University of Alberta

Vessel Icing and Spongy Accretion Modelling

by

Ryan Z Blackmore

A thesis
submitted to the Faculty of Graduate Studies and Research
in partial fulfillment of the requirements for the degree of
Doctor of Philosophy

Department of Earth and Atmospheric Sciences

Edmonton, Alberta
Fall 1996

National Library of Canada
Acquisitions and Bibliographic Services Branch
395 Wellington Street
Ottawa, Ontario
K1A 0N4

Bibliothèque nationale du Canada
Direction des acquisitions et des services bibliographiques
395, rue Wellington
Ottawa (Ontario)
K1A 0N4

Your file *Votre référence*

Our file *Notre référence*

The author has granted an irrevocable non-exclusive licence allowing the National Library of Canada to reproduce, loan, distribute or sell copies of his/her thesis by any means and in any form or format, making this thesis available to interested persons.

L'auteur a accordé une licence irrévocable et non exclusive permettant à la Bibliothèque nationale du Canada de reproduire, prêter, distribuer ou vendre des copies de sa thèse de quelque manière et sous quelque forme que ce soit pour mettre des exemplaires de cette thèse à la disposition des personnes intéressées.

The author retains ownership of the copyright in his/her thesis. Neither the thesis nor substantial extracts from it may be printed or otherwise reproduced without his/her permission.

L'auteur conserve la propriété du droit d'auteur qui protège sa thèse. Ni la thèse ni des extraits substantiels de celle-ci ne doivent être imprimés ou autrement reproduits sans son autorisation.

ISBN 0-612-18018-2

Canada

University of Alberta

Library Release Form

Name of Author: Ryan Z Blackmore

Title of Thesis: Vessel Icing and Spongy Accretion Modelling

Degree: Doctor of Philosophy

Year this Degree Granted: 1996

Permission is hereby granted to the University of Alberta Library to reproduce single copies of this thesis and to lend or sell such copies for private, scholarly or scientific research purposes only.

The author reserves all other publication and other rights in association with the copyright in the thesis, and except as hereinbefore provided, neither the thesis nor any substantial portion thereof may be printed or otherwise reproduced in any material form whatever without the author's prior written permission.

Ryan Blackmore

11391 - 22 Ave
Edmonton, Alberta
Canada T6J 4V8

July 15, 1996

Night of Freezing Spray

The cold sky comes down - the sea rises up to fight
And they meet in confusion, and violence itself is let loose

The vessel buries it's bow deep into the surging wave
Accelerates hard skyward and rolls - diving and driving spray

Hard into the wheelhouse glass - the ice is starting now
The Captain wonders silently, glancing nervously into the barometer's face

How long will the wind stay Nor-west and blow
Nerves start to bristle; now the radar's out

But we know our sister ship is likely just beyond radar's reach - west
Holding strong into the weather -- should be there in the morning too

Can't remember fishing now; too much ice on deck to know what we used to do
Just a controlled terror ebbs and flows, below the men lie remembering courage

And when they go down; they go down fast you know
Funny what's left in dawn's wake - a pop can, a shoe

A page of the Captain's log; two weeks old; what happens next no one knows
Funny how fast the ice comes off; comes off far, far, and deep below.

Ryan Z Blackmore

He spreads the snow like wool
and scatters the frost like ashes.
He hurls down his hail like pebbles.
Who can withstand his icy blast?

Psalm 147: 16,17

"We are lost. The vessel is capsizing. Give our love to our wives and family."

The last radio message from the Ross Cleaveland, one of three vessels which was lost in January 1968 off the coast of Iceland. Synoptic analysis showed strong northerly wind (more than 15 ms^{-1}), low air temperature (-10°C to -15°C), an inflow of cold water from the Greenland Sea, and snowfall. (Panov, 1978; and subsequent references in the prefatory pages are included in the List of References for Chapter 1)

University of Alberta

Faculty of Graduate Studies and Research

The undersigned certify that they have read, and recommend to the Faculty of Graduate Studies and Research for acceptance, a thesis entitled **Vessel Icing and Spongy Accretion Modelling** submitted by **Ryan Z Blackmore** in partial fulfillment of the requirements for the degree of **Doctor of Philosophy**.

Edward Lozowski

Dr. E.P. Lozowski, Supervisor

Dr. L. Makkonen, External Examiner

Dr. T.W. Forest

G W Reuter

Dr. G.W. Reuter

Dr. J.D. Wilson

Date: July 5, 1996

ABSTRACT

This thesis develops an heuristic vessel spray icing model and an exploratory cylinder spray icing model. They are used to study the prediction of vessel spray icing severity.

The physics of vessel spray icing is reviewed in Chapter 1. The resulting overview suggests an elusive phenomenon with many aspects that are as yet understood only in qualitative ways. Two aspects are reviewed in detail: modelling of the distribution of ice accretion over vessels, and the problem of spongy ice growth. This review prepares the background for the model of vessel spray icing of Chapter 2. This model, configured around a non-traditional spray/air heat balance, portrays the overall growth of ice on a vessel in a new and unique way. It accounts for many of the sub-processes of vessel icing while predicting both ice thickness growth rate and overall mass accretion rate for vessels of different size. The model's versatility is illustrated by including an hypothesized nucleated spray icing mechanism that enhances the icing rate significantly (up to 350%) over the original supercooled spray icing mechanism. The problem of spongy ice growth is dealt with in Chapter 3 by modelling the spray icing of a vertical cylinder. In the model the ice has a laminated surficial structure overlain by a falling film of excess liquid flowing over a layer of growing ice called the freezing zone. This new model depends on an analogy between ice growth in the freezing zone and the growth of the tip of a freely-growing ice dendrite, along with traditional thermodynamical elements of spray icing prediction. Using plausible impinging spray temperatures, this model successfully predicts both icing rate and liquid entrapment (i.e. sponginess). It agrees well

with icing data for horizontal rotating cylinders. The model's performance shows that spongy spray ice growth is driven by heat loss from the icing surface, and that it is very sensitive to conditions in the surficial liquid film and the freezing zone. The model's prediction of accretion sponginess is also sensitive to air temperature and spray impingement temperature, which in turn implies the importance of the thermal evolution of the spray in the airstream. Together, the heuristic vessel icing model and the exploratory, spongy spray icing model, demonstrate the importance of the aerodynamics and thermodynamics of spray, as well as the sponginess of the accreted ice, to the rate at which ice accumulates on a vessel under freezing spray conditions.

PREFACE

Man's encounter with the sea has inevitably led to danger, and nowhere has that danger been greater than in the cold oceans of the polar regions. Environmental conditions typical of these regions produce a variety of ice-related problems for sea-going vessels. Icebergs and sea ice are well known for the disasters and the practical difficulties that they bring (Bowyer and Gray, 1990). However, vessels in heavy seas and sub-zero temperatures may encounter another inconvenient and dangerous form of ice, the result of seaspray icing.

Seaspray icing usually occurs under storm conditions. The vessel's interaction with storm-generated wind waves may send volleys of brine over the vessel. Given sufficient heat loss from the brine, the spray may be collected by the vessel to form a brine-laden ice deposit, which, depending on the rate of accretion, may eventually lower the freeboard, raise the centre of gravity, and ultimately promote list and instability of the vessel. These tendencies may be further enhanced by asymmetric ice distribution, and ice accumulations located well above the centre of gravity of the vessel. On occasion atmospheric icing (i.e. freezing rain, wet snow, or freezing fog) may complicate the icing scenario and may add significantly to the overall severity of the icing. However, atmospheric icing, of itself, is not generally considered to be the primary icing threat at sea (Brown and Roebber, 1985). With or without atmospheric icing, vessels capsize and are lost.

Historically, freezing spray has been responsible for the loss of many vessels. Whaling and sealing vessels are known to have sunk due to heavy ice accretion in Arctic waters (Mertins, 1968), and sailing vessels were lost rounding Cape Horn. An interesting account given in *Nature* by Allen (1881) describes the shipwreck of the "Phoenix", a Danish mail ship. The ship encountered a storm with freezing spray, in which the crew were saved only by running the vessel aground, and abandoning ship on the west coast of Iceland.

The danger of seaspray icing to vessels gained greater recognition in the late 1950's, as a result of the loss of British trawlers "Lorella" and "Roderigo" in January 1955. Minsk (1977) suggests that ship icing research was initiated in response to the loss of these vessels by the British Shipbuilding Research Association. As a result cold room ship model tests were carried out in 1955 (Polar Record, 1958). The visibility of the problem grew as cold ocean fishing activity increased, probably the result of better fishing vessels, and increased demand for fish. In 1968 member nations of the Inter-governmental Maritime Organization (IMO) Subcommittee on Safety of Fishing Vessels, began conducting research, obtaining ship icing reports, and publishing on vessel icing.

Shellard (1974) published a list of 81 vessels believed lost primarily due to ice accretion, the earliest recorded loss being that of the "Natset" in the winter of 1942/43. More recent examples of spray icing disasters include the loss of the 300 ft. bulk carrier "Johanna B." and the 420 ft. container ship "Capitan Torres". Both sank December 8, 1989 in the St. Lawrence Bay with a total of 39 fatalities. In February 1988, a Philipino medium-sized fishing trawler capsized off Newfoundland. There was one survivor. In the same area, two seamen were lost from the trawler "Brendan" while attempting to remove ice from its deck. More recently, seaspray ice accretion was named by the Transport Safety Board of Canada as a contributing factor in the sinking of the fishing vessel "Cape Aspy" off the south-west coast of Nova Scotia, January 30, 1993. These incidents show that seaspray icing of ocean-going vessels remains a substantial threat.

The ultimate objective of seaspray icing research is the elimination of vessel losses and the mitigation of dangerous on-board icing conditions. Effective methods and technology for anti-icing (icing prevention) and de-icing (ice removal) would certainly reduce, if not solve, the vessel icing problem. However, as the recent experience documented above indicates, substantial and practical answers to these questions have not been implemented. Therefore, it may prove judicious to address related objectives such as the modelling of the icing process, which will help in the short term, and provide greater knowledge of vessel icing in the long term.

The development of numerical icing models is a desirable objective for a number of reasons. First, reliable and accurate vessel icing models will give predictions of icing to those who need operational forecasts, such as ship captains. Secondly, models will increase understanding of ship icing physics; the resulting knowledge may prove helpful in future anti-icing and de-icing studies and naval architectural design. Third, implementation of vessel icing models into decision-making software packages for ocean routing will likely prove economically beneficial. Finally, numerical models of vessel icing will contribute to the knowledge needed to model icing on other marine structures such as offshore platforms and ice islands.

ACKNOWLEDGEMENTS

Warm thanks to my supervisor, Dr. E.P. Lozowski, not only for his forbearance, encouragement, and help in obtaining financial support, but especially for his acumen and scholarship.

Thanks also to my supervisory committee members Dr. T.W. Forest, Dr. G.W. Reuter, and Dr. J.D. Wilson for their time and attention to this thesis. I am especially grateful to Dr. L. Makkonen for being the external examiner, and for his thoughtful comments.

I would like to acknowledge the work of Dr. W.P. Zakrzewski and his early contribution to this research, as well as the more recent work of John Shi, who shared the results of his spongy icing experiments. I would also thank Mr. R. Brown for his comments and for sharing computer codes and his bibliography.

Special thanks for their support and friendship to Krzysztof Szilder, Tom Flesch, Victor Chung, Russel Sampson and Terry Thompson, and to Laura Smith who deserves particular thanks for helping in the preparation of various manuscripts over the years. I also appreciate Dr. Fairbairn and Dr. Jackson in their capacity as Graduate Chairmen.

I am grateful for financial support by AES and NSERC Research grants and for NSERC, AES, and Province of Alberta scholarships.

Thanks for being there to my friends Dr. Ray and Verna Ellis, Bruce and Coreen Young, Janet Morgan and their families. Finally, heartfelt gratitude to my friend and wife, Heide, for her unflagging vision and patient companionship.

TABLE OF CONTENTS

1. REVIEW OF VESSEL SPRAY ICING PHYSICS 1

1.1 Meteorological Aspects of Vessel Spray Icing 2

1.1.1 Atmospheric icing and spray icing 2

1.1.2 Wind 5

1.1.3 Air temperature 7

1.1.4 Other meteorological factors 9

1.1.5 Synoptic meteorology and vessel icing 10

1.2 Oceanographic Aspects of Vessel Spray Icing 12

1.2.1 Sea-surface temperature 13

1.2.2 Seastate 16

1.2.3 Sea-surface salinity 19

1.2.4 Other oceanographic factors 20

1.3 Seaspray Production 22

1.3.1 Wind-generated seaspray 23

1.3.2 Interaction-generated seaspray 25

1.3.2.1 Initial motion of sea-surface brine 25

1.3.2.2 Seaspray formation 28

1.3.2.3 Seaspray aerodynamics 30

1.3.2.4 Seaspray thermodynamics 31

1.3.3 Vessel-specific factors 33

1.3.3.1 Vessel design 33

1.3.3.2 Vessel dynamic performance 35

1.3.3.3 Vessel operation 36

1.4 Seaspray Ice Accretion 37

1.4.1 Seaspray accretion 37

1.4.2 Seaspray ice growth 40

1.4.3 Seaspray ice distribution on vessels 44

1.5 Modelling Vessel Spray Icing 48
1.5.1 Vessel icing models 48
1.5.1.1. The Kachurin et al. (1974) model 51
1.5.1.2 The Chung et al. (1995) model 54
1.5.2 Modelling spongy spray icing 58
1.5.2.1 The Makkonen (1987) spongy ice growth model . . 60
1.5.2.2 The Zakrzewski et al. (1993) model 64
1.5.2.3 Spongy spray icing structure 69
1.6 Vessel Spray Icing in Context 73
List of References 75

2. AN HEURISTIC MODEL OF VESSEL ICING 89
2.1 Basic Model Assumptions 90
2.2 Modelling Spray Dynamics 93
2.3 Modelling Spray Thermodynamics 94
2.4 Modelling Vessel Spray Flux 95
2.5 Modelling Supercooled Spray Ice Accretion 101
2.6 Modelling Nucleated Spray Ice Accretion 102
2.7 Model Evaluation 105
2.8 Model Sensitivity 110
2.9 Discussion and Conclusions 117
List of References 120

3. AN EXPLORATORY FRESHWATER SPONGY SPRAY ICING MODEL . . 124
3.1 Basic Model Assumptions 125
3.2 Modelling the Falling Film 133
3.3 Modelling the Freezing Zone 142
3.3.1 Freezing zone thermodynamics 144
3.3.2 The interfacial dendritic growth rate 147
3.3.3 Freezing zone thickness 148

3.4 Modelling the Falling Film Thermodynamics 151
3.5 Model Ice Growth Regimes 155
3.5.1 The glaze ice accretion regime 155
3.5.2 The spongy ice accretion regime 156
3.5.3 The porous ice accretion regime 157
3.5.4 Determination of the ice accretion regime 157
3.5.5 Ice accretion sponginess and density 158
3.6 Model Equations 159
3.7 Model Calibration 163
3.7.1 The calibration equations 164
3.7.2 Estimation of the freezing zone parameter 165
3.7.3 Model sensitivity to the freezing zone parameter 167
3.8 Model Performance and Sensitivity 171
3.8.1 Model evaluation with the icing data of Lesins et al. (1980) . 171
3.8.2 Model sensitivity to spray temperature and spray flux 175
3.8.3 Model sensitivity to other model parameters 179
3.8.4 Model evaluation with the icing data of Shi (pers. comm.) . . 182
3.9 Summary Results Conclusions and Recommendations 184
3.9.1 Summary 184
3.9.2 Results 185
3.9.3 Conclusions 186
3.9.4 Recommendations 187
List of References 189

4. CONCLUSIONS 193
4.1 Overview 193
4.2 Conclusions 193
4.3 Recommendations 196
List of References 199

APPENDIX 1: Spray Model Calibration in the Heuristic Vessel Icing Model . . . 201
APPENDIX 2: Spray Collision Geometry in the Heuristic Vessel Icing Model . . 205
APPENDIX 3: Soviet Vessel Icing Data 208
APPENDIX 4: The E-folding Time for Falling Film Development 212
APPENDIX 5: The Mean Period between Droplet Collisions 215
APPENDIX 6: The Reynolds and Rayleigh Numbers for a Falling Film 217
APPENDIX 7: The Algorithm for the Spray Icing Model 219
APPENDIX 8: The Icing Data used to Calibrate the Spray Icing Model 224
APPENDIX 9: The Icing Data used to Evaluate the Spray Icing Model 226
VITAE 228

LIST OF TABLES

Table 2.1 Icing event statistics for comparing the performance of the BLS model and the KA model 106

Table 2.2 Icing event statistics for comparing the performance of the BLS model and the KA model 106

Table 3.1 Predicted falling film thickness and ice fraction for three film path lengths or segment heights 168

Table A3.1 The sixty icing events used to evaluate the performance of the BLS model in Chapter 2 208

Table A3.2 The twelve icing cases used to evaluate the performance of the BLN model in Chapter 2 211

Table A8.1 The Shi spray icing data used to evaluate the spray icing model's freezing zone parameter 225

Table A9.1 The spray icing data used to evaluate the performance of the spray icing model 226

Table A9.2 The spray icing data that was first used to evaluate the freezing zone parameter, and that was then used to compare to model performance 227

LIST OF FIGURES

Figure 1.1 Seaspray ice accretion on the bow of the small Dutch Chemical Tanker "Anna Broere" which went aground near Cape Rozewie 1

Figure 1.2 The frequency of spray generation by a Soviet MFV as a function of heading angle and wave height 27

Figure 1.3 The spray-wetted surface of a 3-D model of a Soviet MFV 30

Figure 1.4 Total collision efficiency versus droplet diameter for a 2.5 cm diameter cylinder 38

Figure 1.5 Total collision efficiency versus droplet diameter for a 1 metre diameter cylinder 39

Figure 1.6 Icing mass flux as a function of liquid water content for a range of spray temperatures (from Lozowski et al., 1995) 43

Figure 1.7 The variation in ice accretion on the superstructure of an unknown Canadian warship 49

Figure 1.8 A nomogram for estimating the icing rate on small Soviet fishing vessels (adapted from Kachurin et al., 1974) 52

Figure 1.9 Schematic 2-D representation of the spongy layer of a hailstone covered by a waterskin (from List, 1990) 70

Figure 2.1 A diagram of a vessel with spray access windows shown 91

Figure 2.2 Plan view of a vessel's bow relative to the waves 97

Figure 2.3 Plan view of a vessel's bow relative to the waves with projected width shown 100

Figure 2.4 Scatter plot for the performance of the Blackmore and Lozowski supercooled model 107

Figure 2.5 Scatter plot of the performance of the computerized version of the Kachurin et al. (1974) nomogram 108

Figure 2.6 Scatter plot of the BLN model, BLS model and KA model for cases of extreme icing 109

Figure 2.7 Sensitivity diagram for air temperature, wind speed and sea-surface temperature 111

Figure 2.8 Sensitivity analysis for significant wave height, sea-surface salinity and fetch 112

Figure 2.9 Model sensitivity to the encountering angle, the vessel speed and the size scaling factor 113

Figure 2.10 Sensitivity analysis of ice growth rate for various models 115

Figure 3.1 A vertical cylinder with two cylinder segments shown 126

Figure 3.2 The model's surficial structure including a falling liquid film adjacent to the freezing zone 130

Figure 3.3 Diagram of the model's surficial structure with mass fluxes and layer thicknesses shown 138

Figure 3.4 Schematic of the model's surficial structure with heat fluxes and temperature profile shown 152

Figure 3.5 The sensitivity of the model's predicted ice fraction to the freezing zone parameter 170

Figure 3.6 Ice fraction as a function of liquid water content for three model spray temperatures compared to the results of Lesins et al. (1980) 172

Figure 3.7 Ice accretion flux versus liquid water content for three spray temperatures compared to the results of Lesins et al. (1980) 174

Figure 3.8 Ice fraction versus spray flux for three spray temperatures and spongy accretion flux and pure ice flux versus spray flux 176

Figure 3.9 Total film thickness, laminar layer thickness, freezing zone thickness, film surface temperature, and icing interface temperature versus spray flux 177

Figure 3.10 Ice fraction versus air temperature for three spray temperatures . . . 180

Figure 3.11 Model-predicted ice fraction as a function of airspeed and relative humidity 181

Figure 3.12 Model versus observed ice accretion flux for icing data 183

Figure A7.1 Flow chart of the spray icing model's algorithm 219

LIST OF SYMBOLS

a	acceleration given to a falling film by the shear stress at the wall (ms^{-2})
a	linearization coefficient for radiative heat transfer at t_s=0°C and t_a=-10°C (Eqn. 1.11, K^3)
a, b	empirical coefficients for the equation that describes the rate of advance of ice crystals growing freely in supercooled water (Eqn. 3.27), and the rate of advance of the icing interface in the spongy icing model (Eqn. 3.45)
A	area of the spray access window of the heuristic vessel icing model (m^2)
A	area of effect for the impact of a droplet on a surface (m^2)
A_1, A_2, B_1, B_2	empirical coefficients of the Bretschneider (1973) seastate model
A_c	area of the windward half of an icing cylinder segment (m^2)
B	vessel's width or beam (m)
B	mass flux of unfrozen brine at an icing surface ($kgm^{-2}s^{-1}$)
B_e	mass flux of brine entrapped by the ice accretion ($kgm^{-2}s^{-1}$)
B_s	mass flux of brine shed from the ice surface ($kgm^{-2}s^{-1}$)
c_1, c_2	constants of integration for Eqn. 3.18
c_p	specific heat capacity of air at constant pressure ($Jkg^{-1}K^{-1}$)
c_w	specific heat capacity of pure water ($Jkg^{-1}K^{-1}$)

C_g magnitude of the group velocity for short waves on a deep sea (ms^{-1})

$\mathbf{C_g}$ group velocity for short waves on a deep sea (ms^{-1})

C_{gr} magnitude of the group velocity relative to the vessel (ms^{-1})

$\mathbf{C_{gr}}$ group velocity vector relative to the vessel (ms^{-1})

C_r freezing zone parameter

C_s phase speed of the significant wave (ms^{-1})

C_w wave phase speed (ms^{-1})

d droplet diameter (m)

d water skin thickness (Fig. 1.9, m)

D diameter of a cylinder accreting ice (m)

e_a equilibrium vapour pressure over a plane surface of water (freshwater or saltwater) for air at the ambient temperature (Pa)

e_s equilibrium vapour pressure over a plane surface of saltwater (of salinity S_0) for air at the surface temperature (Pa)

E collision efficiency of spray droplets with a cylinder

E_{net} net collection efficiency of spray mass by a cylinder

E_s equilibrium vapour pressure over a plane surface of pure water for air at the surface temperature (Pa)

f frequency of the significant wave (Hz)

f_d ice fraction of the accretion's ice matrix

f_e frequency of the a vessel's encounter with the significant wave (Hz)

f_r freezing fraction or the fraction of impinging brine that accretes as pure ice

f_{sp} frequency of a vessel's bow spray production (Hz)

F fetch (m)

F mass flux of brine impinging on an icing surface ($kgm^{-2}s^{-1}$)

F collision of spray mass per unit width of exposure ($kgm^{-1}s^{-1}$)

F_B vessel's freeboard (m)

F_v overall spray collision rate for the heuristic vessel icing model (kgs^{-1})

F_{ws} magnitude of the rate of spray mass impingement on the vessel per unit width of the vessel's upwind projected breadth of wave exposure ($kgm^{-1}s^{-1}$)

$\mathbf{F_{ws}}$ rate of spray mass impingement on the vessel per unit width of the vessel's upwind projected breadth of wave exposure ($kgm^{-1}s^{-1}$)

g acceleration due to gravity (ms^{-2})

h convective heat transfer coefficient ($Wm^{-2}K^{-1}$)

h_s ice growth rate for the heuristic vessel icing model (ms^{-1})

H_s significant wave height (m)

I mass flux of accreted ice and brine (Eqn. 1.3, $kgm^{-2}s^{-1}$)

I mass flux of pure ice (Eqn. 1.20, $kgm^{-2}s^{-1}$)

I ice fraction of the spongy spray ice growth model of Chapter 3

I_0 mass flux of pure ice in the spongy spray ice growth model ($kgm^{-2}s^{-1}$)

I_s the heuristic vessel icing model's ice accretion rate with spray supercooling (kgs^{-1})

I_n ice accretion rate of the heuristic vessel icing model with the nucleated spray icing mechanism (kgs^{-1})

k effective distribution coefficient

k inverse of the e-folding time, t_e, for the development of a falling film from rest (s^{-1})

k, k(I) thermal conductivity of the freezing zone (a function of the ice fraction of the ice matrix, I) of the spongy spray icing model ($Wm^{-1}K^{-1}$)

k^* interfacial distribution coefficient

k_r, k_z empirical constants of the spraying submodel of the heuristic vessel icing model (s^{-1} and s, respectively)

k_w thermal conductivity of water ($Wm^{-1}K^{-1}$)

K constant of proportionality for the empirical spray flux equation of the heuristic vessel icing model

L specific latent heat of fusion for saline spongy ice (Jkg^{-1})

L length of the vessel (m)

L_f specific latent heat of fusion for pure ice (Jkg^{-1})

l_v, L_e, L_v specific latent heat of vaporization for water (Jkg^{-1})

m_1, m_2 empirical coefficients of the Bretschneider (1973) seastate model

m_a mass of air included in an ice accretion (kg)

m_d mass of a spray droplet (kg)

m_i mass of pure ice in an ice accretion (kg)

m_w mass of water in an ice accretion (kg)

n accretion fraction (Eqn. 1.4)

N rate at which droplets affect a point on a surface ($\#s^{-1}$)

N_R flux of droplets passing through a surface (Eqn. A5.1, $\#m^{-2}s^{-1}$)

p, P_a air pressure (Pa)

P period of the significant wave (s)

P upwind projected width of the spray access window (m)

P_c wet shedding perimeter on the windward half of a vertical icing cylinder segment (m)

Pr Prandtl number

P_w wave power encountered per unit width of vessel exposure to the waves (Wm^{-1})

q liquid water content of the spray over a vessel (kgm^{-3})

q_1 heat flux from the freezing zone to the laminar layer at the icing interface of the spongy icing model (Wm^{-2})

q_{12} bulk heat flux from the freezing zone to the laminar layer of the spongy icing model (Wm^{-2})

q_{21} bulk heat flux arising from the transfer (entrainment) of water from the laminar layer into the freezing zone of the spongy icing model (Wm^{-2})

q_{23} bulk heat flux from the laminar layer to the mixed layer of the falling film of the spongy icing model (Wm^{-2})

q_{23} bulk sensible heat flux due to the entrainment of water from the mixed layer to the laminar layer of the falling film of the spongy icing model (Wm^{-2})

q_{i2} flux of sensible heat required to warm the water entering the segment's laminar layer from a segment above (from T_{i2} to T_2) in the spongy spray icing model (Wm^{-2})

q_{i3} flux of sensible heat required to warm the water entering the segment's mixed layer from a segment above (from T_{i3} to T_3) in the spongy spray icing model (Wm^{-2})

q_a rate of heat gain by the air passing through the access window of the heuristic vessel icing model (W)

q_a heat flux at the outer surface of the falling film of the spongy spray icing model (Wm^{-2})

q_b rate of heat loss for the spray passing through the access window of the heuristic vessel icing model (W)

q_c heat flux conducted from the freezing zone across the laminar layer in the spongy icing model (Wm^{-2})

q_v volumetric rate of heat evolution in the freezing zone of the spongy icing model (Wm^{-3})

Q_c convective heat flux at the icing surface (Fig. 1.9, Wm^{-2})

Q_{CC} conductive and convective heat flux at the water skin-air interface (Fig. 1.9, Wm^{-2})

Q_{CP} sensible heat flux at the water skin-air interface (Fig. 1.9, Wm^{-2})

Q_{CCWS} heat flux conducted through the water skin to the water skin-air interface on an icing surface (Fig. 1.9, Wm^{-2})

Q_e evaporative heat flux at the icing surface (Wm^{-2})

Q_{ECS} heat flux due to evaporation, sublimation or condensation at the water skin-air interface (Fig. 1.9, Wm^{-2})

Q_F, Q_I heat flux due to the release of latent heat of fusion at the icing surface (Wm^{-2})

Q_r radiative heat flux at the icing surface (Wm^{-2})

Q_s sensible heat flux at the icing surface (Wm^{-2})

r overall recovery factor for a cylinder (Eqn. 1.11, r=0.79)

r flux ratio for the spray over the vessel in the heuristic vessel icing model

r freezing zone/laminar layer temperature difference ratio (Eqn. A7.1)

r, r^2 correlation coefficient and coefficient of determination, respectively

R mass flux of spray ($kgm^{-2}s^{-1}$)

R_0 mass flux of water entrapped in the ice matrix ($kgm^{-2}s^{-1}$)

R_2 mass flux of water shed from a cylinder segment in the laminar layer of the model's falling film ($kgm^{-2}s^{-1}$)

R_{21} mass flux of water entrained by the freezing zone from the laminar layer of the spongy icing model's falling film ($kgm^{-2}s^{-1}$)

R_3 mass flux of water shed from a cylinder segment in the mixed layer of the model's falling film ($kgm^{-2}s^{-1}$)

R_{32} mass flux of water entrained by the laminar layer from the mixed layer of the model's falling film ($kgm^{-2}s^{-1}$)

R_4 mass flux of spray impinging on the outer surface of the model's falling film ($kgm^{-2}s^{-1}$)

Ra Rayleigh number

R_a mass flux of air entrapped in the ice matrix of the vertical cylinder spray icing model ($kgm^{-2}s^{-1}$)

R_{ae} mass flux of environmental air for the heuristic vessel icing model ($kgm^{-2}s^{-1}$)

R_{as} mass flux of air entrained by the spray over the vessel in the heuristic vessel icing model ($kgm^{-2}s^{-1}$)

R_c mass flux of water down a vertical cylinder segment ($kgm^{-2}s^{-1}$)

Re Reynolds number

RH relative humidity of air

R_{i2} mass flux of water entering the laminar layer of a cylinder segment from the laminar layer of the cylinder segment lying above ($kgm^{-2}s^{-1}$)

R_{i3} mass flux of water entering the mixed layer of a cylinder segment from the mixed layer of the cylinder segment lying above ($kgm^{-2}s^{-1}$)

R_s mass flux of spray ($kgm^{-2}s^{-1}$)

R_T total mass flux of water shed from a cylinder segment in the falling film ($kgm^{-2}s^{-1}$)

R_{ws} mass flux of spray over the vessel in the heuristic vessel icing model ($kgm^{-2}s^{-1}$)

s_b, S_b salinity of the brine on the icing surface (kg (salt) per kg (solution))

Sc Schmidt number

S_i, $\hat{s}$ salinity of the spongy ice (kg (salt) per kg (spongy accretion mass))

S_{ro} salinity of the brine that returns to the sea in the heuristic vessel icing model (kg (salt) per kg (solution))

S_{ss} salinity of the sea-surface brine (kg (salt) per kg (solution))

s_w, S_w salinity of spray (kg (salt) per kg (solution))

t_0 temperature at the envelope of dendrite tips (Fig. 1.9,°C)

t_a, T_a air temperature (°C)

t_s, T_s temperature of the icing surface which is at the equilibrium freezing temperature of the surficial brine (°C)

t_e e-folding time for the development of a falling film beginning with a film at rest (s)

T_0 temperature of the ice matrix and the ice matrix/freezing zone interface of the spongy icing model (°C)

T_1 temperature of the icing interface of the spongy icing model (°C)

T_2 temperature of the laminar layer/mixed layer interface of the spongy icing model's falling film (°C)

T_3 temperature of the mixed layer of the spongy icing model's falling film (°C)

T_4 temperature of the impinging spray droplets of the spongy icing model (°C)

T_f equilibrium freezing temperature of brine (°C)

T_s temperature of the spray over the vessel in the heuristic vessel icing model (°C)

T_{ss} temperature of the sea-surface brine (°C)

T_d droplet temperature or spray impingement temperature (°C)

T_i mean spray impingement temperature (°C)

T_{i2} mean temperature of the water of the film's laminar layer that is entering the cylinder segment from the laminar layer of the cylinder segment lying above (°C)

T_{i3} temperature of the water of the film's mixed layer that is entering the cylinder segment from the mixed layer of the cylinder segment lying above (°C)

T(y) temperature in the freezing zone or the falling film as a function of y (°C)

u fluid flow speed in the falling film (ms^{-1})

u' non-dimensional fluid flow speed in the falling film

u_* friction velocity for the falling film (ms^{-1})

u_a mean fluid flow speed of a falling film (ms^{-1})

U mean speed of the vessel (ms^{-1})

U wind speed in the Bretschneider (1973) seastate model (ms^{-1})

v, V, V_a air speed (ms^{-1})

V_0 rate of advance of the ice matrix/freezing zone interface (ms^{-1})

V_1 rate of advance of the icing interface relative to the liquid of the laminar layer (ms^{-1})

V_{ar} wind speed relative to the vessel in the heuristic vessel icing model (ms^{-1})

$\mathbf{V_{ar}}$ wind vector relative to the vessel in the heuristic vessel icing model (ms^{-1})

V_c rate of advance of an ice crystal growing into bulk supercooled water (ms^{-1})

V_g rate of advance of the icing interface in the glaze ice accretion regime of the vertical cylinder spray icing model (ms^{-1})

V_{HS} rate of advance of the outer surface of a hailstone's the water skin (Fig. 1.9, ms^{-1})

V_{IS} rate of advance of ice dendrites into the water skin on a hailstone (Fig. 1.9, ms^{-1})

V_r, V_{rw} speed of the vessel relative to the waves (ms^{-1})

V_s final horizontal spray speed over the vessel in the heuristic vessel icing model (ms^{-1})

V_{smax} maximum rate of advance of the icing interface in the spongy ice accretion regime of the vertical cylinder spray icing model (ms^{-1})

V_v mean speed of the vessel (ms^{-1})

$\mathbf{V}_v$ mean velocity vector of the vessel (ms^{-1})

V_w wind speed (ms^{-1})

w, W_f liquid water content of airborne spray (kgm^{-3})

We Weber number: ratio of inertial forces to surface tension forces

y dimensional coordinate normal to the substrate with origin at the ice matrix/freezing zone interface (m)

y_0 location of the ice matrix/freezing zone interface (m)

y_1 location of the icing interface (m)

y_2 location of the laminar layer/mixed layer interface (m)

y_3 location of the outer surface of the falling film (m)

(y_1-y_0) thickness of the freezing zone (m)

(y_2-y_1) thickness of the laminar layer of the falling film (m)

(y_3-y_2) thickness of the mixed layer of the falling film (m)

y_t total thickness of the falling film (m)

z height above deck (m)

Z spray access window height in the heuristic vessel icing model (m)

Z_c cylinder segment height in the vertical cylinder spray icing model (m)

Z_{max} maximum spray height above the deck of a vessel (m)

α,γ thermal diffusivity of water ($1.3x10^{-7}$ m^2s^{-1})

α angle between the vessel's heading and the seaway where 0° represents head seas, 90° beam seas, and 180° following seas (degrees,°)

α encountering angle between the vessel's heading and the seaway in the heuristic vessel icing model where 180° represents head seas, 90° beam seas, and 0° following seas (degrees,°)

α_{gr} angle as observed from the vessel between the vessel's heading and the group velocity of the waves in the heuristic vessel icing model where 180° represents head seas, and 0° represents following seas (degrees,°)

α_{ar} angle as observed from the vessel between the vessel's heading and the wind in the heuristic vessel icing model where 180° represents head winds, and 0° represents following winds (degrees,°)

β thermal expansion coefficient for water (68.05×10^{-6} K^{-1})

Γ mass flow rate for a falling film per unit breadth ($kgm^{-1}s^{-1}$)

ΔT supercooling of bulk water into which ice crystals grow (°C)

ΔT temperature difference across the liquid film on a hailstone's surface (°C)

ΔZ maximum height of the spray's trajectory above a vessel's bulwarks (m)

δ thickness of a laminar falling film (m)

δ_{max} maximum laminar layer thickness in the Dukler and Bergelin (1952) model (m)

δ thickness over which dendrites grow or thicken (Fig. 1.9, m)

η non-dimensional coordinate normal to the substrate used to describe the falling film in the spongy icing model

λ "sponginess" or the liquid mass fraction of the predicted ice accretion of the vertical cylinder spray icing model

λ_a air inclusion fraction of the ice accretion of the vertical cylinder spray icing model

μ dynamic viscosity of water (1.79×10^{-3} Nsm^{-2})

ν kinematic viscosity of water (1.75×10^{-6} $m^2 s^{-1}$)

ρ_a density of the air (kgm^{-3})

ρ_{ac} density of the predicted ice accretion of the vertical cylinder icing model (kgm^{-3})

ρ_c radius of curvature of the tip of a freely-growing ice crystal (m)

ρ_i density of ice (kgm^{-3})

ρ, ρ_w density of brine or water (kgm^{-3})

τ, τ_0 shear stress exerted by the falling film at the icing interface of the vertical cylinder spray icing model ($y=y_1$, Nm^{-2})

τ time for spray to rise and fall for a gravitational trajectory over a vessel (s)

τ_d mean period between droplet impacts at a point on a collecting surface (s)

ε ratio of the molecular weight of water vapour to dry air

λ_s, λ_f the liquid mass fraction or sponginess for saline and freshwater accretions, respectively

ξ constant of proportionality (i.e. $\xi=10^{-3}$ kgm^{-4}, Kachurin et al., 1974) in a linear equation describing liquid water, q, over a vessel (kgm^{-4})

σ Stefan-Boltzmann constant (5.67×10^{-8} $Wm^{-2}K^{-4}$)

ω radian frequency of waves (rad s^{-1})

ω_e radian frequency of encounter for a vessel with the waves in its seaway (rad s^{-1})

LIST OF TERMS

Heuristic: (1) of or relating to exploratory problem-solving techniques that utilize self-educating techniques to improve performance (Webster's 3rd New International Dictionary). (2) serving to indicate or point out; stimulating interest as a means of further investigation (Random House Dictionary 2nd Ed. Unabridged). (3) of or relating to a usually speculative formation serving as a guide in the investigation or solution of a problem (American Heritage Dictionary, 2nd College Ed.).

Model: (1) a simplified representation of a system or phenomenon, as in the sciences or economics, with any hypotheses required to describe the system or explain the phenomenon, often mathematically. (2) to simulate (a process, concept, or the operation of a system), commonly with the aid of a computer (Random House Dictionary 2nd Ed. Unabridged).

Physical-empirical model: a vessel icing model that demonstrates or shows an overview of the physical processes of vessel icing and is composed of submodels that describe the subprocesses of vessel icing. (Blackmore)

Statistical model: a vessel icing model that depends only on a statistical relationship between the input parameters and the icing rate. (Blackmore)

Statistical-physical model: a vessel icing model that uses a physical model of spray icing around which the statistics are organized. (Blackmore)

1. REVIEW OF VESSEL SPRAY ICING PHYSICS

Vessel spray icing is a complex phenomenon (Zakrzewski and Lozowksi, 1991). It results from a group of processes that are interrelated and that, even if considered one at a time, may be difficult to fully understand or describe. These processes are controlled by a considerable variety of conditions that influence the onset or severity of freezing spray. Fig. 1.1 shows the variety in shape and thickness of the seaspray ice on the bow of the chemical tanker "Anna Broere".

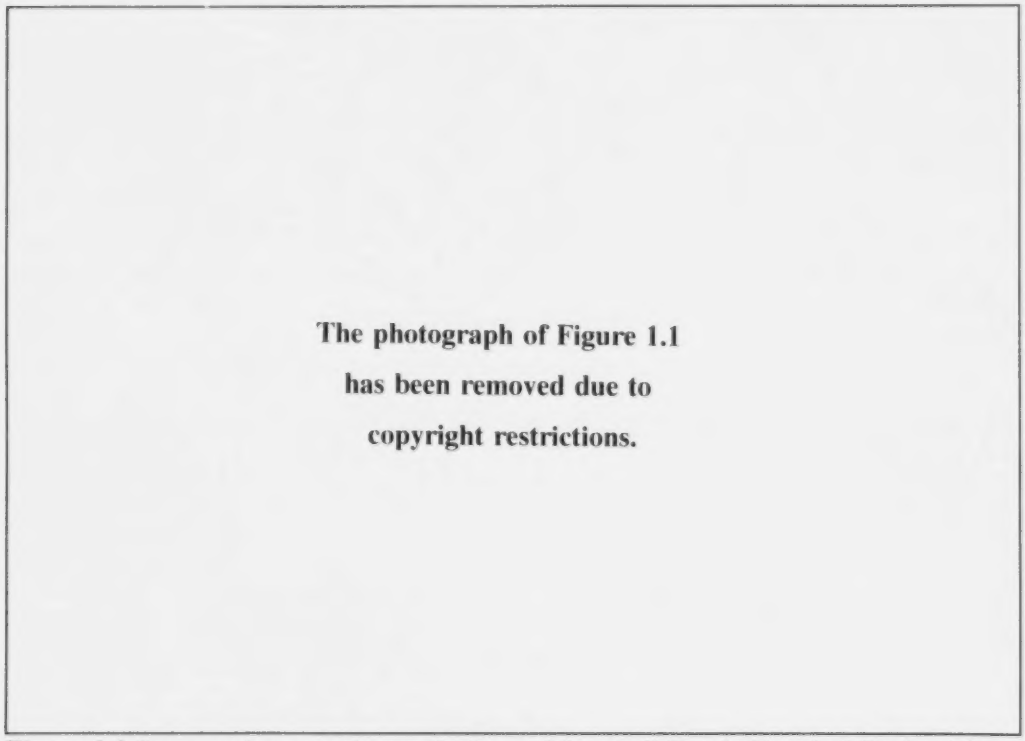

Figure 1.1 Seaspray ice accretion on the bow of the small Dutch Chemical Tanker "Anna Broere" which went aground near Cape Rozewie, (Poland, Southern Baltic Sea), January 1, 1979, (photo courtesy of W.P. Zakrzewski).

This first chapter has the objective of introducing vessel spray icing. This is done in largely descriptive terms in Sections 1.1, 1.2, 1.3, and 1.4, and is followed by a more detailed treatment of modelling in Section 1.5. Section 1.5 begins with a review of the modelling of vessel spray icing, which forms the background for the heuristic model of

spray icing presented in Chapter 2. There follows a review of the physics of spongy spray ice accretion, which provides the background for the exploratory spongy spray icing model of Chapter 3. Section 1.6 gives the reader a sense of the wider context of icing studies within which vessel spray icing research occurs.

The review of vessel spray icing that follows is divided into four sections. Section 1.1 looks at the meteorological conditions that predispose a vessel to seaspray icing, Section 1.2 focuses on oceanographic factors that influence vessel icing, Section 1.3 gives a view of those processes that occur during the transportation of brine to the vessel's icing surface, and Section 1.4 reviews the ice accretion processes that occur on the vessel's surface.

1.1 Meteorological Aspects of Vessel Spray Icing

Vessel spray icing is a multi-faceted process in which meteorological factors play an important part. This section examines the role of meteorological factors in the generation of seaspray, and in the accretion of ice on ocean-going vessels.

1.1.1 Atmospheric icing and spray icing

Atmospheric icing of vessels is discussed here for completeness and because this form of ice accretion may occur coincidentally with seaspray icing. By itself, however, atmospheric icing is most likely not the primary icing threat to ocean-going vessels. Borisenkov and Panov (1972) analyzed reports of over 2000 icing events on Soviet fishing vessels. They found that 89.8% of those events were the result of seaspray icing alone, 6.4% were seaspray combined with fog, rain or drizzle, 1.1% were seaspray with snow, and 2.7% were the result of fog, rain or drizzle alone. They also analyzed vessel icing events in the Arctic, and found 50% were from seaspray, 41% were a combination of seaspray and precipitation, 6% were from precipitation alone, and 3% were from fog alone. Brown and Roebber (1985) examined the relative importance of seaspray with percent frequency data derived from Canadian ship meteorological reports. A percent

frequency range of 81% to 97% is given for icing due to ocean spray for the five regions of the Canadian East Coast. Brown and Roebber (1985) go on to give 56% and 60% frequencies for the occurrence of ocean spray icing in the eastern and western Arctic regions, respectively. Therefore, even though the relative frequency of atmospheric icing is a function of location, seaspray icing appears to be the main threat as far as frequency of occurrence is concerned.

It is also generally accepted that the spray icing of vessels produces more severe ice loadings than does atmospheric icing (Makkonen, 1984a). Shektman (1967), Mertins (1968), Sawada (1970), De Angelis (1974), Makkonen (1984a), and Zakrzewski and Lozowski (1991) acknowledge the potential dangers of atmospheric icing, but due to its reported low frequency and intensity, suggest that seaspray icing is the more dangerous type of vessel icing. This is further confirmed by Brown and Roebber (1985), who report that no cases of ice accretion due to freezing rain produced thicknesses greater than 3.0 cm in the Gulf of St. Lawrence, a region with a relatively high frequency of freezing rain. They also found no ice accretions with thicknesses exceeding 3.0 cm in the Gulf of St. Lawrence for "fog only" cases. They report that freezing spray accounted for the maximum ice accretion thicknesses in all Eastern Canadian waters. There were two areas of local icing maximum: the first, over the Scatarie Bank south of Newfoundland and east of Cape Breton, with a mean ice accretion thickness exceeding 7.0 cm, and the second, off the eastern tip of Anticosti Island in the Gulf of St. Lawrence with a mean ice accretion thickness exceeding 6.0 cm. On the basis of these observations, it is likely that seaspray icing is also the more dangerous form of icing from the point of view of ice loading and vessel stability. However, Makkonen (1984a) points out that the accretion of atmospheric ice during seaspray icing may be important because the accretion of atmospheric ice does not decrease with elevation as it does for seaspray icing. He reasons that atmospheric ice is likely to occur on the uppermost structures of the vessel bringing with it a disproportionately large reduction in vessel stability by virtue of its elevation above the vessel's centre of mass.

Vasil'yeva (1966) examines the synoptic conditions favourable to vessel spray icing. He suggests the possibility of mixed spray icing at sea, especially at the rear of a

cyclone. In the present work, mixed accretion will usually be taken to mean spray icing with snowfall. Of interest here is the entrainment of snow into the seaspray cloud, as well as the collection of snow by the wet icing surfaces of a vessel. Horjen (1990) produced a theoretical icing model which predicts a 200 to 270% increase in the spray icing load during snowfall with a snow concentration of 0.28 gm^{-3} over that without snow, under gale conditions (18-20 ms^{-1} wind speed). Whether the snowfall is wet or dry, and whether or not the icing surface has an exposed liquid film, could also have some influence on the mechanics of snow adhesion and on the ice accretion rates. Wet snow is known to collect on surfaces that are initially dry (Wakahama et al., 1977; Personne and Gayet, 1984).

Borisenkov and Panov (1972) suggest that as a general rule, the lower the temperature and the higher the wind speed, in combination with supercooled precipitation or snow, the higher the probability that an icing event will occur, and the greater the potential icing severity. They report ice thicknesses of at least 20 cm in 50% of their cases, with deck accumulations reaching a maximum of 100 cm under conditions of mixed spray and snowfall. In support of the view that mixed accretion may lead to severe icing, Shektman (1967), suggests that the most severe icing occurs with storm-force winds (25-32 ms^{-1} wind speed) and snowfall. In summary then, although atmospheric icing at sea may not in itself constitute the primary icing threat to vessels, it is likely that atmospheric icing acts with seaspray icing to produce more severe icing, perhaps even the most severe icing.

Brown and Roebber (1985) found that 63% of a group of 960 Canadian Coast Guard vessel icing reports included references to snow. Snowfall may not be the only form of atmospheric precipitation that could enhance seaspray icing rates. Brown and Roebber (1985), on the basis of an analysis of icing data from the Gulf of St. Lawrence and the Labrador Sea-Davis Strait region, suggest that supercooled evaporation fog or sea smoke can also enhance ice accretion thickness. Seaspray icing alone was found to produce on average 5-6 cm thick ice accretions. Evaporation fog alone produced a smaller maximum ice accretion thickness of 3 cm. Seaspray icing with evaporation fog produced a maximum accretion thickness of 17 cm. The maximum accretion thickness

for seaspray icing with evaporation fog, which is much larger than the maximum thickness for evaporation fog alone, or the average for seaspray icing alone, seems to suggest that supercooled fog may act with seaspray to enhance ice accretion thickness. Although an hypothesis, an explanation of how this may occur is presented in Section 2.6, which explores a mechanism in which ice particles such as snow or those that might be present in supercooled fog, could nucleate spray droplets, and thereby enhance icing rates.

1.1.2 Wind

The wind affects seaspray icing of vessels in a number of ways (Zakrzewski et al., 1993). First, the wind is the primary cause of the waves which the vessel encounters. Waves interact with the vessel's hull and give rise to the brine jet which forms bow spray. Swell may also be present in the wave field (Ryerson, 1993), but usually only wind waves are considered in vessel spray icing models. Second, the wind exerts a drag force on the liquid in the brine jet, and carries the resulting spray droplets over the vessel. The vertical gradient of wind speed over the sea surface as well as the disturbance of the wind field by the vessel, are complicating factors which are generally ignored. Usually, the wind speed is assumed to be specified at the standard 10 m height. Third, the wind is responsible for much of the heat loss from the icing surfaces of the vessel. These effects combined suggest that wind speed is very influential in the seaspray icing of vessels.

A fourth factor associated with the wind is its direction relative to the wave field and to the vessel. The impact of relative wind direction on the spray icing of vessels is not yet fully understood. For example, little is known about the effect on spray delivery to a vessel when the wind is not aligned with the motion of the dominant waves. Even for wind that aligns with the dominant wave motion, if it is at an oblique angles to the vessel, it will produce an uneven spray distribution over the vessel and asymmetrical ice loadings (i.e. larger ice loads to the port or starboard of the vessel). Chung (1995) presents a vessel icing model which, along with vessel dynamics and stability analysis,

shows that asymmetric ice loadings have serious consequences for vessel stability. Although Zakrzewski et al. (1993) show that spray icing rate maxima occur near head seas (15° to port and starboard), with little icing at beam seas, and no icing for following seas, much is left to do in verifying their model results and the implications for vessel stability.

The true wind direction may have implications for the spraying and icing of vessels on seasonal time scales. For example, Lundquist and Udin (1977) show that during winter, winds from the northwest through to the northeast are associated with greater icing event frequency and severity in the Baltic Sea. These wind directions are correlated with lower air temperatures behind cold fronts.

Another effect linked to wind direction is exemplified by offshore winds with short fetches. These winds can bring air temperatures that are little modified from the low values typically observed over land or pack ice. Winds from the open ocean, by contrast, will probably have been significantly warmed, at least in the layer near the sea surface. This will tend to moderate the icing severity. In this way, wind direction can work with other factors to affect the spray icing of vessels.

Many researchers (Kachurin et al., 1974; Jessup, 1985; Brown and Roebber, 1985; Zakrzewski, 1987; Overland et al., 1986), implicitly suggest the importance of wind in vessel icing when they focus attention on wind-driven interaction-generated spray. De Angelis (1974), gives a rule for estimating icing potential on the basis of wind speed and air temperature alone. Moderate icing potential, for example, occurs with winds of 13 knots (6.5 ms^{-1}) or greater and with air temperatures of -2°C or lower. Severe icing potential occurs with winds of 30 knots (15 ms^{-1}) or more, and with air temperatures of -9°C or lower.

Shellard (1974) states that a substantial number of investigators give a wind speed threshold for seaspray icing of vessels in the range of Force 5-6 (9.0-13.8 ms^{-1}). Walden (1967) for example, suggests a threshold of Force 4 or less (less than 6.7 ms^{-1}) for a small vessel in short steep waves with cross wave swell, and as much as Force 8 (16.5-19.2 ms^{-1}) for a larger vessel with lower speed. Panov (1976) and Zakrzewski and Lozowski (1991) suggest that the spraying threshold for Soviet medium-sized fishing

vessels (MFV) occurs at approximately 8-9 ms^{-1} wind speed. Thus, the threshold for bow-spray is likely to be a function of wind speed, seastate, vessel size and vessel speed.

Since vessels seeking shelter in freezing spray conditions may enter near-shore waters, local effects may also become important in vessel spray icing. For example the funnelling or channelling of wind around islands or through inlets may affect vessels seeking refuge there. Seaspray icing may have unexpected variations associated with local wind effects.

1.1.3 Air temperature

It is well-known that air temperature significantly influences the icing of vessels (Jessup, 1985; Brown and Roebber, 1985). Zakrzewski and Lozowski, 1991 show that as air temperature decreases the icing rate increases linearly for both the Kachurin et al. (1974) and Comiskey et al. (1984) vessel icing models. This is to be expected as convective heat loss is observed experimentally to depend linearly on the temperature difference between an object's surface (i.e. an icing surface) and the airstream (Holman, 1990). This linear dependence is included in the saline spongy ice growth model of Makkonen (1987) (Eqn. 1.11) and the vessel icing model of Zakrzewski et al. (1993) (Eqn. 1.16), as well as other spray icing models.

Sawada (1962) suggests an air temperature based threshold for the onset of icing of -3°C for all but a very strong wind. In strong wind conditions, icing may occur at temperatures up to -1°C. In addition, according to Sawada (1962), icing becomes very marked at -6°C, and when the air temperature drops to below -8°C, the spray freezes in situ on impingement without running. A more conservative assignment of temperature is given by Shellard (1974), who simply states that, for icing to occur, the air temperature must be lower than the equilibrium freezing temperature of the brine, which varies from 0°C for pure water to approximately -1.9°C for a typical salinity (35 ppt) observed in the open ocean.

The threshold air temperature for the onset of icing and the icing rate at a given air temperature will depend on a number of factors. Two such factors are the intensity

of spray developed as a consequence of the ship/wave interaction, and the initial temperature of the spray brine. These two factors control the supply of sensible heat at the icing surfaces, suppressing or possibly stopping ice growth with a large supply of sensible heat due to warm spray, or encouraging ice growth with increased sensible heat loss due to supercooled impinging spray.

Ship/wave interaction and spray temperature are both affected by fetch. Fetch is defined as the upwind distance over the ocean's surface from the vessel to the sea ice edge or to land. The greater the fetch, the greater the wave height and spray intensity, and the more likely that the temperature of the air will rise as it is heated during its passage over the warm sea surface. Therefore, as a vessel approaches either sea ice or the coast with offshore winds, the air temperature may decrease (Brown and Roebber, 1985). Wave height also decreases, resulting in less spray and hence an unclear overall spray icing tendency.

Sawada (1962), Sawada (1970), Fein and Freiberger (1965), Vasil'yeva (1966), Vasil'yeva (1971), Walden (1967), and BSRA (1957) have suggested that at an air temperature of -18°C or less, the spray freezes in the air, impacting as dry ice crystals which do not stick and so is harmless to vessels. This view is contested by the observational data of Shektman (1967), with icing recorded at air temperatures in the range -19°C to -25°C. Later, Shektman (1968) extended the air temperature based limits for potential icing to the range of 0°C to -29°C, including rapid icing in the temperature range -26°C to -29°C. Borisenkov and Panov (1972) also refute the -18°C air temperature lower limit to vessel spray icing by giving an observed range for icing air temperature of 0°C to -26°C. They further suggest that air temperatures below -18°C lead to rapid icing and an increased, not a diminished, likelihood of disaster. More recently, Overland (1990) takes much the same position by suggesting that the most severe icing in the Bering Sea, Gulf of Alaska, and the Sea of Japan is caused primarily by extreme cold air advection.

It is likely that the large liquid water contents of seaspray that are generated by vessel/wave interaction (Borisenkov and Pchelko, 1975; Ryerson, 1993), will preclude the complete freezing of the spray droplets. Spray with a large liquid water content is likely

to provide significant heating of the entrained air, through the exchange of sensible and latent heat. However, the suggestion that seaspray might partially freeze, especially under the reduced liquid water contents observed to occur at higher elevations over a vessel, seems plausible and may have important consequences. As Borisenkov and Panov (1972) have suggested, very low air temperature may give rise to severe icing, and partial freezing of the airborne spray could play a crucial role in such severe icing. Just such a mechanism has been postulated (Makkonen, 1989; Sackinger and Sackinger, 1987) to explain an acceleration in ice island growth from falling brine spray at an air temperature around -20°C. Such depressed air temperatures may partially freeze the airborne spray. The latent heat evolved would tend to maintain spray droplet temperature close to the equilibrium freezing temperature of the droplet's unfrozen brine. The rate of heat loss from the droplets would thereby remain high throughout the droplets' trajectory, and with it the amount of ice formed in the spray. This, it is argued, increases the ice mass accreted on the ice islands on which the spray falls. In Chapter 2, an analogous nucleated spray icing mechanism is hypothesized to occur in vessel spray icing. It may help to explain severe icing at low air temperatures.

1.1.4 Other meteorological factors

Relative humidity is known to influence spray ice accretion. Lower relative humidity tends to increase ice growth rate due to an increase in the evaporative heat loss from an icing surface. This understanding was used by Wise and Comiskey (1980) in producing an icing prediction nomogram for the northeast Pacific from an existing nomogram for the northeast Atlantic. The winter climate for the Pacific northeast is most notably different from that of the northeast Atlantic by its lower relative humidity (US Naval Weather Service Detachment, 1974).

Another environmental factor that may influence vessel spray icing is solar radiation. Although no studies seem to have taken this into account, solar radiation could appreciably alter the threshold of icing and the icing rate. Convective or evaporative heat loss fluxes characteristic of vessel icing conditions are typically of the order of a few

hundred Wm^{-2}. This is of comparable magnitude to the solar flux reduced by attenuation in the atmosphere and by the angle of inclination of the sun. The presence of clouds will also likely affect the intensity of shortwave radiation at the icing surface. In addition, the albedo of the icing surface will be an important factor since it indicates the fraction of the incident solar radiation that is reflected from the icing surface and that will not participate in the heat balance of the icing surface. Heat exchange due to long wave radiation could also contribute to vessel icing. A comparison of vessel icing between day and night, as well as a comparison between cloudy and clear atmospheric conditions, could be revealing. Radiation effects may account for a component of the "noise" in vessel icing data.

1.1.5 Synoptic meteorology and vessel icing

Borisenkov and Pchelko (1972) show that the majority of ship icing incidents in northern temperate latitudes occur during intrusions of cold air masses southward in autumn, winter, and spring. Ship icing occurs most frequently, well into the cold air mass and to the rear of the low, where northerly, northwesterly, and westerly surface winds typically prevail. The cold air advection at the surface associated with the passage of a cold front may signal the start of strong winds, a condition favourable to vessel icing. Minsk (1977) states that icing may lag the passage of a cold front as the air temperature drops to the values necessary to initiate spray icing. Also, the change in direction and speed of the wind associated with the front may begin to alter the state of the sea, with the establishment of larger waves taking some time. Icing occurs much less frequently ahead of the low with the approach of a warm front.

Kaplina and Chukanin (1974) document an example of the extreme seaspray icing meteorology that is characteristic of the Barents Sea between Norway and Spitzbergen in the month of February. Typically, a large polar low with multiple centres may occupy the region from the southern tip of Greenland to the Kara Sea with influence as far as the Laptev Sea and the North Pole. The periphery of this region is characterized by large pressure gradients and high wind speed. Extreme spray ice thicknesses of 10 cm to 40

cm have been recorded in many instances in this region in February.

As already mentioned, Vasil'yeva (1966), in examining the synoptic conditions favourable to ship icing, included snow and rain at the rear of a cyclone as a characteristic situation. Brown and Roebber (1985) also found, on the basis of a detailed analysis of icing events reported to the Canadian Coast Guard, that a significant portion of these events (63%) were seaspray icing during snowfall. A reason for this coincidence may be the large thermal contrast between the air and the sea surface at the rear of the intense winter cyclones which typically cause freezing spray episodes in the waters of the Canadian East Coast. The warmed air at the surface becomes unstable, producing precipitation, and thereby intermittent mixed accretion conditions.

Winter storms of the Canadian East Coast typically produce snow, rain and freezing precipitation (Stewart and Paternaude, 1988). Stewart et al. (1995) present observations taken over Newfoundland which suggest that there is an organized evolution of precipitation type associated with the passage of troughs, warm fronts and cold fronts. For example, warm fronts exhibited an evolution from snow to ice pellets followed by a transition from freezing rain to rain. They also observed that the airborne mass concentration of precipitation was generally greatest for snow and that wet snow had liquid mass fractions as high as 0.43. The accurate forecasting of precipitation type and intensity is likely to benefit operations at sea (Stewart and Patenaude, 1988).

A particularly intense type of polar low which is triggered by an outbreak of cold arctic air over a relatively warm sea surface has been called an "arctic hurricane" (Businger, 1991). He goes on to suggest that research has largely concentrated on the mid-latitude cyclone and the tropical hurricane, ignoring polar low storms until recently. The arctic hurricane has a structure and physics which are strongly analogous to the well-known tropical hurricane. These violent and fast-forming storms are of concern to vessels in arctic waters, because of their ability to produce freezing spray.

The arctic hurricane is similar to the tropical hurricane in the following characteristics: (1) Satellite imagery reveals a cloud signature similar to the tropical hurricane. A calm "eye" is found at the centre of the cloud with a low barometric pressure and with wall clouds around the relatively calm central region. (2) Wind speeds

in excess of 32 ms^{-1} (the threshold speed for hurricane winds) are observed at the surface about 100 km from the "eye". Like the tropical hurricane, this is a band of very strong winds that enhances the air-sea heat exchange that drives the hurricane. (3) The strong winds occurring in the spiral configuration of the arctic hurricane produces high and confused seas in a way similar to the tropical hurricane.

Arctic and tropical hurricanes also differ: (1) The arctic hurricane is smaller (about 300 km in diameter) than its tropical counterpart (about 1500 km); (2) The arctic hurricane moves more quickly than the tropical hurricane with a typical speed of 30 knots, approximately twice as fast as the tropical storm; (3) The arctic hurricane also forms very quickly with a lifespan in the range of 12-24 hours, compared to a lifespan of 3-7 days for the tropical hurricane. This short lifespan occurs because the arctic hurricane typically forms along the sea ice edge. It develops as it moves out over the relatively warm sea surface, only to encounter pack ice or land again and lose its energy source.

The small-scale, fast-forming, fast-moving and intense nature of these storms produces a significant challenge for forecasters, and for seaspray icing forecasts in particular. The arctic hurricane is usually too small to be detected by the meteorological observational grid, and it is unresolvable by present numerical weather prediction models. Forecasters must rely on an understanding of the general conditions leading to polar lows, on satellite imagery, and on direct observations from vessels in order to predict arctic hurricanes and their dangerous vessel seaspray icing. The arctic hurricane may offer an explanation of the rather sudden icing-related loss of the vessels "Lorella" and "Roderigo" north-north-east of North Cape, Iceland, (67°N. 21°W) in 1955 (Hay, 1956).

1.2 Oceanographic Aspects of Vessel Spray Icing

Even though vessel spray icing is largely governed by meteorological factors, the influence of the sea cannot be ignored. Seaspray icing of vessels is by definition the result of the spray generated from vessel/wave interactions. Vessel/wave interaction, in turn, depends on seastate, the vessel's dynamics, and the way in which the vessel is being

operated. Modelling these factors individually is not a simple task; taken together, they represent a considerable modelling challenge. Factors such as sea-surface temperature and salinity directly influence the growth of ice on the vessel. Indirect effects include the presence of sea ice or frazil ice in the sea surface. Sea ice occurs with a low sea-surface temperature and suppresses waves, two factors with opposite affects on spray icing. To review all the possible oceanographic factors which could influence vessel icing is beyond the scope of this work. Only a brief overview of the most important factors is presented in the following sections.

1.2.1 Sea-surface temperature

The temperature in the ocean generally decreases with depth to a value near the freezing point of water in the deep ocean (Hartmann, 1994). Most of this change occurs in the thermocline, the first kilometre or so of the ocean's depth. Winds and waves produce a mixed layer at the surface of the ocean which has a thickness on the order of tens of meters (Knauss, 1978), and which is usually close to being isothermal (Hartmann, 1994). The sea-surface temperature influences the onset and the severity of seaspray icing of vessels, but the importance of sea-surface temperature on seaspray icing is a matter of controversy, even among those who have observed and collected icing data. Based on an analysis of over 2000 observations of vessel icing, Borisenkov and Panov (1972) found that icing rarely occurs with a sea-surface temperature greater than +6°C. Vasil'yeva (1966) and Sawada (1967) give a sea-surface temperature threshold of +3°C and +4°C, respectively. Mertins (1968) published vessel icing nomograms based on observations made on board German fishing vessels. The sea-surface temperature range used in these nomograms is -2°C to +8°C, implicitly suggesting that icing is likely to be significant only at sea-surface temperatures less than +8°C.

As is evident from the above variety of suggested sea-surface temperature threshold values, a single-parameter description of the seaspray icing threshold may be too simplistic. For example, any threshold to the seaspray icing of vessels should be a function of the intensity of spraying as well as of the sea-surface temperature. Tabata et

al. (1963) used this idea to formulate their hypothesis that spray ice will be removed if enough seawater (i.e. a spray of sufficient intensity) is shipped aboard, even with brine temperatures as low as 0°C.

Other investigators dispute a sea-surface temperature based threshold for vessel icing. Shellard (1974) for example, documents the work of Shektman (1967) in which rapid icing is reported for sea-surface temperatures close to +8°C. Smith (1970) reported icing at a sea-surface temperature of +8°C south of Iceland in conditions of Force 10 to 12 winds (22.5 ms^{-1} to more than 32.6 ms^{-1} wind speed) and air temperatures below -5°C. Perhaps the idea of a sea-surface temperature icing threshold has arisen out of observational experience that may result from the correlation of cold seas with cold air, rather than a true threshold to spray icing originating in the physical processes at work in vessel icing.

Shektman (1968) and Smith (1970) agree that the severity of vessel seaspray icing shows little dependence on sea-surface temperature. Shellard (1974) presented icing data, gathered on United Kingdom fishing vessels, that suggest there is only a slight increase in icing with decreasing sea-surface temperature. Minsk (1977) reports that Soviet experience in the North Atlantic and the Barents Sea shows the influence of the Gulf Stream's warm waters. In particular, he states that if the sea-surface temperature rises above about +2°C, this should be accounted for with a reduced prediction of icing rate. Aside from this, Minsk (1977) suggests that vessel icing is not strongly determined by sea-surface temperature.

Shellard (1974) also notes that sea-surface temperature seems to be of limited significance in many instances, but he offers the proviso that this parameter may be of importance in particular situations. The rapid icing data of Shektman (1967) at sea-surface temperatures close to +8°C is an example. However, Shellard (1974) goes on to concede that this data set was not large enough to be conclusive on this issue. A paper submitted in 1960 to the third session of the WMO Commission for Maritime Meteorology by the Republic of Germany (WMO, 1960) reviews the state of knowledge of vessel spray icing. This report acknowledges the importance of such environmental parameters as air temperature, sea-surface salinity, wind force and the seastate, but unlike

other investigations, it holds that the sea-surface temperature had a great influence on vessel spray ice, and on the ice accretion rate. Overland (1990) supports this view by suggesting that low sea-surface temperatures appear to contribute to severe seaspray icing in the Labrador Sea, Denmark Strait, and Barents Sea. Also, the Overland et al. (1986) vessel icing prediction algorithm exhibits significant sensitivity to sea-surface temperature at near-freezing temperatures. The addition of a cold water data set did not alter substantially the tuning of the original algorithm (Overland et al., 1986). The effect of sea-surface temperature on vessel spray icing may become significant as the sea-surface temperature approaches the equilibrium freezing temperature of the sea-surface brine.

Even though its importance to vessel spray icing remains unclear, sea-surface temperature will have some influence on the temperature of the impinging spray. This is likely because a change in the initial temperature of the spray brine (i.e. the sea-surface temperature) will result in a change in the temperature difference between the entrained air of the spray cloud and the spray droplets. This in turn will lead to a change in the heat transfer between the spray and the air, and the thermal evolution of the droplets along their trajectories in the spray cloud. Other conditions in the spray cloud could also modify the spray impingement temperature and with it the severity of icing.

In fact, other conditions could be as important as the spray's initial temperature. For example, spray liquid of a given initial temperature with sufficiently low flux intensity and sufficiently small droplet diameter could experience a large heat loss to the airstream and a large supercooling en route to the icing surface. Sensible heat loss at the icing surface due to the warming of impinging supercooled spray could result in an increased icing rate. On the other hand, a higher flux of seaspray with much larger droplets at the same initial temperature could produce a reduced heat loss from the droplets to the airstream, little or no supercooling of the spray, and smaller icing rates. If the sensible heat delivered to the vessel's surface were, in this way, to become greater than the heat lost to the environment, then it is possible that no ice would form at all. Each of these situations could occur with the same sea-surface temperature, yet produce significantly different icing rates. A more complete understanding of the role of sea-surface temperature in seaspray icing is a valuable goal for future research although its

importance is likely to be coupled to other factors such as trajectory length, spray flux intensity or droplet size.

1.2.2 Seastate

At a particular wind speed, the seastate can be represented as a wave spectrum. However, in the vessel spray icing literature, seastate is typically described in a simpler way using significant wave height, wave period and wave steepness. Important to the seaspray icing of vessels, is the convergence of two or more systems of waves. This produces "cross seas" (Bowyer and Gray, 1990). Under more extreme conditions, with greater wind speed and wave height, confused "pyramidal seas" may form (Pierson, 1972). Walden (1967) points out that a vessel may roll more severely under these conditions, and that the vessel's interaction with the confused seas will likely produce more spray. An increased spray flux may, under favourable conditions, lead to a greater icing rate, and greater ice loads, which in turn may bring about more extreme vessel motion. Chung (1995) has produced a vessel spray icing model and combined it with a vessel dynamics model for the stern trawler "Zandberg". He presents icing simulations that give rise to asymmetrical ice load distributions which lead to trimming and listing of the vessel. Listing of the vessel leads in turn to large roll motions and to the loss of stability. Therefore, spray and ice accretion are likely to increase during confused seas, as will the probability that the vessel will capsize.

Pierson (1972) analyzed the loss of two trawlers due to crossing wave trains, without the degradation of stability that superstructure icing brings. These vessels are hypothesized to have been lost in confused pyramidal seas which were caused by the refraction of waves. This wave refraction is believed to have been a response to the bottom topography, with varying water depths over shoal areas. Refraction of wave systems also occurs in coastal waters and around islands. In such cases vessels seeking shelter on the leeward side of islands, may encounter hazardous cross seas, while loaded heavily with seaspray ice.

Local currents in coastal waters could also enhance an already dangerous freezing spray condition. Surface currents can increase wave height and can sharply increase wave steepness. For example, a current speed of only 5 knots (2.5 ms^{-1}) can double the wave height, if the current is directed against the motion of the waves (Bowyer and Gray, 1990). They also suggest that currents of 3-6 knots (1.5-3.0 ms^{-1}) are quite common, with extreme current speeds of 15 knots (7.5 ms^{-1}) in the waters of the Canadian East Coast. The arrival of open ocean waves in shallower coastal waters may also cause an increase in wave height and thereby greater seaspray generation. In this case, the wave height tends to increase in response to the local reduction in depth.

Even for long-crested waves on the open ocean, uncomplicated by local effects, the capacity to predict the extent and intensity of spray production by a vessel remains in a relatively primitive state. One exception is the recent work of Chung (1995) which documents the measurement of spray generated by a scale model of the stern trawler "Zandberg". These spraying data were used as the basis for a full-scale spraying model which predicts spraying flux as a function of location on the vessel, vessel speed and significant wave height. Another approach to modelling seaspray production has been presented by Zakrzewski (1987) for the Soviet medium-sized fishing trawler. It is a generalization of the formula proposed by Borisenkov et al. (1975), and describes the variation of spray cloud liquid water content, w (kgm^{-3}), with height, z (m), above the deck:

$$w = 6.46\times10^{-5} H_s V_{rw}^2 \exp\left(-\frac{z}{1.82}\right) \qquad (1.1)$$

where H_s is the significant wave height (m), and V_{rw} is the ship speed relative to the waves (ms^{-1}). Zakrzewski et al. (1993) use this formulation for liquid water content along with a spray cloud model based on the trajectory of a single droplet to determine the location and flux of spray at the vessel's surfaces. As well, Ryerson and Longo (1992) have described their full-scale spray measurements aboard the USCGC MIDGETT, a 2700 ton, 115 m long, high endurance cutter.

Aside from these examples of research into seaspray production, much of the vessel spray icing literature has dealt with the problem of seaspray generation in largely qualitative ways. For example, Woodcock (1953) makes the following points. Small vessels may begin to generate spray by collision with waves in seas that correspond to Force 5 (9.0-11.3 ms^{-1} wind speed, 1.8 m wave height). At Force 6 (11.4-13.8 ms^{-1} wind speed, 2.9 m wave height) the smaller vessels will almost certainly experience spray, especially if moving into the waves. Woodcock (1953) suggests that the spray produced at the threshold wind speed (i.e. 9-11.3 ms^{-1} wind speed) arises from the tops of the waves that interact with the hull. This spray usually does not reach a very high level. Higher wind speeds are required to carry spray to greater heights and further back over the vessel on to the superstructure.

Even though swell, originating at great distances from the area of potential seaspray generation, can alter the frequency and intensity of spray production by a vessel, it is usually not mentioned in the vessel icing literature (except by Ryerson, 1993). Wind waves are usually given the primary credit for the interaction-generated spraying of vessels.

The time dependence of vessel icing that occurs in response to the development and decay of wind waves is not a simple matter, though it may have a considerable bearing on spraying of vessels. Significant growth of wind waves requires a strong wind for an extended time (3-6 hours) from a single direction (Khandekar, 1989; Minsk, 1977). Other factors are also important in the growth of waves. For example, winds of Force 5 (~10.2 ms^{-1} wind speed) with an unlimited fetch require approximately 3.5 hours to develop a significant wave height of 1.2 metres, and winds of Force 7 (~15.1 ms^{-1} wind speed) require approximately 5.5 hours to develop a significant wave height of 3 metres. Also, a small fetch and shallow coastal water will reduce wave size under offshore winds. Where offshore winds or winds off an ice pack occur, spraying and icing of a vessel will probably not be a significant threat within a distance of 1 to 3 miles of the shore or ice edge (Minsk, 1977). Another important factor that can affect the growth and decay of waves is the presence of ice in the sea. Waves on the sea surface are known to decay rapidly when encountering pack ice and grease ice (Martin and Kauffman, 1981).

1.2.3 Sea-surface salinity

The median salinity for the oceans of the world is 34.69 ppt. (Knauss, 1978). Hartmann (1994) shows that the annual-mean salinity of the global ocean has a constant value close to that given by Knauss (1978) below a depth of about 600 m. Hartmann (1994) states that wind and waves produce a mixed surface layer in which salinity is almost independent of depth. This surface layer typically has a depth of tens of meters (Knauss, 1978), and a salinity range in the open ocean from about 33 to 38 ppt (Hartmann, 1994). Hartmann (1994) also states that sea-surface salinities are low at high latitudes because precipitation of freshwater exceeds evaporation. However, heavy snowfall, rain or mixed precipitation such as is often observed in the waters of the Canadian East Coast (Stewart and Patenaude, 1988), could produce local reductions in sea-surface salinity. The extent to which the salinity of the sea-surface brine could be affected is uncertain, and would depend on the mixing of the ocean's surface layer. In the absence of precipitation, sea-surface salinity will remain essentially unchanged during a vessel icing event.

A location in which a vessel might experience a change in sea-surface salinity is the Baltic Sea. The Baltic Sea has brackish water with a variation of salinity from around 15 ppt in the south to around 3 ppt in the northern Gulf of Bothnia (Lundquist and Udin, 1977). This rather large change in salinity occurs over a distance of approximately 1700 km. Therefore, the sea-surface salinity will, for all practical purposes, be constant during a freezing spray event.

Using the model of Kachurin et al. (1974), Lozowski and Gates (1985) show that the icing rate under conditions typical of vessel spray icing increases by approximately 10% when the sea-surface salinity increases from 30 ppt to 35 ppt. Lozowski and Nowak (1985) report experimental observations that are consistent with this predicted trend. However, Makkonen (1987) presents a theory that disputes this tendency for increased icing rate with increasing salinity by suggesting that at temperatures typical of marine icing, the growth rate of saline ice is less than that of freshwater ice. Lozowski and Gates (1985) state that the models of Stallabrass (1980) and Horjen and Vefsnmo (1985) exhibit a similar icing rate sensitivity to that of the model of Kachurin et al. (1974), but with an

opposite tendency. Makkonen (1985) shows with a theoretical model of spray icing that the icing rate for saline water can be either higher or lower than that of pure water spray. He states that the icing rate of saline spray is likely to be higher than the rate for pure water at high spray salinity and high air temperature. Therefore, the tendency of the icing rate remains unclear, even though there is agreement that the icing rate will probably change by less than 10% for the change in salinity that is to be expected during an episode of freezing spray on the open ocean (i.e. a few parts per thousand).

Lozowski and Gates (1985), and Makkonen (1987) point out that the difference in icing rate between freshwater spray (0 ppt) and seaspray (33 ppt) is likely to be substantial. For example, Makkonen (1987) states that the nomogram of Kachurin et al. (1974) predicts rates of seaspray icing that are twice those of freshwater icing for equivalent icing conditions. Therefore, even though the icing rate is not likely to change substantially due to salinity variations on the open seas or on a body of freshwater, it is important to account for the effect of salinity on the rate of spray icing.

1.2.4 Other oceanographic factors

Another form of ice that may have an indirect influence on vessel spray icing, and that is known to occur at the surface of the ocean, is frazil ice. Frazil ice appears in the form of small discs due to anisotropic ice crystal growth rates in the basal plane direction and the radial direction (Forrest and Sharma, 1992). These discs are typically 1-4 mm in diameter and 1-100 μm in thickness. They form as the result of two essential conditions: the supercooling of the brine at the ocean's surface, and the turbulence of the seawater induced by the wind over the ocean (Martin, 1981). Frazil forms in polynyas (large open water areas within pack ice) and arctic leads. If the frazil becomes dense enough to form a slurry, the term "grease ice" is used; otherwise the frazil may appear as an "underwater snow storm" throughout the turbulent layer in which it is growing. Frazil also forms with offshore winds that carry sea ice away from the shore, exposing a near-freezing sea surface to the unmoderated cold air arriving from over the land.

Martin and Kauffman (1981) describe leads in pack ice (defined as openings in the ice with width scales of less than 100 m) where frazil ice growth occurs over the entire open area. The wind produces a surface current which transports the frazil in the downwind direction until it is deposited, often to depths of 0.1 to 0.3 m, against the downwind ice edge. They observed frazil ice in the water 20 m upwind from an advancing grease ice deposit in a small lead. The floating frazil layer can advance upwind until the wind-generated waves of the lead are damped out and frazil formation stops.

Martin and Kauffman (1981) also observe that when grease ice forms in large polynyas, the formations can take the shape of long rows parallel to the wind direction. Dunbar and Weeks (1975) describe the observation of such formations of grease ice in the Gulf of St. Lawrence. Martin and Kauffman (1981) give the theoretical details of how a Langmuir circulation may produce the convergence of frazil ice particles at the sea surface to form these rows of grease ice. This suggests that frazil may be present in polynyas, possibly throughout the water of the polynya.

Vessels that operate in polynyas and leads, can experience seaspray with frazil or grease ice particles, even though the waves may be attenuated by nearby sea ice, or by grease ice. If this occurs, it may have two important implications for the rate of ice accretion during vessel spray icing. First, the frazil ice mass could be directly incorporated into the growing spray ice accretion on the vessel, perhaps in a way similar to that hypothesized and modelled by Horjen (1990) for snow incorporation. Second, the seaspray droplets will be seeded with ice crystals, thereby suppressing the droplet's ability to supercool. This is important because the latent heat evolved during the droplet's freezing maintains a large droplet-to-air temperature difference in the seaspray cloud. Such a large temperature difference maximizes the heat lost by the spray droplets to the cold air, leading to greater icing rates. This mechanism is explored in greater detail in the context of the heuristic vessel icing model presented in Chapter 2.

Brown and Roebber (1985) present a contour map of the mean ice accretion thickness on vessels reporting spray icing during the period 1970-84. There is an accretion thickness maximum east of Anticosti Island in the Gulf of St. Lawrence. They

point out that this observed maximum is difficult to explain, as seasonally expected sea ice coverage in excess of five tenths would likely suppress the spraying and icing of vessels, and thus diminish ice accretion thickness in that area during the crucial months of February and March (Markham, 1980). Markham (1980) shows lower ice coverage toward the centre of the Gulf of St. Lawrence and east of Anticosti Island, with leads forming in the area of the observed spray ice thickness maximum. In addition to the leads that are likely to form east of Anticosti Island, larger areas of open water are also likely to form. For example, Markham (1980) shows a satellite image (Fig. 2, Markham (1980)) of a well-developed area of open water exposed to west-north-westerly wind. Brown and Roebber (1985) report that 80% of the icing events used in their analysis occurred under westerly to northwesterly winds. This suggests that the air at the surface could be largely unmodified in temperature as it moves over Anticosti Island and the sea ice cover that is expected to the west and northwest of the island.

The observed local maximum in spray ice thickness east of Anticosti Island (Brown and Roebber, 1985) may be caused by the effect of frazil ice occurring in the open water in that area. Frazil ice is known to occur in leads (Martin and Kauffman, 1981) and open water exposed to cold windy conditions. For example, Dunbar and Weeks (1975) show a photograph of grease ice rows in the Gulf of the St. Lawrence, west of Anticosti Island (Fig. 6, Jan. 1974). Frazil ice combined with seaspray icing of vessels may prove to be a particularly dangerous condition. An explanation of how frazil might increase the severity of spraying on vessels is presented in Section 1.3.2.4.

1.3 Seaspray Production

Once meteorological and oceanographic conditions are favourable for seaspray icing, it is the collision of spray with the surfaces of the vessel's topside that leads to spray ice growth. Even though wind-generated seaspray may contribute to vessel spray ice accretion, we assume that it is much less important than the spraying generated by vessel/wave interactions (Jessup, 1985; Zakzrewski and Lozowski, 1991). Wind-generated seaspray is dealt with in Section 1.3.1. This is followed by a section on spray generation

due to vessel/wave interaction. Section 1.3.3 deals with the factors of vessel architecture, operation, hydrodynamics, and design.

1.3.1 Wind-generated seaspray

Seaspray generated by the action of the wind drag on the wave tops and by bursting air bubbles at the sea surface (Wu, 1979) is called wind-generated seaspray. This type of seaspray is probably important for enhancing heat and mass transfer between the sea surface and the air (Andreas, 1989), which may in turn affect the sea-surface temperature. The importance of wind-generated seaspray for marine icing depends on whether or not it can deliver a significant amount of brine to the surface of the vessel. Generally, investigators suggest that the intensity of spray from this source is not important (Zakrzewski, 1986; Shellard, 1974).

Shellard (1974) states that wind-generated spray begins to appear at Force 5-6 (9-13.8 ms^{-1}), but that it may not be seen at deck level on a vessel until Force 9 (19.3-22.4 ms^{-1}). However, the appearance of seaspray at deck level, as suggested by Shellard (1974), also depends on the freeboard of the vessel. Monahan (1968) and Wu (1973) reported that wind-generated seaspray begins to form at a wind speed threshold in the range of 7.5 to 9.5 ms^{-1}. As the wind speed increases, the height at which spray is observed also increases. Horjen (1983) proposed that wind-generated spray appears at the 10 meter level at a wind speed of approximately 15 ms^{-1} (Force 7). Wu (1973) state that the concentration of spray droplets in the air increases with wind speed, and decreases with height over the sea surface. Other research also shows that the mean droplet size increases with wind speed and decreases with height above the wave crest level (Preobrazhenski, 1973; Zhuang et al., 1993). Zhuang et al. (1993) showed that a turbulent trajectory simulation can be used to produce seaspray profiles which are affected by upstream fetch and atmospheric stability. Such a simulation could be used to investigate the collision of wind-generated seaspray with a vessel's superstructure as well as its entrainment into the vessel's bow spray cloud.

Wind-generated spray may form as a result of two different mechanisms. Wang and Street (1978) suggest that the tearing of wave crests by the wind will become the dominant mechanism of spray production at higher wind speeds. Brown and Roebber (1985) report general agreement in the literature that bubble bursting is the dominant mechanism of spray production for wind speeds up to 15 ms^{-1}. Zakrzewski (1986) suggested that the liquid water content of wind-generated spray is much lower than that of vessel/wave interaction-generated spray. He also argued that the windborne droplet trajectories will not result in any significant spray delivery to the top side of a vessel.

Finally, wind-generated seaspray could play a role in severe icing, due to its effect on spray nucleation. For example, a vessel in near-freezing sea-surface temperatures and hurricane conditions will encounter air that is filled with seafoam and spray. The spray or foam in the air is likely to supercool and then possibly to nucleate. If nucleation occurs, this airborne mixture of brine and ice could seed the vessel/wave interaction-generated spray droplets with ice crystals. This could lead to accelerated icing according to the nucleated spray icing mechanism described at the end of Section 1.1.3. In addition, this mixture of airborne brine and ice could seed ice crystals directly into the falling film on the icing surfaces of the vessel. The presence of ice particles in the falling liquid film could reduce the supercooling of the surficial liquid from what it would have been otherwise. This assumes that the ice particles would grow, evolving latent heat. We suggest that the latent heat flux in the flowing film would reduce the film's supercooling, increase the film's temperature and increase the difference in temperature between the film and the airstream. This increased temperature difference would increase the icing rate. With rapid growth of these ice crystals or possibly the entrainment of snow, the film might form a slurry with a temperature close to 0°C. This could in turn enhance the convective heat loss from the icing surface to the airstream and consequently the icing rate. Therefore, even though wind-generated seaspray may not contribute to spray icing directly, it could affect vessel spray icing indirectly.

1.3.2 Interaction-generated seaspray

The motion of vessels may lead to green water being shipped on board, some of which may remain as ice, some of which may be kept aboard the vessel by virtue of ice-clogged scuppers, but most of which is shed from the vessel. Overtopping of seawater, may, on the other hand, cause decks to be ice free. Significant sensible heating, the result of large flux intensities, may be sufficient to prevent ice accumulation, and to wash accumulated ice away. While the shipping of green water may bear little hydrodynamic similarity to seaspray formation, it will serve as a point of departure in the discussion of interaction-generated spray.

Interaction-generated seaspray is produced as a result of the vessel's interaction with waves. Brown and Roebber (1985) suggest that the vessel icing literature is consistent in identifying this as the main source of brine for most kinds of marine icing, including vessel spray icing. The process will be analyzed as follows. Section 1.3.2.1 deals with momentum transfer to the bulk brine in the sea surface so as to produce a brine jet at the vessel's hull. Section 1.3.2.2 describes some preliminary ideas to do with spray droplet formation. Sections 1.3.2.3 and 1.3.2.4 deal with the aerodynamics and thermodynamics of the spray cloud over and around the vessel. This review is structured in such a way as to emphasize the difference between those processes that hydrodynamically drive the brine jet and those processes that have to do with the aerodynamics of spray formation and delivery.

1.3.2.1 Initial motion of sea-surface brine

The seastate is itself a challenge to model (Khandekar, 1989), even without attempting to account for the hydrodynamic interaction of the brine with a vessel's hull. However, the problem of the relative motion of sea-surface brine and the vessel may in the first instance be considered from the point of view of seakeeping theory. Overland (1990) reviews the statistical approach to this problem of seakeeping as given by Price and Bishop (1974), and assumes that the onset of spraying relates in a simple way to the shipping of green water. He assumes that seaspraying occurs when 1 in 20 waves are

overtopping the deck under head winds and seas. On the basis of this assumption, Overland (1990) shows that the threshold for the onset of spraying may be related to the length of the vessel.

The initial motion of brine as a result of the hydrodynamic interaction of the hull with the incident wave is an aspect of spray generation that should be modelled. Like the process of wave overtopping, brine jet formation requires sufficient momentum to transport brine from the sea surface. In the case of seaspray formation, the brine jet gives rise to spray droplets which must reach the elevation of the vessel's topside. The frequency of brine jet formation must first be determined.

The frequency of brine jet formation and spraying is not likely to be greater than the frequency with which the vessel encounters the waves (Panov, 1976). Overland (1990) gives the encounter frequency for a vessel with forward motion as:

$$\omega_e = \omega - \frac{\omega^2}{g} U \cos\gamma \qquad (1.2)$$

where ω is the radian frequency of the waves, U is the speed of the vessel, γ is the angle between the vessel's heading and the seaway (180° for head seas, 90° for beam seas, and 0° for following seas), and g is the acceleration due to gravity. Irregular seas and vessel motion will combine to generate spraying frequencies that are very different from the vessel's wave encounter frequency. For example, Ryerson (1993) reports observing double bow splashes for a ship speed of 11 ms^{-1} under intense spraying aboard the U.S. Coast Guard Cutter MIDGETT. Two double spraying events occurred during a 20 minute period with 1.5 m waves and 2.4 m swell. A double spraying event suggests the possibility of developing more than one brine jet at a time for seas with both wind waves and swell. A simple method for predicting the frequency of spraying has been given by Zakrzewski (1987), who suggests that a Soviet medium-sized fishing vessel experiences spraying approximately every second wave encounter. Observations on a large Norwegian whaling ship suggest that a spray jet is produced with every fourth wave encounter (Zakrzewski et al., 1993, Horjen, pers. comm.).

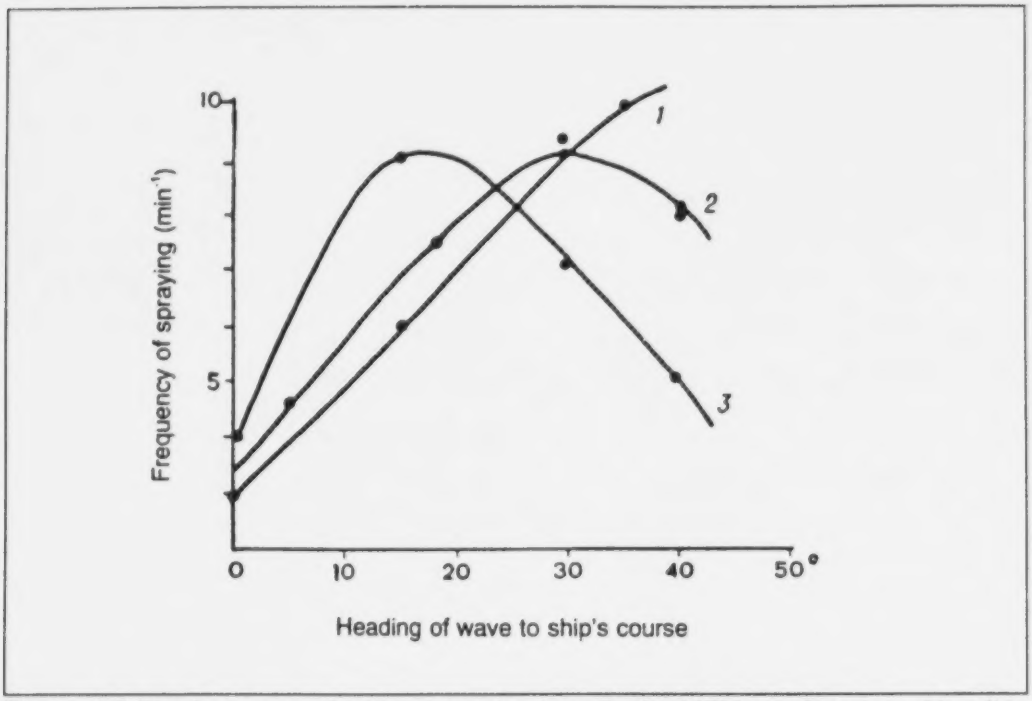

Figure 1.2 The frequency of spray generation by a Soviet MFV as a function of heading angle (0° for head seas) and wave height: (1) 1.0-1.5 m, (2) 2.0-2.5 m, and (3) 3.0-3.5 m. (adapted from Kultashev et al., 1972)

Fig. 1.2 shows a considerable change in the frequency of spraying with vessel heading, and wave height for the Soviet MFV. Following seas may produce no seaspray while head seas will give rise to spray (Zakrzewski et al., 1993). One way to sidestep the difficulty of predicting the irregular way in which vessel/wave interactions occur is to time-average the intensity of spraying. In this way, the problem of predicting the spray generation cycle (i.e. spray on/spray off durations) can be avoided. One also avoids the problem of predicting the variation of spray intensity within an individual spray event. Zakzrewski et al. (1993) and Chung (1995), both model the spray generation cycle with constant spray on/spray off durations and a constant spray flux during the spray-on interval. Another factor that may vary considerably from spray event to spray event is the location along the perimeter of the vessel's hull (Zakrzewski et al. 1988b), where the brine jet forms, giving rise to spray.

Lebiedzinski and Thomas (1993) point out that little research has been done on the spraying of vessels because of the difficulty in scale model simulation of spraying, and because of the great many variables involved. They also state that the process is complex, non-linear, and allows for few simplifying assumptions. They calculated spraying frequency for full-scale, heavy weather tests on the USS "Monterey" (CG-61), a ship with a displacement of 8700 tons and a length of 161 m. These calculations were based on video recordings of the vessel's forecastle and deck, and the visually observed number of spray events over a known time interval (20 min.). They suggest that there is no clear indicator of bow spray formation, but that a vertical bow acceleration of around 0.1 g gave the strongest indication of interaction-generated spray production. They suggest that this indicator, in addition to bow position relative to the incident wave and the sea surface, may eventually lead to a better predictor for the onset of spraying.

Lebiedzinski and Thomas (1993) suggest two mechanisms for spray production in addition to interaction of the bow with the incident wave. A secondary spray was observed to form by wind-stripping of brine from the wet hull. Even though the spray was usually taken aft and away from the topside of this ship, it could be a source of icing spray on other vessels. They also observed secondary spraying associated with vessel-generated or scattered waves. The interaction of these scattered waves (the combined bow, radiated and diffracted waves) with the ambient wave field produced brine jets on the leeward side of the vessel. The turbulent wind in the lee of the vessel formed spray from these brine jets which subsequently recirculated in turbulent eddies back over the vessel, and impinged on the decks.

Kachurin et al., (1974), Kultashev et al., (1972), and Stallabrass (1980), predict the time-averaged spray intensity empirically using significant wave height, vessel speed, and vessel heading. Such formulations are clearly incomplete, but must suffice for the present.

1.3.2.2 Seaspray formation

The hydrodynamic acceleration of bulk seawater to the deck level of a vessel is necessary but not sufficient to produce spray. It may merely result in shipping

greenwater. Spray formation requires that bulk seawater be broken into droplets. The energy to do this may come from the kinetic energy of the brine jet itself, or from the shear stress of the wind on the rising jet.

Since the formation of seaspray droplets from bulk brine brings with it a considerable increase in the free-surface area, the Weber number will to be important (White, 1986). The Weber number, We, is the ratio of inertial forces to surface-tension forces, and for droplet formation it will have values, We≤1. Chin et al. (1991) give a theoretical model of droplet formation for a pure water jet (i.e. a case of Rayleigh jet breakup) from a small diameter orifice (50μm). The droplet size distribution and velocity distribution were measured far enough away from the orifice that droplet formation was complete but close enough that aerodynamic effects (drag) could be ignored. The model predictions compared well to the experimental measurements. The Weber number had a major effect on the droplet size distribution of the spray while the velocity of the jet had a major effect on the droplet velocity distribution. Models of seaspray formation will need to account for the surface tension of brine, the brine jet velocity and aerodynamic drag with the wind.

Scale model experiments on spray formation cannot achieve complete similarity with the full-scale process. Lebiedzinski and Thomas (1993) suggest that if Froude number scaling is used, then scale model vessels produce "spray" drops which become footballs at full scale. Nevertheless, they suggest that scale model testing may still be useful for determining the liquid velocities induced by the vessel's hydrodynamic interaction with waves. Chung (1995) has used this concept as the basis for an empirical spraying model which is described in detail in Section 1.5.1.2.

Chung et al. (1995) have developed an empirical spraying model based on experiments made with a scale model of the hull of the MT "Zandberg". These were carried out at the Institute for Marine Dynamics, NRCC, in St. John's, Newfoundland. This research suggests that the total amount of spray intercepted by the vessel depends on ship speed to the third power. Incorporating this spraying model into a full-scale icing model, Chung et al. (1995) have shown that the icing rate varies rapidly with vessel speed when the latter is less than 5 ms^{-1}. For full-scale vessel speeds above 6 ms^{-1} the

icing rate remains constant due to the large sensible heat flux accompanying the large spray mass fluxes predicted by the model.

1.3.2.3 Seaspray aerodynamics

Once some of the bulk sea-surface brine has been transformed into a spray, the resulting ensemble of droplets will be accelerated by the wind and delivered to the surfaces of the vessel's topside. Many of the approaches to predicting vessel spraying have employed greatly simplified models. For example, Zakrzewski (1987) uses the significant wave height, the vessel's speed relative to the incident waves, and height above deck, to parameterize the distribution of liquid water over a Soviet MFV (Eqn. 1.1). The issue of spray formation is glossed over by assuming a monodisperse spray droplet spectrum with a diameter of 1.25 mm. Fig. 1.3 shows the spray-wetted area on a Soviet MFV (Zakrzewski et al., 1988a).

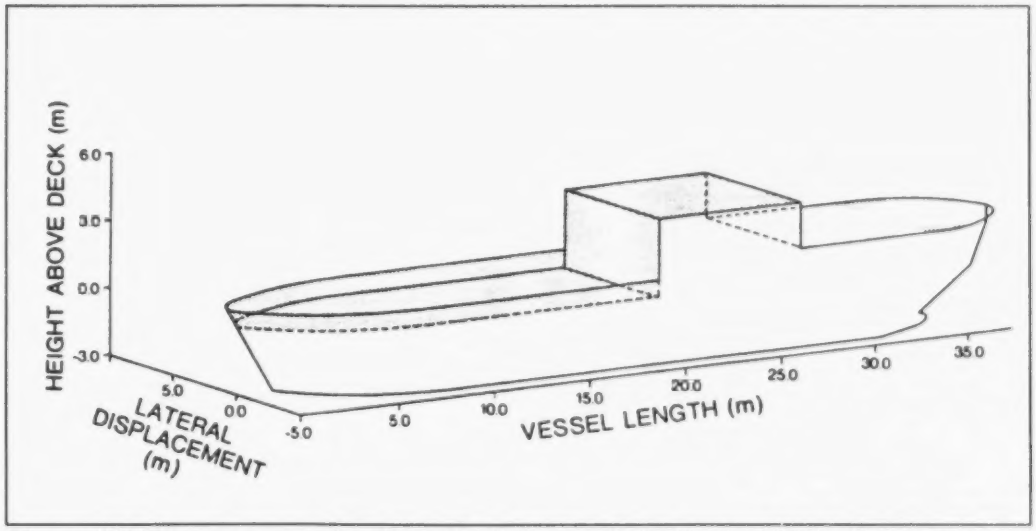

Figure 1.3 The spray-wetted surface of a 3-D model of a Soviet MFV with vessel speed 2 ms^{-1}, wind speed 13 ms^{-1} and head seas (from Zakrzewski et al., 1988a).

Zakrzewski and Lozowski (1987) assume that the spray droplets are initially at rest relative to the vessel over the perimeter of the bow, and that they accelerate from there over the vessel. The aerodynamics of the spray cloud is modelled under the assumption that it will differ little from that of a single droplet. Other spraying models

have been developed recently (Zakrzewski et al., 1993; Chung, 1995) that also depend on modelling the motion of a single droplet.

A single spray event results from the encounter of a non-steady brine jet with the turbulent air flow around a vessel which is moving with 6 degrees of freedom in response to the state of the sea. The brine jet and the spray cloud may be responsible for inducing turbulence within the airstream. The brine jet and the seaspray cloud will probably vary from spray event to spray event due to irregular seas and vessel motion. Perhaps all we can say with certainty at the moment is that the spray droplets will move in the downwind direction. Some of them will be collected by surfaces of the vessel and some will be carried beyond the vessel's topside and returned to the sea.

Large droplets and large liquid water contents occur together in the lower levels of the spray cloud (Panov, 1972; Borisenkov et al., 1975). Since large droplets will fall out of the spray cloud more quickly than small droplets, they will fall out closer to the origin of the spray. This is likely to give rise to a longitudinal gradient of droplet size. Smaller drops will arrive preferentially at higher and more distant vessel surfaces. The smaller droplets which are observed at higher elevations (Borisenkov et al., 1975) are likely to have a velocity close to that of the airstream. By contrast, the largest droplets near the bow will follow essentially gravitational trajectories. In view of these considerations, the liquid water content of the spray cloud is likely to be highest at lower levels, nearer the source of the spray. Chung et al. (1995) observe that the mass flux of spray is described by a negative exponential function with longitudinal distance.

1.3.2.4 Seaspray thermodynamics

The spray cloud will change rapidly in shape and size, deforming in aerodynamic response to the air flow around the vessel's topside. The air temperature will rise because of the heat released during the cooling of the droplets. The temperature changes will depend on the efficiency with which heat is transferred from the spray droplets to the air. This heat transfer depends on the temperature difference between the entrained air and the ensemble of droplets, and the relative velocity of the air and droplets. The spray temperature change will also depend on the ratio of the thermal mass of the spray brine

to the thermal mass of the air with which it interacts. Thus the spray droplet temperature will remain high in those parts of the cloud with high liquid fluxes (expected to occur at lower heights and closer to the spray source). Conversely, lower droplet temperatures are likely to occur in spray at higher elevations and further from the spray source. Since the ice accretion rate is influenced by the spray flux and temperature, one may expect the ice accretion rate to vary downwind from the spray source.

Spray droplets on similar trajectories may experience different thermodynamic processes and as a result may have different thermal histories. For example, some droplets may simply supercool due to the lack of ice nucleators in the droplet. On the assumption that ice nuclei do occur in the sea surface, small droplets are more likely to contain no ice nucleators and supercool in the spray cloud. Large droplets are more likely to contain ice nuclei and may supercool until nucleation occurs, then continue to cool, but more slowly. Minsk (1977) reviewed the freezing and supercooling of droplets in the free atmosphere. Supercooling in the range of -30°C to -40°C prior to freezing is to be expected for quiescent pure water droplets in the diameter range 40 to 120 μm. Brine droplets in a cloud of seaspray are not likely to supercool to this extent because air temperatures over the sea surface are typically not in the range of -30°C to -40°C and because droplet flight times may not be long enough to allow sufficient cooling. The violent mechanics of seaspray delivery, and the possible presence of ice nuclei in seawater probably also preclude it. Biological elements are common in seawater and may act as ice nucleators although no research has been found to confirm this. However, Martin (1981) reports that algae are commonly found attached to frazil ice in cold oceans.

Makkonen (1989) and Sackinger and Sackinger (1987) have hypothesized that nucleation of seaspray droplets occurs in-cloud. Masterson (1992) and Szilder et al. (1991) suggest that nucleated spray may be responsible for an observed increase in ice island building rate when seawater is sprayed into the air at temperatures below approximately -20°C. Droplets containing growing ice crystals evolve latent heat which keeps the droplet's temperature close to the equilibrium freezing temperature of the remaining brine. Since the droplet surface will then be at a higher temperature than if it

had supercooled, the overall heat transfer from the droplet to the air will be enhanced. This mechanism remains hypothetical but if it occurs, a low sea-surface temperature and a low air temperature would enhance it. In addition to droplet supercooling, snow and frazil ice in the sea surface may also initiate the nucleation of spray droplets.

The authors of previous vessel spray icing models have assumed that the spray will supercool. Borisenkov and Pchelko (1972) present a table of final temperature for brine droplets at impact with the ice surface as functions of initial temperature, air temperature and flight time. Other models of droplet heat transfer are also simple. Kachurin et al. (1974) and Stallabrass (1980) consider individual droplets travelling at constant speed over a fixed distance from spray source to icing surface. Other models account for the 3-D motion of single spray droplets over a vessel (Zakrzewski and Lozowski, 1987; Zakrzewski et al., 1993; Chung, 1995). Single droplet spray models do not account for the interaction of the airstream with an ensemble of droplets. Momentum transfer between an ensemble of droplets and the entrained air will result in increased droplet speed and decreased airspeed within the spray cloud. Heat transfer between the droplets and the air will result in decreased droplet temperature and increased air temperature in the spray cloud. Single droplet models assume that the velocity and temperature of the air is constant.

1.3.3 Vessel-specific factors

The design of an ocean-going vessel's superstructure and hull, as well as how it moves in a field of waves, can influence the production, collection and shedding of seaspray, and hence the ice accreted on the vessel. The three areas of design, dynamics and operation are treated separately below, beginning with vessel design.

1.3.3.1 Vessel design

Two aspects of vessel design are likely to influence icing. The first is hull shape, which influences the production of spray. The second is the superstructure design. The structure of the vessel's topside influences the airflow around the vessel, and thereby the

delivery of spray to the vessel's surfaces.

Minsk (1977) notes that ship geometry, including such characteristics as the freeboard and the amount of rigging and other ice-collecting surfaces above deck may alter the severity of icing. The investigation of cylinder icing suggests that small cylinders will experience greater thickness growth rates than large cylinders or flat plates (Minsk, 1977). This occurs because the heat flux from the surface of a cylindrical ice accretion increases with decreasing diameter. To reduce the ice load, exposed structures aboard vessels should be as large as possible while minimizing total surface area.

The British Shipbuilding Research Association carried out tests of a model vessel (BSRA, 1957) which were designed to show the influence of wind heading on icing severity. A scale model (1:12) of a steam trawler (1,115 ton displacement; 55 m length) was exposed to a freshwater spray while the air temperature was kept in the range -6°C to -10°C. The full-scale wind speed was in the range 23 ms^{-1} to 28 ms^{-1}. The loss in metacentric height[1] with a tripod mast was 2/3 of the loss with "normal" rigging for a particular ice load. Even though the weight of ice in each case was the same, the scale model suffered a diminished stability with the "normal" rigging. Therefore, the designer's choice of deck equipment may be important for the spray ice resistance of a vessel. With the wind to stern the model experienced heavy ice growth aft, with little forward of the bridge. With a wind 30° off the bow, there was an increased ice growth rate on the upper rigging, and the model capsized with less than half the ice load that caused it to capsize with head winds.

Kultashev et al. (1972) state that the direction of the vessel's course relative to the wind and waves may affect icing severity. As the wind comes around toward the beam (i.e. 15° to 45° off head winds) the spraying frequency increases, and then it decreases again with beam winds (90° to head winds). They reason that the increasing spray frequency will result in more spray reaching the vessel, and that this will lead to an increased icing severity for courses 15° to 45° off head winds. Sawada (1962) found

---

[1] A decreased metacentric height brings decreased static stability while negative values indicate a statically unstable vessel (Chung, 1995; p. 194-206).

that during sea trials, ice formed most readily on the foreparts of the vessel and that ice accumulations were larger with head winds than with winds astern. The greatest instability was found to occur with beam winds because the ice load was formed along one side of the vessel. Sawada (1962) concluded that the average vessel was in imminent danger of capsizing as the spray ice load approached 15% of the its displacement and that smaller vessels were more prone to capsize. Chung et al. (1995), using an icing model coupled to a dynamics model for the stern trawler "Zandberg" (1225 tonnes displacement), showed that, for winds 15° to starboard, it capsizes with an asymmetrical ice load of 10.2 tonnes, or 8.3% of its displacement.

An important consideration in vessel design is the size of the vessel, as indicated by its displacement. Small and medium-sized vessels are more prone to deteriorating dynamic stability as a result of ice accretion (Zakrzewski and Lozowski, 1991). Shellard (1974) states that spray icing is hazardous for vessels under 1000 tons (i.e. small and medium sized vessels), and that vessels over 10,000 tons are much more resistant to icing. The higher freeboard of larger vessels may cause a reduced spray flux and consequently reduced ice formation. Since larger vessels also have a greater load carrying capacity, a particular ice load is likely to have a diminished impact on the vessel's dynamic performance.

1.3.3.2 Vessel dynamic performance

Vessel motion is affected by the accumulation of ice, which reduces the freeboard, lowers the metacentric height and increases the moments of inertia. Ice deposited at elevations well above deck level may make a considerable contribution to the loss of stability, while simultaneously increasing the sail area of the vessel. This extra sail area increases the heeling moment exerted on the vessel by the wind. Typically for head seas, the ice load is heaviest around the bow. In beam seas the accretion is deposited chiefly along the windward side of the superstructure (Sawada, 1962; Jessup, 1985) producing an asymmetrical ice load. This can induce a considerable list (Chung et al., 1995).

Chung et al. (1995) have undertaken the first modelling of the effect of seaspray icing on the dynamic stability of a vessel. This model is reviewed in Section 1.5.1 below.

It consists of a spray icing model and a vessel dynamics model (Pawlowski and Bass, 1991). A case study of the MT "Zandberg", (length 53 m, beam 11.5 m, displacement 1225 tonnes) shows that asymmetrical ice loading with non-head winds, causes a simultaneous trim and list. Under head seas, the dynamics model predicted that the vessel would capsize after 2.8 hours despite the fact that it still exhibited static stability.

1.3.3.3 Vessel operation

Bardarson (1969) offers advice to skippers on how to operate under freezing spray icing conditions. Following seas (heading downwind) usually lead to a significant reduction in seaspray production. Following seas are defined as that course which sets the motion of the vessel in the same direction as the dominant waves of the seaway. In practise however, this tactic can only be used to reduce the spray icing rate when the mission of the vessel allows for it (Borisenkov and Panov, 1972). This tactic decreases the relative velocity between the vessel and the dominant waves, thereby reducing brine jet formation (at the stern). However, as the waves become larger, following seas become treacherous. The vessel eventually loses maneuverability under these conditions due to overrunning waves, and the tactic usually has to be abandoned (Shellard, 1974).

Beam seas are generally avoided. This orientation to wind and waves causes the vessel to roll excessively, especially as the seas become heavier. It is also a dangerous practice during spray icing events because of the possibility of asymmetric spray ice accretion which can deteriorate the vessel's dynamic performance (Zakrzewski et al., 1993). A common practise among skippers is to set the vessel to head seas, and to maintain course at low speed in order to wait out the adverse weather (Shellard, 1974). This tactic is likely to reduce the spraying intensity and frequency, while exposing a minimum profile to the spray. The size of the spray collision profile for a vessel is a function of the angle of approach of the relative wind. For example, part of the observed increase in icing for a vessel course 15° to 45° off head winds (Minsk, 1977) may be due to a geometrical increase in the spray collision profile of the vessel's topside structure. However, the increase in icing could also be due to other factors such as greater spray flux intensity or a greater extent of spray production along the vessel's perimeter.

In addition to the orientation of the vessel's course to the wind and waves, the vessel speed is important. The vessel icing model of Zakrzewski et al. (1993) shows an approximately quadratic increase in ice load with vessel speed. Shellard (1974) recommends a reduced vessel speed during severe spraying as a means of decreasing the rate of icing while seeking shelter.

The vessel spray icing problem offers significant operational challenges. Operational personnel often work with relatively simple principles in dealing with freezing spray conditions. For example, they may reduce the hazard due to freezing spray by setting a course for warm ocean currents, or by setting a course for the sea ice edge in order to benefit from wave damping. Experience can help, but the complexity of vessel icing remains. A greater knowledge of the physics involved will make decision-making for skippers ultimately more effective and certain.

1.4 Seaspray Ice Accretion

Once spray is generated by the vessel, entrainment by the wind usually results in the distribution of a portion of the spray onto the vessel's external surfaces. Section 1.4.1 deals with the collision of airborne seaspray with those surfaces. Section 1.4.2 looks at the processes at work on the icing surface. In Section 1.4.3, we consider the distribution of ice over the vessel.

1.4.1 Seaspray accretion

Langmuir and Blodgett (1946) developed equations for determining the total collision efficiency for droplets impinging on cylinders and spheres in an aerosol flow. These relationships were verified and improved upon by Lozowski et al. (1983) and Finstad et al. (1988), and show that total collision efficiency depends primarily on the speed of the free airstream, the diameter of the droplets and the diameter of the cylinder or sphere. Typical seaspray droplets (100 μm to 4.0 mm in diameter; Itagaki and Ryerson, 1990) will have a collision efficiency that depends on droplet size. Thus the

collision efficiency must be calculated as a weighted mean over a spectrum of droplet diameters. First, we consider smaller vessel structures by approximating their shape and size by a cylinder of diameter 2.5 cm. Fig. 1.4 consists of isopleths of total collision efficiency for a 2.5 cm diameter cylinder based on the equations of Lozowski et al. (1983) fit to the results of Langmuir and Blodgett (1946).

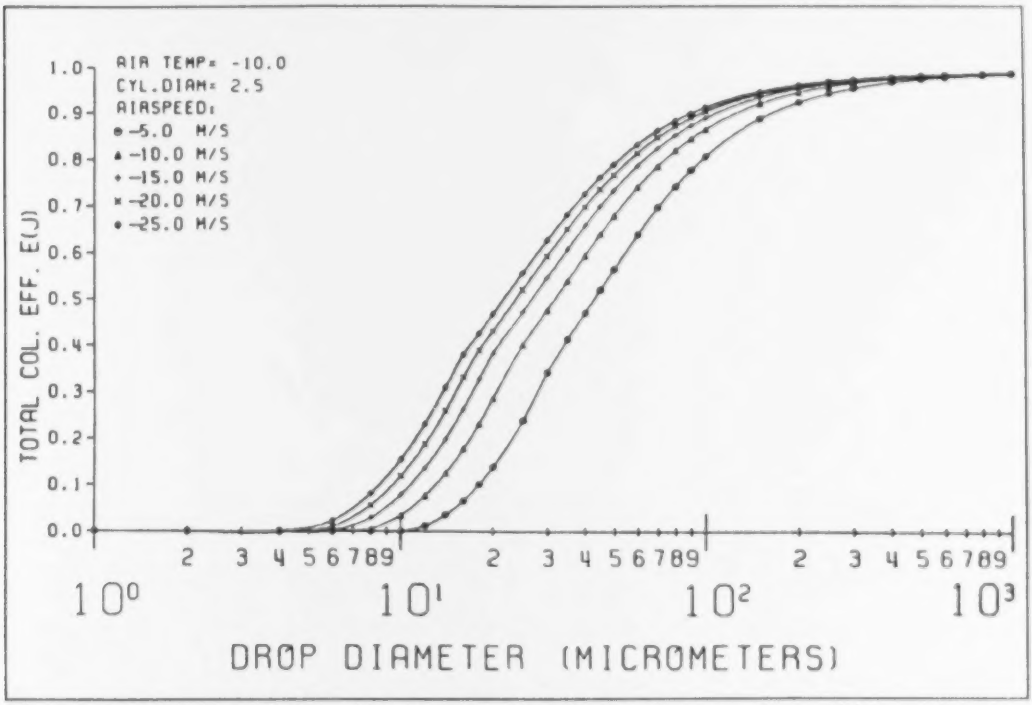

Figure 1.4 Total collision efficiency versus droplet diameter for a 2.5 cm diameter cylinder in an airstream at a temperature of -10°C.

Fig. 1.4 shows that for droplets in the diameter range 100 μm to 1 mm, the collision efficiency varies from 0.8 to 1.0, over a range of airspeeds typical of marine icing conditions. For droplets with diameters in the range 1.0 to 4.0 mm, the collision efficiency is close to unity. Therefore, a total collision efficiency of unity is likely to be a good first approximation for smaller vessel components. In order to consider larger vessel structures we use a cylinder 1 metre in diameter. In this case, Fig. 1.5 shows that for droplets in the diameter range 100 μm to 1 mm, the collision efficiency may vary widely from 0.05 to 0.9. Therefore, a weighted mean over the spectrum of droplet diameters may need to be used for larger vessel structures with seaspray droplets in the

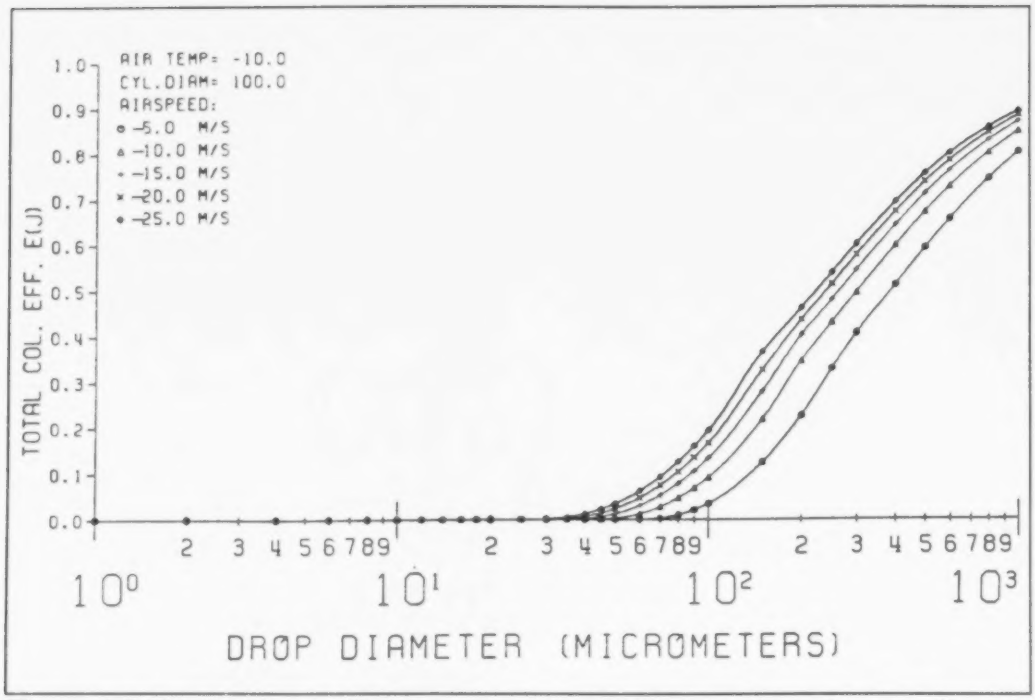

Figure 1.5 Total collision efficiency versus droplet diameter for a 1 metre diameter cylinder in an airstream at -10°C.

range of 100 μm to 1 mm for estimating the impinging spray flux. However, Fig. 1.5 also shows that spray droplets in the range 1.0 to 4.0 mm have collision efficiencies greater than 0.8 for airspeeds typical of marine icing conditions. Therefore, even recent vessel icing models do not account for the variation of seaspray droplet size in estimating collision efficiency, but generally assume a large droplet diameter (i.e. in the range of 1.0 to 4.0 mm) and a collision efficiency of unity (Zakrzewski et al., 1993; Chung et al., 1995).

The spray droplet collision efficiency analysis of Langmuir and Blodgett (1946), Lozowski et al. (1983), and Finstad et al. (1988) depends on a number of assumptions. The primary assumption is that the airflow may be modelled by potential flow. In addition, the droplets do not interact with each other, and their concentration is sufficiently small that they do not influence the flow. As well, they assume that the initial droplet velocity relative to the airstream is zero. Finally, the coalescence efficiency is assumed to be unity. Thus droplet bouncing, shearing or splashing, which might occur

on the wet icing surfaces of a vessel are ignored.

The collision of seaspray with an icing surface could be very different from the above idealization. A spectrum of droplet sizes may develop differing relative airspeeds leading to the possibility of droplet interaction within the seaspray cloud. Turbulence may also enhance droplet interactions.

During the formation of spray droplets from the brine jet, the airspeed relative to the brine will be at its maximum. The droplets will then accelerate as a result of the drag exerted on them by the airstream. Large droplets travelling short distances before impact may not reach dynamical equilibrium with the airstream. Because of such outstanding problems, a collision efficiency of unity and a monodisperse droplet spectrum will have to serve as working assumptions until more realistic spray cloud and droplet collision models are devised. These assumptions are used in recent vessel spray icing models (Blackmore et al., 1989; Zakrzewski et al., 1993; Chung et al., 1995).

1.4.2 Seaspray ice growth

BSRA (1957) reported that air temperatures close to the freezing point coupled with large fluxes of cold spray result in "glaze" ice. This type of ice is dangerous due to its high density and high adhesive strength. If less spray is collected at a lower temperature, a less dangerous "rime" ice formation occurs with a characteristic porous structure. Although the spray icing literature since the BSRA (1957) report does not place any emphasis on the possibility of a seaspray rime icing mode, it does not seem prudent to neglect the possibility entirely. Subsequent soaking of porous rime by unfrozen brine under higher spray fluxes could lead to a very rapid increase in ice load.

Hayhoe (1989) subjected a scale model of an offshore supply vessel (1:100 scale) to a freshwater rime icing spray in a closed-circuit wind tunnel. He measured a maximum increase of 100% in the wind drag (and rolling moment) on the severely iced versus the uniced scale model. The aerodynamic forces and moments exerted on the model by the airstream were measured with a piezoelectric crystal balance. Hayhoe (1989) suggests that increased aerodynamic loading of vessels, coupled with severe ice loading is likely

to reduce the vessel's stability.

Porous seaspray ice accretion could perhaps soak up impinging brine without the need for it to freeze. If large quantities of seaspray were quickly absorbed by a porous ice matrix, asymmetrical vessel loadings might be generated from asymmetrical spray delivery. Even with symmetric spray delivery, the vessel would experience a sudden and substantial increase in load.

Pflaum (1984) has shown that many of the characteristics of natural hailstones are reproduced in wind tunnel experiments when low density riming is followed by wet growth soaking. If porous growth occurs in seaspray icing, brine absorption and subsequent freezing could be as important for vessel icing as it is for hailstone growth.

Ryerson (1993) has attributed part of the difference in the measured deposit density of spray ice between vertically and horizontally oriented surfaces to brine drainage. Seaspray ice accretion, drained of much of its interstitial brine, might provide an opportunity for a rapid increase in loading when spraying resumes.

The spray icing surfaces on vessels are generally assumed to be in the wet icing regime, even though Makkonen (1984a) and Jessup (1985) suggests that different types of icing may occur on a vessel, depending on the location, shape, and size of the icing surface. Wet icing occurs when more liquid collides with the icing surface than can be solidified and incorporated into the spongy ice matrix. The excess brine is shed. The wind speed influences ice growth through both convective heat transfer and spray flux. Convective heat transfer depends on wind speed (i.e. $\sim V^{0.5}$) for many different configurations (flat plates, cylinders, spheres; Incropera and DeWitt, 1990). The transfer of heat away from the icing surface increases with increasing wind speed, thereby increasing the icing rate. As this occurs, the impinging seaspray flux also increases (assuming a constant liquid water content, and a constant collision efficiency). Glukhov (1971) shows that at low wind speeds, the heat loss from the icing surface to the airstream increases more rapidly with wind speed than the sensible heat gain from the impinging spray. For this reason, he suggests that the icing rate increases with wind speed. However, the performance of the freshwater cylinder icing model of Lozowski et al. (1995) suggests that spray temperature as well as the liquid water content must be

accounted for specifically before an icing rate tendency can be predicted.

The glaze ice accretion model of Lozowski et al. (1995) predicts that the icing mass flux may decrease or increase with increasing liquid water content depending upon the spray temperature (Fig. 1.6). The model predicts that for cold spray (T_d=T_a=-15°C) the icing flux increases with increasing liquid water content. This occurs because the sensible heat loss at the model icing surface that warms the impinging cold spray is responsible for an increased icing mass flux. However, as the spray temperature rises, the slope of the icing flux in the "wet" glaze growth model diminishes and becomes zero (a constant icing flux) when the spray is at the freezing point. For warm spray (above the freezing point), the slope is negative, and ice growth is suppressed completely for a spray temperature, T_d=5°C, above a liquid water content of about 15 gm^{-3}. Fig. 1.6 suggests an anti-icing technique in which a sufficiently large continuous spray flux from the sea with negligible cooling might suppress or eliminate ice growth (Lozowski et al., 1995). Fig. 1.6 also shows that the cylinder icing model of Lozowski et al. (1995) predicts a transition to rime icing at low liquid water content. In their model's rime icing mode, all impinging liquid is accreted, giving rise to the large positive slope near 0 gm^{-3}.

If unfrozen liquid is not incorporated by a growing ice accretion, it will give rise to a shedding flow on an inclined icing surface or an icing surface subject to shear stresses and pressure gradients induced by the wind. The unfrozen brine will exhibit an increased salinity due to rejection of salt from the growing ice matrix. A surficial growth instability, driven by the supercooling (and constitutional supercooling) of the brine film on the icing surface, causes crystal growth that traps brine interdendritically in the spray ice matrix. Minsk (1977) suggests that this interstitial brine reduces the effective structural cross-section of the ice and thereby the strength of the ice.

Seaspray ice on vertical surfaces usually increases in thickness downwards (Minsk, 1977). Minsk (1977) suggests that the excess brine drains down the icing surface achieving higher salinity as it descends. Chung and Lozowski (1990) observed and modelled this increase in salinity in the growth of marine icicles. Thus brine inclusions near the bottom of an icing surface may be expected to have increased salinity along with the surficial brine. Blackmore et al. (1989) present a model of the seaspray icing of a

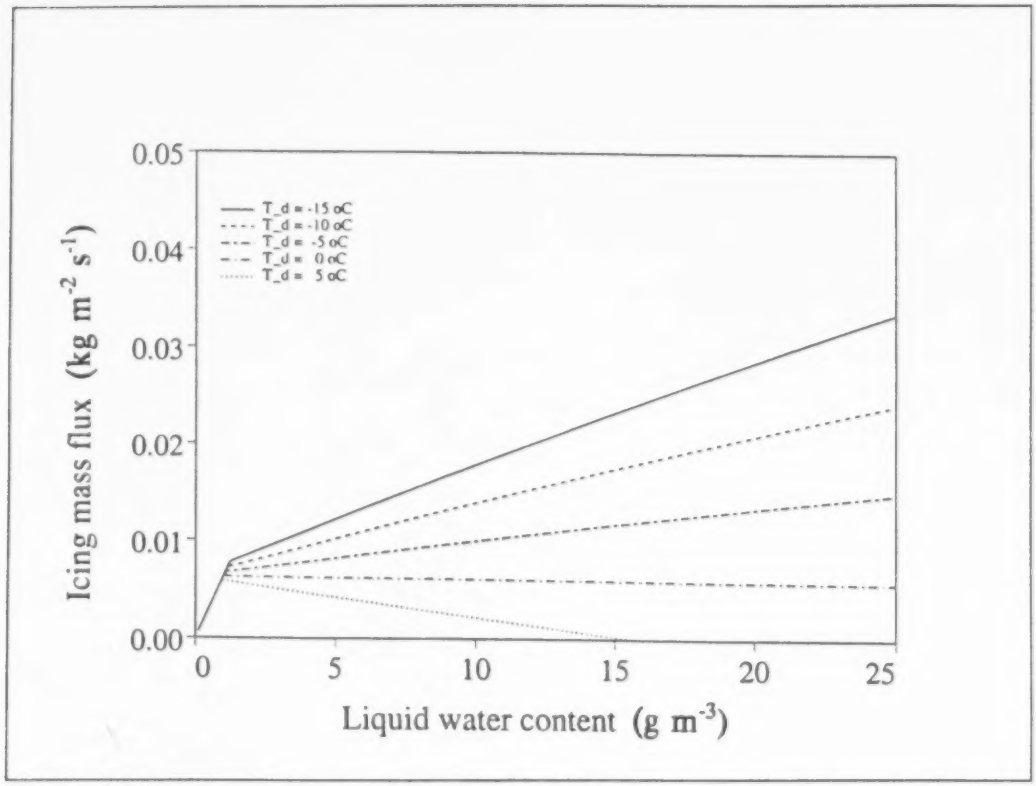

Figure 1.6 Icing mass flux as a function of liquid water content for a range of spray temperatures, T_d, and for T_a=-15°C, V=20 ms^{-1}, and D=0.05 m. (adapted from Lozowski et al., 1995)

ship's mast, which also exhibits this tendency. In the model, they assume that the salinity of the brine incorporated into the ice accretion is the same as that of the surficial brine.

Traditionally, a heat balance equation is used to predict the growth of spray ice. Makkonen (1987), for example, uses a heat balance equation to model the growth of saline spongy ice on a cylinder. This model will be reviewed in detail in Section 1.5.2.1. The heat balance includes convective heat transfer, evaporative heat transfer, viscous heating, sensible heat transfer due to the impinging liquid, and radiative longwave heat transfer from the icing surface. An analogy between the salt entrapment in sea ice growth and that in seaspray icing is used, along with an analogy between sponginess of freshwater icing and the sponginess of seaspray icing, to produce a model that predicts seaspray ice sponginess. The presence of salt in the spray has two principal effects. The

first is to reduce the temperature of the liquid film to the equilibrium freezing temperature of the surficial brine from the 0°C value usually assumed in freshwater icing models. The second is to influence the vapour pressure and hence the evaporative heat loss from the surficial brine. Makkonen assumes that the entrapped interstitial brine has the same salinity as the surficial brine. Analysis of Makkonen's model suggests that a useful estimate of the sponginess of a saline accretion is 0.26. On the other hand, Zakrzewski and Lozowski (1987) use empirical formulations for the vertical distribution of sponginess and salinity of the accretion on a vertical surface in combination with a heat balance equation, to solve for the ice mass accretion rate on a Soviet MFV.

Traditional heat balance approaches to icing rate prediction usually ignore temperature gradients in the surficial liquid film that are normal to the icing surface and usually do not specify or account for a surficial structure. An exception is the modelling of the effect of surface roughness on the heat transfer coefficient by Makkonen (1984b).

Detailed modelling of the growth of spongy ice with a well-defined structure is very recent. Consequently, the review of vessel icing models, that will be presented in Section 1.5.1, will describe only models which employ a traditional heat balance as their central physical concept. The heuristic vessel icing model presented in Chapter 2 also uses a heat balance equation to predict overall vessel icing. Section 1.5.2 gives a detailed review of two recent approaches to the modelling of spongy spray ice growth. This review provides the context for the freshwater spongy ice growth model of Chapter 3.

1.4.3 Seaspray ice distribution on vessels

The flux of seaspray which impinges on a vessel's surface is a function of the spray flux near the spray's source and the distance from the source. If the spray flux intensity is small, the airstream will lose little momentum to the spray, and the spray trajectories will be relatively long. If the spray flux intensity is large, the airstream will be slowed by the drag on the droplets, and the spray trajectories will be shorter. Zakrzewski (1987) shows that the liquid water content (Eqn. 1.1) and the spray flux decreases rapidly with height over the deck of a Soviet MFV. Therefore, trajectories at

low height over the deck are likely to be shorter than trajectories at higher elevation. In addition, larger droplets with large terminal fall speeds are likely to follow gravitational trajectories more closely than are smaller droplets, and will therefore impinge on the vessel nearer the spray source. Borisenkov and Panov (1972) proposes that large liquid water contents tend to occur with large model droplet diameters in collision-generated seaspray. If high liquid water contents occur with larger droplets, their shorter trajectories will bring larger fluxes to surfaces of the vessel nearer the spray source. Once the formation of the brine jet at the vessel's hull and the subsequent formation of the airborne seaspray droplets of the spray cloud is more completely understood, the influence of spray flux intensity will be more readily included in spray trajectory analysis over a vessel. Following this reasoning, the spray flux is expected to decline with distance from the spray origin. The effect of spray flux has not yet been considered in the modelling of spray trajectories over a vessel.

Even though the intensity of the spray flux has not been taken into account in the modelling of spray aerodynamics, models to predict the spray flux distribution over vessels have been produced, (Zakrzewski et al. (1993) and Chung et al. (1995)). However, they employ only single droplet trajectory modelling. Such models still require a number of assumptions. For example, the spray droplet source region must be specified along with the initial droplet velocity, droplet diameter, and the airflow around the vessel.

The distribution of seaspray and the resulting spray ice distribution over the vessel is important to the vessel's operation. The effect of the ice load on vessel stability is not a simple matter to estimate (Chung et al., 1995). An asymmetric (port-starboard) distribution will produce list and deteriorate the vessel's dynamic performance (Chung et al., 1995). With head winds and seas, maximum ice growth is likely to occur on a vessel's bow. Under severe icing conditions in the Baltic Sea, the Soviet MFV "Piarnu" accreted a maximum ice thickness of 50 cm at its bow with decreasing thickness toward the wheelhouse and with height up the rigging and superstructure (Rybnikov, 1975). Hayhoe (1991) also shows a similar ice thickness tendency for scale-model icing tests. Allen (1881) reports that the mail steamer "Phoenix" (450 tonnes displacement) accreted enough ice on the forecastle that the trim at the bow decreased and the propeller was

almost out of the water. With the rudder and propeller even partially out of the water, a vessel is not likely to be able to maintain its course. For many years, the vertical distribution of the ice load has been believed to degrade vessel stability (BSRA, 1957). The scale model experiments of Hayhoe (1989) and the numerical modelling of Chung (1995) confirm this.

The operations aboard a vessel may be affected by the ice distribution as well. For example, icing may allow work to go ahead as usual or it may put a stop to work due to slippery and treacherous decks or due to equipment that will not function under a layer of accreted ice. Ice at specific locations may also affect safety equipment and communications equipment. Frozen up scuppers may prevent spray brine and green water drainage. The resulting accumulation of brine will further reduce the vessel's stability and increase the operational hazard aboard the vessel. A better ability to predict the distribution of ice accretion on vessels should result in a greater capability to design more functional ice-free work areas.

The distribution of ice accretion on a vessel will also be a function of its ability to first nucleate on a surface and then to adhere to the surface. This idea lies behind the search for ice-phobic surfaces. The initiation of spray ice growth on metal surfaces requires an air temperature of -3°C or less (Minsk, 1977). The ice appears to have a loose bond with the metal surface initially, but the strength of adhesion rapidly increases to a maximum in 1.5 to 2 hours.

Makkonen (1984a) states that for atmospheric ice on sea structures, adhesive failure is the most likely mode in which is ice lost. In this mode, it is a very thin layer of ice near the substrate that is relevant to the failure. He also suggests that the initially deposited layer of ice is often formed nearer the wet growth limit than is most of the rest of the deposit which may typically form by rime accretion. Therefore, it is likely that atmospheric ice will adhere to a substrate with a strength proportional to the ice fraction of the initial accretion where the initial accretion grew spongy. Sponginess may also reduce the adhesive strength of marine spray ice, and for this reason, the modelling of sponginess could be important to the future prediction of the adhesive strength of marine ice.

The initiation of spray icing appears to be hampered by wooden decks (Kliuchnikova, 1971). A slush seems to form which is readily flushed away by greenwater on the deck. It may be that the type of paint or varnish applied to the wood is important (Stallabrass, 1980).

Borisenkov and Pchelko (1972) reported that under headwinds and seas the bow accretes ice while other parts of a Soviet MFV further aft, may have slight or no icing at an air temperature close to -3°C with low wind speeds (7-10 ms^{-1}). They indicate that for wind speeds up to 25 ms^{-1} the ice accretion generally occurs on the forward half of a Soviet MFV. Under these circumstances, the drag force exerted on the spray by the wind is not sufficient to deliver spray to all parts of the vessel. Reduced spray near the stern is to be expected as a result of the interception of spray by the superstructure in the case of head winds and seas. With increased wind speed, and decreasing air and spray temperatures, more of the vessel is likely to be covered with spray and ice (Minsk, 1977); however, the stern of the vessel is typically not iced even when the heading is downwind. This is probably because the vessel is steaming in the same direction as the waves, thereby reducing the intensity of vessel/wave interaction, and the resultant spray flux. A shadowing effect also occurs under beams seas and winds. In this case, ice is prone to grow on the windward side of the superstructure with less ice accreted on the leeward side (Sawada, 1962).

Minsk (1977) cites investigations of spray icing on the Soviet MFV "Professor Somov" in which the distribution of ice was observed to have a substantial variation over the vessel. For example, horizontal surfaces had a variation in the percentage of total ice loading of 30% to 70% while vertical surfaces had a variation of 15% to 40%. The ice accretion on complex horizontal and vertical surfaces (e.g. instruments and equipment) showed a variation of 5% to 30% while simpler cylindrical objects (e.g. masts, spars, and rigging) showed a variation of 0% to 30%. Based on spray icing measurements aboard the large U.S. Coast Guard Cutter, MIDGETT, Ryerson (1993) found that, on average, vertical surfaces accreted only 71% as much ice mass as horizontal surfaces. Ryerson (1993) also reports that ice growth and ice ablation may occur simultaneously at different locations on a vessel. Fig. 1.7 shows the rather considerable variation in ice accretion

thickness that can occur on a vessel's superstructure.

1.5 Modelling Vessel Spray Icing

The modelling of vessel spray icing has two practical purposes. The first purpose is to develop engineering approaches to anti-icing and de-icing. A second purpose is to enhance the understanding of vessel spray icing physics. This understanding can then be used to improve the forecasts of freezing spray conditions. An accurate forecast of the onset and severity of a freezing spray episode would be helpful in vessel operations and ocean routing, and should help to reduce the inconvenience and danger of spray icing.

1.5.1 Vessel icing models

Various models to predict vessel spray icing have been developed over the years, including those of Kachurin et al. (1974), Stallabrass (1980), Overland et al. (1986), Zakrzewski and Lozowski (1987), Horjen and Carstens (1989), Blackmore et al. (1989), Zakrzewski et al. (1993), and Chung et al. (1995).

Most spray icing algorithms may be categorized as either (1) statistical models, (2) statistical-physical models, or (3) physical-empirical models. Statistical models do not account for the physics of vessel spray icing except insofar as the wise choice of input parameters is a matter of physics. These statistical models are based on correlations between the input parameters and vessel icing data.

Like statistical models, statistical-physical models depend on the assumption that the forecast situations will differ little from comparable events in the data set. However, statistical-physical models depend on a physical submodel around which the statistics have been organized. This is done to capture more of the physics involved, with the expectation that this will produce a better predictor of icing. The physical submodels used in these statistical-physical models have been surprisingly complex in some cases, (Kachurin et al., 1974) with little evidence to demonstrate that such complexity is essential to model performance.

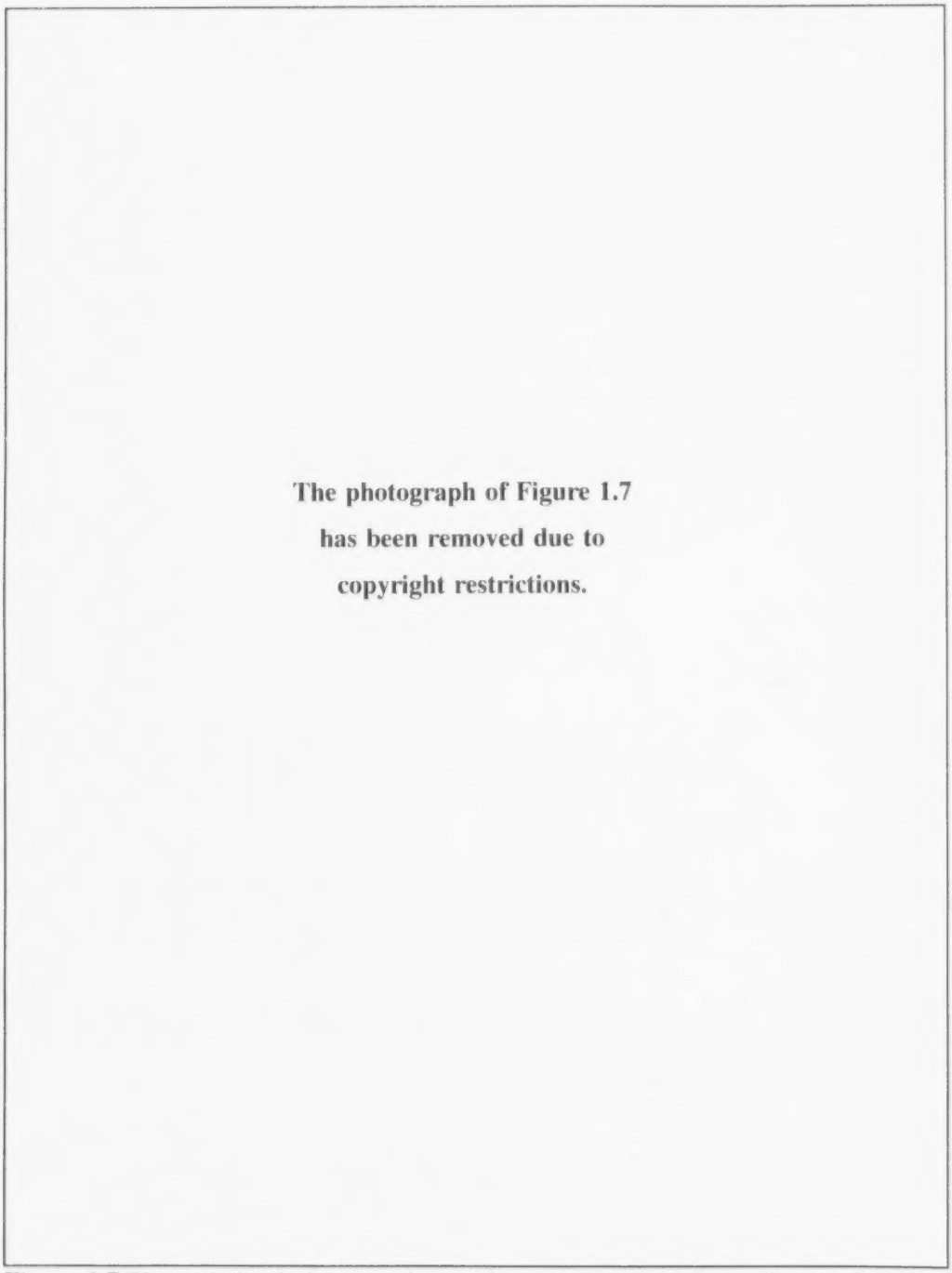

Figure 1.7 The variation in ice accretion on the superstructure of an unknown Canadian warship during the Second World War. No Canadian ships were lost to spray icing during the war years. (courtesy of the Naval Museum of Alberta)

Physical-empirical models are more recent. This type of model is structured in such a way as to account more completely for the physical processes of vessel icing. The physical-empirical model may have no statistical dependence on vessel icing data. However, this type of model is likely to include submodels which do have some empirical dependence. For example, a submodel of spray distribution may be used which has empirical dependence on spray data. In this case, the modeller may represent some of the processes of vessel spray icing more explicitly, but may need to invoke a proliferation of submodel assumptions, thereby ending with as much or more empirical dependence as in the statistical-physical models.

The Kachurin et al. (1974) model is an example of a statistical-physical model. It predicts ice loading rates for a Soviet medium-sized fishing vessel by means of a statistical correlation. The physical portion of the model simulates ice growth on a cylinder. The ice load on a ship is then determined via a statistical relationship between cylinder ice thickness and total ship load derived from a ship icing data set. The user must have confidence that this correlation will not change between icing events in the original data set and those events for which he will have forecasting responsibility.

More complicated physical-empirical models (Zakrzewski and Lozowksi, 1987; Blackmore et al., 1989; Zakrzewski et al., 1993; Chung, 1995) are not certain to perform better than simpler statistical models. More complex models like these exhibit greater modelling detail and flexibility by virtue of having more submodels to describe the details of the vessel icing process. However, the considerable number of processes to be taken into account forces increased prudence in the choice of what to simulate and how to do it. This may in the end result in as much empirical dependence within the submodels as the simple statistical models have on their data sets. In fact, unimportant processes may acquire an undue importance, with a resulting sensitivity to irrelevant physical parameters. Thus a physical-empirical model requires insight into which of the vessel spray icing processes to model, which to disregard, and how to do the actual modelling without excessive empirical dependence.

Aside from the choice of input parameters, statistical models such as Sawada (1967), Mertins (1968) and Wise and Comiskey (1980) have little dependence on the

physics of vessel icing. Statistical-physical models such as Borisenkov and Pchelko (1972), Kachurin et al. (1974), Stallabrass (1980), and Overland et al. (1986), and physical-empirical models such as Zakrzewski and Lozowski (1987), Horjen and Carstens (1989), Zakrzewski et al. (1993) and Chung (1995), all employ an icing surface heat balance equation to predict the rate of ice growth. The vessel icing models of Kachurin et al. (1974) and Chung (1995) are reviewed in some detail below as examples of a statistical-physical model and of a physical-empirical model, respectively. This review is meant to give a sense of the context in which the heuristic modelling of Chapter 2 was performed.

1.5.1.1. The Kachurin et al. (1974) model

Kachurin et al. (1974) regarded a purely theoretical approach to vessel spray icing prediction as both unsuitable and unpromising due to the complexity of vessel icing. The complexity of both the vessel's structure and that of the spray cloud are offered as examples. Kachurin et al. (1974) also eschewed the statistical modelling approach used in making the first maps of vessel icing probability (Shektman, 1968) with the observation that to obtain sufficiently high statistical validity, it would be necessary to conduct an enormous number of observations. However, he thought that a correlation might be sought between vessel icing severity under observed hydrometeorological conditions and a simple theoretical icing model. The theoretical model is for a cylinder, 50 cm in diameter, oriented horizontally and transverse to the spray-laden airflow.

The hydrometeorological conditions from the vessel icing data were used as inputs for the cylinder icing model. Kachurin et al. (1974) carried out a statistical correlation between the observed icing rates (tonnes hr^{-1}) on an entire ship, and the ice growth rates (cm hr^{-1}) calculated with the theoretical cylinder icing model. For an icing data set limited to cases with winds no more than 40° off head winds, a correlation coefficient of $r=0.96\pm0.02$ was achieved. The resulting model gives an estimate of maximum icing rates for small displacement fishing boats. This proviso is given because much of the calibrating data were taken on Soviet medium-sized fishing vessels (40 m length; 450 tonnes displacement).

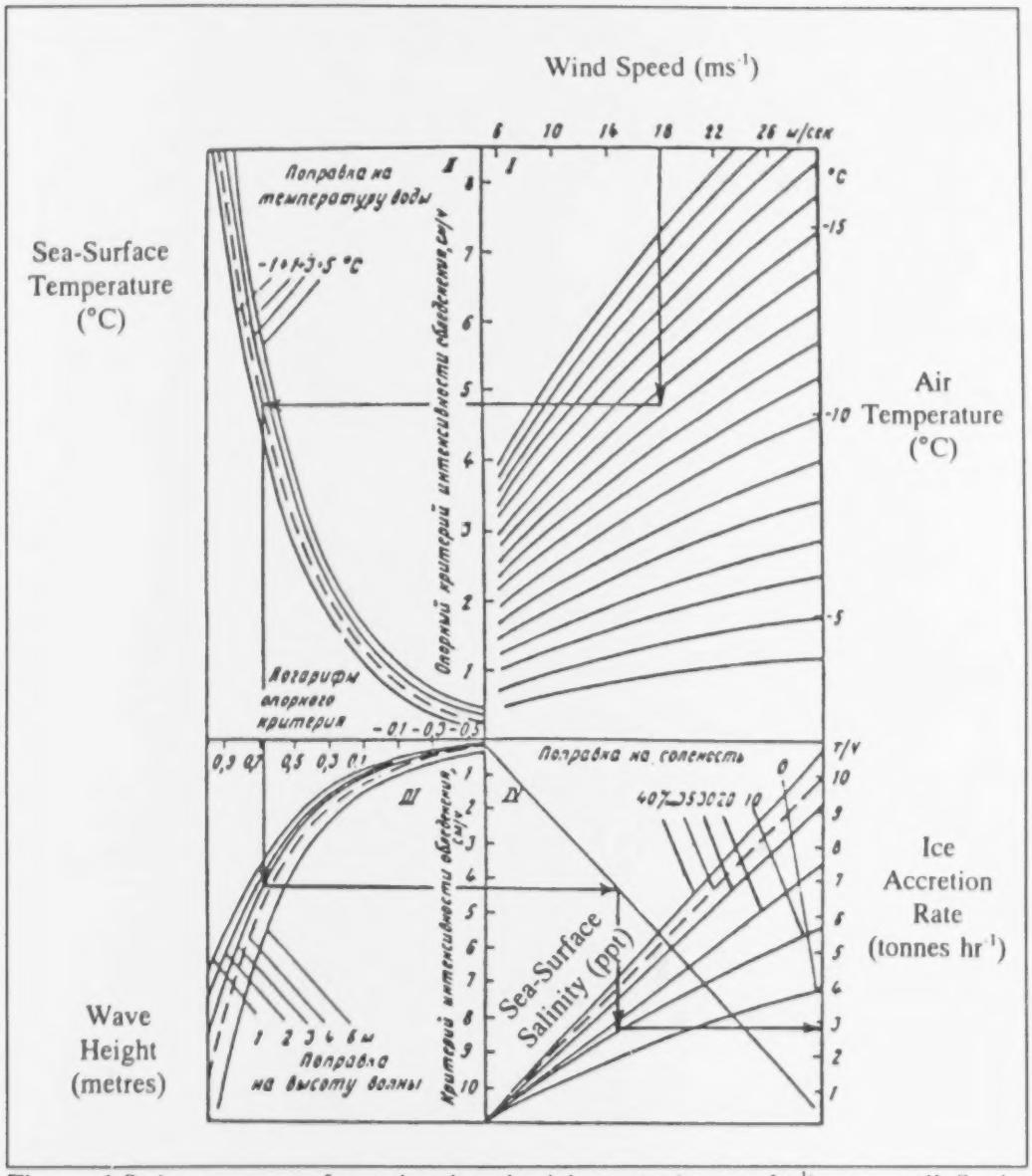

Figure 1.8 A nomogram for estimating the icing rate (tonnes hr^{-1}), on small Soviet fishing vessels (adapted from Kachurin et al., 1974).

Kachurin et al. (1974) reduced their findings into the form of a nomogram in order to make the model readily available to those needing vessel icing estimates. This nomogram is shown in Fig. 1.8. An example of how to use the nomogram (Jessup, 1985) is shown using the arrows in Fig. 1.8. Beginning with a wind speed of 18 ms^{-1}, isopleths

of air temperature -13.5°C, sea-surface temperature +1.0°C, significant wave height 3 m, and sea-surface salinity 15 ppt are followed to arrive at an icing rate of approximately 2.8 tonnes hr^{-1}.

A summary of the physical assumptions and concepts of the Kachurin et al. (1974) model are provided below:

1) The accretion of ice on the cylinder is axisymmetric. Ice sponginess is ignored.

2) The processes of brine collision and shedding are continuous without the complication of intermittent spraying and its influence on shedding. The ice growth rate is steady, and in the wet growth regime.

3) The spray droplets are 2 mm in diameter and are assumed to have a collision efficiency of 1.0. Kachurin et al. (1974) state that the effect of droplet temperature on the calculated icing rate is relatively small. Nevertheless, a model of the motion and cooling of a single droplet is used with a 10 m trajectory to calculate the spray impingement temperature.

4) Any conductive heat loss from the accretion to the cylindrical substrate is neglected. The liquid film on the icing surface is assumed to be well-mixed. Jessup (1985) states that the model is capable of accounting for salt diffusion at the icing interface but that this capability is not used.

5) The conductive heat transfer through the surface liquid film is accounted for in the heat balance, along with convective and evaporative heat loss to the airstream, sensible heat transfer due to spray impingement, and the evolution of latent heat at the icing surface.

6) The thickness of the liquid film is assumed to be constant.

7) The wind speed, air temperature, sea-surface temperature and sea-surface salinity are input parameters in the cylinder icing model. The sea-surface temperature is used as the initial droplet temperature in the droplet cooling model.

8) The wave height (required by the nomogram of Fig. 1.8) is used to estimate the liquid water content for the cylinder icing model. Kachurin et al. (1974) state that wave height is the chief factor governing the liquid water content of the cloud that impinges on the vessel. They give a linear equation for liquid water content where $q=\xi H_s$,

H_s is the wave height, and $\xi=10^{-3}$ kgm^{-4}. This equation is based on observations by L.I. Gashin during the sixth Atlantic expedition of the Soviet MFV "Aysberg" for sailing speeds of 6-8 kt (3-4 ms^{-1}), and for winds no more than 40° off head winds.

Brown and Roebber (1985) have reviewed this model, and note that the numerical values of the theoretical cylinder icing rate (cm hr^{-1}), and the observed vessel icing rates (tonnes hr^{-1}) have a ratio of 1:1, with a surprisingly low degree of scatter. They found that the nomogram overpredicts the icing rates in a Canadian trawler icing data set by a factor of 3. This may not be as inconsistent as it appears since Kachurin et al. (1974) give the proviso that the nomogram provides a maximum icing rate for small displacement fishing vessels.

The Kachurin et al. (1974) model has two salient characteristics. The first is that a traditional heat balance equation forms the core of the model. The second is that oceanographic, hydrodynamic, and spray formation and delivery considerations are all compressed into the liquid water content equation, $q=\xi H_s$. This stands in significant contrast to the detailed and extensive effort expended in producing the cylinder icing model itself. Kachurin et al. (1974) offer no justification for this modelling emphasis, relying rather on the intuitive similarity between the icing physics of a cylinder and that of an entire ship.

1.5.1.2 The Chung et al. (1995) model

Chung (1995), and Chung et al. (1995) set out to model the accretion of ice and its distribution over a vessel, with the intention of examining its influence on the dynamic performance. The MT "Zandberg", a stern trawler, was idealized using a finite panel geometry model. A seaspray icing model was produced for the topside, and a dynamic model was used to predict the vessel's motions in a wave field while loaded with spray ice. Chung (1995) embraced many of the physical-empirical modelling methods and assumptions that had been developed and presented by Zakrzewski et al. (1993). Unlike the Kachurin et al. (1974) model, Chung's work was not intended to result in a forecasting algorithm.

Chung (1995) represented the Zandberg's ice collecting surface by flat plates, one for the foredeck, one for the forward face of the wheelhouse, and one for the top of the wheelhouse. The vessel's mast was represented by a cylinder standing atop the wheelhouse. These surfaces were subdivided into grid cells, each of an area less than 1 m^2. The distribution of the spray and ice accretion over the vessel is determined by calculating the spray flux and ice load for each grid cell.

Chung (1995) used an empirical spray flux formulation developed from data. The data were measured in experiments with a scale model (1:13.43) of the MT "Zandberg". It was self-propelled through head seas in the clearwater wave tank at the Institute for Marine Dynamics, NRCC, in St. John's, Newfoundland. Since these scale model tests did not include the effect of wind drag on the spray, wind drag in the full-scale model is introduced by numerical simulation of a 1.75 mm diameter spray droplet trajectory in a uniform wind field. This trajectory calculation, and the empirical spray flux calculation is carried out for each grid cell.

The spraying model predicts spray impingement with an assumed collision efficiency of unity. It also models the thermal evolution of a single droplet. The spray impingement temperature at input is needed in order to determine the sensible heat term in the local heat balance equation.

The following points provide an overview of the model, corresponding to the eight points in the overview of the Kachurin et al. (1974) algorithm in Section 1.5.1.1:

1) The spray and ice are distributed over an idealized geometrical approximation to the superstructure of the MT "Zandberg". The spongy accretion is taken to have a constant liquid fraction of 0.26 (Makkonen, 1987).

2) The processes of brine collision and shedding, and the growth of ice, are modelled taking into account spray intermittency. The spray delivery cycle consists of an interval of "spray-on" followed by "spray-off" conditions. The icing surface is assumed to be in the wet icing mode. Consequently, the model has the ability to account for the shedding of excess brine from a grid cell. In the model, shedding occurs only to the grid cell immediately below, on the vertical surfaces of the wheelhouse and the mast. The surficial liquid is modelled as a falling laminar film whose thickness is computed.

On horizontal surfaces there is no physical shedding mechanism and the film is considered to be stationary with a maximum thickness of 1mm. Unfrozen brine in excess of this thickness simply vanishes.

3) The spraying is assumed to have a constant duration of 3.5 seconds. The interval between sprays is estimated using the formula of Panov (1971) for Soviet medium-sized fishing vessels. A time step of one second was selected for the icing calculation, and this time step is applied during both the "spray-on" and the "spray-off" portions of the spraying cycle. The total ice mass is assumed to be proportional to the number of spray cycles in the icing event. While ice accretes during the spraying cycle, there may be a film of excess brine left on the ice surface at the end of the cycle. The effect of this residual brine is not easy to include in the model without having to calculate over the entire time series of cycles in the icing episode. In order to avoid this, Chung (1995) followed Zakrzewski et al. (1993), by ignoring any liquid left on the icing surface at the end (and similarly at the beginning) of a spray cycle.

4) Conductive heat loss to the substrate is neglected in the Chung (1995) model. As in Kachurin et al. (1974), the transport of salt in the liquid film normal to the icing surface is neglected, although salinity effects in the liquid film have been included. The effect of salinity on the equilibrium freezing temperature, vapour pressure, brine viscosity and specific heat is included in modelling the liquid film.

5) Conductive heat transfer through the surficial brine film is not included explicitly in Chung's model. Rather, it follows the traditional surface heat balance approach. The conventional heat balance includes the convective, evaporative, radiative, sensible and latent heat terms.

6) The thickness of the liquid film in the Chung (1995) model is computed but it is limited to a maximum thickness of 1 mm. The surfaces are taken as planar, with no curvature effects accounted for in the case of the mast.

7) Air temperature, relative humidity, sea-surface temperature, wind speed, fetch, wind direction relative to the vessel, vessel speed, and sea-surface salinity are the input parameters of the model.

8) The Kachurin et al. (1974) model uses the observed significant wave height, H_s, as an input parameter for the nomogram. Chung (1995) used wind speed and fetch and the fully-developed deep ocean wave model of Bretschneider (1973) to estimate the significant wave height, H_s, for the spraying model. The spraying model used by Chung (1995) is based on scale-model testing with the Zandberg hull. These experiments suggest that spraying intensity is proportional to vessel speed to the third power, and significant wave height to the seventh power. The range of full-scale significant wave height that is valid for use in the model is 2 to 5 m. The range of full-scale vessel speed for which the model is valid is 2.5 to 8 ms^{-1}. Unlike Kachurin et al. (1974), the spraying empiricism is not limited to a vessel speed of 6-8 knots (3-4 ms^{-1}) but like Kachurin et al. (1974) it is limited to vessel headings close to head seas. This is because the scale model was tested under head seas only. However, the direction of the wind relative to the vessel may be varied, permitting an azimuthal variation in seaspray delivery and ice accretion over the vessel. The spraying model used by Chung (1995) treats intermittent spray while the Kachurin et al. (1974) model assumes continuous spray.

Chung (1995) used the physical-empirical modelling approach. He used empirical submodels within a physical framework to produce the overall vessel icing model. Kachurin et al. (1974) used a statistical-physical approach, based on a statistical correlation between their cylinder icing model and a vessel icing data set. Chung (1995) modelled the spraying process and the spray ice distribution whereas Kachurin does not. However, the lack of reliable local heat transfer coefficients over the surface of the vessel may offset the gain of modelling the superstructure with greater geometrical verisimilitude than Kachurin et al. (1974). The continuous spray icing model of Kachurin et al. (1974) sidesteps a considerable number of difficult intermittent spray icing problems. However, it is not certain whether this simplification leads to enhanced predictive capability.

Over the long term, a physical-empirical approach such as that used by Chung (1995) must be taken in order to examine the relative importance of the various vessel icing subprocesses, and the influence of their modelling assumptions. In this way, the processes of spray generation and ice growth may eventually become more completely

understood, so that more accurate models will follow. However, better data sets will be required in the future in order to perform more reliable model validation.

For all their differences, the Kachurin et al. (1974) model and the Chung (1995) model are similar in three ways:

1) A traditional heat balance equation is at the core of both models.

2) The modelling of spray generation in both models is empirical, with little theoretical basis, even though the empiricism used by Chung (1995) has a substantial experimental basis.

3) The ice accretion sponginess is modelled by assuming a constant liquid mass fraction for the accretion. Kachurin et al. (1974) assumed a liquid fraction of 0.0, and Chung (1995) assumes a liquid fraction of 0.26.

The third point shows the rather naive way in which the ice accretion sponginess has been modelled heretofore. Chapter 3 of the present thesis describes a first attempt to model freshwater spongy spray ice growth physically, with a surficial structure that includes a falling liquid film as well as a dendritic icing interface. In preparation for Chapter 3, current approaches to the modelling of spongy spray icing are reviewed next.

1.5.2 Modelling spongy spray icing

Spray ice growth often occurs coincident with the entrapment of a portion of the impinging spray liquid by the ice matrix. Under these circumstances, the ice accretion is said to be spongy, and the degree of sponginess is often quantified by the liquid mass fraction (cf. Eqn. 3.52). Accretion sponginess is also described by the ice mass fraction or more succinctly the ice fraction (cf. Eqn. 1.25). The possibility of liquid entrapment by the ice accretion's crystalline matrix was first recognized by Fraser et al. (1952). Ludlam (1950) suggested that hailstones which fall in cumulonimbus clouds may contain liquid water. He formulated the first approach to spongy ice accretion modelling by simply neglecting it in his cylinder icing model. Many modellers have since followed his example, despite the fact that List (1963) concluded that the maximum mass accretion rate for hail likely occurs under spongy growth conditions. Later, the possibility of such

liquid entrapment in hailstones was inferred by Knight (1968) and again by List (1977).

The phenomenon of sponginess is observed in both freshwater and saline spray ice formation. Freshwater sponginess has been observed in hailstones, icicles, and experimental cylinder ice accretions. Saline spongy ice formations have been observed in spray icing on ships and in sea ice growth (Makkonen, 1987). Zakrzewski and Lozowski (1987) measured sponginess in the range of 8% to 20% as a function of height on the front face of the superstructure of the RFT "Wilfred Templeman". Modelling the sponginess of spray ice accretion is important for ice load prediction due to the weight of the entrapped brine (Makkonen, 1987; Zakrzewski and Lozowski, 1991). Savyel'ev (1971) states that 50% sponginess may be expected as a maximum value in saline ice formed on ocean-going vessels. This value implies a mass loading 100% larger than would be predicted thermodynamically on the basis of heat transfer considerations alone.

For both saltwater and freshwater, predicting spongy ice growth has remained largely an intractable problem. This has occurred because most accretion modelling has followed the traditional thermodynamic heat balance approach without engaging the problems of spongy surficial structure and physics. In more recent years however, the seaspray ice accretion models of Makkonen (1987), Zakrzewski and Lozowski (1987), and Zakrzewski et al. (1993) have attempted to account for sponginess through analogies and empiricisms for saline spray icing. For freshwater icing, List (1990), Lock and Foster (1990) and Makkonen (1990) have advanced conceptual views of the processes at work. However, essentially no modelling, based on analogy, empiricism or physics has been published for the freshwater case.

With these things in mind, we now present a review of Makkonen's analogy for predicting saline spongy ice accretion. This will be followed by an overview of the spongy growth empiricism of Zakrzewski et al. (1993). This will be followed by a brief review of the experimental work of Lock and Foster (1990), List (1990), and Makkonen (1990), in order to provide a context for the exploratory freshwater cylinder icing model of Chapter 3.

1.5.2.1 The Makkonen (1987) spongy ice growth model

Makkonen (1987) presents a physical-empirical model of salt incorporation into seaspray ice, that is founded upon an analogy with salt entrapment in sea ice growth. He starts with the principle of salt mass conservation at the spongy spray icing surface. As pure ice crystals form, the rejected salt increases the surficial brine's salinity. A portion of the surficial brine is trapped in the growing ice matrix to form brine pockets, and the remaining brine is shed. The conservation of salt is expressed by:

$$FS_w = IS_i + (F-I)S_b \tag{1.3}$$

where F is the mass flux of the brine impinging on the icing surface, I is the mass flux of the accreted ice and incorporated brine, S_w, S_i and S_b are the salinities of the spray brine, the spongy ice and the surficial brine, respectively.

Dividing Eqn. 1.3 by FS_b, and using the accretion fraction (n=I/F), we have:

$$\frac{S_w}{S_i}\frac{S_i}{S_b} = n\frac{S_i}{S_b} + (1-n) \tag{1.4}$$

The "interfacial distribution coefficient" k^* is defined as:

$$k^* = \frac{S_i}{S_b} \tag{1.5}$$

This parameter specifies the non-equilibrium capture of salt at the advancing solid/liquid interface.

The effective distribution coefficient, k, is defined as:

$$k = \frac{S_i}{S_w} \tag{1.6}$$

It describes the overall salt entrapment efficiency at the growing seaspray icing surface. Rearranging Eqn. 1.4 and substituting k and k^* results in:

$$k=\frac{k^*}{1-(1-k^*)n} \tag{1.7}$$

Since no experimental data are available to determine k^* in spongy seaspray icing, Makkonen proposes an analogy with salt entrapment in sea ice growth. There is a considerable body of experimental work on the interfacial distribution coefficient, k^*, for the entrapment of salt in sea ice. Weeks and Ackley (1982) document this work, and the constitutional supercooling model that provides a useful empirical framework for predicting the salt distribution in the growing dendritic layer on the underside of the sea ice. Weeks and Lofgren (1967) and Cox and Weeks (1975), suggest that $k^* \rightarrow 0.26$ as the growth rate of the sea ice diminishes to zero. The value of k^* in this zero-growth limit is used in the analogy with spray icing. Makkonen suggests that seaspray icing may be analogous to sea ice growth between the planar growth regime and the dendritic growth regime which ensues from constitutional supercooling.

Next Makkonen (1987) shows that k^* for seaspray icing may be interpreted as the sponginess of the accretion. In the limit, as spray salinity, $S_w \rightarrow 0$, the saline sponginess approaches that of the freshwater case. This concept is expressed by:

$$0.26 \approx k^* \approx \lambda_s \approx \lambda_f \tag{1.8}$$

where λ_s and λ_f are the liquid mass fractions for saline and freshwater ice accretions, respectively.

Assuming that $k^*=0.26$, Eqns. 1.5, 1.6, and 1.7 may be used to solve for the ice accretion salinity S_i, in terms of the salinity of the impinging brine S_w:

$$S_i=\frac{0.26}{1-0.74n}S_w \tag{1.9}$$

In a similar way, the salinity of the brine film can be shown to be:

$$S_b=\frac{1}{1-0.74n}S_w \tag{1.10}$$

Makkonen (1987) then suggests that those factors which control n will control the overall ice accretion salinity and the surficial brine salinity. Consequently, such factors as air temperature and the dimensions of the icing surface will influence the salt mass distribution at the icing surface. These factors are accounted for by a cylinder icing model (Makkonen, 1984b) that estimates the accretion fraction, n, for freshwater icing. The accretion fraction is given by:

$$n=\frac{h}{FL}\left[(t_s-t_a)+\frac{\varepsilon L_e}{c_p P_a}(e_s-e_a)-\frac{rv^2}{2c_p}\right]+\frac{c_w(t_s-t_d)}{L}+\frac{\sigma a(t_s-t_a)}{FL} \qquad (1.11)$$

where Makkonen (1987) defines the variables as follows: h the convective heat transfer coefficient, F the flux of water to the surface, t_a the air temperature, t_s the temperature of the icing surface, t_d the spray droplet temperature, L the specific latent heat of freezing at t_s, ε the ratio of the molecular weights of water vapour and dry air (ε=0.622), L_e the latent heat of vaporization, c_p the specific heat of air at constant pressure, P_a the air pressure, e_s and e_a the saturation vapour pressures at the surface temperature and dew-point temperature, respectively, r the overall recovery factor (r=0.79) of a cylinder, as described by Lozowski et al. (1979), c_w the specific heat capacity of water, σ the Stefan-Boltzmann constant, and $a=8.1 \times 10^{-7} K^3$ (evaluated at t_a=-10°C and t_s=0°C by Makkonen (1984b)).

The overall heat transfer coefficient h in Eqn. 1.11 incorporates the effect of a rough icing surface on the heat transfer. This is accomplished by using a numerical boundary layer model of heat transfer (Makkonen, 1985). The model requires as input an estimate of the roughness of the cylindrical accretion surface.

Equation 1.11 was formulated for freshwater. Makkonen (1987) suggests that three salinity effects should be accounted for in order to model saline spongy spray icing. The first is that the equilibrium freezing temperature of the surficial brine t_s is less than 0°C. Makkonen states that the equilibrium freezing temperature of surficial brine as a function of salinity may be approximated by:

$$t_s = -54 S_b - 600 S_b^3 \qquad (1.12)$$

where S_b is the salinity of brine[2] on the ice surface. The salinity of the surficial brine will also reduce the equilibrium vapour pressure over the surface. This second affect is approximated by (Witting, 1908; Arons and Kientzler, 1954):

$$e_s = (1 - 0.537 S_b) E_s \qquad (1.13)$$

where E_s represents the equilibrium vapour pressure over a pure water surface. These two effects alter the transport of vapour and heat from the icing surface.

The third salinity effect is apparent in calculating the specific latent heat of the spongy ice deposit. The latent heat of fusion of saline spongy ice is linearly proportional to the pure ice mass fraction of the accretion. Since the liquid mass fraction is S_i/S_b (Makkonen, 1987), the latent heat of fusion of a spongy accretion is given by:

$$L = \left(1 - \frac{S_i}{S_b}\right) L_f \qquad (1.14)$$

where L_f is the specific latent heat of fusion of pure ice at the temperature of the surficial film.

Makkonen (1987) suggests an iterative procedure to solve for accretion salinity and ice mass growth rate. He reports that the ratio of the mass accretion rate for freshwater spongy icing to that for spongy saline icing is less than unity for typical marine atmospheric conditions. He concludes that a dendritic substructure occurs at the icing surface for all spray icing conditions, and that this dendritic growth entraps surficial brine into the matrix. He also suggests that the sponginess is essentially constant over a range of growth conditions, but that the sponginess is likely to increase with increasing spray salinity. Makkonen (1987) also suggests that the interfacial distribution coefficient k^* is approximately constant and equal to 0.26 for spray icing. He argues that a good first approximation for modelling the sponginess of a spray ice accretion is to assume that the

---

[2] The salinity, S_b, for Eqns. 1.12 and 1.13 has units of kg (salt) per kg (solution).

interfacial distribution coefficient, k^*, equals the liquid fraction and has a value of about 0.26. This practical modelling assumption is readily incorporated into any traditional heat balance approach to spray ice modelling. As will be seen in the following section, Zakrzewski et al. (1993) effectively adopt this value for the liquid fraction of accreted ice.

1.5.2.2 The Zakrzewski et al. (1993) model

This section presents a recent spongy spray icing model. It will be compared to the approach used by Makkonen (1987), which was reviewed in Section 1.5.2.1. The overall structure and approach of the Zakrzewski et al. (1993) model is very similar to that of the Chung (1995) vessel icing model. This is because the Chung (1995) model for the MT "Zandberg" is patterned after the Zakrzewski et al. (1993) model for seaspray icing of the Coast Guard Cutter MIDGETT. Zakrzewski et al. (1993) describe the MIDGETT's superstructure in great detail, using 1381 grid cells on 143 components. They have thereby produced the most comprehensive and detailed topside icing model currently available. The vessel icing is subdivided into two groups of processes, spraying and icing. The icing module depends upon the predictions and output of the spraying module. These modules have two time scales. The first is the forecasting time step, during which the input parameters remain constant. This represents the long-time scale for environmental and operating conditions. The second time scale is shorter and has to do with the modelling of the spraying and icing cycle. This intermittent spraying process is modelled in much the same way as Chung et al. (1995), described in Section 1.5.1.2.

Zakrzewski et al. (1993) model the seastate, the spray jet liquid water content distribution, the spray jet geometry, the spray jet generation frequency, single spray droplet motion and cooling, and finally the spray flux delivery to each of the topside grid cells. This gives the necessary information to calculate the accretion of pure ice on the basis of a heat balance for each grid cell. The pure ice growth flux on each cell gives the needed information for the spongy portion of the spray icing model. Once the spongy spray icing flux (i.e. pure ice and entrapped brine) is known for each of the vessel's surficial grid cells, the ice growth distribution is known, and the overall icing load may

be calculated for the vessel.

The heat balance at the icing surface of each grid cell is composed of five heat flux components:

$$Q_l = Q_c + Q_e + Q_r + Q_s \tag{1.15}$$

where the convective heat flux, Q_c, the evaporative heat flux, Q_e, the radiative heat flux, Q_r, and the sensible heat flux, Q_s, sum to equal the latent heat flux evolved due to pure ice formation, Q_l. Each heat flux component is presented below with the purpose of establishing the traditional heat balance approach of Eqn. 1.15.

The convective heat flux (Zakrzewski et al. 1993) is:

$$Q_c = h(T_s - T_a) \tag{1.16}$$

where T_a is the air temperature, T_s is the equilibrium freezing temperature of the surface brine, and h is the local convective heat transfer coefficient. The convective heat transfer coefficient was taken to be a constant on all the grid cells of a particular vessel component. Vessel components were described as either planar or cylindrical with an appropriate Nusselt number formulation applied to each.

The evaporative heat flux term is:

$$Q_c = \frac{\varepsilon l_v}{p c_p}\left(\frac{Pr}{Sc}\right)^{0.63} h(e_s - e_a) \tag{1.17}$$

where ε is the ratio of the molecular weights of water vapour and dry air, l_v is the specific latent heat of vaporization at 0°C, p is the ambient atmospheric pressure, c_p is the specific heat of air at constant pressure, Sc is the Schmidt number for air (0.595), Pr is the Prandtl number for air (0.711), e_s is the saturation vapour pressure over the surficial brine, and e_a is the partial pressure of water vapour in the free airstream.

The radiative heat flux term is:

$$Q_r = 4.4(T_s - T_a) \tag{1.18}$$

which is a linear estimate of the black body radiative heat exchange between the surface

and the surrounding airstream.

The sensible heat flux is:

$$Q_s = R c_w (T_s - T_i) \tag{1.19}$$

where R is the brine flux from both impinging spray and the runoff from other grid cells, c_w is the specific heat of the brine, and T_i is the mean temperature of the incoming brine flux.

The final heat balance term is the pure ice growth term:

$$Q_l = l_f I \tag{1.20}$$

where l_f is the specific latent heat of fusion of pure ice at 0°C, and I is the mass flux of ice for the grid cell. Solving for the mass flux of ice from Eqn. 1.15 results in:

$$I = \frac{Q_c + Q_e + Q_r + Q_s}{l_f} \tag{1.21}$$

Eqn. 1.21 cannot be solved directly because the temperature of the brine, T_s, is initially unknown. To circumvent the problem, we assume that the surficial brine temperature is equal to its equilibrium freezing temperature. Makkonen (1987) suggests the following approximation of equilibrium freezing temperature as a function of brine salinity:

$$T_s = -54 s_b - 600 s_b^3 \tag{1.22}$$

where T_s is the equilibrium freezing temperature, and s_b is the salinity of the surficial brine.

Once the temperature of the surficial brine has been determined from Eqn. 1.22, it is only necessary to determine the salinity of the surface brine in order to solve Eqn. 1.21. This is done by developing equations which invoke brine mass conservation and conservation of the mass of salt in the brine film.

The overall conservation of brine mass is:

$$R = I + B \tag{1.23}$$

where B is the flux of brine that remains unfrozen.

The mass conservation of salt is established using the empirical results of Panov (1976) and Zakrzewski (1987), which give the overall accretion salinity, $\hat{s}$, as 75% of that of the impinging brine, s_w, i.e.:

$$\hat{s} = 0.75 s_w \tag{1.24}$$

This relation implies an effective distribution coefficient, k=0.75.

The ice fraction of the accretion is:

$$f_d = \frac{I}{I + B_e} \tag{1.25}$$

where f_d is the fraction of the accretion's mass which is in the solid phase and B_e is the flux of brine entrapped in the accretion. By contrast, the freezing fraction, $f_r = I/(I+B)$ is that fraction of the brine mass entering the grid cell which remains as pure ice.

The overall accretion salinity, given empirically by Eqn. 1.24, is defined as:

$$\hat{s} = \frac{s_b B_e}{I + B_e} \tag{1.26}$$

Together, Eqns. 1.25 and 1.26 can be used to show that:

$$f_d = 1 - \frac{\hat{s}}{s_b} \tag{1.27}$$

Transforming Eqn. 1.25 results in:

$$B_e = I\left(\frac{1}{f_d} - 1\right) \tag{1.28}$$

which shows that the surficial brine flux that is entrapped by the ice matrix is a function of the pure ice mass flux and the accretion's ice fraction. The unfrozen flux of brine B, is:

$$B = B_e + B_s \tag{1.29}$$

where B_s is the flux of shed brine. Conservation of salt mass at the icing surface may be expressed as:

$$s_w R = s_b B \tag{1.30}$$

This system of eight equations (Eqns. 1.21-1.30, excluding the dependent Eqns. 1.27 and 1.28) is solved by the method of Blackmore et al. (1989) for the eight variables B, B_e, B_s, f_d, $\hat{s}$, S_b, T_s, I. For freshwater spray icing, Zakrzewski et al. (1993) assume f_d=0.80 (an "average" value for spongy freshwater icing). Also, if f_d becomes less than 0.5 on the basis of the above set of equations, it is reset to 0.5. This is done because accretions with ice fractions smaller than this may not have sufficient mechanical integrity to remain structurally intact.

Since some of the implicit assumptions of this model are not readily apparent, they are summarized here:

1) The surface brine is of uniform temperature (the equilibrium freezing temperature) throughout the thickness of the film. This implies that the film is well-mixed.

2) Because the temperature of the brine is uniform, conduction of heat through the film is not explicitly modelled (i.e. no conductive term is included in the heat balance Eqn. 1.15).

3) Heat transmission from the icing surface to the outer surface of the brine film occurs without resistance.

4) There is no gradient of salinity in the brine film.

5) Ice crystal growth at the icing surface is assumed to occur with no supercooling (i.e. at the equilibrium freezing temperature of the surficial brine). For this reason, the growth mechanism by which the crystal growth front advances is not unspecified, although a crystal growth front with a supercooling close to the equilibrium freezing temperature of the liquid may have an interface that is close to being planar.

All of these points, except (4), have been implicit in traditional models of freshwater spray icing. For this reason, even though both Zakrzewski et al. (1993) and Makkonen (1987) have different ways of importing empiricism, the traditional heat balance and an implicit icing surface structure provide the basic framework of both models. Although Zakrzewski et al. (1993) and Makkonen (1987) have expanded the understanding of the structure of spray icing to include the substrate, ice matrix, freezing zone of ice dendrites and surficial liquid film, both authors have approached the modelling problem by ignoring the physics of the freezing zone and the liquid film. The following section will give a brief overview of the structure of the spray icing surface as it is presently understood.

1.5.2.3 Spongy spray icing structure

The surficial structure of growing spongy ice consists of an accretion matrix that adheres to the substrate, a freezing zone (the ice crystal growth layer in which the ice accretion matrix is being formed), and a surficial liquid layer that lies between the external surface of the freezing zone and the airstream.

List (1990) offers experimental evidence and theoretical arguments in support of an emerging physical picture (Fig. 1.9) of the processes at work at the surface of a gyrating spongy hailstone. List's focus is on the physics of the liquid film, including the supercooling of the surface liquid. He mentions the necessity of an ice crystal growth layer (or freezing zone) and then largely ignores this layer since it lies behind the envelope of the ice front. In this layer the temperature is assumed to relax from a supercooled value at the ice front, to the equilibrium freezing temperature in the spongy ice-water matrix. List (1990) also suggests that the freezing zone is probably only a fraction of the thickness of the surficial liquid film (at the equator of a hailstone). These icing surface structures are shown in Fig. 1.9 where temperatures, interfacial growth velocities and heat fluxes are also indicated.

List (1990) states that artificial hailstones grown in a wind tunnel environment routinely exhibit a supercooling of up to 5°C at the outer surface of the liquid film. He gives a theoretical analysis showing that laminar water films up to 1 mm in thickness are

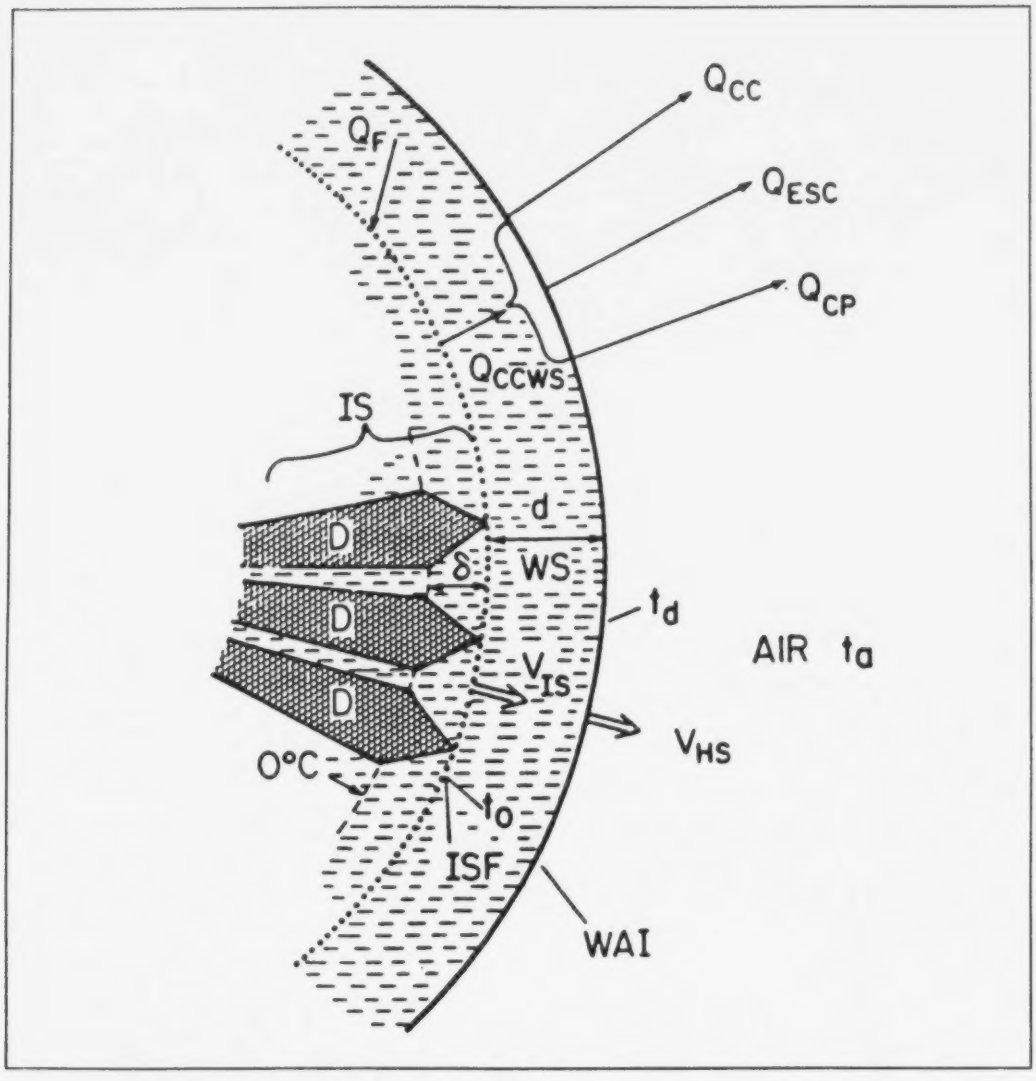

Figure 1.9 Schematic 2-D representation of the spongy layer (IS) of a hailstone covered by a waterskin (WS). The latent heat of freezing, Q_F, is released at the ice-sponge front (ISF). The equivalent heat energy flux, Q_{CCWS}, is conducted through the water skin to the water skin-air interface (WAI) from where it is passed on to the air through the conduction and convection term, Q_{CC}, the evaporation, sublimation or condensation term, Q_{ECS}, and the sensible heat term, Q_{CP}. The idealized ISF, the envelope of the tips of the growing dendrites (D), is at the temperature, t_0, and advances at the speed V_{IS} into the water skin of thickness, d. WS retains its thickness because of the accretion of cloud water at the WAI (at t_d) which advances at the speed V_{HS} (=V_{IS}). In reality, the dendrites require time to thicken over a depth, δ. Only behind that (neglected) layer will ice and water be at the equilibrium temperature, 0°C (from List, 1990).

consistent with molecular conduction of heat from the freezing zone to the outer surface of the liquid film. This implies a linear temperature profile through the laminar water film.

Lock and Foster (1990), in contrast to List (1990), focus on the nature of the freezing zone itself, and the formation of the ice matrix in the vicinity of the forward stagnation point of a disc placed perpendicular to a supercooled icing aerosol. The accretion was allowed to grow on an ice-free steel disc, which was initially at a temperature close to that of the accretion to be formed. The experimental observations and theoretical arguments presented by them have to do with the influence of factors such as airspeed, air temperature, liquid-water content, and spray salinity on the ice fraction and the ice growth rate. Lock and Foster (1990) made macroscopic observations of two spray ice morphologies, and suggest that they correspond to two modes of ice growth in the freezing zone.

Lock and Foster (1990) say that both freshwater and saline spray icing exhibited a mushy ice growth mode at air temperatures below about -15°C. A macroscopic examination of this deposit showed an accretion with a fine crystalline structure, similar to slush, with a random crystal orientation and low strength. They hypothesize that this is due to the nucleation of water, within the freezing zone immediately adjacent to the water film. They surmise that supercooling in the spray droplets is the driving condition for the isotropic growth of the many small ice crystals that form the ice matrix. The normalized accretion thickness was linear with time. This can be readily explained on the basis of a conventional heat balance analysis.

Lock and Foster (1990) also observed a columnar ice growth mode with a coarse structure at air temperatures above -10°C. Even though they did not use thin section analyses to determine the crystallographic direction, they suggest that long cellular dendrites form with the a-axis parallel to the ice growth direction. This accretion showed greater structural integrity than the accretion in the mushy growth mode, and fractured along well-defined grain boundaries. This ice growth mode was associated with a logarithmic increase in the normalized mass with time. A conventional heat balance model fails to give a clear explanation for this non-linear accretion rate.

Understanding the modes of growth that may occur in spray icing is likely to depend on understanding the nature of ice crystal growth at the icing interface. For example, Knight (1968) suggests that spongy growth is the result of the morphology of the icing interface. Makkonen (1990) states that the morphology of an ice-water interface changes from planar to cellular and then to dendritic with increased supercooling. These ice-water interface morphologies may account in part for the macroscopically observed columnar (cellular) and mushy (dendritic) icing modes reported by Lock and Foster (1990).

Makkonen (1990) presents a theory for predicting the solid fraction of an ice matrix formed by axisymmetric parabolic dendrites. He examines the heat balance at the dendritic interface and assumes that the crystals grow without changing shape. An important result is that the solid fraction of the crystal matrix is relatively insensitive to growth conditions, as proposed earlier by Makkonen (1987). Makkonen (1990) shows that an assumed ice crystal shape at the icing interface along with a heat balance and a known supercooling can be used to predict the ice fraction for a freshwater spray ice accretion.

This review of the work of List (1990), Lock and Foster (1990), and Makkonen (1990) provides a context for the surficial structure postulated in the exploratory spray ice growth model of Chapter 3. The work of Makkonen (1987) and Zakrzewski et al. (1993) is used as the basis for the spray ice accretion model of Chapter 3.

Even though the traditional heat balance at the outer surface of the spray ice accretion maintains its key importance in spray icing physics, the modelling of accretion characteristics such as sponginess will depend on more complete models of the surficial structure and the morphological processes involved. Therefore, spray icing models of the future will probably account for the hydrodynamics and thermodynamics of the surficial liquid film as well as the crystal growth mechanisms at work in forming the final spray ice matrix. Other problems involving the mechanical nature of spray ice (e.g. strength and adhesion) may be approached once the morphology of the spray ice becomes predictable. Advances in this area, as well as in the macroscopic prediction of icing rates for vessels, are likely to become the stimulus for comparable advances in other areas of glaciology.

1.6 Vessel Spray Icing in Context

Vessel spray icing occurs within the context of marine icing, which in turn occurs within the realm of atmospheric icing. Atmospheric icing itself occurs within the larger context of all kinds of ice formation within the earth's cryosphere such as sea ice growth and glacier formation. This discussion is limited to research areas that bear the fundamental nature of spray icing; namely the presence of a substrate or an object on which an aerosol may first collect and then freeze. The interrelatedness of all such spray icing leads to the supposition that research in one area may open up interesting possibilities in another area. Lozowski and Gates (1991) suggest that all areas of icing research share much in common, and that artificial barriers between the various fields should be reduced by increased communication and sharing of information.

Vessel spray icing is a case of marine icing in which the dynamics of the free-floating vessel play an important part. In a similar fashion, offshore platforms and other floating structures such as buoys may also experience seaspray icing. Seaspray icing of fixed structures including natural objects on the shoreline, port facilities or fixed drilling platforms may occur as a result of wave impact. Marine icing usually is characterized by large droplets or splashes of brine. This kind of spray generation is likely to occur for vessels on large bodies of freshwater as well.

The conditions for freshwater icing are, generally, quite different from the marine case. For example, freezing rain causes a variety of difficulties in the non-marine environment, including icing of aircraft on the ground and in the air, transmission line icing, road icing and the loss of agricultural crops. In other situations, rime icing may occur. This is often seen in mountainous areas where rime may coat trees, transmission lines and towers. These kinds of atmospheric icing, along with wet snow accretion, can disable meteorological instrumentation and remote communications equipment.

Hail is a form of icing well-known for its potential to destroy crops and property. Hail growth studies first brought to light the problem of spongy ice growth, and provide the foundation for the current studies of sponginess in marine spray icing. Therefore, a question born first in the investigation of hailstones will be answered, at least in part, by

work directed toward the marine icing problem.

Even though marine icing conditions are often quite different from those of atmospheric icing, many of the processes involved have a similar nature. For example, aircraft icing occurs in supercooled clouds with small droplets, low liquid water contents, and the high airspeeds associated with flight. In contrast, vessel spray icing occurs with relatively warm spray and large droplets, high liquid water contents, and high surface wind speeds. However, the icing processes may have much in common. In all cases, for example, the heat transfer is from the icing surface toward the cold airstream, and droplets must collide with the icing surface in order to form the surface liquid film of wet icing. Also, dendritic growth of ice at the icing surface is likely to account for the sponginess observed in both marine and atmospheric icing. The similarities in all kinds of spray icing can serve as the basis for interrelating, comparing and transferring research results from one area of investigation to another.

A clearer understanding of the physics of spray icing will likely produce more effective engineering responses to spray icing problems. For example, anti-icing and de-icing problems do not yet have effective generally applicable engineering solutions. Fundamental research into the physics of spray icing should continue in the hope that such engineering solutions will appear along with more accurate models for forecasting the various icing hazards. The present work is designed to add specifically to the knowledge of vessel spray icing and spongy ice growth, but it may also serve as a resource for research in other areas of spray ice accretion.

List of References

Allen, J. A., 1881: A singular case of shipwreck. *Nature*, June 2, 1881, 106-107.

Andreas, E. L., 1989: Thermal and size evolution of spray droplets. CRREL Rep. 89-11, U.S. Army Cold Regions Research and Engineering Laboratory, Hanover, NH, 37 pp.

Arons, A. B. and Kientzler, C. F., 1954: Vapour pressure of sea-salt solutions. *Trans. Amer. Geophys. Union,* **35,** 722-728.

Bardarson, H. R., 1969: Icing of ships. *Jökull,* (Iceland) **19**, 107-120.

Blackmore, R. Z., W. P. Zakrzewski and E. P. Lozowski, 1989: Ice growth on a ship's mast. In: Proceedings of the 10th International Conference on Port and Ocean Engineering under Arctic Conditions, (POAC), Lulea, Sweden, Vol. 3, 1440-1453.

Borisenkov, Ye.P., and V. V. Panov, 1972: Fundamental results and perspectives in research into the hydrometeorological aspects of ship icing. Arkt. Antarkt. Nauc-Issled Inst. T298, Leningrad, 5-33. [in Russian]

Borisenkov, Ye.P., and I. G. Pchelko, Eds., 1972: Indicators for forecasting ship icing. Arkt. Antarkt. Nauc-Issled Inst., Leningrad. [in Russian] [also as CRREL Draft Translation 481 (AD-A030 113), U.S. Army Cold Regions Engineering and Research Laboratory, Hanover NH, 60 pp.]

Borisenkov, Ye.P., and I. G. Pchelko, 1975: Indicators for forecasting ship icing. CRREL Draft Translation 481 (AD-A030 113), U.S. Army Cold Regions Engineering and Research Laboratory, Hanover NH, 60 pp.

Borisenkov, Ye.P., G. A. Zablockiy, A. P. Makshtas, A. I. Migulin and V. V. Panov, 1975: On the approximation of the spray cloud dimension. Arkt. Antarkt. Nauc-Issled Inst., Trudy No. 317, Gidrometeoizdat, Leningrad, 121-126. [in Russian]

Bowyer, P. J., and J. M. Gray, 1990: East coast marine weather manual. General Weather Services, Atmospheric Environment Service, Bedford, NS, 88 pp.

Bretschneider, C. L., 1973: Prediction of waves and currents. *Look Lab, Hawaii,* **3(1),** 1-17.

Brown, R. D., and P. Roebber, 1985: The scope of the ice accretion problem in Canadian waters related to offshore energy and transportation. Rep. 85-13, Canadian Climate Center, Downsview, Ont., 295 pp. [unpublished manuscript]

BSRA (British Shipbuilding Research Association), 1957: Trawler-icing research. BSRA Rep. No. 221, London.

Businger, S., 1991: Arctic hurricanes. *Amer. Sci.* **79,** 18-33.

Chin, L. P., P. G. Larose, R. S. Tankin, T. Jackson, J. Stutrud and G. Switzer, 1991: Droplet distributions from the breakup of a cylindrical liquid jet. *Phys. Fluids A,* **3(8),** 1897-1906.

Chung, K. K., 1995: Ship icing and stability. Ph.D. Dissertation. University of Alberta, 184 pp.

Chung, K. K., and E. P. Lozowski, 1990: On the growth of marine icicles. *Atmosphere-Ocean,* **28,** 393-408.

Chung, K. K., Lozowski, E. P., J. S. Pawlowski and Q. Xu, 1995: Ship icing and stability. In: Proceedings of the 1st Asian Computational Fluid Dynamics Conference, Jan. 16-19, Hong Kong, Vol. 1, 275-280.

Comiskey, A. L., L. D. Leslie and J. L. Wise, 1984: Superstructure icing and forecasting in Alaskan waters. Unpublished draft report submitted by the Arctic Environmental Information and Data Centre to Pacific Marine Environmental Laboratory (NOAA), Seattle, 39 pp.

Cox, G. E. N., and W. F. Weeks, 1975: Brine drainage and initial salt entrapment in sodium chloride ice. CRREL Report 354, U.S. Army Cold Regions Research and Engineering Laboratory, Hanover NH, 85 pp.

De Angelis, R. M., 1974: Superstructure icing. *Mar. Wea. Log*, **18,** 1-7.

Dunbar, M., and W. F. Weeks, 1975: Interpretation of young ice forms in the Gulf of St. Lawrence using side-looking airborne radar and infrared imagery. CRREL Report 337, U.S. Army Cold Regions Research and Engineering Laboratory, Hanover NH, 46 pp. [also as Defense Research Establishment Ottawa (DREO) Report 711]

Fein, N., and A. Freiberger, 1965: Survey of the literature on shipboard ice formation. *Nav. Eng. J.*, **77,** 849-855. [also in Tech. Memo. No. 2, Naval Applied Science Lab., Brooklyn, N.Y., 15 pp.]

Finstad, K., E. P. Lozowski and E. M. Gates, 1988: A Computational investigation of water droplet trajectories. *J. Atmos. Ocean. Tech.*, **5(1),** 160-170.

Forest, T. W., and R. Sharma, 1992: Growth rates of frazil ice discs. In: Proceedings of the 11th International Association for Hydraulic Research Symposium on Ice (IAHR), Banff, Canada, Vol. 2, 723-734.

Fraser, D., C.K. Rush and D. Baxter, 1952: Thermodynamic limitations of ice accretion instruments. NRC NAE Laboratory Report LR-32.

Glukhov, V. G., 1971: Evaluation of ice loads on high structures from aerological observations. Arkt. Antarkt. Nauchno-Issled. Inst., Trudy No. 283 GGO, Gidrometeoizdat, Leningrad, 3-11. [in Russian] [also Trans. Soviet Hydrology; Selected papers, Vol. 3, 1971, 223-228]

Hartmann, D. L., 1994: *Global physical climatology*. Academic Press, San Diego, 411 pp.

Hay, R. F. M., 1956: Meteorological aspects of the loss of LORELLA and RODERIGO. *Mar. Obs.*, **26(172),** 89-94.

Hayhoe, R. D., 1989: An experimental study of ice accretion and wind loading on offshore supply boats. Ph.D. Dissertation. Heriot-Watt University, 188 pp.

Hayhoe, R. D., 1991: An experimental investigation of shipboard ice accretion. In: Proceedings of the Institute of Marine Engineers, London, UK, 18 pp.

Holman, J. P., 1990: *Heat transfer.* McGraw Hill, New York, 714 pp.

Horjen, I., 1983: Mobile platform stability. MOPS Subproject 02-Icing (MOPS Report No. 7). Norwegian Hydrodynamic Lab., Report NHL 283021.

Horjen, I., 1990: Numerical modelling of mixed snow and sea spray icing. In: Proceedings of the 10th International Association for Hydraulic Research (IAHR) Symposium on Ice, 945-960.

Horjen, I., and T. Carstens, 1989: Numerical modelling of sea spray icing on vessels. In: Proceedings of the 10th International Conference on Port and Ocean Engineering under Arctic Conditions (POAC), Lulea, Sweden, 694-704.

Horjen, I., and S. Vefsnmo, 1985: A numerical sea spray model including the effect of a moving water film. In: Proceedings of the International Workshop on Offshore Winds and Icing, Halifax, NS, 152-164.

Incropera, F. P., and D. P. DeWitt, 1990: *Introduction to heat transfer.* John Wiley and Sons, New York, 824 pp.

Itagaki, K., and C. Ryerson, 1990: A universal flying particle camera. In: Proceedings of the Fifth International Workshop on Atmospheric Icing of Structures, Tokyo, p. B2-1-(1)-B2-1-(4).

Jessup, R. G., 1985: Forecast techniques for ice accretion on different types of marine structures, including ships, platforms and coastal facilities. Marine Meteorology and Related Oceanographic Activities, Rep. 15, WMO, Canada, 90 pp.

Kachurin, L. G., L. I. Gashin and I. A. Smirnov, 1974: Icing rate of small displacement fishing boats under various hydrometeorological conditions. *Meteorologiya i Gidrologiya*, **3**, 50-60. [in Russian]

Kaplina, T. E., and K. I. Chukanin, 1974: Synoptic conditions of especially heavy icing of commercial ships. CRREL Draft Trans. 411, ADA-003215, U.S. Army Cold Regions Research and Engineering Lab., Hanover, NH, 172-177. [also, Brachnell: Met. Off. Trans. No. 877. Original Document: Arkt. Antarkt. Nauc-Issled. T298, 168-172, in Russian]

Khandekar, M. L., 1989: Operational analysis and prediction of ocean wind waves. *Coast. Estuar. Stud.*, **33,** Springer-Verlag, 214 pp.

Kliuchnikova, L. A., 1971: Physical processes controlling the icing of the deck of medium-sized fishing vessels. In: Theoretical and experimental investigations of conditions of icing on ships. Arkt. Antarkt. Nauchno-Issled. Inst., Gidrometeoizdat, Leningrad, 16-25. [in Russian]

Knauss, J. A., 1978: *Introduction to physical oceanography.* Prentice-Hall, London, 338 pp.

Knight, C. A., 1968: On the mechanism of spongy hailstone growth. *J. Atmos. Sci.*, **25,** 440-444.

Kultashev, Ye. N., N. F. Malakhov, V. V. Panov and M. V. Schmidt, 1972: Spray icing of fishing vessels of classes SRT (medium-sized fishing vessel) and SRTM (medium-sized freezing trawler). Arkt. Antarkt. Nauc-Isssled. Inst. Trudy No. 298, 125-136. [in Russian] [Bracknell, Met. Off. Trans. No. 875. Also, CRREL Draft Translation No. 411, ADA-003215, 1974]

Langmuir, I., and K. Blodgett, 1946: Mathematical investigation of water droplet trajectories. In: *Collected works of Irving Langmuir,* Vol. 10, Gen. Ed.: C. G. Suits, Pergamon Press, 1960, pp. 348-393. [also as Army Air Forces TR 5418, Feb. 1946]

Lebiedzinski, K. , and W. L. Thomas III, 1993: Prediction of bow spray frequency for a naval combatant. In: Proceedings of the 12th International Conference on Port and Ocean Engineering under Arctic Conditions, (POAC), Hamburg, Vol. 2, 824-834.

List, R., 1963: General heat and mass exchange of spherical hailstones. *J. Atmos. Sci.*, **20,** 189-197.

List, R., 1977: Ice accretions on structures. *J. Glaciol.*, **19**, 451-465.

List, R., 1990: Physics of supercooling of thin water skins covering gyrating hailstones. *J. Atmos. Sci.*, **47(15),** 1919-1925.

Lock, G. S. H., and I. B. Foster, 1990: Experiments on the growth of spongy ice near a stagnation point. *J. Glaciol.*, **36(123),** 143-150.

Lozowski, E. P., and E. M. Gates, 1985: Marine icing models: how do they work and how good are they? In: Proceedings of the International Workshop on Offshore Winds and Icing, Halifax, Nova Scotia, Oct. 7-11, 102-122.

Lozowski, E. P., and E. M. Gates, 1991: On the modelling of ice accretion. In: *Freezing and Melting Heat Transfer in Engineering*, K. C. Cheng and N. Seki, eds., Hemisphere Publishing Corp., 615-660.

Lozowski E. P., A. M. Kobos, and L. G. Kachurin, 1995: Influence of the surface liquid film on cylinder icing under marine conditions. In: Proceedings of the 14th International Conference on Offshore Mechanics and Arctic Engineering (OMAE), Copenhagen, Vol. IV, Arctic/Polar Technolog ASME 199, 115-122.

Lozowski, E. P., and A. Novak, 1985: The design and construction of an outdoor marine icing facility. Prepared under contract no. KM147-4-1255, for the Atmospheric Environment Service, Canadian Climate Centre, Downsview, ON, 36 pp.

Lozowski, E. P., J. R. Stallabrass and P. F. Hearty, 1979: The icing of an unheated non-rotating cylinder in water droplet-ice crystal clouds. Rep. No. LTR-LT-96. National Research Council Canada, Ottawa.

Lozowski, E. P., J. R. Stallabrass and P. F. Hearty, 1983: The icing of an unheated, non-rotating cylinder. Part I: A simulation model. *J. Climate Appl. Meteor.*, **22,** 2053-2062.

Ludlam, F.H., 1950: The composition of coagulation elements in cumulonimbus. *Q. J. R. Meteorol. Soc.*, **76,** 52-58.

Ludlam, F.H., 1951: Heat economy of a rimed cylinder. *Q. J. R. Meteorol. Soc.*, **77**, 663-666.

Lundqvist, J., and I. Udin, 1977: Ice accretion on ships with special emphasis on Baltic conditions. Res. Rep. 23. Winter Navigation Research Board, Swedish Meteorological and Hydrological Institute, 32 pp.

Makkonen, L., 1984a: Atmospheric icing on sea structures. CRREL Monograph 84-2, U.S.A. Cold Regions Research and Engineering Laboratory, Hanover, NH, 92 pp.

Makkonen, L., 1984b: Modelling of ice accretion on wires. *J. Climate Appl. Meteor.*, **23**, 929-939.

Makkonen, L., 1985: Heat transfer and icing of a rough cylinder. *Cold Reg. Sci. Tech.*, **10,** 105-116.

Makkonen, L., 1987: Salinity and growth rate of ice formed by sea spray. *Cold Reg. Sci. Tech.*, **14,** 163-171.

Makkonen, L., 1989: Formation of spray ice on offshore structures. In: Working Group on Ice Forces, 4th State-of-the-Art Report, CRREL Special Report 89-5, U.S.A. Cold Regions Research and Engineering Laboratory, Hanover, NH, 277-309.

Makkonen, L., 1990: Origin of spongy ice. In: Proceedings of the 10th International Association for Hydraulic Research (IAHR) Ice Symposium, Espoo, Finland, 1022-1030.

Markham, W. E., 1980: Ice atlas - eastern Canadian seaboard. Atmospheric Environment Service, Toronto.

Martin, S., 1981: Frazil ice in rivers and oceans. *Ann. Rev. Fluid. Mech.*, **13**, 379-397.

Martin, S., and P. Kauffman, 1981: A field and laboratory study of wave damping by grease ice. *J. Glaciol.*, **27(96),** 283-313.

Masterson, D. M., 1992: Ambient temperature effects on spray ice island construction using saline (sea) and fresh water. In: Proceedings of the 11th International Conference on Offshore Mechanics and Arctic Engineering (OMAE), June 7-14, 1992, Calgary, AB, Vol. 4, 51-58.

Mertins, H. O., 1968: Icing on fishing vessels due to spray. *Mar. Obs.*, **38(221),** 128-130.

Minsk, L. D., 1977: Ice accumulation on ocean structures. CRREL Rep. 77-17, U.S. Army Cold Regions Research and Engineering Laboratory, Hanover, NH, 47 pp.

Monahan, E. C., 1968: Sea spray as a function of low elevation wind speed. *J. Geophys. Res.*, **73(4),** 1127-1137.

Overland, J. E., 1990: Prediction of vessel icing for near-freezing temperatures. *Wea. Forecasting*, **5(1),** 62-77.

Overland, J. E., C. H. Pease, R. W. Preisendorfer and A. L. Comiskey, 1986: Prediction of vessel icing. *J. Climate Appl. Meteor.*, **25(12),** 1793-1806.

Panov, V. V., 1971: On the frequency of splashing the medium fishing vessel with sea spray. Theoretical and experimental investigations of the conditions of the icing on ships. Gidrometeoizdat, Leningrad, 87-90. [in Russian]

Panov, V. V., 1972: The estimation of the spray droplet temperature and ice accretion salinity during spray icing of ships. Investigation of the physical nature of ship icing. Arkt. Antark. Nauc-Issl. Inst., Trudy No. 298. Gidrometeoizdat, Leningrad, 44-50. [in Russian] [CRREL Draft Translation 411, ADA-003215, 1974, 1-30]

Panov, V.V., 1976: Icing of ships. Arkt. Antark. Nauc-Issled Inst., Trudy No. 334, Gidrometeoizdat, Leningrad, 4-25. [in Russian]

Panov, V. V., 1978: Icing of Ships. *Polar Geography*, **2**, 166-186.

Pawlowski, J. S., and D. W. Bass, 1991: A theoretical and numerical model of ship motion in heavy seas. Trans. SNAME, 31 pp.

Personne, P., and J. F. Gayet, 1984: Etude théorique et étude expérimentale en soufflerie du phénoméne d'accretion de givre sur les lignes électriques aériennes. *J. Rech. Atmos.*, **18,** 263-279.

Pierson, W. J., 1972: The loss of two British trawlers--a study in wave refraction. *J. Navigation,* **25(3),** 291-304.

Pierson, W. J., G. Neumann, R. W. James, 1955: Practical methods for observing and forecasting ocean waves by means of wave spectra and statistics. U.S. Navy Hydrographic Office, H. O. Publications, No. 603.

Pflaum, J. C., 1984: New clues for decoding hailstone structure. *Bull. Am. Met. Soc.*, **65(4),** 583-593.

Polar Record, 1958: Research on anti-icing precautions for ships. *Polar Record,* **9(58),** 36-39.

Preobrazhenskii, L. Yu., 1973: Estimate of the content of spray-drops in the near-water layer of the atmosphere. *Fluid Mechanics Soviet Research,* **2(2),** 95-100. [in Russian]

Price, W. G., and R. E. D. Bishop, 1974: *Probabilistic Theory of Ship Design*, New York: J. Wiley and Sons, 311 pp.

Rybnikov, B. N., 1975: Analysis of the unique icing of the medium-sized fishing trawler "Piarnu". In: Arkt. Antarkt. Nauchno-Issled. Inst., Trudy No. 317, Gidrometeoizdat, Leningrad, 132-140. [in Russian]

Ryerson, C. C., 1993: Superstructure spray ice accretion on a large U.S. Coast Guard cutter. In: Proceedings of the 6th International Workshop on the Atmospheric Icing of Structures (IWAIS), Sept. 20-23, 1993, Budapest, 280-285.

Ryerson, C. C. and P. Longo, 1992: Ship superstructure icing: data collection and instrument performance on the USCGC MIDGETT Research Cruise. USA Cold Regions Research and Engineering Laboratory, CRREL Report 92-23, 56 pp.

Sackinger, W. M., and P. A. Sackinger, 1987: On the freezing of sprayed sea water to produce artificial sea ice. In: Proceedings of the 9th International Conference on Port and Ocean Engineering under Arctic Conditions (POAC), Fairbanks, AS, 581-590.

Savyel'ev, B. A., 1971: Structure, chemical content and strength of the accretions formed on different materials. "Zhizn' ziemli" No. 7, 23-33. [in Russian]

Sawada, T., 1962: Icing on ships and its forecasting. *J. Jpn. Soc. Snow Ice*, **24,** 12-14. [also in *Bull. Hakodate Mar. Obs.*, **9, (1962).** Trans. No. 2357, Nav. Res. and Dev. Admin., MOD, London, 1971]

Sawada, T., 1967: A forecasting method for ship icing near the Kuril Islands. Tokyo, Japan Meteorological Agency. *J. Meteor. Res.*, **18,** 15-23. [also in Bull. Hakodate Mar. Obs., 14, 1969]

Sawada, T., 1970: Ice accretion on ships in the northern part of the Sea of Japan. *Bull. Hakodate Mar. Obs.*, **15,** 29-35.

Shektman, A. N., 1967: Hydrometeorological conditions of icing on ships. Nauc-Issl. Inst., Aeroklimatologii, Trudy No. 45, Gidrometeoizdat, Moscow, 51-63. [in Russian]

Shektman, A. N., 1968: Probability and intensity of icing of sea-going ships. Nauc-Issl. Inst., Aeroklimatologii, Trudy No. 50, Gidrometeoizdat, Moscow, 55-65. [in Russian]

Shellard, H. C., 1974: The meteorological aspects of ice accretion of ships. Marine Science Affairs, Rep. No. 10, WMO-No. 397, World Meteorological Organization, Geneva, 34 pp.

Smith, D. P., 1970: Trawler safety off Iceland. *Mar. Obsr.*, **40,** 24-31.

Stallabrass, J. R., 1980: Trawler icing: a compilation of work done at N.R.C. Mech. Eng. Rep. MD-56, N.R.C. No. 19372, National Research Council, Ottawa, 103 pp.

Stewart, R. E., and L. M. Patenaude, 1988: Rain-snow boundaries and freezing precipitation in Canadian East Coast winter storms. *Atmos. Ocean*, **26,** 377-398.

Stewart, R. E., D. T. Yiu, K. K. Chung, D. R. Hudak, E. P. Lozowski, M. Oleskiw, B. E. Sheppard, and K. K. Szeto, 1995: Weather conditions associated with the passage of precipitation type transition regions over Eastern Newfoundland. *Atmos. Ocean*, **33(1),** 25-53.

Szilder, K., T. W. Forest and E. P. Lozowski, 1991: A comparison between different construction methods of ice islands. In: Proceedings of the 10th International Conference on Offshore Mechanics and Arctic Engineering (OMAE), Stavanger, Vol. 4, 9-15.

Tabata, T., S. Iwata and N. Ono, 1963: Studies of ice accumulation on ships. Part I. *Low Temp. Sci. Ser. A.*, No. 21, 173-221. [Trans. by E. R. Hope, Ottawa. NRC, TT-1318, 1968, 42 pp]

U. S. Naval Weather Service Detachment, 1974: Marine Climatic Atlas of the World, Vol 1. North Atlantic Ocean. NAVAIR 50-1C-528, 388 pp.

Vasil'yeva, G. V., 1966: Hydrometeorological conditions promoting the icing of marine ships. *Rybnoye Khozyastvo*, **12,** 43-45. [in Russian] [also Trans. T486R, Defense Research Board, Ottawa, 1967]

Vasil'yeva, G. V., 1971: Hydrometeorological conditions involved in the icing of marine vessels. *Tr. Gidromettsentra SSSR*, **87,** 82-92. [in Russian] [also Bracknell (UK) Met. Off. Trans. 848, 11 pp]

Wakahama, G., D. Kuroiwa and K. Goto, 1977: Snow accretion on electric wires and its prevention. *J. Glaciol.*, **19,** 479-487.

Walden, H., 1967: Zur frage der quantitativen vorausbestimmung der schiffsvereisung. *Der Seewart*, **28 H2,** 58-62.

Wang, C. S., and R. L. Street, 1978: Measurements of spray at an air-water interface. *Dyn. Atmos. Oceans*, **2(2),** 141-152.

Weeks, W. F., and S. F. Ackley, 1982: The growth, structure and properties of sea ice. CRREL Monograph 82-1, U.S. Army Cold Regions Research and Engineering Lab, Hanover, NH, 136 pp.

Weeks, W. F., and G. Lofgren, 1967: The effective solute distribution coefficient during the freezing of NaCl solutions. *Phys. Snow Ice, Inst. Low Temp. Sci.*, **1,** 579-597.

White, F. M., 1986: *Fluid mechanics*. McGraw Hill, New York, 732 pp.

Wise, J. L., and A. L. Comiskey, 1980: Superstructure icing in Alaskan waters. NOAA Special Rep., Pacific Marine Environmental Laboratory, Seattle, WA, 30 pp. [NTIS PB81-135188]

Witting, R., 1908: A study on water level variations and water exchange in the Finnish sea areas. Finlandische Hydrographisch-Biologische Untersuchungen, 2, 173 pp. (in German).

WMO, 1960: Icing of ships. WMO Commission for Maritime Meteorology Third Session, Utrecht, CMM-III Doc. 5, submitted by the Fed. Rep. of Germany.

Woodcock, A. H., 1953: Salt nuclei in marine air as function of altitude and wind force. *J. Meteor.*, **10,** 362-371.

Wu, J., 1973: Spray in the atmospheric surface layer: laboratory study. *J. Geophys. Res.*, **78(3),** 511-519.

Wu, J., 1979: Spray in the atmospheric surface layer: review and analysis of laboratory and oceanic results. *J. Geophys. Res.*, **84(C4),** 1693-1704.

Zakrzewski, W. P., 1986: Icing of ships. Part I: Splashing a ship with spray. NOAA Tech. Memo., ERL PMEL-66, Pacific Marine Environmental Laboratory, Seattle, WA, 74 pp.

Zakrzewski, W. P., 1987: Splashing a ship with collision-generated spray. *Cold Reg. Sci. Tech.*, **14(1),** 65-83.

Zakrzewski, W. P., and E.P. Lozowski, 1987: The application of a vessel spraying model for predicting the ice growth rates and loads on a ship. In: Proceedings of the 9th International Conference on Port and Ocean Engineering under Arctic Conditions (POAC), Fairbanks, AS, Vol. 3, 591-603.

Zakrzewski, W. P., and E. P. Lozowski, 1991: Modelling and forecasting vessel icing. In: *Freezing and Melting Heat Transfer in Engineering*, K. C. Cheng and N. Seki, eds., Hemisphere Publishing Corp., 661-706.

Zakrzewski, W. P., E. P. Lozowski, and R. Z. Blackmore, 1988a: The use of a ship spraying/icing model to estimate the effect of the direct spray flux on the icing rate. In: Proceedings of the 4th International Symposium on Atmospheric Icing of Structures (IWAIS), Paris, 399-404.

Zakrzewski, W. P., E.P. Lozowski, and D. Muggeridge, 1988b: Estimating the extent of the spraying zone on a sea-going ship. *Ocean Engineering*, **15(5),** 413-430.

Zakrzewski, W. P., E. P. Lozowski, W. L. Thomas, M. Bourassa, R.Z. Blackmore, K. Szilder and A. Kobos, 1993: A three-dimensional time-dependent ship icing model. In: Proceedings of the 12th International Conference on Port and Ocean Engineering under Arctic Conditions (POAC), Vol. 2, Hamburg, 857-873.

Zhuang, Y., E. P. Lozowski, J. D. Wilson and G. Bird, 1993: Sea spray dispersion over the ocean surface: a numerical simulation. *J. Geophys. Res.* **98(C9),** 16547-16553.

2. AN HEURISTIC MODEL OF VESSEL ICING[1]

The heuristic model of vessel icing presented here and by Blackmore and Lozowski (1994) is developed under the modelling rationale given at the end of Chapter 1, and is intended for the purpose of exploring and investigating vessel icing physics. We suggest a theoretical framework for vessel icing based on the sequence of physical processes which constitute ship icing. Such a framework may be used to help maintain the "big picture" of vessel icing physics, allowing work to proceed on aspects of the problem while keeping the overall context and perspective. As an example, we present the following heuristic model which accounts for the four vessel icing subprocess areas as presented in Chapter 1. The four subprocess areas are (1) the state of the atmosphere and ocean, (2) vessel dynamics/spray generation hydrodynamics, (3) thermodynamics and dynamics of spray, and (4) thermodynamics and hydrodynamics of icing surfaces. In addition to modelling with these four subprocess areas of vessel icing in mind, we attempt to produce a model characterized by simplicity, and universality, with icing severity indicated on a numerical scale. In addition the model is to be heuristic in nature and purpose, being readily modifiable and useful for the exploration and investigation of various aspects of vessel spray icing.

Therefore, the present work introduces a physical-empirical model in which the many assumptions used are stated explicitly, and in which empiricism is limited to a single component of the model. An empirical submodel is used to describe the vessel's spray generation, and calibration of this submodel is based on ship spraying field data. As an heuristic model it has the potential for investigating many aspects of ship icing but one question was considered central at the outset. This question has to do with the relative importance of the physical processes in the spray cloud as compared to the processes at work on the icing surfaces in bringing about ice accumulation. With this purpose in mind, the model was formed in such a way that the in-cloud dynamics and

---

[1] A version of this chapter has been published. Blackmore and Lozowski (1994). Int. J. Offshore Polar Eng. 4(2): 119-126.

thermodynamics are of primary importance in the model's physics. This is contrary to most vessel icing models which either neglect the spray phase of ship icing outright or emphasize the icing surface physics with only a partial attempt to consider the spraying subprocesses.

In the following sections the model is described, its performance is compared with data and with the performance of other models, and its sensitivity is examined. Finally, as a secondary demonstration of the model's heuristic potential, a mechanism for severe icing is hypothesised as an example, included in the model physics, and then explored.

2.1 Basic Model Assumptions

In an attempt to increase their usefulness, many vessel icing models maintain generality by neglecting vessel size and shape altogether. We suggest simplicity as an alternative, and model vessel shape and size above the water line by the vessel's length, L, beam, B, and freeboard, F_B, as shown in Fig. 2.1. The resulting rectangular parallelepiped collects spray and accretes ice only on the upper rectangular surface. The collected spray is assumed to pass through the vertically oriented access "windows" (shown in Fig. 2.1) on the perimeter of the upper surface. The wind accelerates the spray in such a way that it passes through one of these access windows and impinges on the rectangular upper surface representing the vessel's top side. The total flux of brine is a product of the spray flux intensity and the upwind projected area of the access window. This projected area depends not only on the vessel's length and beam but also on the vessel's encountering angle. The encountering angle describes the vessel's orientation to the waves and is defined as the angle between the direction of wave travel and the direction of the ship's heading. The encountering angle is 180° for head seas, 90° for beam seas and 0° for following seas.

The model avoids the complication of cyclical spray generation due to periodic encounter with waves by assuming continuous spray. This simplification may have important ramifications. Brown and Roebber (1985) suggest that the rapid temporal variation in spray observed over vessels is likely to have a significant effect on the mass

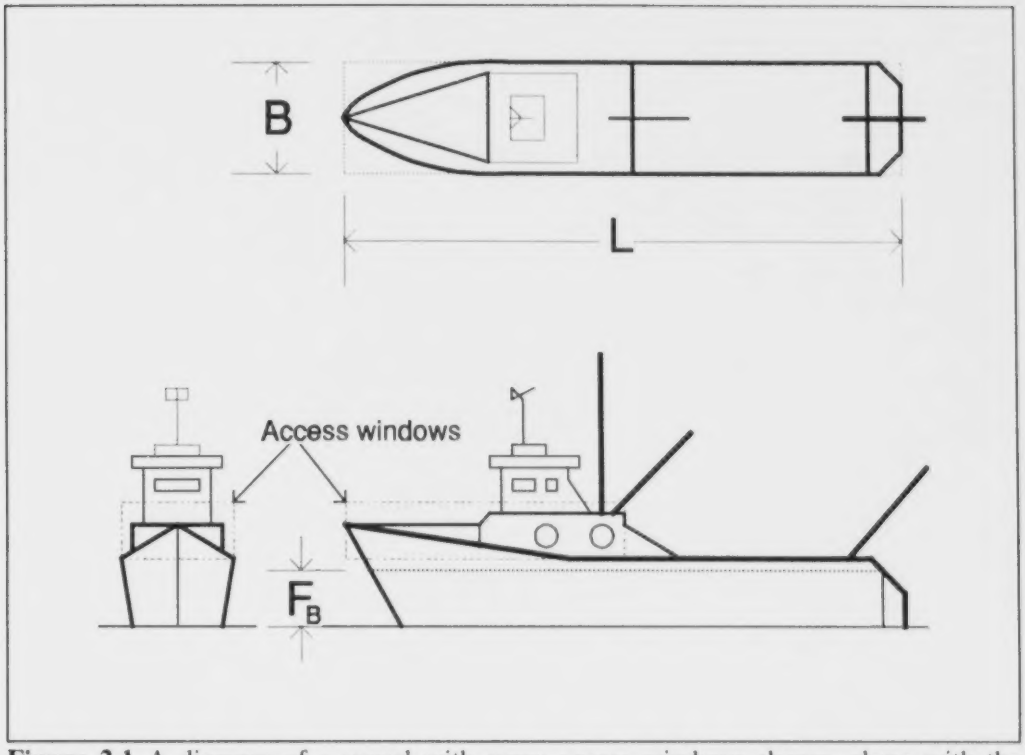

Figure 2.1 A diagram of a vessel with spray access windows shown, along with the characteristic rectangle in plan view.

and energy transfers at the ice accretion surface. Modelling these surface processes is difficult, but modelling intermittent spray delivery itself may be even more difficult, since the frequency, intensity and distribution of spray probably depends in a complex way on seastate, vessel operation and hull design.

The complexities inherent in the dynamic and thermodynamic evolution of sea spray are sidestepped by assuming that the attainment of dynamic and thermodynamic equilibrium is complete before the spray impinges on the vessel. Thermodynamic equilibrium here means that the entrained air, which is initially at the ambient temperature, T_a, comes to thermal equilibrium with the spray brine. The temperature of the spray over the vessel, T_s, therefore, is assumed to be the temperature of both the air and brine in the spray downwind of the access window. In this way, the spray brine undergoes cooling from the sea-surface temperature, T_{ss}, to the spray temperature, T_s.

The concept of dynamic equilibrium is invoked to describe the generation and rafting of spray over the vessel. Initially at rest relative to the vessel, spray droplets are accelerated by the wind to the final horizontal spray speed, V_s, in the frame of reference of the vessel. The spray-entrained air decelerates from an initial relative speed, V_a, to that of the spray, V_s. The environmental wind field is assumed to be uniform both vertically and horizontally, with deformation by both the spray cloud and the vessel neglected.

Blackmore and Lozowski (1992) suggest that a vessel enveloped in a spray cloud that is hypothesized to be continuous would eliminate much of the need for the conventional convective heat transfer approaches typically seen in numerical vessel spray icing models. The spray moves through the access window and over the vessel. The air is warmed by interaction with the droplets of brine, and flows over the vessel even after the spray falls out on to the vessel. Blackmore and Lozowski (1993) offer the assumption that there may be negligible turbulent transport or mixing of colder external environmental air to the vessel's surface, at least over the components of the vessel which are experiencing spray collection. Furthermore, there may be little convective loss of heat from the vessel's icing surfaces to the air, because the entrained air has the same temperature, T_s, as the deposited droplets that form the outer skin of the liquid film on the vessel's icing surfaces. Therefore, the heat transfer modelling normally used to account for convective heat loss from the various components on the vessel may be neglected, at least within the context of a model such as the present one, which invokes thermodynamic equilibrium in a steady two phase flow consisting of air and liquid droplets.

Another thorny modelling issue often dealt with only in more complex physical-empirical models is the inclusion of brine in the growing spray ice, also known as spongy growth. We assume that the spray ice is solid primarily to maintain the model's simplicity. However, we also suggest that if supercooling in the liquid film is responsible for ice accretion sponginess (Makkonen, 1987), it must also be responsible for a decrease in the temperature difference between the liquid film and the airstream. An increase in spray ice mass accretion as a result of an increase in sponginess might be partially offset by the reduction that would accompany the decrease in overall heat loss. In this way

modelling the ice accretion mass may be largely insensitive to the supercooling-sponginess assumption used. Since we cannot resolve this question here, the ice accretion temperature is set equal to the equilibrium freezing temperature of the surface runoff brine, and the accretion is assumed to be solid, which is appropriate for a liquid film without supercooling. The performance of the spongy spray icing model presented in Chapter 3 shows (Fig. 3.10) that as spray supercooling decreases, the sponginess of accreted ice is also likely to decrease until the accretion consists of solid ice.

The growth of ice is modelled in a simple way that is independent of the hydrodynamics of the surface brine. For the present we will discuss only the case of supercooled spray. This supercooling heat flux from the spray brine needed to generate a non-supercooled liquid film, balances the latent heat release at the icing surface. This heat balance is used as the basis for calculating the rate of ice growth. In so doing, many issues such as salt mass balance, surface brine film run-off patterns, and liquid entrapment may be either dealt with in simple way or may be set aside.

The model output consists of an overall vessel ice accretion rate and a characteristic ice thickness growth rate based on the supposition that the ice accretes uniformly. Ten input parameters are used: (1) the wind speed, V_w, (2) the ship's speed, V_v, (3) the encountering angle, α, (4) the fetch, F, (5) the air temperature, T_a, (6) the sea-surface temperature, T_{ss}, (7) the sea-surface salinity, S_{ss}, (8) the vessel length, L, (9) the vessel beam, B, and (10) the freeboard, F_B.

2.2 Modelling Spray Dynamics

Brine droplets ejected from the sea surface by collision with the vessel are prone to a greater momentum exchange with the wind than is bulk seawater closer to the sea surface. The wind is probably responsible for the majority of the spray droplet separation and acceleration from the collision-generated jet of seawater. Our description of the spray rafting process is based on conservation of momentum. Since little is known about the collision-generated jet we assume a homogeneous source region for the rafted spray. We associate this source region with the spray access window by assuming that the brine

from the jet is transformed into spray at or near the spray access window. Therefore we are suggesting that at the window, the momentum of the upstream environmental air is distributed between the spray-entrained air and the airborne brine of the spray cloud. Another of our premises is that the brine in the spray jet initially has no momentum relative to the vessel. The vessel is also presumed to have only a constant linear velocity relative to the sea surface. We further assume that the air and brine reach a final velocity, V_s, in an inertial coordinate system fixed to the vessel. The resulting momentum conservation can be expressed as:

$$\rho_a V_a = w V_s + \rho_a V_s \tag{2.1}$$

where ρ_a is the density of the air, V_a is the upstream environmental air speed relative to the vessel, V_s is the spray speed (i.e. air and droplet speed) downstream of the access window, and w is the average liquid water content of the spray cloud. The terms in Eqn. 2.1 may be interpreted as either momentum per unit volume (i.e. $kgms^{-1}m^{-3}$) or as mass flux intensities (i.e. $kgm^{-2}s^{-1}$). Therefore, Eqn. 2.1 can be rewritten as:

$$R_{ae} = R_{ws} + R_{as} \tag{2.2}$$

where R_{ae} is the mass flux intensity of the environmental air flow, R_{ws} is the flux intensity of the spray liquid, and R_{as} is the flux intensity of the entrained air. The terms flux intensity or flux are used hereafter to mean mass flux intensity, as defined above. The present model also assumes that a homogeneous brine flux intensity characterizes the entire cloud. Such effects as varying liquid flux intensity with height and with distance from the spray access window are therefore not accounted for.

2.3 Modelling Spray Thermodynamics

The spray brine is cooled by the entrained air from T_{ss} to T_s, and the rate of heat loss, q_b, for the flux of spray passing through the access window is:

$$q_b = c_w R_{ws} A (T_{ss} - T_s) \tag{2.3}$$

where c_w, the specific heat of pure water, is used to represent the specific heat of sea water, A is the area of the spray access window, T_{ss} is the temperature of the sea surface, and T_s is the spray temperature. The forced convective heat transfer which is primarily responsible for this energy exchange is dependent on the relative motion between the spray droplets and the air. Thus, a further implicit assumption of the model is that thermodynamic equilibrium must be attained either before or at the same time as dynamic equilibrium.

The rate of heat gain by the air is q_a:

$$q_a = c_p R_{as} A (T_s - T_a) \tag{2.4}$$

where c_p is the specific heat of air at constant pressure and T_a is the environmental air temperature. Since the rate of heat loss by the brine must equal the rate of heat gain by the air (i.e. $q_a = q_b$), Eqns. 2.3 and 2.4 may be combined and used to derive an expression for the spray temperature:

$$T_s = \frac{c_w T_{ss} r + c_p T_a}{c_w r + c_p} \tag{2.5}$$

where r is the flux intensity ratio (i.e. $r \equiv R_{ws}/R_{as}$). The flux intensity ratio, r, is calculated using an empirically determined value of R_{ws} (see Eqn. 2.10a), and R_{as} from Eqn. 2.2.

2.4 Modelling Vessel Spray Flux

Collision-generated sea spray results from the vessel's interaction with waves, and therefore depends substantially on the seastate. We model seastate based on Bretschneider (1973), and assume long-crested waves, for a deep fully-developed sea. The significant wave height, H_s, and significant wave phase speed, C_s, are given by:

$$H_s = A_1 \left(\frac{U^2}{g} \right) \tanh \left[B_1 \left(\frac{gF}{U^2} \right)^{m_1} \right] \tag{2.6a}$$

$$C_s = A_2 U \tanh\left[B_2\left(\frac{gF}{U^2}\right)^{m_2}\right] \qquad \textbf{(2.6b)}$$

where U is the wind speed (ms^{-1}) at the 10 meter height, F is the fetch (m), g is the gravitational acceleration (ms^{-2}), and A_1=0.283, B_1=0.0125, m_1=0.42, A_2=1.2, B_2=0.077, and m_2=0.25. Eqns. 2.6a and 2.6b are valid for the wind speed range 10 to 100 knots (5.1 to 51.4 ms^{-1}) and for the fetch range 1 to 1000 nautical miles (1.85 to 1852 km). Since Eqns. 2.6a and 2.6b are deep sea equations, and since the group speed for short waves on a deep sea is half the phase speed (i.e. $C_g=C_s/2$), the group velocity is readily available for use in the spray generation equations developed below. Following Horjen and Carstens (1989), we suggest that spray generation is related in a simple way to the rate of power transmission by the waves in the vessel's seaway, Doppler shifted by the vessel's motion. The wave power encountered per unit width of vessel exposure to the waves is (Khandekar, 1989):

$$P_w = \frac{1}{8}\rho_w g H_s^2 C_{gr} \qquad \textbf{(2.7)}$$

where ρ_w is the density of seawater, H_s is the significant wave height, and $\mathbf{C_{gr}}$ is the magnitude of the group velocity relative to the vessel (Fig. 2.2). We assume that the vessel moves steadily through the wave field without acceleration from either ship/wave interaction or from a change in course. The group velocity relative to the vessel, shown in the vector triangle on the left in Fig. 2.2, can be represented by the vector equation:

$$\mathbf{C_{gr}} = \mathbf{C_g} - \mathbf{V_v} \qquad \textbf{(2.8)}$$

where vectors are represented in the text with bold type, and where $\mathbf{V_v}$ is the vessel's velocity, and $\mathbf{C_g}$ is the group velocity of the significant waves. The group velocity in Eqn. 2.8 may be interpreted as either the velocity of wave energy (i.e. as in Eqn.2.7), or as the velocity of a group of waves.

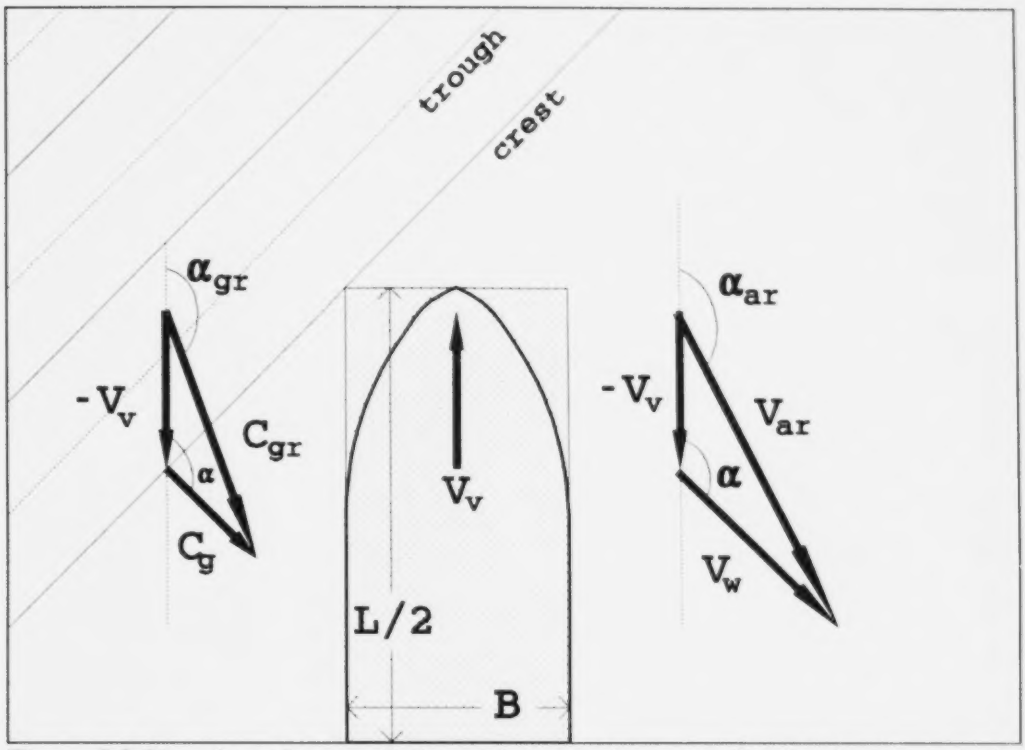

Figure 2.2 Plan view of a vessel's bow relative to the waves. Wind and group velocity vector triangles are shown on the right and left, respectively.

In order to justify a functional form for F_{ws}, the spray flux impinging on the vessel, per unit width of the vessel's upwind projected breadth of wave exposure (units of $kgm^{-1}s^{-1}$), the Buckingham Π theorem may be invoked. The variables assumed to be important are, ρ_a the air density, H_s the significant wave height, F_B the freeboard, and C_{gr} the relative group velocity. We sought a functional form similar to that of Eqn. 2.7 on the hypothesis that wave power is related in a simple way to spray generation. Therefore, $\mathbf{F_{ws}}$ may be written as:

$$\mathbf{F_{ws}} = K \rho_a \frac{H_s^2}{F_B} \mathbf{C_{gr}} \qquad \textbf{(2.9)}$$

where the constant K may be thought of as the dimensionless group formed from the selected variables which produces an equation for $\mathbf{F_{ws}}$ that is similar in form to Eqn. 2.7.

The freeboard is included in Eqn. 2.9 because we expect that the collected collision-generated spray mass will decrease with an increase in freeboard. Since F_{ws} is a function of R_{ws} and Z, the spray access window height (i.e. $F_{ws}=R_{ws}Z$), we propose that:

$$R_{ws} = k_r \rho_a \left(\frac{H_s^2}{F_B} \right) \tag{2.10a}$$

$$Z = k_z C_{gr} \tag{2.10b}$$

where k_r and k_z are empirical constants with units of s^{-1} and s, respectively. It can be shown that k_r and k_z are 0.15 s^{-1} and 0.085 s, respectively. These values are derived in Appendix 1 on the basis of field data for spraying of the Soviet medium-sized fishing vessel (MFV) "Narva" (Zakrzewski, 1987).

The central rationale for the partition of Eqn. 2.9 into Eqns. 2.10a and 2.10b is that Eqn. 2.10b follows the form of the equation for the maximum height of spray over a Soviet medium-sized fishing vessel (Zakrzewski et al., 1988). This equation is given in Appendix 1 as Eqn. A1.6 (i.e. $Z_{max}=0.535V_r$). However, Eqn. 2.10a contains the ratio (H_s/F_B) which is known to be important in the seakeeping of vessels, and Kachurin et al. (1974) suggest that the liquid water content over a vessel may depend on the significant wave height (i.e. $w=\xi H_s$, $\xi=10^{-4}$ kgm^{-4}). Both H_s and the ratio H_s/F_B are contained in Eqn. 2.10a and may help to give a partial explanation for its form.

In order to derive equations for spray generation for the entire vessel, the angle of encounter with the relative group velocity, and the magnitude of the relative group velocity C_{gr} need to be calculated. The magnitude of the relative group velocity, C_{gr}, is used in Eqn. 2.10b to determine the time-averaged spray access window height, Z. The equations required to solve for C_{gr} and α_{gr} are derived in Appendix 2.

In order to calculate the final velocity and temperature of the spray, the value of the air velocity relative to the vessel (V_a in Eqn. 2.1) must be known. Therefore, in an analogous manner to that used above for $\mathbf{C_{gr}}$, the velocity of air relative to the vessel, $\mathbf{V_{ar}}$ is determined by the vector equation:

$$\mathbf{V_{ar} = V_w - V_v} \qquad (2.11)$$

The vector triangle on the right in Fig. 2.2 shows this vector sum. The method and equations used to solve for V_{ar} and α_{ar} are given in Appendix 2.

The hydrodynamics of the spray jet during the interaction of the vessel's hull with waves are poorly understood. Even though the recent splash-generation experiments of Sampson et al. (1996) compare very well with the scale-model bow splashing experiments of Chung (1995), much research remains to be done on the hydrodynamics of the brine-hull interaction. Determining the extent of spray generation along the vessel's perimeter remains a difficult problem. We suggest, as a first attempt at a spraying submodel, that the hull/wave interaction produces a spray jet along half the vessel's length. Zakrzewski et al. (1988) give data which suggests that for a 25 ms^{-1} wind speed and beam seas, the extent of spray generation may approach half the vessel's length (i.e. 0.44L). Spray generation over half the vessel length may therefore be an overestimate. In the model we assume that the spraying occurs along the port side of the vessel but by symmetry of the process, the results apply equally well for spraying on the starboard side. The extent of the spray jet along the perimeter of the ship, along with the encountering angle, α_{gr}, allows the determination of the upwind projected width of the spray access window, P. The equations for the projected width and their derivation are given in Appendix 2. The spray access window area is therefore:

$$\mathbf{A = PZ} \qquad (2.12)$$

Fig. 2.3 shows that the relative group velocity, $\mathbf{C_{gr}}$, is perpendicular to the projected width, P, and that the relative wind velocity, $\mathbf{V_{ar}}$, is not (even though the absolute wind and group velocity are parallel). Therefore, only that component of $\mathbf{V_{ar}}$ along $\mathbf{C_{gr}}$ is perpendicular to the width P. This component of the relative wind is assumed to be the source of momentum for the spray. This component of the relative wind vector is defined here to be $\mathbf{V_a}$, and its magnitude, V_a, was used in Eqn. 2.1 to determine the momentum available for the rafting of spray over the vessel. The particulars of the derivation and use of V_a in the model are given in Appendix 2.

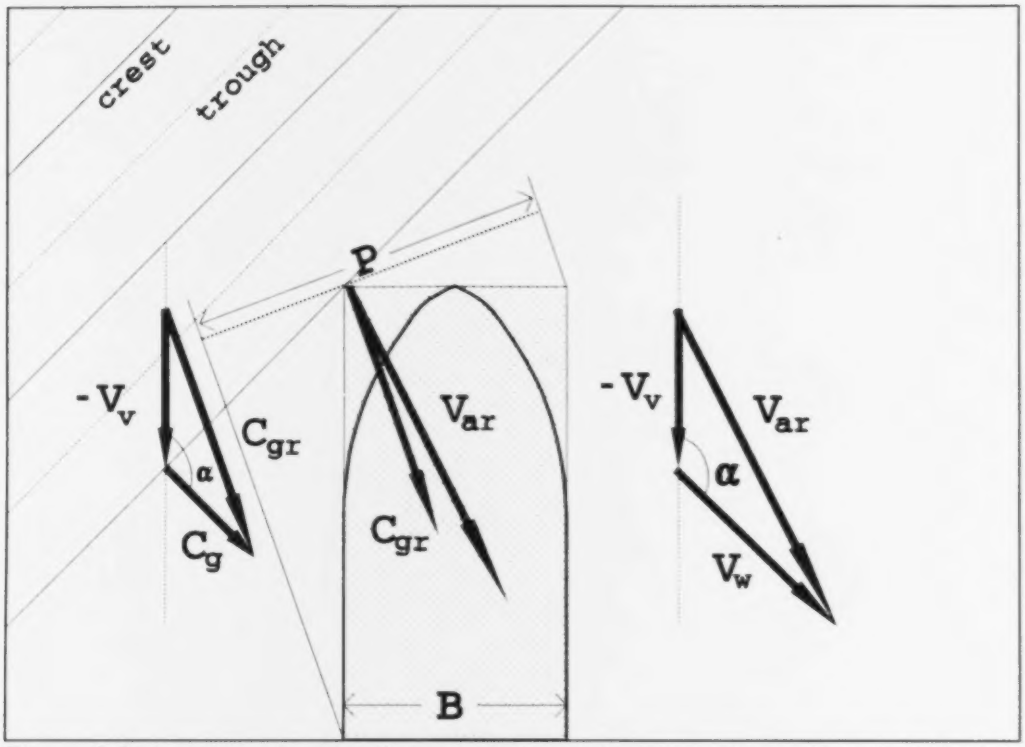

Figure 2.3 Plan view of a vessel's bow relative to the waves. The projected width, P, is shown with the relative wind and group velocity vectors.

Since the projected width of the spray access area, and the flux intensity of spray have now been determined, the overall spray flux, F_v, is:

$$F_v = AR_{ws} \tag{2.13}$$

Under actual spraying conditions, a portion of the spray is collected by the vessel and the remaining spray passes over and around it, back to the sea. We assume that all the spray passing through the access window (i.e. F_v, Eqn. 2.13) impinges on some surface of the vessel. That spray which passes around the access window returns directly to the ocean.

2.5 Modelling Supercooled Spray Ice Accretion

The primary assumption here is that the spray is cooled by the environmental air in such a way that the droplets may supercool below the brine's equilibrium freezing temperature. In the model, if the spray supercools, icing is predicted, and if the spray does not supercool, icing is not predicted. Therefore, we suggest that for the purpose of a simple model, the in-cloud heat loss associated with the supercooling of the collected brine flux, q_s, may be set equal to the flux of latent heat associated with the vessel's ice accretion rate, q_{lf}. This leads to:

$$c_w R_{ws} A(T_f - T_s) = L_f I_s \tag{2.14}$$

where T_f is the freezing temperature of the brine, L_f is the latent heat of fusion, here approximated as the latent heat of fusion for pure water, and I_s is the overall ice accretion rate for the vessel under the supercooling scenario. The heat balance expressed in Eqn. 2.14 is different from the heat balances used in most spray icing models in that it assumes a final thermodynamic equilibrium between the spray liquid and the entrained air as opposed to the more traditional summation of heat transfer components at the icing surface.

The equilibrium freezing temperature of brine, T_f, which is required for the heat balance in Eqn. 2.14, has been expressed as a function of salinity, S_b, by Makkonen (1987) as:

$$T_f = -54S_b - 600S_b^3 \tag{2.15}$$

The overall vessel icing rate, I_s, may then be expressed as:

$$I_s = R_{ws} A \frac{c_w}{L_f}(T_f - T_s) \tag{2.16}$$

Once the overall vessel icing rate is known, the thickness growth rate, typically in cm hr^{-1}, can readily be determined using the assumption that ice accretes on only half of the model's rectangular topside area. In general, ice forms forward for head seas, aft

for following seas, and on the windward side for beam seas (BSRA, 1957; Hayhoe, 1989). Nevertheless, our assumption represents a considerable simplification in the modelling of spray ice distribution. No specific assertion concerning the distribution of ice on an actual vessel's superstructure or deck is intended or possible with this model.

Using the rectangular topside model of a vessel along with the above ice distribution rationale leads to:

$$h_s = \frac{I_s}{\rho_i\left(\frac{BL}{2}\right)} \tag{2.17}$$

where h_s is the ice growth rate for the vessel, and ρ_i is the density of the ice accretion taken to be that of pure ice, $\rho_i = 917\ kgm^{-3}$.

2.6 Modelling Nucleated Spray Ice Accretion

As mentioned above, the present model is intended for investigative purposes, and because it has a relatively uncomplicated structure, it may be modified to examine different aspects of the problem. In order to demonstrate this capability, we present model and equation development which is used to explore a hypothesized severe icing mechanism, namely nucleated spray. In a later section, the model will be compared with data that may represent severe icing cases.

The modified or nucleated model's premise is that the sea spray droplets freeze partly in transit and hence contain ice crystals in such quantity that the temperature of the droplets is well represented by the equilibrium freezing temperature of the unfrozen brine in the droplet. The source of the ice nuclei is unclear, but we hypothesize three possibilities. The first is that frazil ice or grease ice (Martin and Kauffman, 1981) may be present in the sea as a result of sufficient heat loss to the air under conditions of wave induced turbulence. Recent work in the Weddell Sea for example (Weeks and Ackley, 1982) has shown that sea ice may consist of more than 50% frazil. Even though frazil ice formation is less likely in the Arctic basin, the Labrador Sea, and other areas

frequented by vessels, than in the Weddell Sea, we propose that this is a possible mechanism for nucleated sea spray.

A second hypothesized mechanism is the nucleation of spray droplets as a result of cooling during the rafting of the spray (Makkonen, 1989; Sackinger and Sackinger, 1987). Szilder et al. (1991) postulate that an observed increase in ice island building rate for air temperatures less than -20°C might be due to the mechanism of droplet nucleation. Apart from low air temperatures, the conditions required to trigger this mechanism in vessel spray icing are unclear.

A third possible mechanism for the introduction of ice crystals into the spray is snow. Brown and Roebber (1985) show that 62.8% of a group of 960 Canadian Coast Guard icing reports included references to snow. They recommend further that work be done on mixed snow and spray, and suggest that snow may have an important effect on ship icing. Horjen (1990) found theoretically a 200 to 270% increase in the spray icing load during snowfall (snow concentration of 0.28 gm^{-3}) over that without snow, for gale conditions (18-20 ms^{-1}). Unlike Horjen (1990), however, we do not account for, or include, the accumulation of actual snow mass within the growing ice on the vessel. Another significant effect that snow may have on ship icing is to cool the sea surface to the freezing point, and then become a source of ice particles for the sea-surface brine, after it has reached the freezing temperature. Thus prolonged snowstorm conditions may help reduce sea temperatures and set the scene for nucleated spray.

In order to derive an equation for the ice growth rate under nucleation conditions, we equate the in-cloud heat gain by the air (Eqn. 2.4), q_a, to the sum of q_{lf}, the flux of latent heat associated with the ice formation, and q_{ws}, the sensible heat given up by the brine. The heat balance equation is:

$$c_p R_{as} A(T_s - T_a) = L_f I_n + c_w R_{ws} A(T_{ss} - T_s) \qquad \textbf{(2.18)}$$

where T_s represents the spray temperature and where I_n is the overall ice accretion rate for the vessel under the nucleation assumption. The spray temperature, T_s, of Eqns. 2.18 and 2.19, is assumed to be the final equilibrium temperature of the nucleated spray (i.e. a mixture of ice and brine) that impinges on the vessel. Therefore, as is explained in

more detail below, the ice-brine mixture is at the equilibrium freezing temperature of the brine. For this reason we suggest that the spray temperature is the equilibrium freezing temperature of the liquid portion of the spray (i.e. $T_s=T_f$), which results in a heat balance very different from that of the supercooled vessel icing model of Section 2.5 (Eqn. 2.16). The overall vessel icing rate with the nucleated spray assumption, I_n, is:

$$I_n = R_{ss}A\left(\frac{c_p}{L_f}\right)(T_s - T_n) - R_{ws}A\left(\frac{c_w}{L_f}\right)(T_{ss} - T_s) \qquad (2.19)$$

As with the supercooled icing model, we assume that all of the spray ice is accreted on the vessel, and that the ice forms a solid deposit without entrapped brine. This assumption is used here as the basis for modelling the conservation of salt mass, and ultimately as the basis of another equation for I_n. The rate of salt mass collection inherent in the brine impinging on the vessel (i.e. the term on the left side of Eqn. 2.20) must balance the rate of salt mass runoff (i.e. the term on the right side of Eqn. 2.20):

$$R_{ws}AS_{ss} = (R_{ws}A - I_n)S_{ro} \qquad (2.20)$$

where S_{ss} is the salinity of the sea surface (i.e. the initial brine salinity), and S_{ro} is the salinity of the runoff brine that returns to the sea. Eqn. 2.20 is rearranged so as to give a second equation for the nucleated ice accretion rate:

$$I_n = R_{ws}A\left(1 - \frac{S_{ss}}{S_{ro}}\right) \qquad (2.21)$$

Since the mass of ice formed during the spraying process is assumed to stay on the vessel as a solid deposit, the concentrated spray brine salinity and the runoff brine salinity are reasoned to be the same. In this way, the salinity of the run-off brine and the spray temperature can be related through the equilibrium freezing relationship (Makkonen, 1987) as:

$$T_s = -54S_{ro} - 600S_{ro}^{\ 3} \qquad (2.22)$$

Eqns. 2.19, 2.21 and 2.22 are solved for the three variables I_n, T_s, and S_{ro} using

the bisection method (Press et al., 1990, p. 243). Once I_n is known, the ice thickness growth rate, h_n, can be calculated in a way analogous to Eqn. 2.17.

2.7 Model Evaluation

In order to test the model, a group of sixty icing events was chosen from the Zakrzewski and Lozowski (1989) data set. Cases were selected where all the required input variables were listed or where a reasonable estimate for a missing value could be given, especially missing parameters with low model sensitivity. Where the original data contains a parameter range, an average over the range was used in the model evaluation. A sea-surface salinity of 32.5 ppt was assumed for all events except those from the Baltic Sea where 5 ppt was used. For most of the selected cases, vessel length, beam, and freeboard are specified by Zakrzewski and Lozowski (1989), but sometimes only vessel length is available. In these cases beam and freeboard were estimated using geometrical similarity to the Soviet MFV. The seastate in all cases was modelled on the assumption of a 200 nm fetch with a fully developed sea. The only exceptions were cases from the Baltic Sea for which a fetch of 100 nm was used. Where ice growth rates in cm hr^{-1} were given in the data, they were converted to data icing rates in tonnes hr^{-1} using Eqn. 2.17. These data are listed in Appendix 3.

The model's performance was subjected to the statistical analysis recommended by Willmott (1982). In this approach a number of statistics are reported including, (1) the number of data (N), (2) the observed and predicted mean values (OM, PM), (3) the observed and predicted standard deviations (OSD, PSD), (4) the slope and y-intercept of the regression line (b, a), (5) the mean bias error and the mean absolute error (MBE, MAE), (6) the root mean square error (RMSE), (7) the systematic and unsystematic RMSE ($RMSE_s$, $RMSE_u$), and (8) the Willmott index of agreement (d). Even though Willmott (1982) suggests that the coefficient of determination, r^2, is of little importance in model evaluation, we report it because of its familiarity. These statistics were calculated for predictions made by (1) the Blackmore and Lozowski (1994) heuristic model with supercooling spray (BLS), and (2) a version of the Kachurin et al. (1974)

nomogram computerized by the AES of Canada (KA model) for the sixty cases of the above mentioned data set. The statistics are presented in Tables 2.1 and 2.2.

TABLE 2.1 Icing event statistics for comparing the performance of the BLS model and the KA model against each other and data. All statistics have units of tonnes hr^{-1}, except b.

	OM	PM	OSD	PSD	b	a
BLS	2.27	2.30	2.05	2.52	0.875	0.307
KA	2.27	2.44	2.05	1.67	0.489	1.325

TABLE 2.2 Icing event statistics for comparing the performance of the BLS model and the KA model against each other and data. All statistics have units of tonnes hr^{-1}, except d and r^2.

	MBE	MAE	RMSE	$RMSE_S$	$RMSE_U$	d	r^2
BLS	0.024	1.23	1.78	0.25	1.76	0.83	0.51
KA	0.163	1.34	1.69	1.05	1.32	0.76	0.36

Fig. 2.4 shows a scatter plot for the BLS heuristic model. The OM and PM for the BLS model performance are very similar and the model shows a moderately larger standard deviation than the observations. The regression line shows a slope not far from that of the diagonal, and a low intercept value. Together, the slope and intercept imply a low bias in model performance. The MBE shown in Table 2.2 is small but the larger MAE suggests a somewhat larger variation in predicted icing rates than does the MBE. This is confirmed by the large value of RMSE in Table 2.2. With a small value of $RMSE_s$, and with an $RMSE_u$ ~ RMSE, it is apparent that the model has a small component of systematic error.

Fig. 2.4 exhibits an apparent bimodal behaviour in the range 3 to 6 tonnes hr^{-1} where the data appear to "avoid" the diagonal. This bimodality may be due to developing seas or nearshore winds (i.e. smaller H_s than expected) on the one hand, and heavier seas than expected (i.e. winds dropping off with insufficient time for appreciable wave decay or open ocean waves where the fetch is larger than expected) on the other. Comiskey et al. (1984) have also reported a bimodality like this in their model's comparison with data.

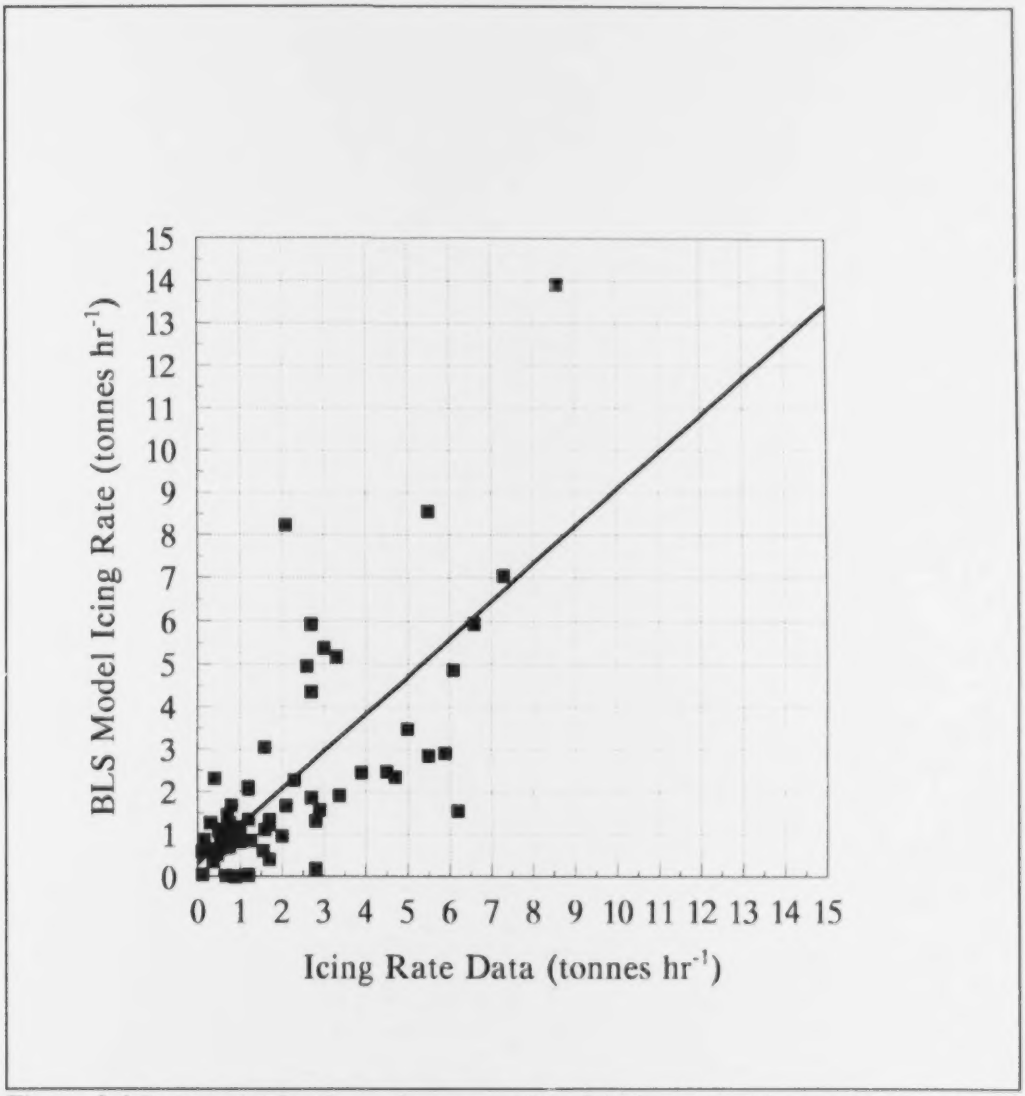

Figure 2.4 Scatter plot for the performance of the Blackmore and Lozowski supercooled model (BLS) against sixty cases of Soviet icing data from Zakrzewski and Lozowski (1989).

Fig. 2.5 shows the KA model performance compared against the same data set used for Fig. 2.4. Once again the OM and PM are similar but show a slightly larger discrepancy than for the BLS model. The PSD in this case is clearly less than that of the OSD of the data. The slope of the regression line given in Table 2.2 is low. With the high value of intercept, this suggests that the KA model performs with more bias than

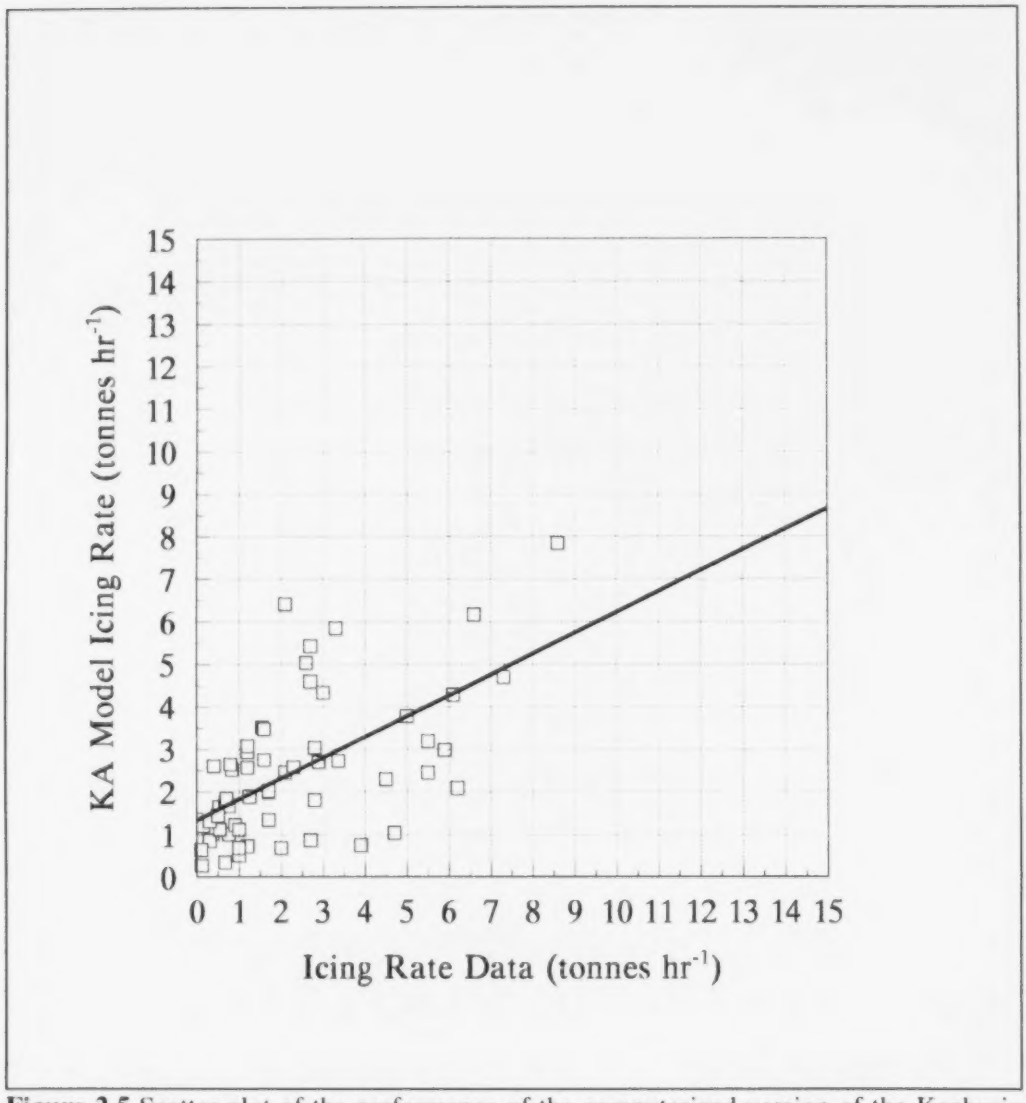

Figure 2.5 Scatter plot of the performance of the computerized version of the Kachurin et al. (1974) nomogram for sixty icing events taken from Zakrzewski and Lozowski (1989).

the BLS model. This is confirmed by the values of MBE and MAE. The KA model performance gives an RMSE which is slightly better than that of the BLS model. However, large values of $RMSE_s$ and $RMSE_u$ suggest that the KA model has a comparatively large systematic error. The Willmott index of agreement in Table 2.2 is lower than for the BLS model, but may not be significantly lower.

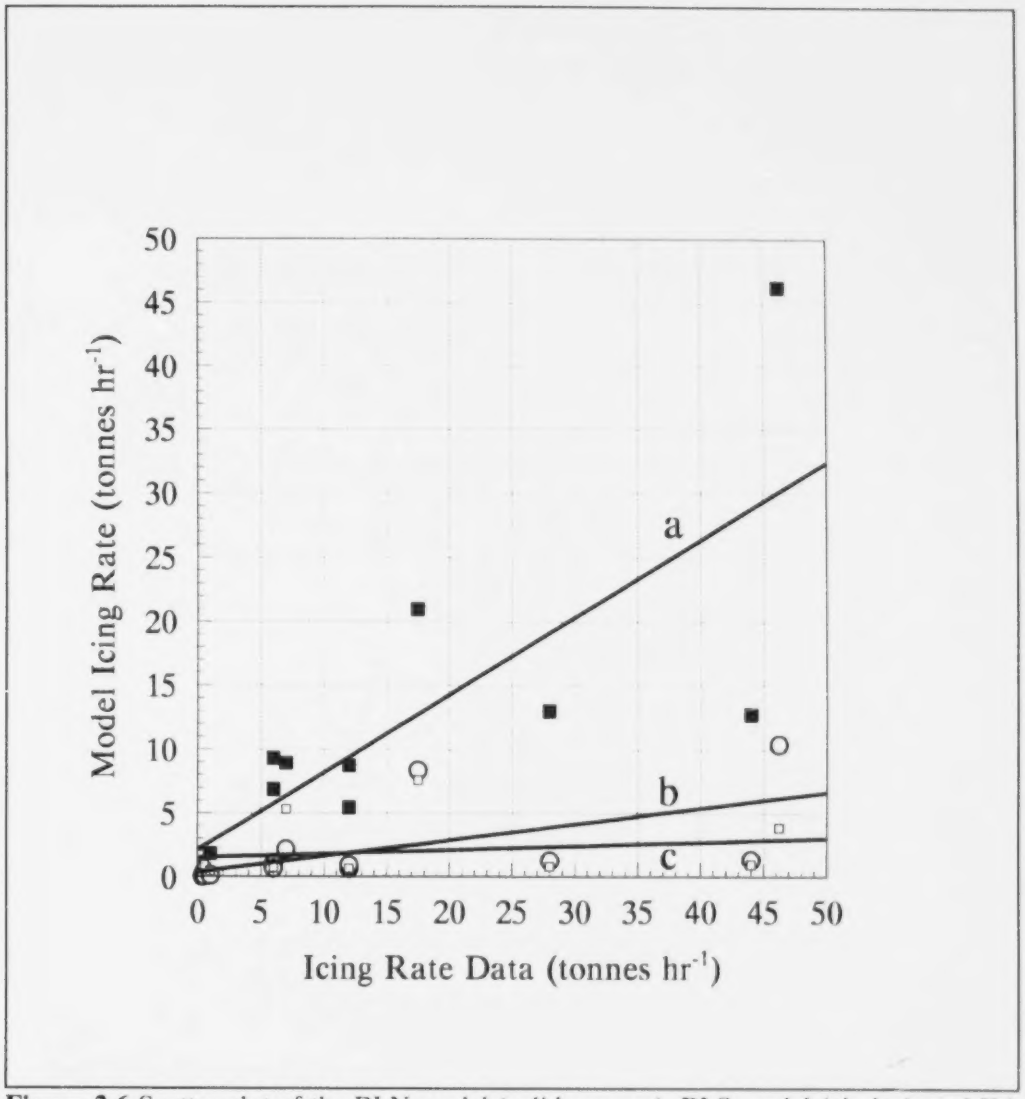

Figure 2.6 Scatter plot of the BLN model (solid squares), BLS model (circles), and KA model (small open squares) vs extreme icing data. Regression lines for (a) the BLN model, (b) BLS model, and (c) KA model vs extreme icing data.

After examining the data of Zakrzewski and Lozowski (1989) again, we found an additional twelve cases which were not included in the sixty cases used for Figs. 2.4 and 2.5. These cases were originally neglected because of what seemed to be anomalously large icing rates compared with the other data and with icing rates from the KA model (see Fig. 2.6). We suggest that these cases of anomalously large icing rate may be due

to the nucleated spraying mechanism as described in the Blackmore and Lozowski nucleated spraying model (BLN). If these cases are anomalously large because of the nucleated spraying mechanism, then aside from near-freezing sea-surface temperatures, the conditions necessary for this mechanism remain unclear and may require substantial work to identify.

In Fig. 2.6, curves "a", "b", and "c" are the regression lines for the BLN, BLS, and KA models, respectively. The slopes for curves "a", "b" and "c" are 0.61, 0.13, and 0.03, respectively, showing that the BLN model is in better agreement with observation than either the BLS, or the KA model. For the most extreme icing case in Fig. 2.6, the BLN model predicts an icing rate approximately 350% larger than the BLS model.

2.8 Model Sensitivity

The sensitivity of the BLS model was investigated for a Soviet MFV given a standard condition consisting of V_v = 1 ms^{-1}, V_w = 20 ms^{-1}, α = 180 degs, T_a = -10 °C, T_{ss} = 1 °C, and S_{ss} = 35 ppt. For fully developed seas, this condition results in a significant wave height of 6 m.

Fig. 2.7 shows the sensitivity of the BLS model to wind speed, air temperature, and sea-surface temperature. Air temperature and wind speed are influential parameters. This is in agreement with much of the vessel icing literature (Lozowski and Gates, 1985). The sea-surface temperature has a relatively mild effect on the icing rate, and qualitatively, this also agrees with the vessel icing literature (Minsk, 1977).

Fig. 2.8 shows that the model sensitivity to significant wave height and fetch may be considerable, and comparable to the influence of air temperature and wind speed (Fig. 2.7). In the present model, the significant wave height is estimated on the basis of Eqn. 2.6a, and for this reason the significant wave height and the fetch are not independent. The icing rate shows much less sensitivity to sea-surface salinity than to wave height or fetch, and indicates a decrease in icing rate with increasing salinity. Since sea-surface salinity may typically not vary strongly on the open ocean, the model suggests that this parameter may have little influence in vessel icing.

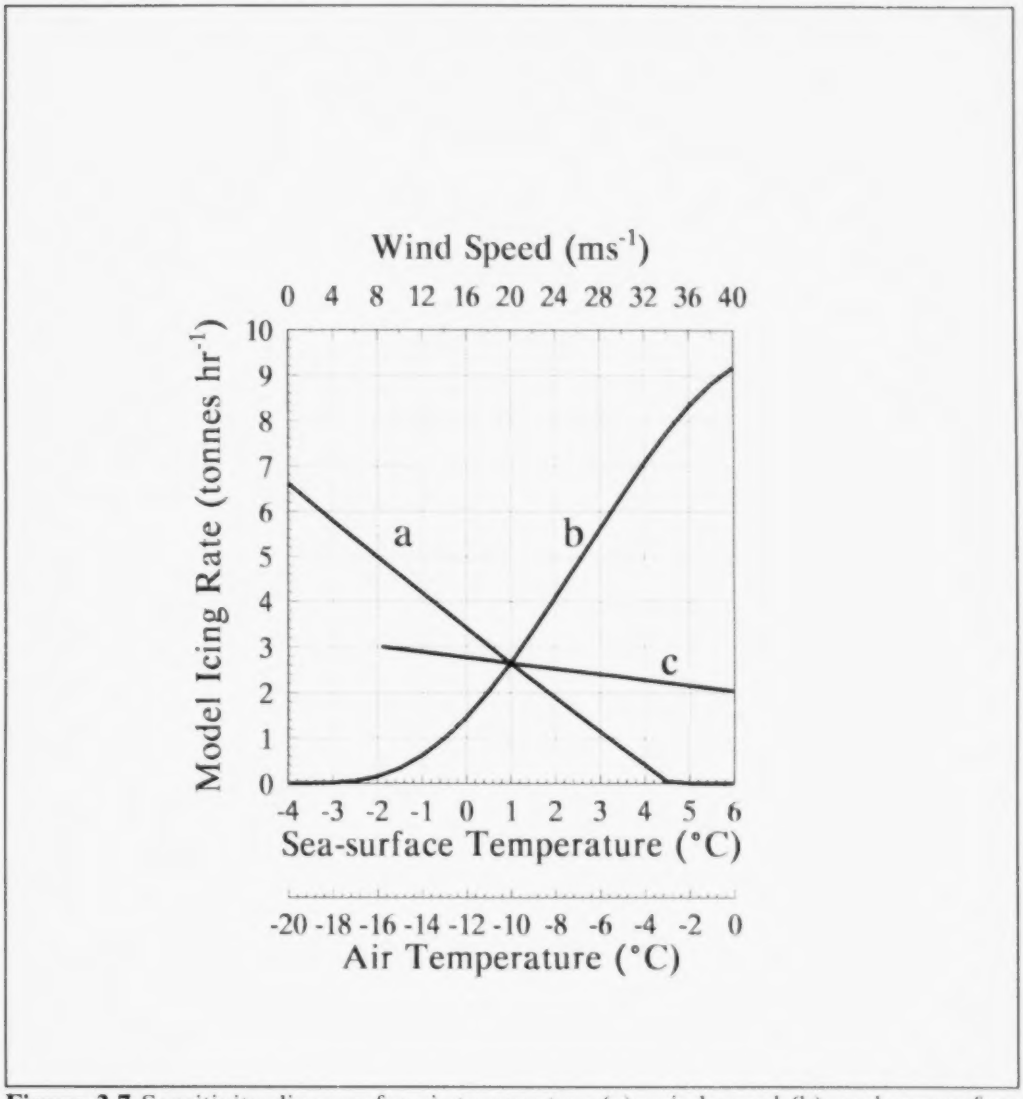
Wind Speed (ms-1)
0 4 8 12 16 20 24 28 32 36 40
Model Icing Rate (tonnes hr-1)
10 9 8 7 6 5 4 3 2 1 0
a
b
c
-4 -3 -2 -1 0 1 2 3 4 5 6
Sea-surface Temperature (°C)
-20 -18 -16 -14 -12 -10 -8 -6 -4 -2 0
Air Temperature (°C)

Figure 2.7 Sensitivity diagram for air temperature (a), wind speed (b), and sea-surface temperature (c) under the standard condition.

Fig. 2.9 shows model icing rate sensitivity to vessel speed, encountering angle, and the size scaling factor. Icing rate here has a strong dependence on the encountering angle with a maximum around 110 degrees (i.e. close to beam seas) and a minimum for following seas. The vessel speed for a Soviet MFV is limited to ~2.5 ms^{-1} for the conditions specified, and with it the icing rate is also limited. However, the model suggests that a vessel with the characteristic size of an MFV and greater speed may

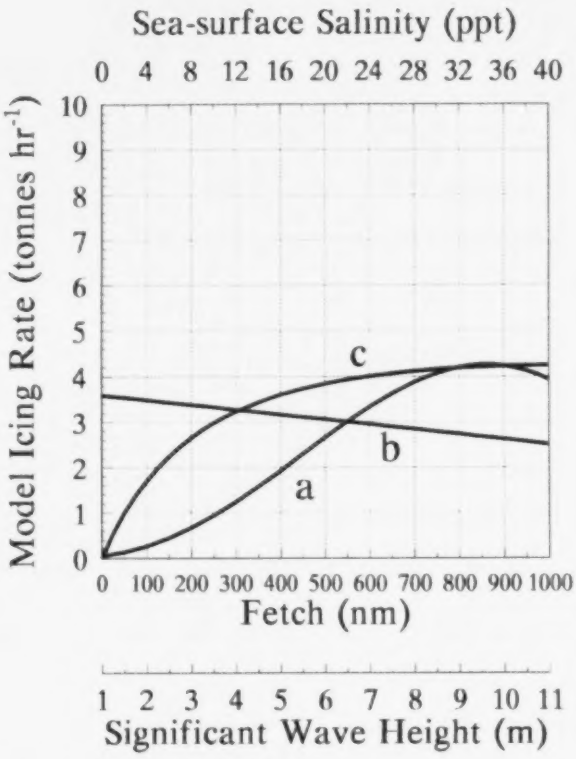

Figure 2.8 Sensitivity analysis for significant wave height (a), sea-surface salinity (b), and fetch (c) for the standard condition.

experience a considerable increase in icing. The size scaling factor was multiplied by the characteristic linear dimensions of an MFV in order to examine the ice growth rate (cm hr^{-1}) sensitivity to vessel size. The ice growth rate (ordinate on the right side of Fig. 2.9) is notably sensitive to the scaling factor for factors of 2 or less (i.e. lengths less than 80 m). Ice thickness growth rates appear to become very sensitive to scaling factor for factors less than unity, showing no icing for very small vessels and very large ice growth

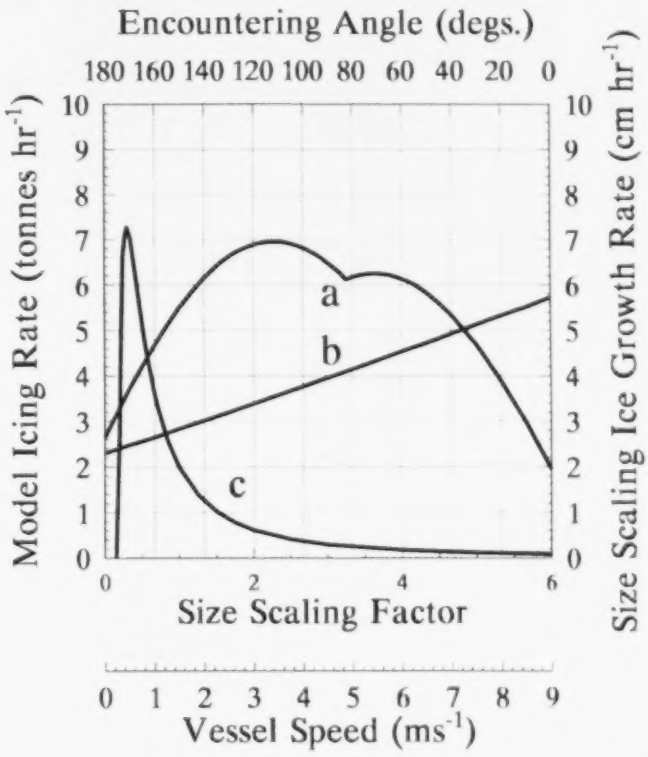

Figure 2.9 Model sensitivity to the encountering angle (a), the vessel speed (b), and the size scaling factor (c). The encountering angle is 180° for head seas, 90° for beam seas, and 0° for following seas.

rates for scaling factors in the range 0.3 to 0.4. The lack of icing associated with scaling factors close to zero is caused by a reduction in the vessel's freeboard. Eqn. 2.9 suggests an increase in spray flux with decreased scaling factor and freeboard. With a large spray flux, the entrained air may not produce spray supercooling, and hence no icing would occur. As the scaling factor becomes large, the spray flux becomes much smaller, and

this, combined with the larger accretion area, (i.e. BL/2; Eqn. 2.17) results in small thickness growth rates. For scaling factors in the 0.3 to 0.4 range, the icing rate (tonnes hr^{-1}) coincides with a relatively small vessel accretion area which accounts for the sharp peak in thickness growth rate of Fig. 2.9.

The sensitivity to scaling factor suggests that the overall mass accretion rate needs to be related to the particular vessel (i.e. to vessel size). This is because a given mass accretion rate may be insignificant for a large vessel, but disastrous for a smaller one. The smaller vessel may experience a significant increase in spray collection area and sail area (not modelled in the present work). The increase in collection area could in a time-dependent fashion accelerate the rate of ice growth and the increased sail area could increase the overturning moment for the vessel, ultimately reducing stability. Vessel icing prediction methods that do not account for the vessel size may yield underestimates of spray icing danger.

Fig. 2.10 is similar to the sea-surface temperature sensitivity diagram presented by Makkonen et al. (1991). The condition specified by Makkonen et al. (1991) is the same as the standard condition described above, except that the significant wave height is 8 m. (Fig. 2.10, curves a and b). The BLS model with an 8 m wave height (curve a) shows a larger ice growth rate than the Stallabrass (1980) model (S model), but less than the KA model or the Overland (1990) model (O model). The BLN model (curve b) shows a higher ice growth rate and a higher sensitivity than the other models with the exception of the O model.

Makkonen et al. (1991) present their diagram (similar to Fig. 2.10) to show the strong brine-temperature sensitivity of the Overland et al. (1986) algorithm at low sea-surface temperatures. In this way, they intend to support their position that the Overland et al. (1986) algorithm is theoretically deficient. Because the present work is not based on an icing surface heat balance in the way the Overland et al. (1986) algorithm is, it can shed little light on the issue except possibly in one way. Curves b and g suggest the possibility that a nucleated spray icing mechanism may be responsible for actual icing rates and icing rate sensitivities larger than would be expected with predictions from surface heat transfer models such as the Stallabrass (1980) and KA models. If this is so,

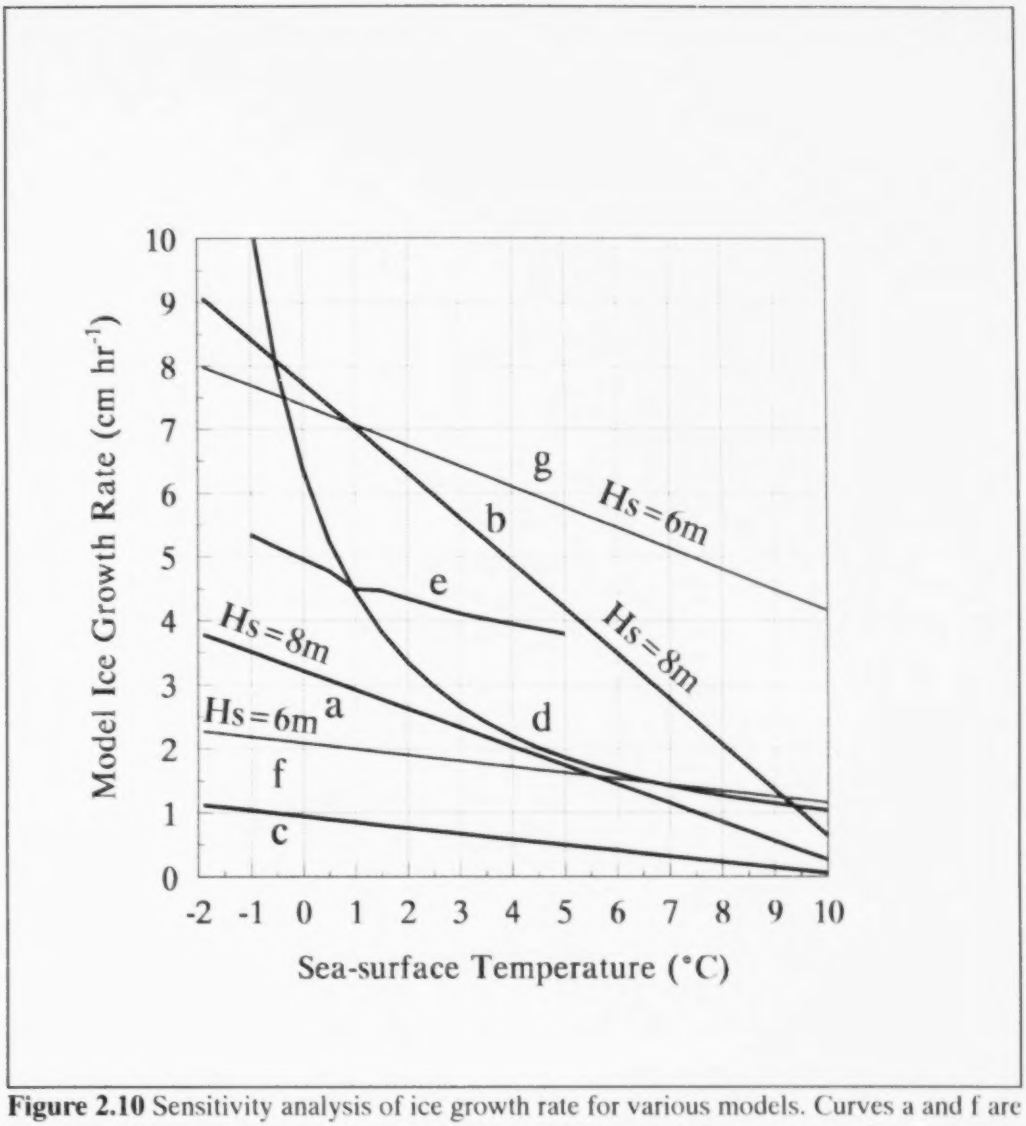

Figure 2.10 Sensitivity analysis of ice growth rate for various models. Curves a and f are for the BLS model. Curves b and g are for the BLN model. Curves c, e and d are for the S, KA, and O models.

then the data used by Overland et al. (1986) and Overland (1990) may have nucleated spraying events that coincide well with their theoretical approach to modelling. This view is supported by the BLN model's performance at low sea-surface temperatures (Fig. 2.10, curve b) where both the icing rates and icing rate sensitivity are somewhat similar to the Overland (1990) algorithm.

The BLS model reveals a significant change in sea-surface temperature sensitivity with seastate. This is apparent from Fig. 2.10 as curve "a" is for H_s=8 m and curve "f" for H_s=6 m. For a sea-surface temperature close to 5.5 °C, a change of significant wave height from 6 m to 8 m will bring little change in icing rate. It appears that for a higher sea-surface temperature (i.e. T_{ss}>5.5 °C), heavier seas mean a decrease in ice growth rate, while for a lower sea-surface temperature, heavier seas will bring an increased ice growth rate. At the "cross-over" temperature the increased potential for icing as a result of heavier seas (i.e. more spray) is just offset by the decreased potential for icing as a result of the warmer sea surface brine. For the BLN model the situation is analogous except that this "cross-over" sea-surface temperature, shown at the intersection of curves "b" and "g", is lower.

Fig. 2.10 also shows that curves a and b will intersect close to 11°C on the sea-surface temperature axis (i.e. with an ice growth rate of 0 cm hr^{-1}). This occurs because the spray supercooling in both the BLS and BLN models is 0 °C at a sea-surface temperature of about 11 °C. In this way, a limit to ice growth based on sea-surface temperature is apparent for the standard condition. This limit appears to be above the 6°C to 8°C limit proposed by some early vessel icing investigators (Minsk, 1977; Borisenkov and Pchelko, 1972). For a significant wave height of 6 m (curves f and g) this sea-surface based ice growth limit moves to a much higher temperature. A further reduction in the significant wave height causes the sea-surface temperature curve to approach the horizontal orientation, suggesting that the sea-surface temperature limit increases to very large and unrealistic values. In this case, the icing becomes spray-generation-limited and the icing rate approaches zero at all sea-surface temperatures as the significant wave height approaches zero. Therefore, the model suggests that an ice growth limit is a function of both sea-surface temperature and seastate. Thus, the apparent limit may have been a climatological feature of cold oceans and not be based on the physics of ship icing itself.

2.9 Discussion and Conclusions

The heuristic modelling described in the above sections gives attention to the four subprocess areas of vessel icing, namely, (1) the state of the atmosphere and ocean, (2) vessel dynamics/spray generation hydrodynamics, (3) thermodynamics and dynamics of spray, and (4) thermodynamics and hydrodynamics of icing surfaces. In each of these subprocess areas we use a combination of empiricism and physical principle to model vessel spray icing. In this way, the entire vessel icing process is accounted for in the model development.

The model uses simple physics. An example of this is the use of a heat balance based on the assumption of complete air/spray heat exchange without the traditional heat transfer components seen in many icing models. It is easy to forget that the heat transfer correlations traditionally used to model the heat transfer components are themselves empiricisms often with many constraints. These correlations may be valid for uniform single phase flow, and are usually without liquid films flowing on the object's surface. These correlations are also usually limited to smaller objects and depend on an assumption concerning the air flow deformation due to the presence and motion of the vessel and the spray cloud relative to the vessel. Therefore, the much simpler air/spray heat balance presented here could model the heat transfer processes as effectively as the more complex empirical heat transfer correlations.

The use of a parallelepiped approximation to the vessel's shape above the water line results in an icing model that in a simple way takes into account the essential nature of many different types and classes of vessel without causing the model to become specialized to one type or class of vessel. Historically, the great variety of vessels that may be present during a freezing spray episode has been a problem for spray icing prediction.

The goal of modelling precision is satisfied in that most of the aspects of the physical processes of ship icing were dealt with by explicit assumptions, physical principles, or empirical submodels. The goal of output precision is met in that this model has numerical output (i.e. ice mass accretion and thickness growth rates). Many icing

predictors in the past have used categorical schemes for describing icing intensity and have, thereby, exhibited less output precision.

Therefore the present heuristic model of vessel icing, simpler in physics than some models of vessel icing, demonstrates a considerable universality while maintaining precision. The empiricism for the model's spray generation is based on Soviet field data for spraying of an MFV. The primary heuristic issue addressed in the present work has to do with the spray/air heat balance used to calculate the spray ice accretion rate. The model performs well against data and the KA model. We suggest that the heuristic model's successful performance in comparison to the KA model implies that our emphasis on the spraying process rather than the surface icing processes produced a model with realistic performance. On the basis of our approach, we are not suggesting that the spraying processes are more important than the surface processes but only that more work deserves to be done on establishing more clearly their relative importance. However we do recommend, on the basis of the present work, that it would be prudent to emphasize the spraying process more in future modelling than has been done in the past.

The model's usefulness in exploring a hypothetical severe icing mechanism (i.e. the BLN model) has been demonstrated by examining twelve selected cases of extreme icing. Since conditions necessary to trigger nucleated spray are not clear, the selection of extreme icing cases of this kind remains subjective. Also, since vessel icing data sets may contain cases of nucleated or partially nucleated spray, some of the noise or error in these data sets may arise from this uncertainty.

The model has also been used to examine icing sensitivity to nine model parameters. Air temperature, wind speed, vessel size and encountering angle, were found to have a strong influence on vessel icing for a chosen standard condition. Fetch, significant wave height (dependent on fetch in the BLS model) and vessel speed were found to have a moderate influence on vessel icing severity, while sea-surface temperature (for the BLS model) and sea-surface salinity had a mild influence. A hypothesized nucleated spraying mechanism was numerically tested. These tests showed that the nucleated spray icing mechanism produced a marked increase in icing rate and

in the sensitivity of the icing rate to the sea-surface temperature. Finally, the model shows that a universal sea-surface-temperature-based-limit to spray icing is not likely.

List of References

Blackmore, R. Z., and E. P. Lozowski, 1992: An uncomplicated model of ship icing. In: Proceedings of the 11th International Association for Hydraulic Research Symposium on Ice (IAHR), Banff, Canada, Vol. 2, 607-621.

Blackmore, R. Z., and E. P. Lozowski, 1993: An heuristic freezing spray model of vessel icing. In: Proceedings of the 3rd International Society of Offshore and Polar Engineering Conference (ISOPE), Singapore, Vol. 2, 648-654.

Blackmore, R. Z., and E. P. Lozowski, 1994: An heuristic freezing spray model of vessel icing. *Int. J. Offshore Polar Eng.*, **4(2)**, 119-126.

Borisenkov, Ye. P., and I. G. Pchelko, Eds., 1972: Indicators for forecasting ship icing. Arkt. Antarkt. Nauc-Issled Inst., Leningrad. [in Russian] [also as CRREL Draft Translation 481 (AD-A030 113), U.S. Army Cold Regions Engineering and Research Laboratory, Hanover NH, 60 pp.]

Borisenkov, Ye.P., G. A. Zablockiy, A. P. Makshtas, A. I. Migulin and V. V. Panov, 1975: On the approximation of the spray cloud dimension. Arkt. Antarkt. Nauc-Issled Inst., Trudy No. 317, Gidrometeoizdat, Leningrad, 121-126. [in Russian]

Bretschneider, C. L., 1973: Prediction of waves and currents. *Look Lab, Hawaii*, **3(1)**, 1-17.

Brown, R. D., and P. Roebber, 1985: The scope of the ice accretion problem in Canadian waters related to offshore energy and transportation. Rep. 85-13, Canadian Climate Centre, Downsview, Ont., 295 pp. [unpublished manuscript]

BSRA (British Shipbuilding Research Association), 1957: Trawler-icing research. BSRA Rep. No. 221, London.

Chung, K. K., 1995: Ship icing and stability. Ph.D. Dissertation. University of Alberta, 184 pp.

Comiskey, A. L., L. D. Leslie and J. L. Wise, 1984: Superstructure icing and forecasting in Alaskan waters. Unpublished draft report submitted by the Arctic Environmental Information and Data Centre to Pacific Marine Environmental Laboratory (NOAA), Seattle, 39 pp.

Hayhoe, R. D., 1989: An experimental study of ice accretion and wind loading on offshore supply boats. Ph.D. Dissertation. Heriot-Watt University, 188 pp.

Holman, J. P., 1990: *Heat transfer.* McGraw Hill, New York, 714 pp.

Horjen, I., and T. Carstens, 1989: Numerical modelling of sea spray icing on vessels. In: Proceedings of the 10th International Conference on Port and Ocean Engineering under Arctic Conditions (POAC), Lulëa, Sweden, 694-704.

Kachurin, L. G., L. I. Gashin and I. A. Smirnov, 1974: Icing rate of small displacement fishing boats under various hydrometeorological conditions. *Meteorologiya i Gidrologiya*, **3**, 50-60. [in Russian]

Khandekar, M. L., 1989: Operational analysis and prediction of ocean wind waves. *Coast. Estuar. Stud.*, **33,** Springer-Verlag, 214 pp.

Lozowski, E. P., and E. M. Gates, 1985: Marine icing models: how do they work and how good are they? In: Proceedings of the International Workshop on Offshore Winds and Icing, Halifax, Nova Scotia, Oct. 7-11, 102-122.

Makkonen, L., 1987: Salinity and growth rate of ice formed by sea spray. *Cold Reg. Sci. Tech.*, **14,** 163-171.

Makkonen, L., 1989: Formation of spray ice on offshore structures.In: Working Group on Ice Forces, 4th State-of-the-Art Report, CRREL Special Report 89-5, U.S. Army Cold Regions Research Engineering Lab, Hanover, NH, 277-309.

Makkonen, L., R.D. Brown and P.T. Mitten, 1991: Comments on "Prediction of vessel icing for near-freezing sea temperatures." *Wea. Forecasting,* **6,** 565-567.

Martin, S., and P. Kauffman, 1981: A field and laboratory study of wave damping by grease ice. *J. Glaciol.*, **27(96),** 283-313.

Minsk, L. D., 1977: Ice accumulation on ocean structures. CRREL Rep. 77-17, U.S. Army Cold Regions Research and Engineering Laboratory, Hanover, NH, 47 pp.

Overland, J. E., 1990: Prediction of vessel icing for near-freezing temperatures. *Wea. Forecasting,* **5(1),** 62-77.

Overland, J. E., C. H. Pease, R. W. Preisendorfer and A. L. Comiskey, 1986: Prediction of vessel icing. *J. Climate Appl. Meteor.*, **25(12),** 1793-1806.

Press, W. H., B. P. Flannery, S. A. Teukolsky and W. T. Vetterling, 1990: *Numerical recipes. The art of scientific computing (Fortran version).* Cambridge University Press, 702pp.

Sackinger, W. M., and P. A. Sackinger, 1987: On the freezing of sprayed sea water to produce artificial sea ice. In: Proceedings of the 9th International Conference on Port and Ocean Engineering under Arctic Conditions (POAC), Fairbanks, AS, 581-590.

Sampson, R. D., K. K. Chung and E. P. Lozowski, 1996: A simple experiment to measure the splash mass produced by a free-falling buoyant sphere impacting a deep quiescent liquid. J. Colloid and Interface Sci., (in press).

Stallabrass, J. R., 1980: Trawler icing: a compilation of work done at N.R.C. Mech. Eng. Rep. MD-56, N.R.C. No. 19372, National Research Council, Ottawa, 103 pp.

Szilder, K., T. W. Forest and E. P. Lozowski, 1991: A comparison between different construction methods of ice islands. In: Proceedings of the 10th International Conference on Offshore Mechanics and Arctic Engineering (OMAE), Stavanger, Vol. 4, 9-15.

Weeks, W. F., and S. F. Ackley, 1982: The growth, structure and properties of sea ice. CRREL Monograph 82-1, U.S. Army Cold Regions Research and Engineering Lab, Hanover, NH, 136 pp.

Willmott, C. J., 1982: Some comments on the evaluation of model performance. *Bull. Amer. Meteor. Soc.*, **63,** 1309-1313.

Zakrzewski, W. P., 1987: Splashing a ship with collision-generated spray. *Cold Reg. Sci. Tech.*, **14(1),** 65-83.

Zakrzewski, W. P., and E.P. Lozowski, 1989: Soviet marine icing data. Report 89-2, Canadian Climate Center, 125 pp.

Zakrzewski, W. P., and E. P. Lozowski, 1991: Modelling and forecasting vessel icing. In: *Freezing and Melting Heat Transfer in Engineering*, K. C. Cheng and N. Seki, eds., Hemisphere Publishing Corp., 661-706.

Zakrzewski, W. P., E. P. Lozowski, and R. Z. Blackmore, 1988: The use of a ship spraying/icing model to estimate the effect of the direct spray flux on the icing rate. In: Proceedings of the 4th International Symposium on Atmospheric Icing of Structures (IWAIS), Paris, 399-404.

3. AN EXPLORATORY FRESHWATER SPONGY SPRAY ICING MODEL

The review of saline spray icing given in Chapter 1 suggested that much is left to be learned about spongy accretion. Included in Chapter 1 are the details of a model of spongy ice accretion for seaspray (Makkonen, 1987), which is based on an analogy with freshwater spongy spray icing. This analogy has allowed considerable insight into the ice accretion process, including an increased awareness of the importance of the dendritic growth likely to occur in spongy spray icing, which is also observed in sea ice growth. The modelling approach presented in this Chapter for freshwater spray icing is based on an analogy with freely-growing ice crystals in bulk supercooled water. An increased understanding of freshwater spongy accretion is likely to help advance the understanding of spongy saline spray icing.

The present approach is in contrast to many traditional ones in which spongy spray icing is modelled without clearly specified modelling assumptions concerning the structure of the icing surface. This lack in traditional modelling might be taken to suggest that the surficial liquid film is of uniform temperature and that the icing surface may have a surficial structure of little importance to the icing process. As a consequence, the hydrodynamics of the film, and its possible influence on the icing process are typically not considered. Also not considered is that layer of growing dendritic ice which lies between the liquid film and the crystalline ice matrix of the spongy accretion. Even though it has been known for some time that the macroscopic characteristics of spray icing are the product of ice crystal growth at the microscopic scale (Knight, 1968), most models have not accounted for these factors explicitly. To rectify this deficiency, a new exploratory theoretical model is presented which reinforces many earlier insights, while providing new insight into the physics of the spongy spray icing process. The model predicts the ice accretion rate as well as the rate of inclusion of water into the ice accretion matrix. It is formulated for a specific icing configuration, namely that of a vertical cylinder segment.

A general description of the model, its assumptions, and its structure is given in Section 3.1. The equations for the hydrodynamic submodel of the falling film are given in Section 3.2. An approach to modelling the surficial layer of growing dendritic ice, or what will hereafter be referred to as the freezing zone, is given in Section 3.3. The thermodynamics of the model appear in Section 3.4. The icing regimes that arise from the model's structure and that characterize the model's performance are discussed in Section 3.5. A list of model equations and a brief discussion of the approach used to solve them is given in Section 3.6. Section 3.7 gives the method used to evaluate an empirical parameter needed by the model for completeness. Once the empirical parameter is estimated, model sensitivity and performance can be evaluated. This evaluation is presented in Section 3.8. Finally, conclusions and recommendations are presented in Section 3.9.

3.1 Basic Model Assumptions

A fundamental assumption of the present model is that ice is accreted under constant environmental conditions to yield steady-state ice growth on a vertically oriented circular cylinder segment of specified length. A series of cylinder segments may be used to model a cylinder of greater length, and to discretize the mathematical problems of spray and ice distribution. Such a configuration of cylinder segments, each of height, Z_c, is shown in Fig. 3.1. In this way, ship mast icing or the icing of other vertically oriented cylindrical components of a vessel could be simulated. The main reason for choosing a vertical orientation of the cylinder has to do with the availability of a gravitational film flow model to describe the flow of liquid down a vertical surface. This strategy was adopted in order to use the vertical falling liquid film model of Dukler and Bergelin (1952), to apply it in the case of a vertical cylinder, and to concentrate on other aspects of the spongy spray icing problem. The primary objective is to produce a complete, although preliminary and configuration-specific, approach to spongy accretion modelling. The use of this model has given the opportunity to examine the potential influence of a falling film on spray ice accretion.

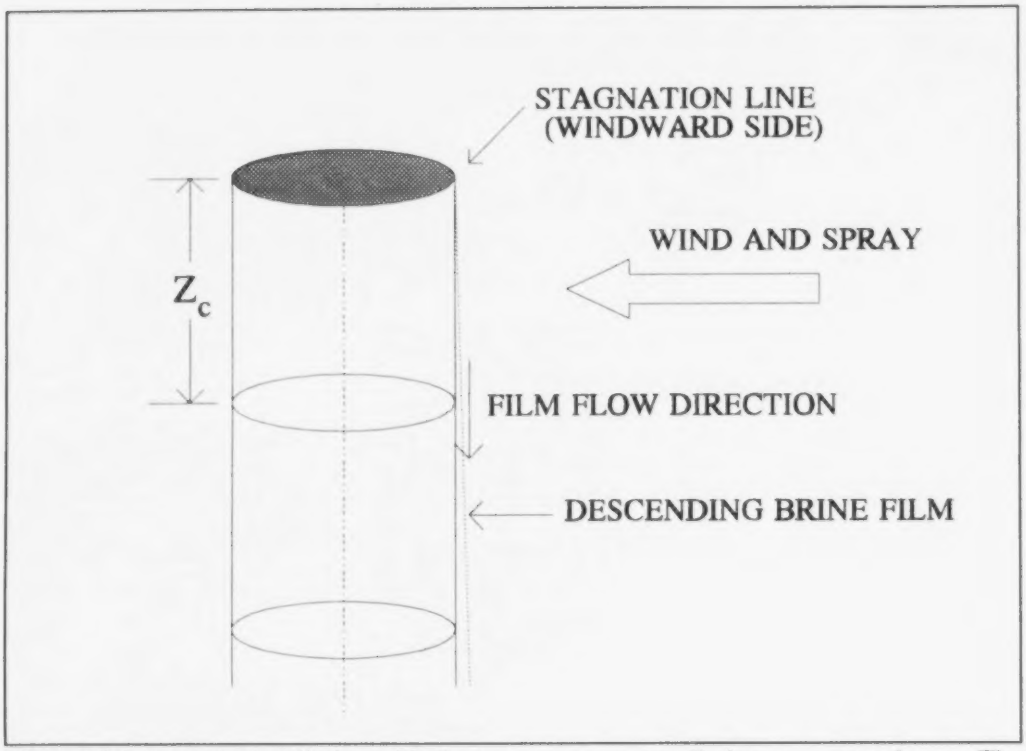

Figure 3.1 A vertical cylinder with the two uppermost cylinder segments shown. The cylinder segment height is Z_c. Only the windward half of the cylinder receives impinging spray which forms a falling liquid film.

Fig. 3.1 shows that the wind and spray motion are perpendicular to the axis of the cylinder. It also indicates that the spray droplets collide with the liquid film moving down the icing surface. The collision efficiency parameterization of Finstad et al. (1988), gives a collision efficiency of unity over a considerable range of wind speed for droplets greater than 2.0 mm in diameter. However, since Ryerson and Longo (1992) measured a range of droplet diameters from 100 μm (i.e. the smallest droplet size measured) to 4 mm, simulating the collision of seaspray on a cylinder will likely not be a trivial matter. In order to keep this aspect of spray icing uncomplicated, a monodisperse droplet population is assumed with a known collision efficiency, independent of the spray flux intensity. In this way, the difficulties of simulating seaspray impingement are sidestepped for the purpose of maintaining the main modelling focus on the spongy ice growth problem. The cylinder's curvature is neglected inasmuch as a uniformly distributed spray

flux over the windward side of the cylinder is assumed. This assumption was also made to maintain simplicity, and to model the average hydrodynamic condition for the windward side of the icing surface.

The model's falling liquid film moves only vertically, and no horizontal component of film velocity is allowed for in the falling film submodel. This allows no surficial liquid flow from the windward side toward the leeward side of the cylinder, and implies that the model accretion is added uniformly to the windward side of the cylinder. The ice mass which is being accreted on the icing surface is removed from the falling film as the liquid flows over the ice in the segment.

If the model is run for a single-segment, liquid is collected by the windward side of the cylinder and is shed along the lower boundary of the segment. If the model is run as a series of segments (as in Fig. 3.1), liquid flows into a segment from the segment immediately above, while impinging water joins the flow over the windward half of the segment. If the accretion is spongy, water either exits a segment as part of the falling film, or is accreted as a matrix of crystalline ice and entrapped liquid. The ice crystal interface grows due to the supercooling of the liquid in the falling film. If the supercooling is sufficiently large, aggressive crystal growth may occur which entraps the liquid at the freezing zone/laminar layer interface. For the sake of brevity, the freezing zone/laminar layer interface will hereafter be referred to as the icing interface, shown in Fig. 3.2. Makkonen (1988) has assumed that the rate of advance of the tip of an icicle is related to the degree of supercooling near the ice/water interface at the icicle's tip. He reports that a model based on this assumption compares very well with experimental measurements of the growth rates of icicle length. An analogous assumption that the rate of advance of the icing interface depends on the supercooling in the vicinity of the interface is used in the present model.

Conservation of water substance is used as a modelling principle, ensuring that the incoming mass of water is equal to the sum of the accreted mass and the mass of water leaving the segment. Heat energy must also be conserved at the icing surface. In the present model, the latent heat of fusion is assumed to evolve within the freezing zone. This layer may be thought of as that surficial region in which the structure of the ice

matrix is in the process of being formed. The latent heat of fusion is assumed to evolve uniformly throughout the freezing zone, and is conducted away from its outer surface through the laminar sublayer of the falling film. In turn, the outer surface of the falling film loses heat by convective, evaporative, and radiative heat transfer to the external air flow.

In Section 3.3.1, the model's freezing zone will be shown to have a parabolic temperature profile. This temperature profile depends upon the assumption of uniform thermal conductivity throughout the freezing zone. Uniform conductivity in turn implies a uniform distribution of liquid and solid water substance in the freezing zone. This group of modelling assumptions is used in Section 3.3 to produce a description of latent heat evolution and conduction within the freezing zone.

Adjacent to the freezing zone is a film of falling liquid which is shed from the icing surface. Dukler and Bergelin (1952) present a falling liquid film model that is used here to describe the film's hydrodynamics. Recent work on falling films appears to focus on certain specific issues rather than on the general modelling of falling films. For example, one issue is the flow transition from a continuous laminar layer to rivulet flow with dry patches of substrate between rivulets. Trela (1988) presents a theoretical approach to predicting the breakdown of the liquid film into rivulet flow on a vertical surface. This characteristic of a falling film could be of interest for vertical icing surfaces near the wet/dry icing transition. However, in the present approach, the complication of rivulet flow is neglected. Another issue in falling film modelling has to do with the propagation of waves down the falling liquid film. Even for laminar falling films, waves of large and small amplitude relative to the mean film thickness may propagate down the film (Fulford, 1964). The larger waves may have an amplitude two to five times the thickness of the much slower moving falling film (Wasden and Dukler, 1989). In addition, Wasden and Dukler (1989) suggest that a large fraction of the total mass flow is likely to occur in these falling waves and that these waves may be very influential with respect to heat and mass transfer from the surface of the falling film. Similar waves propagating along the surficial liquid films on icing surfaces could also influence the growth of the ice. However, in the present approach, the complication of surficial film

wave propagation is neglected in order to maintain model simplicity. The model assumes a steady flow and does not account for either rivulet flow or surficial wave propagation.

Here we assume that a laminar layer is formed next to the vertical wall, with buffer and turbulent layers forming only if there is a sufficiently large film flow. The details of the model are presented more fully in Section 3.2. For the present purpose, the buffer and turbulent layers are combined and are referred to as the mixed layer. We assume that the mixed layer offers no resistance to heat transfer as the liquid in the layer is assumed to be thoroughly mixed by turbulence. This layer is likely to have a temperature profile normal to the icing interface that is almost isothermal. The model assumes an idealized isothermal temperature profile in the mixed layer while not accepting the usual implication that no heat can be transferred through such a layer. In addition, it is assumed that the advancing dendritic ice forms an icing interface adjacent to the laminar layer in such a way that the hydrodynamics of the laminar layer are unchanged from those of the smooth wall assumed by Dukler and Bergelin (1952).

A summary of the surficial structure discussed above is presented in Fig. 3.2. The vertical cross-section given in Fig. 3.2 shows the ice accretion matrix adhering to the substrate. The height of the cylinder segment is Z_c. Steady-state transport of heat and mass occurs across the boundaries of the segment. Even though the freezing zone, the laminar layer, and the mixed layer are constant in thickness with time, they are moving away from the substrate and have moving boundaries. We assume that no vertical heat or mass transport occurs within the model's ice matrix and freezing zone. On the other hand, heat and mass are transported in the vertical direction in both the laminar and the mixed layers. Heat and mass are also transported horizontally between the surficial layers. Heat and mass are conserved for each of the model's surficial layers and thereby for the icing surface as a whole.

The model assumes a steady-state ice growth condition with constant impinging spray flux, while the surficial layers remain constant in thickness with time, on each segment. The ice matrix, on the other hand, is stationary (i.e. fixed to the substrate) while growing in thickness at a constant rate. Therefore, in the frame of reference of the substrate, the surficial layers may be thought of as moving away from the substrate (to

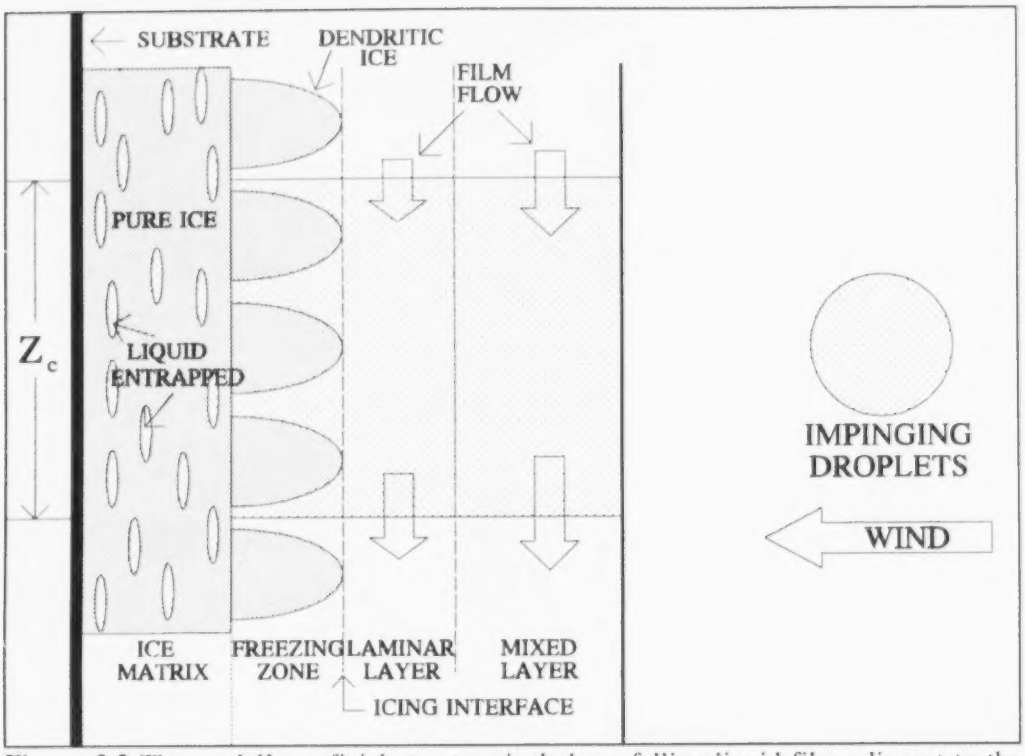

Figure 3.2 The model's surficial structure includes a falling liquid film adjacent to the freezing zone. The mixed layer may or may not be present, depending on the flux of excess liquid.

the right in Fig. 3.2) at a rate equal to the growth rate of the ice matrix. Since the density of water decreases with solidification, the rate of advance of the ice matrix will be slightly greater than the velocity at which liquid enters the freezing zone at the icing interface. As a result, water in the vicinity of the icing interface will have a small component of velocity away from the substrate. However, once the water substance has become part of the ice matrix, we assume that it has no motion relative to the substrate.

Fig. 3.2 may also be viewed from a second frame of reference, as if the observer were fixed relative to the freezing zone and the layers of the falling film and not fixed relative to the substrate. In this case, the substrate will appear to move to the left at a rate equal to the growth rate of the ice matrix. The velocity of the water toward the icing interface is slightly less than the velocity of the ice matrix as it is formed in the freezing zone and emerges at the freezing zone/ice matrix interface. Thus water enters the freezing

zone at the icing interface and emerges to the left having formed an ice matrix. Equations are developed in the following sections that are valid in either of the frames of reference described above and that ensure steady-state mass conservation for these layers. Once the heat balance for the laminar and mixed layers has been established for the segment's falling film (Section 3.4), the temperature profile for the layers can be determined. In this way, the temperature (or equivalently the supercooling) at the icing interface may be determined.

The rate of advance of the icing interface is estimated using an analogy with individual freely-growing ice dendrites in bulk supercooled water. Since the supercooling of the bulk water controls the rate of growth of the ice crystal, we assume that the supercooling at the icing interface controls the rate of growth of the model's ice matrix. This interfacial supercooling is defined as the absolute value of the difference between the liquid temperature and the liquid's equilibrium freezing temperature at the icing interface. The equilibrium freezing temperature is taken to be 0°C for pure water at a pressure of one atmosphere. Since the temperature profile in the falling liquid film is calculated, and with it, the interfacial supercooling, an estimate of the interfacial growth rate is made possible.

Once the rate of advance of the icing interface and the mass flux of pure ice formed in the freezing zone have been estimated, it is possible to define three accretion regimes for the model. These regimes are: (1) the glaze ice accretion regime, (2) the spongy ice accretion regime, and (3) the porous ice accretion regime. The rationale used in the definition of each of these regimes is presented next, in preparation for the derivation of the equations which describe them in Section 3.5.

The glaze ice accretion regime occurs in the model when the volumetric accretion rate of solid ice, as calculated on the basis of a heat balance in the freezing zone, exceeds the volumetric accretion rate based on the model's crystal growth speed. In this situation, the model's ice accretion rate is based on the model's overall heat balance with ice sponginess and porosity neglected. Thus when the glaze icing regime is calculated, the ice growth rate is based on a solid accretion morphology, and all excess water is assumed to form the surficial liquid film and is shed from the icing surface. No mechanism is

proposed here to explain how such a solid icing morphology may come about. Knight and Knight (1968) have made observations of hard ice growth (i.e. solid icing) in hailstones and have suggested that these hailstones show a different crystallographic structure than hailstones with a spongy structure.

If the crystal growth speed exceeds the growth speed under the morphological assumption of solid ice, a portion of the liquid film is first entrained into the freezing zone and then subsequently entrapped by the ice matrix. The model's spongy ice accretion regime occurs under these conditions. As in the glaze ice accretion regime, the excess liquid that is not entrapped in the advancing ice matrix, forms the falling film. This regime of the model may have the potential to simulate naturally occurring spongy ice. The occurrence of spongy ice has been well-known for years (Fraser et al., 1952; List, 1959), and the basic mechanism of surficial liquid entrapment by aggressive dendritic ice growth has been suggested by many investigators (Macklin and Ryan, 1962; List, 1963; Knight, 1968). The present model does not account for the observed (Macklin, 1977) formation of air bubbles in the spongy ice matrix. The appearance of these bubbles from air initially dissolved in the impinging water is neglected. Thus the model's spongy ice accretion regime yields an accretion composed only of ice and water. The model's spongy ice accretion regime is given more attention than the other two regimes in the sections that follow because of its potential for predicting spongy ice accretion.

There is a third modelling regime. If the crystal growth rate is so large that all of the available excess liquid is incorporated into the advancing ice matrix, then the porous ice accretion regime occurs. Because of the high speed of ice crystal growth in this regime, air may become trapped in the accretion, taking up any remnant interstitial volume not occupied by the entrapped water. For this reason, the model's porous accretion is less dense than the glaze or spongy accretions. In this respect the porous ice accretion regime bears some resemblance to rime icing with its low accretion density. No observations have yet been advanced that suggest the bulk entrapment of air into the ice accretion as suggested in this regime, although the appearance of bubbles in accreted ice is observed frequently in hailstones near the wet-dry growth transition (Macklin, 1977). For the moment, therefore, this modelling regime, like the other ice accretion regimes,

is considered a modelling hypothesis. The particulars of each regime are given in greater detail in Section 3.5 along with their mathematical descriptions.

3.2 Modelling the Falling Film

Spray icing often occurs with a surficial flow of excess liquid which is in the process of being shed from the icing surface. This section describes the falling film submodel used to obtain the mass fluxes that are needed to ensure conservation of water substance and to estimate the sensible heat fluxes at the icing surface. The falling film submodel also yields the laminar layer thickness that is essential for estimating the conductive heat flux in the laminar layer (Section 3.4). The falling liquid film model of Dukler and Bergelin (1952) for a smooth vertical surface is used here. Dukler and Bergelin (1952) use the universal velocity distribution equation for turbulent flow of von Kármán (1939) in which the non-dimensional film flow rate is defined as:

$$u^{+} = \frac{u}{u_*} \tag{3.1}$$

where u is the velocity of the fluid in the film, and u_* is the friction velocity (Eqn. 3.3). The non-dimensional coordinate normal to the substrate is:

$$\eta = \frac{u_* \rho (y - y_1)}{\mu} \tag{3.2}$$

where ρ is the density of the liquid, μ is the dynamic viscosity of the liquid, y is the dimensional coordinate normal to the wall with origin at the ice matrix/freezing zone interface, and y_1 is the location of the icing interface (Fig. 3.3). The friction velocity is defined as:

$$u_* = \sqrt{\frac{\tau_0}{\rho}} \tag{3.3}$$

where τ_0 is the shear stress at the "wall" (i.e. $y=y_1$).

These parameters form the basis of the well-known Prandtl mixing length model (Schlichting, 1979). This model describes fluid flow near a wall with three characteristic film layers. The layer in contact with the wall is the laminar sublayer in which molecular transport of momentum, heat and mass dominates. The next layer is often called either the buffer layer or the transition layer in which turbulent and viscous effects are of comparable importance. Farther away from the wall, bulk mixing dominates and this layer is termed the turbulent layer. The Prandtl mixing length hypothesis results in a set of well-known equations (e.g. Holman, 1990) that are used to describe the velocity profile with the non-dimensional variables given in Eqns. 3.1 and 3.2. The laminar layer is specified by:

$$u^+ = \eta \qquad 0<\eta\leq 5 \tag{3.4}$$

where Eqn. 3.4 describes the film's laminar layer with or without an accompanying buffer or turbulent layer. The buffer layer is specified by:

$$u^+ = 5.0\ln(\eta) - 3.05 \qquad 5<\eta\leq 30 \tag{3.5}$$

and the turbulent layer is specified by:

$$u^+ = 2.5\ln(\eta) + 5.5 \qquad 30<\eta \tag{3.6}$$

In order to account for the surficial fluxes of water substance, the non-dimensional flow speeds of the laminar, buffer and turbulent layers given in Eqns. 3.4, 3.5 and 3.6 can be integrated in a piecewise fashion according to the general equation:

$$\Gamma = \mu \int_0^{\eta} u^+ d\eta \tag{3.7}$$

where Γ is the total mass flow rate per unit breadth of the falling film.

The equation development for the continuity of mass is done on the basis of mass flux intensity, since the impinging mass of spray intercepted by the cylinder is naturally described in terms of its mass flux intensity. Describing the liquid flow in a film which moves parallel to the icing surface is not as naturally represented in this way. However,

this is achieved by converting the mass flow per unit breadth, Γ, in units of $kgm^{-1}s^{-1}$ to mass flux intensity in units of $kgm^{-2}s^{-1}$ with:

$$R_c = \frac{\Gamma P_c}{A_c} = \frac{\Gamma}{Z_c} \qquad (3.8)$$

where P_c is the wet-shedding perimeter on the windward half of the cylinder segment (i.e. P_c is half the cylinder circumference), A_c is the area of the windward half of the same cylinder segment, and R_c is the segment's mass flux intensity of shed liquid in units of $kgm^{-2}s^{-1}$. For brevity, the term flux will be used hereafter to mean mass flux intensity.

Substituting Eqn. 3.4 into Eqn. 3.7 and converting to mass flux units using Eqn. 3.8 results in:

$$0<\eta\leq 5 \qquad R_2 = 0.5\mu\eta^2 Z_c^{-1} \qquad (3.9)$$

where R_2 is the liquid flux in the segment's laminar layer. If the film submodel suggests the development of the falling film beyond a laminar layer, η=5 denotes the surface which separates the laminar sublayer from the buffer layer. If the laminar layer is fully developed without such a mixed layer, then η=5 is the non-dimensional coordinate at the outer surface of the falling film. The mass flux for this fully developed laminar layer (Eqn. 3.9, η=5) is:

$$R_2 = 12.5\mu Z_c^{-1} \qquad (3.10)$$

If η lies in the range $0<\eta<5$, then neither a buffer nor a turbulent layer is present, but only the laminar layer itself. In this case, the total mass flux of the falling film, R_T, occurs as a laminar film (i.e. $R_T=R_2$) without an outer mixed layer[1]. If η=0, there is no film flow.

In order to derive an equation for estimating the film's total mass flux, R_T, with a buffer layer present, Eqns. 3.4 and 3.5 are integrated to yield:

---

[1] The mixed layer is composed of a buffer layer and a turbulent layer, provided a turbulent layer is present.

$$R_T = \mu(12.5 - 8.05\eta + 5.0\eta\ln(\eta))Z_c^{-1} \qquad 5<\eta\leq 30 \qquad (3.11)$$
$$R_3 = R_T - R_2$$

where R_3 is the flux in the mixed layer. The range given for η in Eqn. 3.11 describes the limits of the buffer layer's extent and not the integration limits. In this case, the mass flux in the mixed layer, R_3, is also the mass flux in the buffer layer.

In order to derive an equation for estimating the film's total mass flux, R_T, with all three layers present, Eqns. 3.4, 3.5, and 3.6 are integrated to yield:

$$R_T = \mu(-63.8 + 3.0\eta + 2.5\eta\ln(\eta))Z_c^{-1} \qquad \eta>30 \qquad (3.12)$$
$$R_3 = R_T - R_2$$

where R_T is the total mass flux for a falling film with a laminar, buffer and turbulent layer present, and where R_3 is the flux for the mixed layer.

The falling film submodel described above is used to estimate the surficial film flow with the parameters R_2 and R_3 as shown in Fig. 3.3. We now turn our attention to the role of the falling film in establishing a heat balance for the surficial liquid. An important part of this heat balance involves the conduction of heat through the laminar layer, which depends inversely on the laminar layer's thickness (y_2-y_1). The estimation of the laminar layer thickness starts by substituting Eqn. 3.3 into Eqn. 3.2 to give:

$$\eta = \frac{u_*\rho(y-y_1)}{\mu} = \frac{\sqrt{\frac{\tau_0}{\rho}}\rho(y-y_1)}{\mu} \qquad (3.13)$$

Fig. 3.3 shows the icing interface at the tips of the ice dendrites ($y=y_1$). This surface is taken to be the lower boundary of the falling film. The shear stress exerted by the falling film at the icing interface, τ_0, is estimated in a simple way for a steady-state falling film without wind shear, and with the gravitational body force on the liquid taken into account:

$$\tau_0 = \rho g y_T \tag{3.14}$$

where g is the acceleration due to gravity, and y_T is the total thickness of the liquid film (i.e. $y_T = y_3 - y_1$). The steady-state assumption is valid for falling water films up to a thickness of approximately 200 μm (i.e. Re≈33). For greater film thickness, waves appear on the surface of the film with agitated waves beginning to form at the onset of turbulent film flow (i.e. Re≈1100) with a thickness of approximately 660 μm. At a greater film thickness, larger waves are likely to form which will eventually account for most of the flow of water in the film. At even greater rates of flow, water may cascade along the wall, accelerating under the gravitational body force, with little momentum transfer to the wall. Since the present falling film model does not account for waves or cascading flow, the momentum transfer to the wall and hence the shear stress at the wall are taken to be constant with time and given by Eqn. 3.14.

Eqn. 3.14 can be combined with Eqn. 3.13 to yield:

$$\eta = \frac{\sqrt{y_T g \rho}}{\mu}(y - y_1) \tag{3.15}$$

Eqn. 3.15 and Eqns. 3.9 to 3.12 are used to calculate the laminar layer flux, R_2, the mixed layer flux, R_3, the laminar layer thickness, $(y_2 - y_1)$, and the falling film thickness, y_T. A more complete description of how these equations are used in the model is left to Section 3.6 where they are presented in context with the other model equations.

Dukler and Bergelin (1952) show that use of the von Kármán velocity profile gives experimentally verified film thickness, as a function of film flow rate and the physical properties of the fluid flow, over the complete viscous to turbulent flow range. These theoretical equations agree closely with measurements of film thickness for freshwater flow (without wind stress) on a vertical stainless steel plate well into the turbulent regime, with a film thickness of up to 0.71 mm. The equations predict a laminar to turbulent film transition which agrees closely with observation (i.e. Re ≈ 1000, Eqn. A6.2). Nevertheless, the use of the Dukler and Bergelin (1952) model in the context of the present spray icing model involves a number of limitations and assumptions.

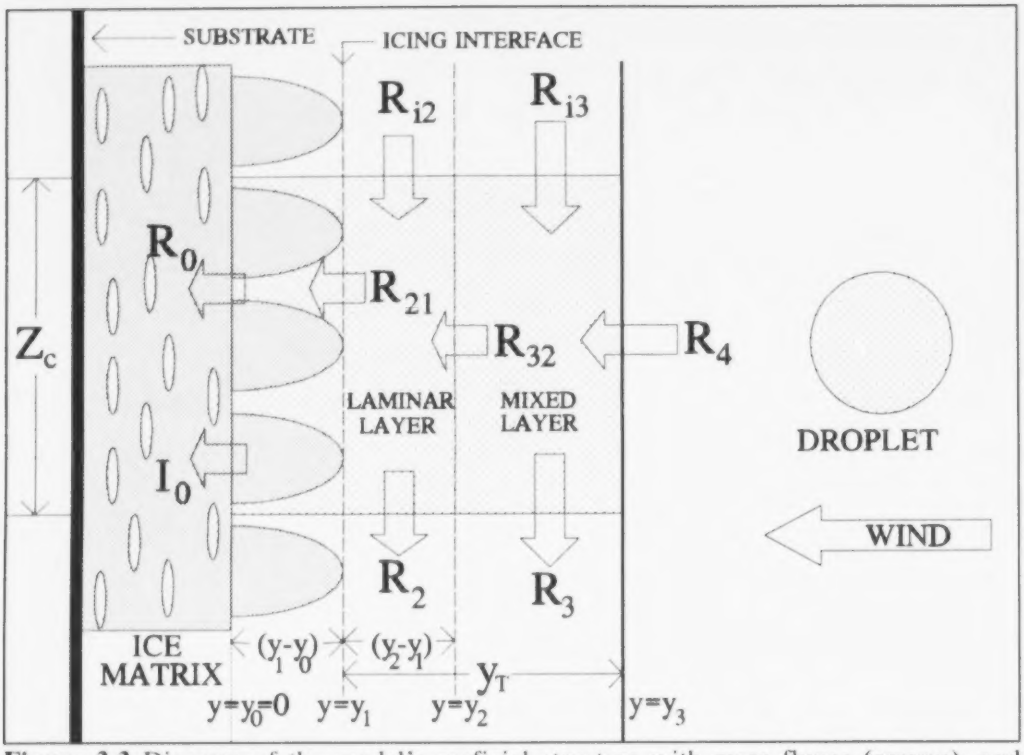

Figure 3.3 Diagram of the model's surficial structure with mass fluxes (arrows), and layer thicknesses shown.

The spray icing model requires the assumption that a flat plate is not significantly different from an idealized cylindrical icing surface. This should introduce little error if the film thickness remains small compared to the radius of the cylinder. For this reason, the model should probably not be used for cylinders less than about 1 cm in diameter. Another effect that is neglected in the present work is the wind stress on the liquid film.

While the empirical equations describing the falling film assume a hydrodynamically smooth substrate, icing surfaces are probably not hydrodynamically smooth; in fact, they may have substantial microscopic roughness from dendritic penetration into the laminar sublayer of the film. Fulford (1964) in reviewing the effects of wall roughness on film flow, suggests that increased wall roughness (i.e. roughness elements of a few 100μm) initiates turbulence in falling films at lower Reynolds numbers than would otherwise occur. As a result heat transfer through the film is likely to

increase. Because the roughness of the icing interface is unknown, it appears prudent to use the laminar layer of the Dukler and Bergelin (1952) model as the basis for describing conductive heat transfer in the falling film. Surficial irregularities that are very large compared to the film thickness are known to produce back-mixing patterns in falling films (Fulford, 1964). Flow patterns like these may occur around macroscopic irregularities such as ridges and hollows that are observed to develop during ice accretion (Roos and Pum, 1974). These complications of film flow and heat transfer are beyond the scope of the present work and are therefore neglected.

The excess water film associated with spray icing may also be very different from falling films in which there are no disturbances such as impinging spray or wind stress. In marine icing, colliding droplets with diameters as large as 1 or 2 mm are to be expected. These spray droplets will strike the liquid film and spread out. It is likely that at least the outer regions of the liquid film will be significantly affected by these impinging droplets, since the droplet diameters may be significantly larger than the film thickness (a few tenths of a millimetre). The impact of the impinging droplets on the mixed layer of the falling film is almost certain to further enhance the surficial wave formation and the turbulent mixing that is observed in falling films under quiescent external conditions. This enhanced mixing would tend to reduce the temperature gradient in the mixed layer of the film normal to the icing surface. Therefore, without specific observational evidence concerning falling films under droplet bombardment, the assumption that the mixed layer is isothermal seems to be a prudent one. As well, this isothermal mixed layer assumption forms a natural modelling progression from the well-tested and successful traditional assumption that the entire film is well-mixed.

Another important issue in vessel spray icing is the effect of cyclical spraying. Appendix 4 presents an analysis of a film of water that is initially at rest on a vertical wall, and that is used to estimate an e-folding time for the development of a laminar falling film. In the analysis, an initially motionless water film is used to simulate the beginning of a spraying event, and we show that an e-folding time of about 0.003 s is required for the establishment of a laminar layer of 100 μm thickness. This duration is much smaller than the time scale of a vessel spraying event. Zakrzewski and Lozowski

(1991) suggest that the spray duration typical of a Soviet medium sized fishing vessel ranges from 1 to 3 seconds. Therefore, a laminar falling film probably will form quickly and will be present on a vessel's icing surface during the spraying event. However, in the context of the present model, we sidestep this complexity by assuming that the spraying is continuous.

In Appendix 5 we estimate the mean period between droplet impacts at a point on the surface to be about 0.02 s. This estimate depends on the assumption that the droplet's impact on the surface disturbs the liquid film significantly over an area with a radius twice that of the impinging droplet. The estimate is calculated for a droplet diameter of 1 mm and for a spray flux of 10 $kgm^{-2}s^{-1}$, which is a very large flux even for the spraying of vessels. The estimated mean period between droplet collisions (0.02 s) is significantly longer than that calculated for the development of a steady laminar layer (0.003 s) of thickness 100 μm which is initially motionless (Appendix 4). Therefore, on the assumption that the establishment of a laminar falling film can be used to describe the re-establishment of a film following a droplet impact, a falling laminar film of at least 100 μm will probably form on a wet icing surface between droplet collisions under most spraying conditions. Therefore, the present modelling assumption of a laminar layer next to the freezing zone is likely to be a good one.

In Appendix 6, an analysis is given for the laminar layer as defined in the falling film model of Dukler and Bergelin (1952). We show that the maximum laminar layer thickness is about 200 μm with a maximum fall speed of about 22 cm s^{-1} at the outer surface of the film (at η=5). This gives a Reynolds number based on film thickness of 33, which is much smaller than the value of Re≈1800 that is given as the criterion for the development of turbulence in a falling film (Incropera and DeWitt, 1990). Therefore, we expect the laminar layer of the Dukler and Bergelin (1952) model to be a robust hydrodynamic feature that will resist transition to turbulent flow, possibly even under spray droplet bombardment.

The conservation of water substance for the falling film on a cylinder segment may be expressed as:

$$R_{i2} + R_{i3} + R_4 = I_0 + R_0 + R_2 + R_3 \qquad (3.16)$$

where R_{i2} is the laminar layer mass flux entering the segment from the segment above, R_{i3} is the mixed layer mass flux entering the segment, R_4 is the flux of impinging spray, I_0 is the flux of solid ice that forms the framework of the spongy ice matrix, R_0 is the flux of water incorporated into the ice matrix, R_2 is the flux of water shed from the segment in the laminar layer, and R_3 is the flux of water shed from the segment in the mixed layer. The variables of Eqn. 3.16 are all shown in Fig. 3.3., which also shows R_{21}, the mass flux of water transferred from the film's laminar layer into the freezing zone ($R_{21}=I_0+R_0$), and R_{32}, the mass flux of water entrained into the laminar layer from the mixed layer. Fig. 3.3 shows a falling film with a sufficient impinging flux of water to produce a mixed layer. If the surficial water flux is so small that only a laminar layer exists, then the spray is assumed to impinge on the laminar layer directly (i.e. $R_4=R_{32}$, $R_{i3}=R_3=0$).

The algorithm which solves the icing model equations uses a recursive method, that begins by calculating the hydrodynamics of the falling film under an initial assumption that no icing is occurring (i.e. all impinging liquid is flowing down). The thermodynamic equations which are described in the following sections are then solved on the basis of this "no icing" falling film. With this initial estimate of the accretion flux of water substance (i.e. R_0+I_0), the hydrodynamic equations of the liquid film are then recalculated. Once new film hydrodynamics are established which account for the accretion flux, new thermodynamics are calculated, and so on. This process is repeated until the laminar layer thickness, (y_2-y_1), changes within an acceptably small error limit, eventually rendering an acceptable solution to the icing equations. A more detailed account of this procedure is provided in Appendix 7. The falling film equations used in the model as well as those that describe other physical aspects of the icing model are given in Section 3.6. The way in which the freezing zone is modelled is described next.

3.3 Modelling the Freezing Zone

Following Knight (1968), Roos and Pum (1974), Makkonen (1987), Lock and Foster (1990), and List (1990), we assume spongy ice to result from dendritic ice growth at the accretion surface. List (1990) refers to a layer of ice lying between the spongy ice matrix and the surficial liquid on a hailstone. In this section such a layer is also hypothesized, and is modelled as a zone of dendritic ice and water of thickness, y_1-y_0 (Fig. 3.3). In a way similar to List (1990), we suggest that this zone is that region over which the ice accretion evolves from its liquid state in the laminar film layer to its final equilibrium state in the ice matrix. This region is referred to as the freezing zone.

The freezing zone is assumed to contain an ensemble of ice crystals that are growing in close proximity to one another with a uniform tip growth rate. This uniform growth rate will ensure that the ice crystal tips remain in the plane of the icing interface as represented in Fig. 3.3. Kurz and Fisher (1986) show that the growth of an ensemble of dendrites is complex and the theory for such growth is not well developed. Therefore, modelling the freezing zone explicitly as an ensemble of ice dendrites appears for the moment to be a considerable problem in its own right. However, modelling the growth of the freezing zone by analogy with the growth of a freely-growing ice dendrite seems more plausible.

Tirmizi and Gill (1987) state that even for individual freely-growing crystals in a bulk supercooled liquid, there is an adequate theory for only the simplest cases, with no natural or forced convection. Moreover, data on dendrite tip geometry are still not available. Therefore, modelling the icing interface and the freezing zone by analogy with freely-growing ice dendrites is likely to require a number of assumptions. Modelling the freezing zone may be further complicated by the possibility that surficial ice crystal growth may occur in different modes. For example, Lock and Foster (1990), have observed and reported macroscopic evidence for columnar and mushy regimes in freshwater spray icing. Crystallographic factors such as ice crystal orientation and size, as well as other unknown factors, are likely to be responsible for these observed regimes. Accounting for such ice growth modes would escalate the model's already considerable

complexity. Hence, a relatively simple approach to modelling the freezing zone was sought, in order to achieve a first working model of spongy spray icing.

Our approach to modelling the freezing zone is based on three concepts. The first is that ice grows in such a way that the latent heat of fusion is released homogeneously throughout the freezing zone. As will be shown below, the evolution and conduction of latent heat is used as the basis for solving for the temperature profile in the freezing zone. This temperature profile is then used to give an estimate of the supercooling in the vicinity of the growing ice dendrite tips.

The second modelling concept arises from crystal growth theory (Tirmizi and Gill, 1987) which suggests that the linear growth rate of a freely-growing dendrite is controlled largely by the supercooling of the bulk liquid into which the dendrite is growing (in the vicinity of the crystal tip). The empirical relationship developed by Tirmizi and Gill (1987) for freely-growing ice crystals in supercooled water will be used to describe the rate of advance of the model's icing interface. Therefore, in the present approach we assume an equality between the rate of advance of a freely-growing ice dendrite tip in a semi-infinite volume of supercooled water, and the rate of advance of an ensemble of ice crystals with a known crystal tip supercooling. This approach of using a freely-growing dendritic growth rate model to estimate the growth rate of glaze ice was used by Kachurin and Morachevskii (1966) under the conditions of aircraft icing. In a similar way, List (1990) also used an ice crystal growth rate formulation to investigate the physics of water skins on hailstones.

The third concept used to evoke our model of the freezing zone has to do with estimating its thickness. We propose the idea that the freezing zone thickness may be related to the morphology of the tip of a freely-growing dendrite. Since crystal growth theory does not, at present, give a strong physical basis for modelling the growth of an ensemble of ice dendrites, a set of simple physical assumptions are employed instead. First, we assume that the interfacial ice dendrites grow in a way that preserves their shape with time (Makkonen, 1990). We further assume that the ice dendrites which grow at the interface have a radius of curvature similar to that observed by Tirmizi and Gill (1987). However, unlike the simple ice dendrites observed by Tirmizi and Gill (1987),

secondary dendritic growth in an ensemble of dendrites may be largely suppressed by the growth of neighbouring ice dendrites. That is, the heat evolved by nearby dendrites reduces the supercooling of the water interdendritically, so that the primary growth direction is normal to the interfacial surface. One morphological assumption which has the merit of simplicity, is that the freezing zone thickness is proportional to the radius of curvature of a freely-growing dendrite tip. In order to test this concept, the freezing zone thickness in the present model is linearly proportional to the radius of curvature of a freely-growing ice dendrite tip. The details of the concept are presented in Section 3.3.3.

3.3.1 Freezing zone thermodynamics

Returning now to the first concept, we assume that the latent heat of fusion produced by the growing ice is released homogeneously throughout the freezing zone. No particular dendritic growth mechanism or morphology from crystal growth theory is invoked to describe the evolution of latent heat within the layer. A simple and useful submodel results.

The conduction and evolution of heat in the freezing zone is described by a particular case of the one-dimensional steady-state heat diffusion equation. The differential equation for this problem is well known (Incropera and DeWitt, 1990):

$$\frac{d}{dy}\left(k\frac{dT(y)}{dy}\right) + q_v = 0 \qquad (3.17)$$

where k is the thermal conductivity of the freezing zone, T(y) is the temperature in the freezing zone, y is the coordinate normal to the surface with origin $y=y_0=0$ at the interface (Fig. 3.4), and q_v is the constant volumetric rate of heat evolution in the freezing zone. If the thermal conductivity is assumed to be independent of y, the general solution to Eqn. 3.17 is:

$$T(y) = -\frac{q_v}{2k}y^2 + c_1 y + c_2 \qquad (3.18)$$

and since the ice matrix is a freshwater accretion, the temperature at y=0 is $T=T_0=0°C$. Also, because there is no heat conduction within the spongy ice matrix or at the ice matrix/freezing zone interface, the gradient of temperature, $dT/dy = 0$ at y=0. Using both of these boundary conditions, the particular solution for Eqn. 3.17 is:

$$(T_0 - T_1) = \frac{q_v(y_1 - y_0)^2}{2k} \qquad (3.19)$$

where k is the thermal conductivity of the freezing zone, and where temperatures and distances are as shown in Fig. 3.4. In Eqn 3.19 and subsequently, we use the convention that heat fluxes which tend to increase the enthalpy of a zone or layer have positive values.

In Section 3.6 we show that the ratio of the temperature differences across the freezing zone and the laminar layer can be used to express the effect of these two surficial structures on the heat balance of the icing surface. We will now derive this temperature ratio starting with Eqn. 3.19. First, the volumetric rate of evolution of latent heat in the freezing zone q_v, may be written:

$$q_v = \frac{q_1}{(y_1 - y_0)} \qquad (3.20)$$

where q_1 is the heat flux from the freezing zone to the laminar layer (cf. Fig. 3.4). This heat flux is given by:

$$q_1 = I_0 L_f - c_w(I_0 + R_0)(T_0 - T_1) \qquad (3.21)$$

where L_f is the specific latent heat of fusion for pure water at 0°C, and c_w is the specific heat of pure water at 0°C. The first term on the right-hand-side of Eqn. 3.21 is the flux of heat evolved due to ice formation in the freezing zone and the second term is the flux of sensible heat required to warm the accreting mass flux, (I_0+R_0) from its temperature at the icing interface to its temperature in the ice matrix.

A heat balance at the icing interface is now introduced in order to derive an alternate expression for q_1. The heat balance at the interface is:

$$q_1 - q_c = 0 \tag{3.22}$$

where q_c is the heat flux conducted from the freezing zone across the laminar layer. Because a linear temperature profile prevails through the laminar layer, the heat flux q_c must be constant. Therefore, the flux of heat conducted from the freezing zone to the laminar layer may be written:

$$q_1 = q_c = k_w\left(\frac{T_1 - T_2}{y_2 - y_1}\right) \tag{3.23}$$

where T_2 is the temperature at the laminar layer/mixed layer interface. Substituting Eqn. 3.23 into Eqn. 3.20 results in another expression for the volumetric rate of generation of latent heat in the freezing zone:

$$q_v = k_w \frac{(T_1 - T_2)}{(y_2 - y_1)(y_1 - y_0)} \tag{3.24}$$

Substituting this expression into Eqn 3.19 results in:

$$(T_0 - T_1) = \frac{k_w}{2k}\frac{(y_1 - y_0)}{(y_2 - y_1)}(T_1 - T_2) \tag{3.25}$$

which may be further transformed into:

$$\frac{(T_0 - T_1)}{(T_1 - T_2)} = \frac{k_w}{2k}\frac{(y_1 - y_0)}{(y_2 - y_1)} \tag{3.26}$$

This expression for the ratio of the temperature differences across the freezing zone and the laminar layer will be used in the model's equation development in Section 3.6. It is also a useful parameter for solving the model's equations and appears again in the model's algorithm (in Appendix 7) as well as the model's computer code. Before Eqn. 3.26 can be used, however, a means of determining the ratio of layer thicknesses $(y_1 - y_0)/(y_2 - y_1)$ must be found. This is done in Section 3.3.3, below. First however, we will

consider, in Section 3.3.2, the approach used to model the rate of advance of the icing interface based on the single crystal growth empiricism of Tirmizi and Gill (1987).

3.3.2 The interfacial dendritic growth rate

Crystal growth theory (Chalmers, 1964) has long recognized that the linear growth rate at the tips of dendrites is a function of the supercooling of the bulk liquid into which the dendrite is growing. The dendritic growth rate is expressed as:

$$V_c = a(\Delta T)^b \qquad (3.27)$$

where a and b are empirical coefficients, and ΔT is the supercooling of the bulk liquid. Tirmizi and Gill (1987) made measurements of the growth rates and the dimensions of freely-growing ice crystals. The supercooling of water in a 5.0 cm diameter spherical container was controlled to ±0.005°C and observed with considerable accuracy (±0.0015°C). Ice crystals were nucleated at one end of a capillary tube and emerged from the other end of the capillary that was located at the centre of the spherical container. The growing ice crystal was observed photographically to determine its growth rate and dimensions with the help of a mounting which allowed for 360° rotation of the spherical chamber. Tirmizi and Gill (1987) say that this mounting made it possible to measure the linear crystal growth rate more accurately than had been done previously. Also, this apparatus served well in achieving the simultaneous and accurate measurement of ice crystal growth rate and ice crystal dimensions while observing the ice crystal morphology.

Tirmizi and Gill (1987) report $a=1.87X10^{-4}$ and b=2.09 (Eqn. 3.27) for ice crystal growth in pure water where V_c is the crystal growth rate in ms^{-1}, and ΔT is the supercooling in °C. They recommend these values of a and b for $\Delta T>0.2$°C. They found that at the slower crystal growth rates which are characteristic of lower supercoolings (i.e. $\Delta T<0.2$°C), natural convection in the bulk liquid controlled the crystal growth rate and hence Eqn. 3.27 was not valid. However, in the context of the present icing model, should a growth rate estimate be required at a supercooling of less than 0.2°C, we follow

the example of List (1990). He used the values of a and b (Eqn. 3.27) for ice growth rate in bulk water as given by Hobbs (1974) which are valid over the supercooling range, $2°C<\Delta T<6.5°C$. List (1990) extrapolated the formulation of Hobbs (1974) down to 0°C, arguing that the equation gives an expected and reasonable ice growth rate tendency as the supercooling approaches 0°C. That is, as the supercooling $\Delta T \rightarrow 0°C$, the growth rate also approaches zero. Kachurin and Morachevskii (1966) also use this assumption and an equation with the form of Eqn. 3.27 in modelling the rate of advance of the crystallization front. Experience in using the present spray icing model suggests that the crystal growth rate calculation is usually made for a supercooling, $\Delta T>0.2°C$. Consequently the crystal growth rate equation of Tirmizi and Gill (1987) was employed in the model over the entire range of supercooling. Next, the Tirmizi and Gill (1987) model of ice crystal tip morphology will be used to estimate the freezing zone thickness.

3.3.3 Freezing zone thickness

The third requirement for modelling the freezing zone is to determine its thickness. We propose that the radius of curvature of the tip of a freely-growing ice crystal be used as a basis for this estimate. Tirmizi and Gill (1987) observed that at low supercoolings (i.e. $\Delta T \approx 0.06°C$), ice crystals grow as basal plane disks, and that disks with serrated edges begin to form at bulk supercooling of $\Delta T=0.12°C$. Partially developed ice dendrites start to occur at $\Delta T=0.15°C$, and fully developed dendrites appear at $\Delta T=0.53°C$. Tirmizi and Gill (1987) give the radius of curvature at the tip of a growing ice crystal, ρ_c, at two bulk water supercoolings ($\rho_c=264\mu m$ at $\Delta T=0.1°C$; $\rho_c=80\mu m$ at $\Delta T=1.1°C$). They suggest that the radius of curvature is a function of ΔT^{-1} by expressing these two empirical results as $\rho_c=26.4\Delta T^{-1}\ \mu m$ at $\Delta T=0.1°C$ and $\rho_c=88.0\Delta T^{-1}\ \mu m$ at $\Delta T=1.1°C$. On the assumption of a linear relationship between ρ_c and ΔT^{-1}, and these observations, the radius of curvature may be expressed as:

$$\rho_c = 6.16\times10^{-5} + \frac{2.024\times10^{-5}}{\Delta T} \qquad (3.28)$$

where ρ_c is in units of metres and ΔT is in °C.

In the present approach, Eqn. 3.28 is used, on the assumption that $\Delta T=(T_0-T_1)$, to form a linear inverse relationship (Eqn. 3.29) between the thickness of the freezing zone and the supercooling at the icing interface. We assume that the freezing zone thickness is linearly proportional to the radius of curvature of the freely-growing ice crystal (i.e. $(y_1-y_0)=C_r\rho_c$). We postulate this proportionality in order to obtain a working model of spongy accretion, but it requires experimental verification. Consequently, the freezing zone thickness may be written:

$$(y_1 - y_0) = C_r \left(6.16\times10^{-5} + \frac{2.024\times10^{-5}}{(T_0 - T_1)}\right) \qquad (3.29)$$

where C_r is a constant of proportionality, referred to here as the freezing zone parameter. Eqn. 3.28 shows that at low supercooling, the radius of curvature of the tip of an ice crystal is large. This is in qualitative agreement with the macroscopic experimental observations of Lock and Foster (1990) who say that at high air temperatures (probable low film supercooling) coarse columnar ice crystals form the accretion's ice matrix. Such coarse columnar ice crystals are likely to have had large radii of curvature. They also observed that at low air temperatures (probable high film supercooling) a fine grained accretion with small crystal size occurred. Our working assumption in the present model is therefore that coarse ice crystals, with tips of large radii of curvature, grow in freezing zones of greater thickness than do smaller, finer ice crystals. The hypothesis that the freezing zone thickness is proportional to the radius of curvature of the freely-growing ice crystal will remain speculative until crystallographic observations of the freezing zone are made.

Eqn. 3.29 suggests that as $\Delta T\rightarrow0$°C, the freezing zone thickness, (y_1-y_0) becomes unbounded. However, since the ice accretion model usually does not predict icing interface supercoolings of less than 0.2°C, extremely large values of freezing zone

thickness do not arise. For example, the minimum value of supercooling which occurred in calculating the results of Section 3.8 is $(T_0-T_1)=0.238°C$ with a resulting freezing zone thickness of $(y_1-y_0)=197\mu m$.

Substituting Eqn. 3.29 into Eqn. 3.26 we obtain an expression for the freezing zone/laminar layer temperature difference ratio:

$$\frac{(T_0-T_1)}{(T_1-T_2)}=\frac{C_r}{(y_2-y_1)}\left(6.16\times10^{-5}+\frac{2.024\times10^{-5}}{(T_0-T_1)}\right)\frac{k_w}{2k} \qquad (3.30)$$

Since the freezing zone is a composite of liquid water and ice, it is reasonable to expect that its conductivity will be a function of its ice fraction. Even if the detailed freezing zone morphology were known, a difficult composite materials conduction problem would follow. Since this is not known, however, we estimate k as follows. We take the thermal conductivity at the ice matrix/freezing zone interface (y=0) to be identical with that of the spongy ice matrix:

$$k(I)_{y=0}=k_i I+k_w(1-I) \qquad (3.31)$$

where I is the ice fraction of the ice matrix and where k_i and k_w are the thermal conductivities of pure ice and liquid water, respectively. The thermal conductivity at the icing interface is taken be k_w. The thermal conductivity of the freezing zone is then taken to be the mean of k_w and $k(I)_{y=0}$:

$$k=\frac{k_w}{2}\left[I\left(\frac{k_i}{k_w}-1\right)+2\right] \qquad (3.32)$$

Substituting this expression into Eqn. 3.30 yields:

$$\frac{(T_0-T_1)}{(T_1-T_2)}=\frac{C_r}{I\left(\frac{k_i}{k_w}-1\right)+2}\left(\frac{6.16\times10^{-5}}{(y_2-y_1)}+\frac{2.024\times10^{-5}}{(T_0-T_1)(y_2-y_1)}\right) \qquad (3.33)$$

Next, the model's surficial heat balance equations will be derived.

3.4 Modelling the Falling Film Thermodynamics

The assumption has already been made that conductive heat transfer occurs in the laminar layer of the falling film. We will also assume that the mixed layer offers no resistance to heat transfer. This notion is consistent with thorough turbulent mixing and a resulting isothermal temperature profile. Under this set of assumptions, it is possible to write heat balance equations for the laminar and mixed layers. If no mixed layer is present, the mixed layer's heat balance equation (Eqn. 3.34) reduces to a heat balance at the outer surface of the laminar film. The convention is adopted here that those fluxes of heat which increase the enthalpy of a layer have positive values, and those fluxes which decrease the enthalpy of a layer have negative values. The heat balance for the mixed layer (or for the outer surface of the laminar layer if there is no mixed layer) is (cf. Fig. 3.4):

$$q_{i3} + q_c + q_a = 0 \qquad (3.34)$$

where q_{i3}, is the flux of sensible heat required to warm the incoming water in the mixed layer from T_{i3} to T_3 as it flows across the upper boundary of the cylinder segment, q_c, is the conductive heat flux that originates in the freezing zone and that is directed through the laminar layer into the mixed layer (appearing at the outer surface of the laminar layer as a component of the heat flux term q_{32} (Eqn. 3.44)), and q_a, is the net heat flux at the outer surface of the falling film. Each of these fluxes is described in more detail below.

The sensible heat flux, q_{i3}, required to warm the vertically inflowing liquid from T_{i3} to T_3 in the mixed layer, is:

$$q_{i3} = c_w R_{i3}(T_{i3} - T_3) \qquad (3.35)$$

where R_{i3} is the mass flux which flows into the mixed layer of the cylinder segment under consideration from the mixed layer of the segment lying above (Fig. 3.3), T_{i3} is the temperature of the incoming mixed layer fluid, and T_3 is the temperature of the mixed layer in the segment under consideration. Both T_{i3} and T_3 represent vertically averaged temperatures for their respective cylinder segments. Thus we approximate the continuous

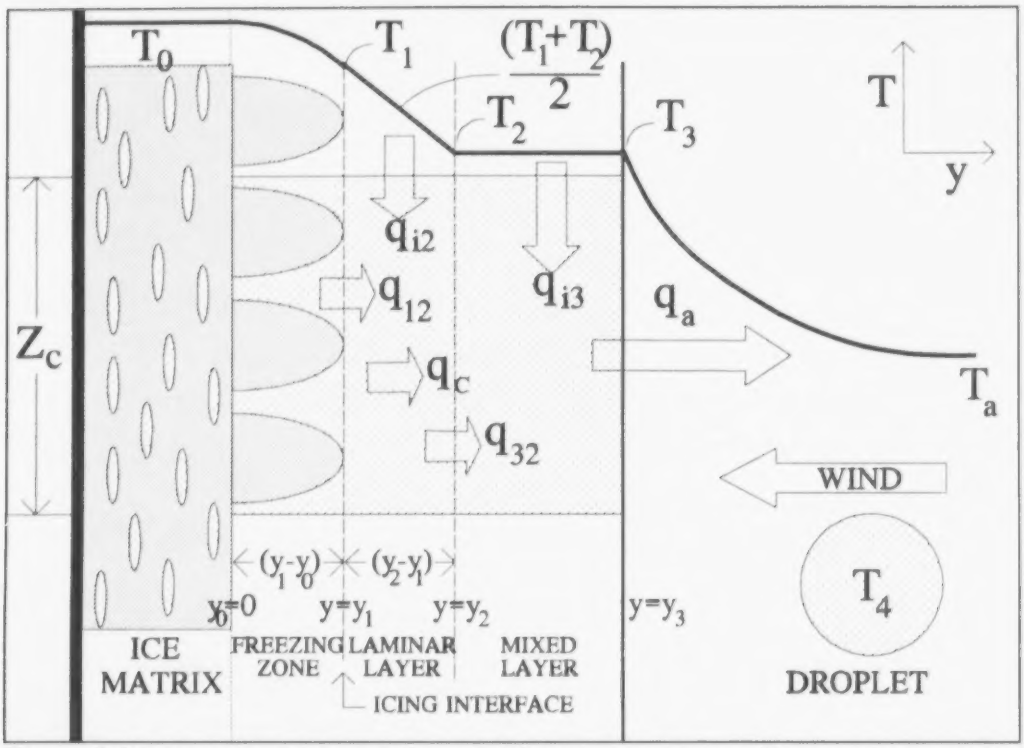

Figure 3.4 Schematic of the model's surficial structure with heat fluxes and temperature profile shown. The temperature axis is parallel to the icing surface with decreasing temperature in the downward direction.

variation of the mixed layer's temperature with height using finite averages over Z_c. This approach is taken for all of the characteristics of the falling film. For example, layer thickness, mass flux, heat flux and temperature are represented in this way, as well as output parameters such as the accretion flux and the ice fraction.

The conductive heat flux, q_c, is:

$$q_c = k_w \frac{(T_1 - T_2)}{(y_2 - y_1)} \tag{3.36}$$

The net heat flux at the outer surface of the falling film is:

$$q_a = -[h(T_3 - T_a) + \frac{\varepsilon h L_v}{c_p P_a}\left(\frac{P_r}{S_c}\right)^{0.63}(e_3 - RHe_a) + \sigma a(T_3 - T_a) + c_w R_4(T_3 - T_4)] \quad (3.37)$$

where h is the convective heat transfer coefficient, ε is the ratio of the molecular weights of water and dry air (0.622), L_v is the specific latent heat of vaporization, c_p is the specific heat of air at constant pressure, P_a is the ambient air pressure, e_a and e_3 are the saturation vapour pressures at temperatures T_a and T_3, respectively, RH is the relative humidity of the air, σ is the Stefan-Boltzman constant, and a is a linearization constant for thermal radiation (8.1×10^{7} K^3). The right-hand-side of Eqn. 3.37 consists of the convective, evaporative, radiative, and sensible heat flux terms respectively (Makkonen, 1984). The $2/\pi$ factor to be found in the last term of the comparable equation given by Makkonen (1984) does not appear in Eqn. 3.37. In the present work, this factor, which accounts for the distribution of the spray over the cylinder surface, is included in the definition of R_4. Eqns. 3.34 through 3.37 comprise the mathematical description of the mixed layer's heat balance.

The equation describing the heat balance of the laminar layer is:

$$q_{i2} + q_{12} + q_{32} = 0 \quad (3.38)$$

where q_{i2} is the sensible heat flux required to warm the vertically inflowing liquid in the laminar layer, q_{12} is the bulk heat flux from the freezing zone to the laminar layer, and q_{32} is the bulk heat flux from the laminar layer to the mixed layer, (Fig. 3.4).

The sensible heat flux required to warm the vertically inflowing liquid in the laminar layer is:

$$q_{i2} = c_w R_{i2}\left(T_{i2} - \frac{T_1 + T_2}{2}\right) \quad (3.39)$$

where R_{i2} is the mass flux into the laminar layer of the cylinder segment under consideration from the laminar layer of the segment above (Fig. 3.4); T_{i2} is the mean

temperature of the incoming laminar layer flux, and $(T_1+T_2)/2$, is the mean temperature of the laminar layer for the segment under consideration (Fig. 3.4).

Heat is exported into the laminar layer from the freezing zone, and some portion of this heat is used to warm the flux of water entrained by the freezing zone. This heat flux is:

$$q_{12} = q_1 + q_{21} \tag{3.40}$$

where q_1 is the heat flux from the freezing zone into the laminar layer (Eqn. 3.21), and q_{21} is the bulk sensible heat flux arising from the transfer (entrainment) of liquid from the laminar layer into the freezing zone. This sensible heat flux due to loss of liquid from the laminar layer is:

$$q_{21} = c_w R_{21}\left(\frac{T_1 + T_2}{2} - T_1\right) \tag{3.41}$$

where R_{21} is the mass flux of water transferred from the film's laminar layer into the freezing zone ($R_{21}=I_0+R_0$, Fig. 3.3), and where $(T_1+T_2)/2$ represents the mean temperature of the laminar layer. Heat fluxes q_1 and q_{21} are not shown in Fig. 3.4 in order to maintain the figure's simplicity. Substitution of Eqns. 3.41 and 3.21 into Eqn. 3.40 results in:

$$q_{12} = I_0 L_f + c_w R_{21}\left(\frac{T_1 + T_2}{2} - T_0\right) \tag{3.42}$$

The bulk heat flux between the laminar and mixed layers is:

$$q_{32} = q_{23} - q_c \tag{3.43}$$

where q_c is the conductive heat flux from the laminar layer into the mixed layer (Eqn. 3.36), and q_{23} is the bulk sensible heat flux due to entrainment of liquid from the mixed layer into the laminar layer. The bulk heat flux between the laminar and mixed layers is thus:

$$q_{32} = -c_w R_{32}\left(\frac{T_1+T_2}{2} - T_2\right) - k_w \frac{(T_1-T_2)}{(y_2-y_1)} \qquad (3.44)$$

3.5 Model Ice Growth Regimes

Although future models are likely to account for more of the crystallographic aspects of spray ice accretion, we begin here with a relatively simple model based on Eqn. 3.27:

$$V_1 = a(T_0 - T_1)^b \qquad (3.45)$$

where V_1 here is the rate of advance of the icing interface ($y=y_1$) relative to the liquid of the laminar layer (Fig. 3.4). V_1 is used in the model to specify three ice accretion regimes: (1) the glaze ice accretion regime, (2) the spongy ice accretion regime, and (3) the porous ice accretion regime. We will describe each regime in turn in Sections 3.5.1, 3.5.2, and 3.5.3.

3.5.1 The glaze ice accretion regime

In order to determine which icing regime prevails for a particular icing condition, it is first necessary to determine the ice flux, I_0. We assume here that I_0 is known. Since glaze ice is assumed to be solid, the rate of advance of the icing interface is:

$$V_g = \frac{I_0}{\rho_w} \qquad (3.46)$$

where ρ_w is the density of pure water. The density of water is used in Eqn. 3.46 because it is liquid water and not ice that prevails in the plane of the ice crystal tips at the icing interface ($y=y_1$) where V_g is defined. If the rate of advance of the icing interface, based on a solid growth morphology, V_g, equals or exceeds the rate of advance given by the ice crystal growth model, V_1 (see Eqn. 3.45), then the glaze ice accretion regime is

assumed to occur, and V_1, the rate of advance of the icing interface ($y=y_1$) is set equal to V_g. The glaze ice accretion regime is more likely to occur under conditions where the supercooling at the icing interface, (T_0-T_1), is small. On the other hand, if $V_g<V_1$, then either the spongy or porous ice accretion regime will prevail, and V_1, the rate of advance of the icing interface ($y=y_1$) retains its value according to Eqn. 3.45.

3.5.2 The spongy ice accretion regime

Since air bubble formation is neglected, the spongy ice accretion considered here consists of only ice and water. The rate of advance of the icing interface in the spongy ice accretion regime is:

$$V_1 = \frac{I_0 + R_0}{\rho_w} \tag{3.47}$$

where I_0/ρ_w represents the accretion of solid ice and R_0/ρ_w represents the entrapment of water. The spongy ice accretion regime will prevail as long as sufficient water is available. If the ice accretion flux, becomes equal to the entire liquid flux that is available for accretion, ($I_0+R_0=R_{i2}+R_{i3}+R_4$), then the fastest possible rate of advance for the icing interface is achieved under the spongy ice accretion regime, and the shedding fluxes for the laminar and mixed layers are zero. Substituting this expression into Eqn. 3.47 gives the maximum rate of advance of the icing interface:

$$V_{smax} = \frac{R_{i2} + R_{i3} + R_4}{\rho_w} \tag{3.48}$$

Therefore, the spongy ice accretion regime is defined to occur in the model over the V_1 range, $V_g<V_1\leq V_{smax}$.

3.5.3 The porous ice accretion regime

The porous ice accretion regime occurs when the predicted crystallographic rate of advance of the icing interface, V_1, exceeds the maximum rate of advance of the icing interface for the spongy regime ($V_1 > V_{smax}$). In this case, the mass flux shed from the segment is assumed to be zero, and all of the water directed onto the icing surface of the cylinder segment is accreted in either the solid or liquid phase. Since the accretion of all the available water substance is not sufficient to produce a deposit growth rate equal to V_1 if it is composed of only water and ice, voids in the ice matrix are assumed to form. The rate of advance of the icing interface for the porous ice accretion regime is:

$$V_1 = \frac{R_{i2} + R_{i3} + R_4}{\rho_w} + \frac{R_a}{\rho_a} \qquad (3.49)$$

where ρ_a is the density of the entrapped air, and where R_a is the mass flux of air included in the growing accretion. This equation defines and determines R_a.

3.5.4 Determination of the ice accretion regime

In Sections 3.5.1, 3.5.2 and 3.5.3, the rate of advance of the icing interface, V_1, was used as the criterion for determining the model icing regime. However, in the development of the model's algorithms and computer code, two mass flux parameters are used instead to determine the model icing regime. The result is equivalent to using V_1, but the procedure yields a less complex algorithm.

The first parameter is R_0, the flux of water entrapped by the ice matrix, while the second is R_a, the mass flux of air entrapped in the ice accretion. The first parameter is used to identify glaze icing cases, and we define R_0 as:

$$R_0 = V_1 \rho_w - I_0 \qquad (3.50)$$

For known ice flux, I_0, and rate of advance of the icing interface, V_1 (Eqn. 3.45), the value of R_0 is used to test for the glaze ice accretion regime. If we find that $R_0 \leq 0$, the

glaze ice accretion regime prevails, and we set $R_0=0$. If $R_0>0$, either the spongy or porous ice accretion regime occurs and the value of R_0 is accepted as the flux of water entrapped by the ice matrix.

The second parameter, that is used as a criterion in determining the occurrence of the porous ice accretion regime, R_a, is defined with Eqn. 3.49:

$$R_a = \frac{\rho_a}{\rho_w}(V_1\rho_w - R_{i2} - R_{i3} - R_4) \tag{3.51}$$

If $R_0>0$, and $R_a\leq 0$, the spongy ice accretion regime occurs, and we set the mass flux of entrapped air, $R_a=0$. If $R_0>0$, and $R_a>0$, the porous ice accretion regime prevails, and the value of R_a is accepted as the flux of entrapped air at the icing surface.

3.5.5 Ice accretion sponginess and density

The "sponginess" of a sample of ice, λ, is defined to be its liquid mass fraction:

$$\lambda = \frac{m_w}{m_i + m_w + m_a} \tag{3.52}$$

where m_w is the mass of the entrapped water, m_i is the mass of ice, and m_a is the mass of air included in the accretion. The mass of entrapped air is usually neglected being small. However, because air is trapped in the porous ice accretion regime and because air inclusion may have a significant effect on accretion density, we retain the effect of air inclusion in the equations that follow. Using mass fluxes, sponginess may be defined equivalently:

$$\lambda = \frac{R_0}{I_0 + R_0 + R_a} \tag{3.53}$$

The air inclusion fraction may similarly be written as:

$$\lambda_a = \frac{R_a}{I_0 + R_0 + R_a} \tag{3.54}$$

An equation for the accretion density, ρ_{ac}, may be derived as follows. First, the rate of advance of the ice matrix/freezing zone interface is:

$$V_0 = \frac{I_0}{\rho_i} + \frac{R_0}{\rho_w} + \frac{R_a}{\rho_a} = \frac{I_0 + R_0 + R_a}{\rho_{ac}} \tag{3.55}$$

Next, the ice fraction may be written in terms of the sponginess and the air inclusion fractions as:

$$I = 1 - \lambda - \lambda_a \tag{3.56}$$

Eqns. 3.55 and 3.56 can be combined to give:

$$\rho_{ac} = \frac{\rho_w \rho_i \rho_a}{\lambda \rho_i \rho_a + \lambda_a \rho_w \rho_i + I \rho_w \rho_a} \tag{3.57}$$

Once the icing regime has been determined, accretion characteristics such as ice fraction (Eqn. 3.56), air inclusion fraction (Eqn. 3.54), and accretion density (Eqn. 3.57) can be calculated.

3.6 Model Equations

The model equations developed throughout Sections 3.2 to 3.5, are brought together and summarized here to make them more accessible. For symbol meanings, we refer the reader to the List of Symbols or to the original text in which they were introduced. We start with the equations that describe the falling film. The thickness of the falling film (cf. Eqn. 3.15) for both turbulent and laminar conditions is:

$$(y_3 - y_1) = \left(\frac{\mu\eta}{g^{1/2}\rho}\right)^{\frac{2}{3}} \tag{3.58}$$

The total mass flux for the falling film (laminar or turbulent) is:

$$R_T = R_2 + R_3 \tag{3.59}$$

where the falling film fluxes (R_T, R_2, R_3) are determined for a laminar falling film, a falling film with a mixed layer consisting of a buffer layer, and a falling film with a mixed layer consisting of buffer and turbulent layers. For a falling laminar film with no mixed layer present (cf. Eqns. 3.9 and 3.59):

$$\begin{aligned} &R_2 = 0.5\mu\eta^2 Z_c^{-1};\ R_3 = 0 \\ &R_T = R_2 \qquad\qquad 0 < \eta \le 5 \\ &(y_3 - y_1) = (y_2 - y_1);\ y_3 = y_2 \end{aligned} \tag{3.60}$$

For a falling laminar film with mixed layer consisting of a buffer layer only (cf. Eqns. 3.10, 3.11, and 3.15 with η=5):

$$\begin{aligned} &R_2 = 12.5\mu Z_c^{-1};\ R_3 = R_T - R_2 \\ &R_T = \mu(12.5 - 8.05\eta + 5.0\eta\ln\eta)Z_c^{-1} \qquad 5 < \eta \le 30 \\ &(y_2 - y_1) = \frac{5\mu}{\sqrt{g(y_3 - y_1)\rho}} \end{aligned} \tag{3.61}$$

For a falling film with mixed layer composed of buffer and turbulent layers (cf. Eqns. 3.10, 3.12 and 3.15 with η=5):

$$\begin{aligned} &R_2 = 12.5\mu Z_c^{-1};\ R_3 = R_T - R_2 \\ &R_T = \mu(-63.8 + 3.0\eta + 2.5\eta\ln\eta)Z_c^{-1} \qquad \eta > 30 \\ &(y_2 - y_1) = \frac{5\mu}{\sqrt{g(y_3 - y_1)\rho}} \end{aligned} \tag{3.62}$$

The conservation of water substance for the falling film is expressed as:

$$R_{i2} + R_{i3} + R_4 = I_0 + R_0 + R_2 + R_3 \tag{3.63}$$

The ratio of the temperature differences across the freezing zone and the laminar layer is:

$$\frac{(T_0 - T_1)}{(T_1 - T_2)} = \frac{k_w}{2k}\frac{(y_1 - y_0)}{(y_2 - y_1)} \tag{3.64}$$

where the freezing zone thickness is:

$$(y_1 - y_0) = C_r\left(6.16\times10^{-5} + \frac{2.024\times10^{-5}}{(T_0 - T_1)}\right) \tag{3.65}$$

The mean thermal conductivity of the freezing zone, k, is:

$$k = \frac{k_w}{2}\left[I\left(\frac{k_i}{k_w} - 1\right) + 2\right] \tag{3.66}$$

where the ice fraction, I, is:

$$I = \frac{I_0}{I_0 + R_0 + R_a} \tag{3.67}$$

The heat balance equation for the mixed layer or for the outer surface of the laminar falling film in the event that no mixed layer is present, is (cf. Eqn. 3.34):

$$\begin{aligned} &k_w\frac{(T_1 - T_2)}{(y_2 - y_1)} - h(T_2 - T_a) - \frac{\varepsilon h L_v}{c_p P_a}\left(\frac{P_r}{S_c}\right)^{0.63}(e_2 - RHe_a) \\ &-\sigma a(T_2 - T_a) + c_w R_{i3}(T_{i3} - T_2) - c_w R_4(T_2 - T_4) = 0 \end{aligned} \tag{3.68}$$

where we have used T_2=T_3. The heat balance for the laminar layer is (cf. Eqn. 3.38):

$$\begin{aligned} &c_w R_{i2}\left(T_{i2} - \frac{T_1 + T_2}{2}\right) + I_0 L_f + c_w(I_0 + R_0)\left(\frac{T_1 + T_2}{2} - T_0\right) \\ &- c_w R_{32}\left(\frac{T_1 + T_2}{2} - T_2\right) - k_w\frac{(T_1 - T_2)}{(y_2 - y_1)} = 0 \end{aligned} \tag{3.69}$$

The mass flux of water entrained into the laminar layer from the mixed layer is (see Fig. 3.3):

$$R_{32} = R_{13} + R_4 - R_3 \tag{3.70}$$

Establishing the ice accretion regime begins with the equation for estimating the rate of advance of the icing interface:

$$V_1 = a(T_0 - T_1)^b \tag{3.71}$$

Based on this rate of advance, V_1, an estimate of the mass flux of entrapped water, R_0, (which is used as a criterion for determining the occurrence of the glaze ice accretion regime) is:

$$R_0 = V_1 \rho_w - I_0 \tag{3.72}$$

An estimate of the mass flux of entrapped air, R_a, (which is used as a criterion for discerning the occurrence of the porous ice accretion regime) is:

$$R_a = \frac{\rho_a}{\rho_w}(V_1 \rho_w - R_{12} - R_{13} - R_4) \tag{3.73}$$

Once R_0 and R_a are known, (Eqns. 3.72 and 3.73) the icing regime is established according to the following criteria: (1) if $R_0 \leq 0$, the glaze ice accretion regime occurs with $R_0=0$ and $R_a=0$; (2) if $R_0>0$ and $R_a \leq 0$, the spongy ice accretion regime occurs with a mass flux of entrapped water, R_0 and a mass flux of entrapped air, $R_a=0$, and (3) if $R_0>0$ and $R_a>0$, the porous ice accretion regime occurs with a mass flux of entrapped water, R_0, and a mass flux of entrapped air, R_a. Once R_0 and R_a are known, along with the pure ice flux, I_0, the ice fraction and ice accretion density can be estimated according to the equations of Section 3.5.5.

An examination of the equations of this section shows that there is an empirical parameter (C_r in Eqn. 3.65) that must be evaluated before the model is complete. Once that parameter has been specified, there are 16 variables to solve for. These are: R_2, R_3, R_{32}, R_T, η, y_3, y_2, y_1, I, I_0, R_0, R_a, T_3, T_1, k, and V_1 where T_2 is not explicitly included

because $T_2=T_3$. Other parameters that appear in the equations are either (1) parameters that describe the physical properties of air, water, or ice (e.g. ρ, μ, etc.), or (2) parameters that are known on the basis of external input conditions (e.g. h, e_a), or (3) input parameters (e.g. T_a, RH, V_a, T_4, R_4). There are 16 independent model equations (Eqns. 3.58 to 3.74). Thus the number of equations is sufficient to solve for the model's variables and to yield an ice accretion prediction. The algorithm used to solve the equations of the model is described in Appendix 7, along with a listing of the model's computer code on diskette. In the next section, the question of evaluating the empirical parameter, C_r, is addressed.

3.7 Model Calibration

This section presents the method used to calibrate the model. Calibration in the present context means determining the value of the freezing zone parameter, C_r, (cf. Eqn. 3.65), under the assumption that C_r is indeed a constant of the problem. Determination of this parameter is possible if the rate of advance of the icing interface (the ice growth rate) and the ice fraction are both known experimentally. However, if the thickness of the freezing zone relates to the radius of curvature of a freely-growing ice crystal in a more complex way than we have assumed, the freezing zone parameter may not be a constant but may be a more complicated function of conditions at the icing surface. However, in order to achieve a working model, we persist with the assumption that the freezing zone parameter is a constant. Nine spongy icing experiments performed at the University of Alberta are used to estimate C_r. The mean value of C_r based on these observations is used in the model for the sensitivity and performance analysis of Section 3.8. Because of the uncertainty in C_r, the sensitivity of the model's prediction to variation in C_r, will be examined for a "representative" icing condition.

3.7.1 The calibration equations

The method used to derive an equation for C_r, is first to produce an alternate expression for the freezing zone/laminar layer temperature ratio to that given by Eqn. 3.33, and then to equate the two expressions. First, the ice fraction, I, defined in Eqn. 3.67, may be written:

$$I = \frac{I_0}{I_0 + R_0} \tag{3.74}$$

where we assume for the present that there is no air inclusion (R_a=0). Using Eqn. 3.47, the ice accretion flux may be expressed as:

$$(I_0 + R_0) = V_1 \rho_w \tag{3.75}$$

Next, the expression for q_1 (Eqn. 3.21) is transformed to give:

$$q_1 = (I_0 + R_0)\left[L_f\left(\frac{I_0}{I_0 + R_0}\right) - c_w(T_0 - T_1)\right] \tag{3.76}$$

Eqns. 3.74 and 3.75 are then substituted into Eqn. 3.76 and give:

$$q_1 = V_1 \rho_w [L_f I - c_w(T_0 - T_1)] \tag{3.77}$$

Substituting the expression for V_1 (Eqn. 3.71) into Eqn. 3.77, and then introducing the resulting equation for q_1 into Eqn. 3.23 (i.e. q_1=q_c) results in:

$$a(T_0 - T_1)^b \rho_w [L_f I - c_w(T_0 - T_1)] = k_w \frac{(T_1 - T_2)}{(y_2 - y_1)} \tag{3.78}$$

Eqn. 3.78 may be transformed to give an expression for the freezing zone/laminar layer temperature difference ratio:

$$\frac{(T_0-T_1)}{(T_1-T_2)} = \frac{k_w}{a(T_0-T_1)^{b-1}\rho_w\,[L_f I - c_w(T_0-T_1)]\,(y_2-y_1)} \tag{3.79}$$

Finally, this ratio is equated to that given by Eqn. 3.33 to yield an expression for C_r:

$$C_r = \frac{[I(k_i-k_w)+2k_w]\,[L_f I - c_w(T_0-T_1)]^{-1}}{a\rho_w[6.16\times10^{-5}(T_0-T_1)^{b-1}+2.024\times10^{-5}(T_0-T_1)^{b-2}]} \tag{3.80}$$

Eqn. 3.80 may be used to estimate C_r if the ice fraction, I, and the supercooling at the icing interface, (T_0-T_1) are known. The supercooling at the icing interface, (T_0-T_1), is not likely to be measured experimentally, but it may be inferred on the basis of Eqn. 3.71 for a known value of V_1. Most icing measurements will be of V_0, the rate of advance of the ice matrix, and not V_1. Therefore, using Eqns. 3.47 and 3.55, and with R_a=0, the rate of advance at the icing interface is:

$$V_1 = V_0\left[1 + I\left(\frac{\rho_w}{\rho_i}-1\right)\right]^{-1} \tag{3.81}$$

Together, Eqns. 3.81, 3.45, and 3.80 can be used to determine C_r, from observations of V_0 and I.

3.7.2 Estimation of the freezing zone parameter

The case of hailstone growth (List 1990) is used here to illustrate the estimation of C_r. List (1990) states that temperatures below the freezing point of water occur in the water skins which form on hailstones. He also states that supercooling as high as 5°C is routinely observed at the water skin-air interface. On the basis of this observation, he suggests that the water skins which cover the growth regions of hailstones are probably laminar, with thicknesses of up to approximately 1 mm. The water skins on hailstones may be quite different from the falling films on a vertical icing surface. Whatever the differences may be for the water films of these two icing configurations, we assume that

their freezing zones are similar. The present approach to model calibration and the example that follows depends on the equation development of Section 3.7.1 which reveals that in order to estimate C_r, only conditions in the freezing zone and at the icing interface need to be considered. The difficulties of accounting for or measuring the characteristics of the many surficial liquid films that may occur under various icing configurations and conditions are therefore sidestepped.

List (1990) measured an ice growth rate of 2.0 mm min^{-1} on a 2 cm gyrating spheroid, with a water skin thickness of 1 mm and an estimated ice fraction, I=0.5. He does not give the wind tunnel conditions that produced these ice growth parameters. However, with $V_0=1.667X10^{-5}ms^{-1}$, Eqn. 3.81 may be used to calculate $V_1=1.60X10^{-5}ms^{-1}$. Equation 3.45 may then be used to calculate $(T_0-T_1)=0.31°C$. This value of supercooling is close to the value calculated by List (1990) of 0.307°C. He used the equation of Hobbs (1974) which has the same form as Eqn. 3.27 with values for a and b of $2.8X10^{-4}$ and 2.39, respectively. Therefore, even though these values of a and b differ from those used in the present model (i.e. $1.87X10^{-4}$ and 2.09), calculation of supercooling at the icing interface is, for this icing condition, substantially unaffected by the choice of ice crystal growth rate model. Finally, Eqn. 3.80 is used to estimate $C_r=1.64$.

Using the method illustrated above, spongy spray icing measurements made in the Marine Icing Wind Tunnel at the University of Alberta (Shi, pers. comm.) were used to calculate values of the freezing zone parameter. Shi measured ice growth rates and ice fractions on a slowly rotating (0.1 Hz) horizontal cylinder of 4 cm diameter. The ice growth rates were determined in the centre of the accretion from the measured experiment duration and the final accretion diameter. Ice from the central portion of the accretion was also used to establish the ice fraction of the deposit by calorimetry.

The Marine Icing Wind Tunnel at the University of Alberta (Foy, 1988) has a vertical working section in which airspeed was varied from 10 to 30 ms^{-1}, and the air temperature from 0°C to -30°C. The air flow (directed downward) carried spray from nozzles located above the rotating cylinder to the surface of the ice accretion on the cylinder. The spray cooled en route to the ice accretion but the spray temperature was not measured. The spray flux was measured prior to each icing run by collecting spray

with a sponge placed in the airstream. The air temperature, wind speed, spray flux, ice growth, and ice accretion sponginess were measured for eighteen cases. The first nine cases are used here to estimate the value of the freezing zone parameter; these data are tabulated in Appendix 8. The remaining nine cases are documented in Appendix 9 and are used for model performance evaluations in Section 3.8.4. The first nine cases yield a range for the freezing zone parameter of $1.09 \leq C_r \leq 1.56$, with a mean value of 1.33, and a standard deviation of 0.16. This mean value is used in the model for the performance evaluations and sensitivity analysis of Section 3.8. Both sets of nine icing cases include a variety of icing conditions, such as a considerable variation of wind speed (10 ms^{-1} to 30 ms^{-1}) and air temperature (-2°C to -20°C). While the first group of icing cases was chosen arbitrarily for calibrating the model, the second group would have produced a similar value for C_r of 1.43.

3.7.3 Model sensitivity to the freezing zone parameter

Because of the range of values estimated for C_r, the model sensitivity to variations in C_r will now be examined. The results of the sensitivity analysis are shown in Fig. 3.5 near the end of this section. The environmental conditions used for this analysis are the ones that will be used as a standard condition for sensitivity analysis to other parameters in Section 3.8. It is also the standard condition used in the freshwater icing experiments reported by Lesins et al. (1980) on a horizontal cylinder of diameter 1.9 cm. For the present purpose, we have chosen the diameter of the vertical cylinder to be 1.9 cm with a single cylinder segment of the same height, Z_c=1.9 cm. The air temperature is -10°C, and the airspeed 18.0 ms^{-1}. The temperature of the impinging spray is assumed to be midway between the freezing point and the temperature of the air (i.e. T_4=-5°C). The liquid water content of the spray is 15 gm^{-3}, and the droplets have a diameter of 90μm. The cylinder collision efficiency calculated from the equations of Finstad et al. (1988) for these conditions is E=0.92. Thus the spray flux (with collision efficiency accounted for) is 0.249 $kgm^{-2}s^{-1}$. The relative humidity of the airstream is assumed to be 90%.

For the present purpose, we have chosen the diameter of the vertical cylinder to be 1.9 cm with a single cylinder segment of the same height, Z_c=1.9 cm. A model configuration with cylinder segment height equal to its diameter, D, was chosen in order to simulate the length over which excess surficial water will flow on a horizontal cylindrical icing surface such as the ones investigated by Lesins et al. (1980). Lozowski et al. (1995) propose a liquid film flow length of πD/4 for excess water on the windward surface of a horizontal icing cylinder. Their film flow model estimates the film thickness on the icing surface using the wind shear on the cylinder's surface. For a cylinder with rotation and wind shear neglected, the maximum length over which the liquid might flow under its gravitational body force is πD/2. Since a surficial flow length equal to the cylinder's diameter lies between these two estimates (πD/4 and πD/2), the cylinder diameter, D, was used in our vertical cylinder icing model (Z_c=D) to simulate icing on horizontal cylinders. Table 3.1 shows the sensitivity of the model's surficial liquid film thickness and ice fraction to film flow length (i.e. Z_c). For a variation in the film flow length from πD/4 to πD/2, the predicted film thickness was within 20% of that predicted for a flow length of D. For the same variation in film flow length the predicted ice fraction was within 5% of that which was estimated for a flow length of D. Therefore, the choice of cylinder segment height (i.e. flow path length) has a significant influence on the film thickness while having a relatively modest effect on the accretion's ice fraction. Film thicknesses of several hundred micrometres have been proposed by Kachurin et al. (1974) for vessel icing conditions and by List (1990) for hailstone growth. Lozowski et al. (1995) shows that for a 5 cm diameter horizontal cylinder (with no icing) and a large impinging spray flux (2 $kgm^{-2}s^{-1}$) that a maximum film thickness of 280 μm is to be expected. Therefore, until a more complete description of the way in which liquid

Table 3.1 Predicted falling film thickness, (y_3-y_1), and ice fraction, I, for three film flow path lengths or segment heights, Z_c. (conditions as given in Section 3.7.3)

Z_c	πD/4 (1.5 cm)	D (1.9 cm)	πD/2 (3 cm)
(y_3-y_1)	88.3 μm	95.7 μm	112 μm
I	0.545	0.557	0.584

films depend on gravitational body force, wind shear and surface geometry becomes available, a model-predicted film thickness of ~96μm (for the present standard condition) is likely to provide a satisfactory basis on which to make a comparison between the predictions of a vertical cylinder icing model and icing data for horizontal cylinders.

The falling liquid film and the ice growth on a vertical cylinder of height, D, can be modelled in the single-segment mode (Z_c=D) or in the multi-segment mode (Z_c=D/N) where N is the number of segments. The multi-segment mode produces greater vertical resolution for the model's output (i.e. I, (I_0+R_0), (y_3-y_1)). However, for the standard icing conditions as described above, the model in multi-segment mode with N=10, estimates ice accretion flux, (I_0+R_0) and an ice fraction, I, that is within 5% of the values predicted by the model in single segment mode. Therefore, we use single segment mode (Z_c=D) for all of the sensitivity analyses and for all of the model comparisons with horizontal icing data that follow in Section 3.8. We sidestep the extra computational effort of the multi-segment mode because it has little effect on the largely qualitative results of the sensitivity analyses, and because the extra resolution is not likely to reflect the icing on horizontal cylinders more realistically.

The spongy spray icing model was run for values of the freezing zone parameter in the range $1.0 \le C_r \le 2.0$ in order to illustrate the sensitivity of the model's ice fraction to this parameter. Fig. 3.5 shows that the ice fraction, I, has a substantial dependence on C_r. An increase in C_r from 1.0 to 2.0 results in a decrease in the ice fraction from 1.0 to approximately 0.2. On the other hand, the flux of pure accreted ice calculated by the model, I_0, increases by only 1.4% over this range of C_r. This suggests that the rather substantial increase in total accretion flux calculated by the model, (I_0+R_0), from 0.018 $kgm^{-2}s^{-1}$ to 0.089 $kgm^{-2}s^{-1}$ is largely the result of the increase in sponginess. Hence the model's prediction of spongy ice accretion flux and ice fraction are strongly dependent on the value of C_r.

An increase in the freezing zone parameter has the effect of increasing the thickness of the freezing zone (Eqn. 3.29), which in turn causes the supercooling at the icing interface to increase. This increased supercooling results in an increased rate of advance of the icing interface and hence increased sponginess, as more of the surficial

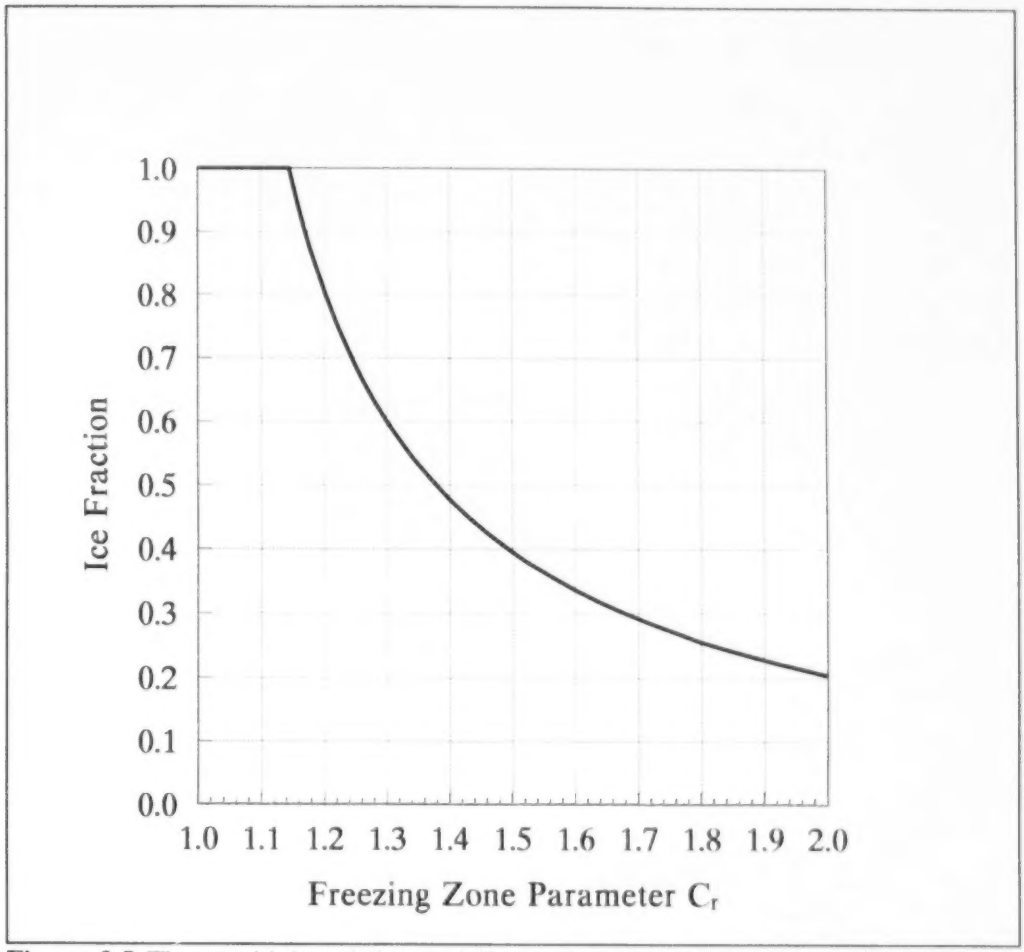

Figure 3.5 The sensitivity of the model's predicted ice fraction to the freezing zone parameter, C_r. (other conditions given in text)

water is entrained by the freezing zone and then entrapped in the advancing ice matrix. This enhanced surficial water entrapment also has the effect of reducing the thickness of the falling film, thereby increasing the film surface temperature, the external heat transfer and hence the flux of pure ice, although only slightly. Therefore, the total ice accretion flux, the ice fraction of the spongy accretion, and the thickness of the falling film depend substantially on the freezing zone parameter, and the surficial structure of the model.

3.8 Model Performance and Sensitivity

The model's performance is examined by comparing the model's prediction of ice fraction and ice accretion flux with the results of experiments performed by Lesins et al. (1980). Following this, the sensitivity of the model to spray flux, spray temperature, air temperature, air velocity, and relative humidity is presented. This is done by varying one parameter at a time from the standard icing condition specified in Section 3.7.3. Finally, the model's performance is compared to ice accretion and ice fraction observations made in the Marine Icing Wind Tunnel at the University of Alberta (Shi, pers. comm.).

3.8.1 Model evaluation with the icing data of Lesins et al. (1980)

Lesins et al. (1980) performed freshwater icing experiments in a refrigerated wind tunnel using a slowly rotating (0.5 Hz) cylinder of diameter 1.9 cm. The cylinder was oriented horizontally 1.8 m above nozzles that produced spray with a mean volume droplet diameter of 90μm. An airflow with a speed of 18 ms^{-1} carried the spray up to the cylinder, cooling the droplets en route. The initial spray temperature at the nozzles was about 0°C and Lesins et al. (1980) estimate a spray temperature close to that of the airstream at the location of the cylinder. The liquid water content was varied from 2 to 40 gm^{-3} while air temperature was varied from -2 to -20°C.

Even though the comparison of the results of Lesins et al. (1980) for a horizontal slowly rotating cylinder, with the performance of our spongy spray icing model for a non-rotating vertical cylinder is not ideal, we persist in the comparison on the basis of similarities in heat transfer with the airstream and spray collision with the cylinder. For both configurations spray collision will occur on the windward half of the cylinder and the collision efficiency will be the same for both configurations. The loss of heat from the two cylinder configurations will be similar because of the same air speed and cylinder diameter. In order to make the best comparison possible, the model cylinder segment length, Z_c, was set equal to its diameter, D=1.9 cm. In section 3.7.3 we propose this segment length because it is approximately the length of the surficial water shedding path

on the surface of a horizontal cylinder. The resulting comparisons of ice fraction, I, and ice accretion flux, (I_0+R_0), are shown in Figs. 3.6 and 3.7, respectively.

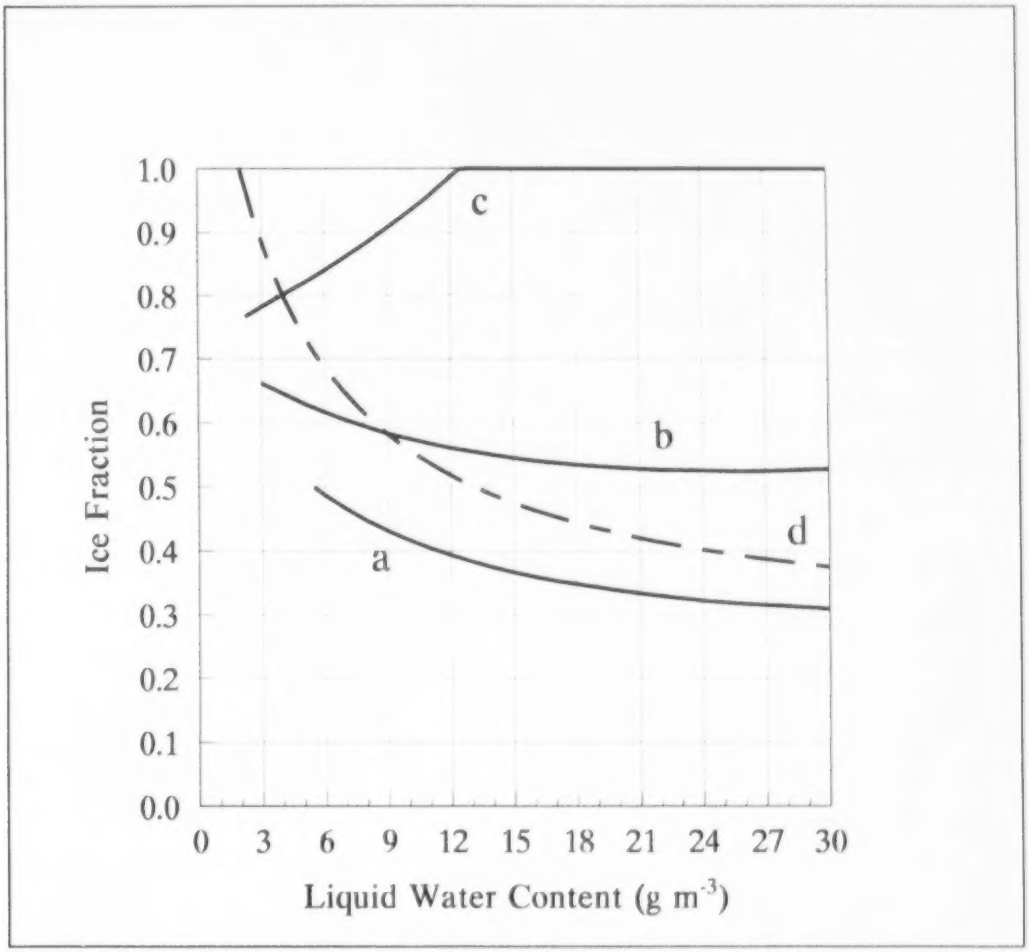

Figure 3.6 Ice fraction as a function of liquid water content for model spray temperatures (a) T_4=-10°C, (b) T_4=-5°C, (c) T_4=0°C, compared with (d) the result of Lesins et al. (1980).

Lesins et al. (1980) measured the thickness of the ice accreted on the cylinder along with the ice fraction of a sample of the accretion. These measurements were used to calculate the net collection efficiency. The net collection efficiency , E_{net}, is defined by Lesins et al. (1980) as the ratio of the mass growth rate by permanently accreted water to the total mass flow rate in the volume swept out by the cylinder. A least squares best fit was applied to the data to give empirical equations for the net collection

efficiency, E_{net}, and the ice fraction, I, as functions of air temperature, T_a, and liquid water content, W_f. The resulting empirical relationship for the net collection efficiency has been used to plot curve "d" in Fig. 3.7 which shows ice accretion flux, (I_0+R_0), as a function of liquid water content at air temperature, T_a=-10°C. Their empirical relation for ice fraction, I, as a function of liquid water content at an air temperature, T_a=-10°C, is shown as curve "d" in Fig. 3.6.

Fig. 3.6 shows the model-predicted ice fraction as a function of liquid water content for the standard condition of Lesins et al. (1980), with a spray temperature, T_4, of -10°C, -5°C, and 0°C. These three spray temperatures are presented because the actual spray temperature at the cylinder was not measured. Curves "a" and "b" in Fig. 3.6 appear qualitatively similar to the empirical result of Lesins et al. (1980), while the warm spray curve "c" exhibits an opposite tendency with glaze ice at high liquid water contents. Curve "c" shows an increasing ice fraction with increasing liquid water content (up to ~12.5gm^{-3}) due to an increased contribution of sensible heat by the relatively warm impinging spray (T_4=0°C). An increased contribution of sensible heat at the outer surface of the falling film due to warm spray accounts for an increased portion of the convective and evaporative heat loss to the airstream. This brings with it a reduction in that portion of heat loss to the airstream which originates in the freezing zone. Hence, a reduction in the rate at which heat is conducted from the freezing zone and the rate at which pure ice grows in the freezing zone. Decreased heat conduction in the freezing zone and at the icing interface is accompanied by a decreased thermal gradient. A decreased thermal gradient in the freezing zone leads to decreased supercooling at the icing interface. Reduction in the supercooling at the icing interface leads to a decreased rate of advance of the icing interface and reduced entrapment of water by the ice matrix. Therefore, the ice fraction of the accretion increases with increasing liquid water content until the glaze ice accretion regime occurs with an ice fraction of unity.

The low spray temperature curves "a" and "b" show an increasing sponginess (decreasing ice fraction) with increasing liquid water content. This decreasing ice fraction with increasing liquid water content results from the impingement and warming of supercooled spray. Thus sensible heat loss augments the convective and evaporative heat

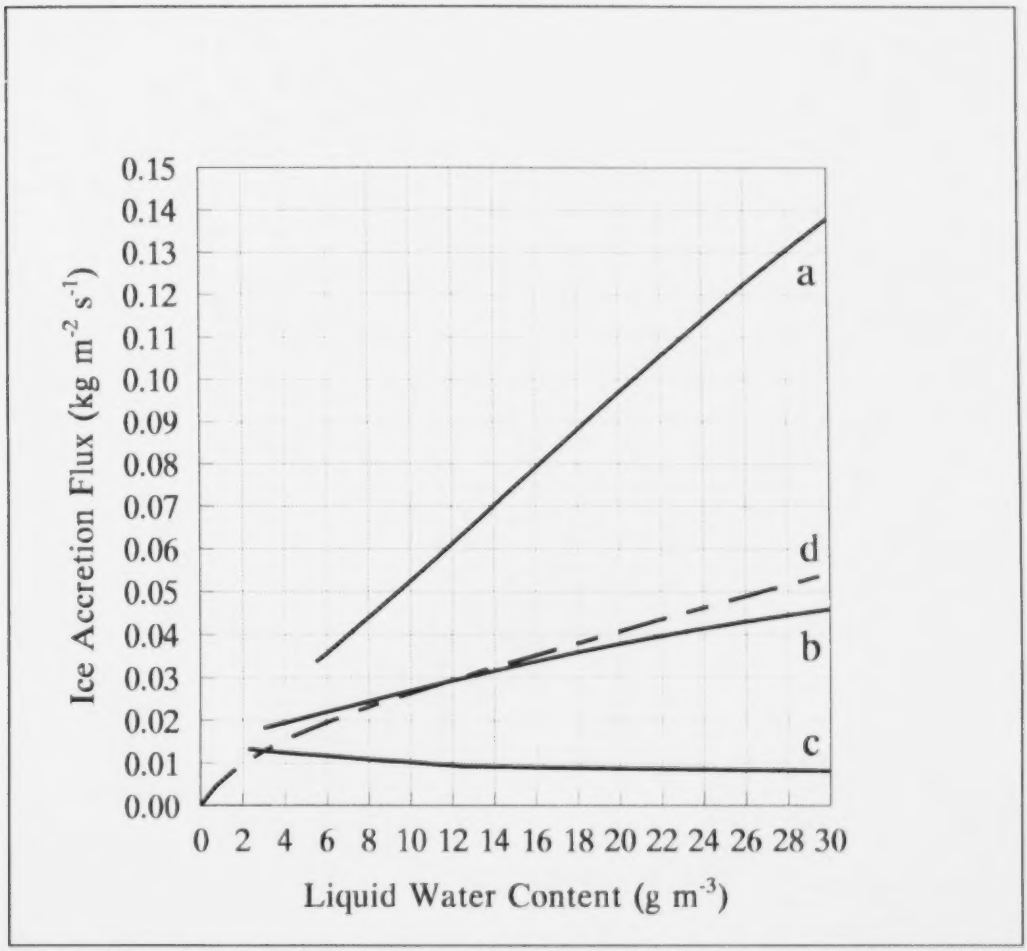

Figure 3.7 Ice accretion flux versus liquid water content for spray temperatures (a) T_4=-10°C, (b) T_4=-5°C, (c) T_4=0°C, compared with (d) for the result of Lesins et al. (1980).

loss at the outer surface of the falling film, and is responsible for an increased pure ice growth flux, I_0, in the freezing zone. The increasing evolution of latent heat of fusion leads to a rising temperature gradient in the freezing zone. This increased thermal gradient leads to a larger supercooling at the icing interface and to an increased rate of advance at the icing interface. Therefore, more water is incorporated into the ice matrix and the ice fraction decreases with increasing spray liquid water content as shown in curves "a" and "b" of Fig. 3.6.

Curves "a", "b", and "c" in Figs. 3.6 and 3.7 are truncated near 0 gm^{-3} because the model does not converge to a solution at low liquid water contents. This lack of convergence occurs with very thin falling films. There may be a minimum critical film thickness below which a steady-state falling film can no longer exist (Kachurin and Morachevskii, 1966). This condition presumably verges on rime icing. The prediction of rime icing is straightforward since all impinging liquid freezes. However, it is not built into the present spongy spray icing model.

Fig 3.7 shows the model's prediction of the ice accretion flux, (I_0+R_0), as a function of liquid water content under the same condition used in Fig. 3.6. Curve "a" represents the ice accretion flux with a spray temperature of -10°C. Overprediction of the rate of advance of the icing interface leads to the overprediction of sponginess that is in turn responsible for the overprediction of ice accretion flux in curve "a". A spray temperature of -5°C (curve "b") produces generally good agreement between the model-predicted ice accretion flux and that measured by Lesins et al. (1980). Curve "c", for a spray temperature of 0°C, considerably underpredicts the ice accretion flux over much of the liquid water content range. In this case, underprediction of the rate of advance of the icing interface produces the underprediction of the sponginess that is responsible for the underprediction of ice accretion flux in curve "c".

3.8.2 Model sensitivity to spray temperature and spray flux

Fig. 3.8 shows a sensitivity analysis of model-predicted ice fraction under the same conditions used in Fig. 3.6. In Fig. 3.8, spray flux replaces liquid water content as abscissa. Fig. 3.8 covers a much greater range of liquid water content than does Fig. 3.6 (i.e. 5.5 gm^{-3} to 555 gm^{-3}). The same three spray temperatures are considered in both figures. Curve "c", for a spray temperature of 0°C shows essentially the same result as curve "c" of Fig. 3.6. Curve "b", for a spray temperature of -5°C shows a more complicated tendency in ice fraction with increasing spray flux. However, curve "a", with a spray temperature of -10°C is chosen here for detailed analysis. To help with this analysis, Fig. 3.8 also displays the ice accretion flux (curve "d", I_0+R_0) and the ice flux

(curve "e", I_0) corresponding to "a". Curve "a" in Fig. 3.8 suggests that there are three regions based on the ice fraction tendency.

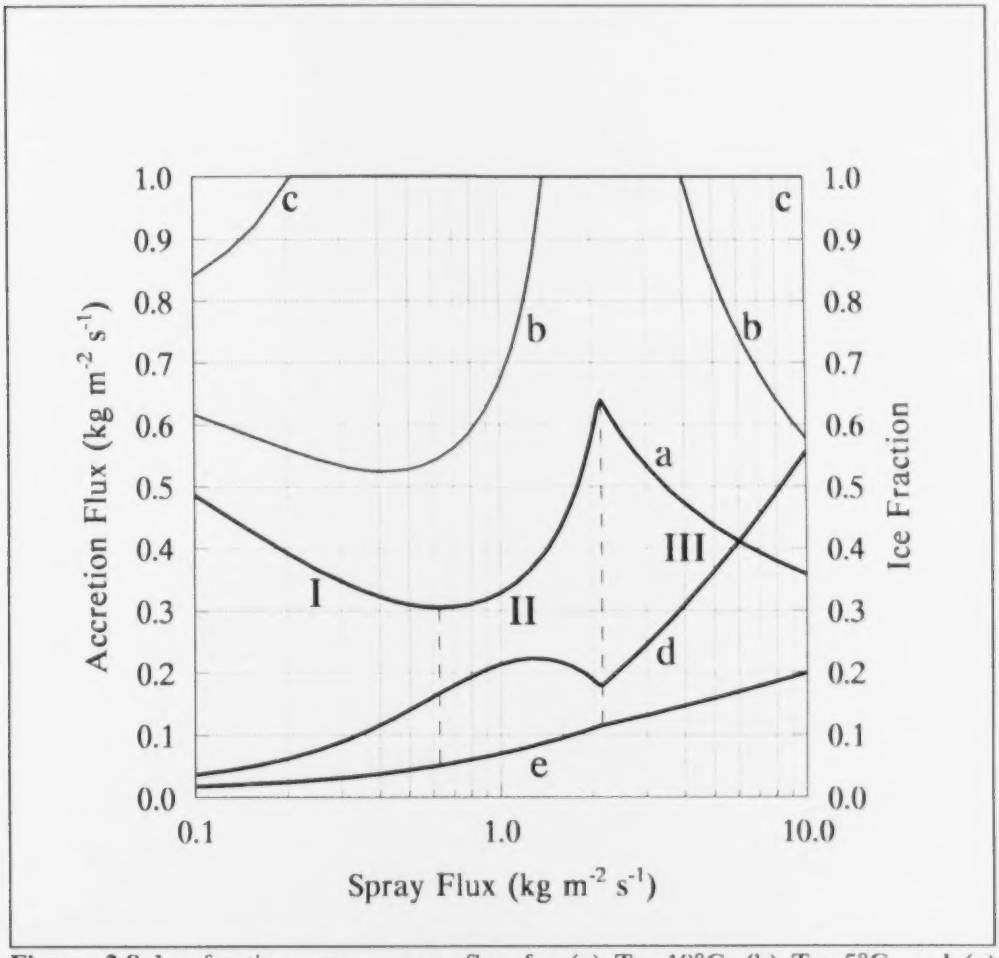

Figure 3.8 Ice fraction versus spray flux for (a) T_4=-10°C, (b) T_4=-5°C, and (c) T_4=0°C. Spongy accretion flux (d) and pure ice flux (e) versus spray flux for T_4=-10°C.

Region I extends from a flux of 0.1 kgm^{-2}s^{-1} to 0.63 kgm^{-2}s^{-1}. It has already been discussed in connection with Figs. 3.6 and 3.7 which have a comparable flux range. In this region, the ice fraction decreases as the ice accretion flux increases. The discussion of region I, given in connection with Figs. 3.6 and 3.7, suggests an explanation for these tendencies, but neglects some aspects of the model's structure. Here, Fig. 3.9 is introduced to help with a more complete interpretation of region I. Fig. 3.9 shows the

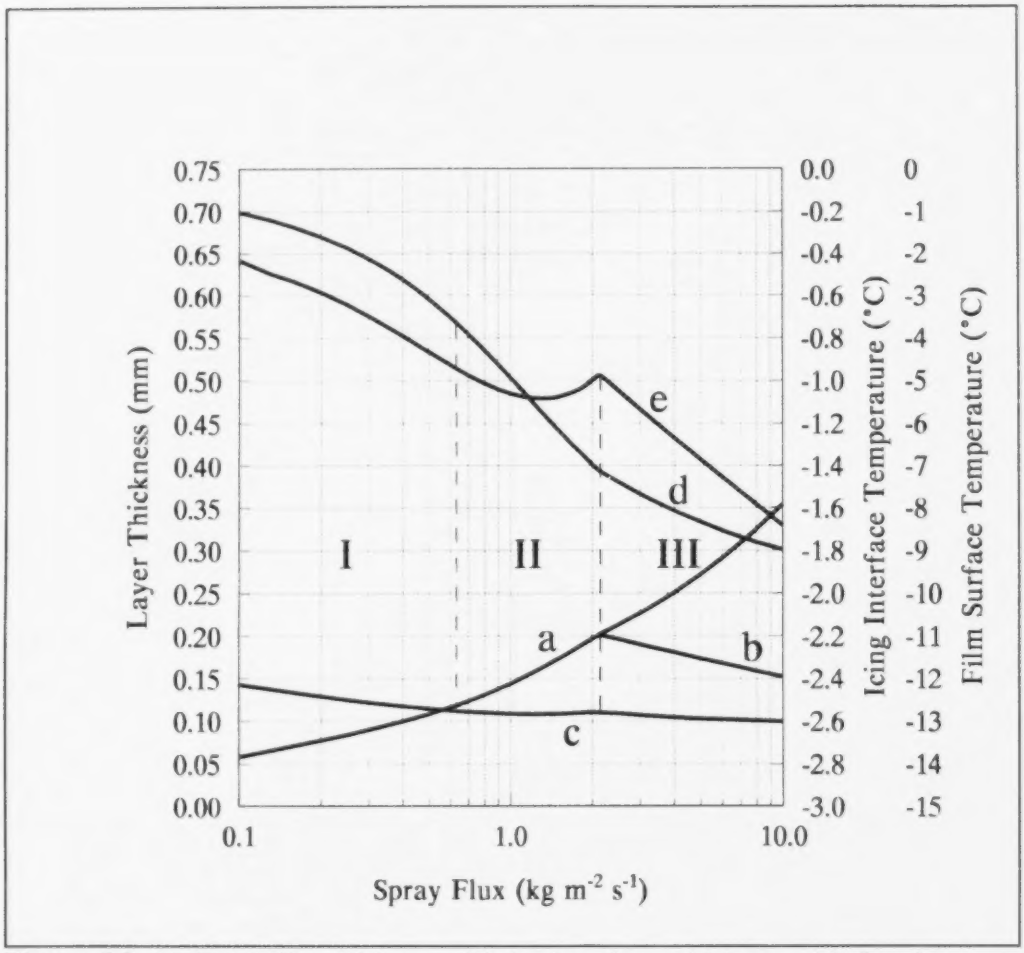

Figure 3.9 (a) Total film thickness, (b) laminar layer thickness, (c) freezing zone thickness, (d) film surface temperature, and (e) icing interface temperature versus spray flux. (conditions as given in Section 3.7.3)

total film thickness (curve "a"), the laminar layer thickness (curve "b"), the freezing zone thickness (curve "c"), the film surface temperature (curve "d") and the icing interface temperature (curve "e").

In region I, the freezing zone thickness decreases while the film thickness increases. Perhaps more important for determining the ice fraction and accretion flux is the decline in the icing interface temperature, which causes the rate of advance of the icing interface to increase. As a result, the sponginess and spongy ice accretion flux both increase. Also, in region I, the temperature of the outer surface of the film is decreasing

(Fig. 3.9, curve "d"). This has the effect of decreasing the heat loss from the film to the airstream. However, due to the substantial increase in the sensible heat loss at the outer surface of the film as the spray flux rises, the overall heat loss increases, giving rise to an increasing pure ice flux in region I.

Region II occurs in the spray flux range 0.63 $kgm^{-2}s^{-1}$ to 2.15 $kgm^{-2}s^{-1}$. In region II, the ice fraction increases with increasing spray flux while the ice accretion flux rises to a local maximum before falling again. As the spray flux increases, the flux of shed water on the icing surface also increases. The increasing film thickness in region II leads to a decreasing film surface temperature. This decreases the convective, evaporative and radiative heat loss from the film to the airstream. However, the increase in sensible heat loss that accompanies an increased flux of supercooled impinging spray, more than compensates for the reduction in heat transfer to the airstream. This results in an increasing ice flux.

The thickness of the freezing zone is nearly constant in region II, and the temperature of the icing interface changes by less than 0.2°C while reaching a local minimum. This local minimum in the icing interface temperature corresponds to a local maximum in the spongy ice accretion flux. This demonstrates the sensitivity of the ice accretion flux to the icing interface temperature. Even though the ice accretion flux in region II reaches a maximum and then decreases, the overall heat loss from the outer surface of the falling film continues to increase as it did in region I. Over the first half of region II (0.63 $kgm^{-2}s^{-1}$ to 1.40 $kgm^{-2}s^{-1}$), the increase in overall heat loss produces an increasing ice flux, and a small increase in the ice fraction. However, over the second half of region II (1.4 $kgm^{-2}s^{-1}$ to 2.15 $kgm^{-2}s^{-1}$), the rate of advance of the icing interface decreases, with the result that the ice fraction increases rapidly.

The increase in ice fraction in region II brings about the decreasing icing interface temperature, that is responsible for reducing the rate of advance of the icing interface and the ice accretion flux. Eqn. 3.32 shows that the mean thermal conductivity of the freezing zone is linearly proportional to the accretion's ice fraction. As a result, the thermal gradient in the freezing zone decreases and along with it the icing interface supercooling. Therefore, even though the heat flux conducted from the freezing zone increases in region

II, as is evident from the increase in the pure ice flux, the increase in thermal conductivity of the zone produces a reduced thermal gradient, and with it a diminished icing interface supercooling. Therefore, the effect of ice fraction on the thermal conductivity of the freezing zone is responsible for reducing the rate of advance of the icing interface, and the ice accretion flux in region II.

At the onset of region III there is a discontinuity in the slope of both the ice fraction and ice accretion flux curves. This slope discontinuity is associated with the development of the mixed layer at a flux of about 2.15 $kgm^{-2}s^{-1}$. Fig. 3.9 shows that at this flux the icing interface temperature begins to drop again with increasing spray flux. This occurs because the sensible heat flux needed to warm the impinging spray as it forms the mixed layer, is responsible for a considerable increase in the growth rate of ice in the freezing zone. The icing interface temperature must therefore drop substantially in order to provide a sufficiently large conductive heat flux through the freezing zone. In addition, the decreasing ice fraction in region III leads to a decreasing thermal conductivity in the freezing zone, an increasing thermal gradient across it (and the laminar layer) and an increasing supercooling at the icing interface. As a result, the rate of advance of the icing interface increases rapidly with increasing spray flux and gives rise to a decreasing ice fraction and an increasing ice accretion flux in region III.

3.8.3 Model sensitivity to other model parameters

Fig. 3.10 shows the sensitivity of the model-predicted ice fraction to air temperature, under the standard condition of Lesins et al. (1980) (see Section 3.7.3). Curve "a" is for spray temperature equal to the air temperature, curve "b" for a spray temperature equal to the mean of the air temperature and the spray's equilibrium freezing temperature, (0°C), and curve "c" for a spray temperature of 0°C. All three curves show that the model-predicted ice fraction is a strong function of air temperature, in contrast to the experimental findings of Lesins et al. (1980). They state that within a relative error of ±8%, the calorimetrically measured ice fraction was constant over the air temperature range, $-4°C \geq T_a \geq -16°C$ while varying from 0.37 to 1.0 with spray liquid water content.

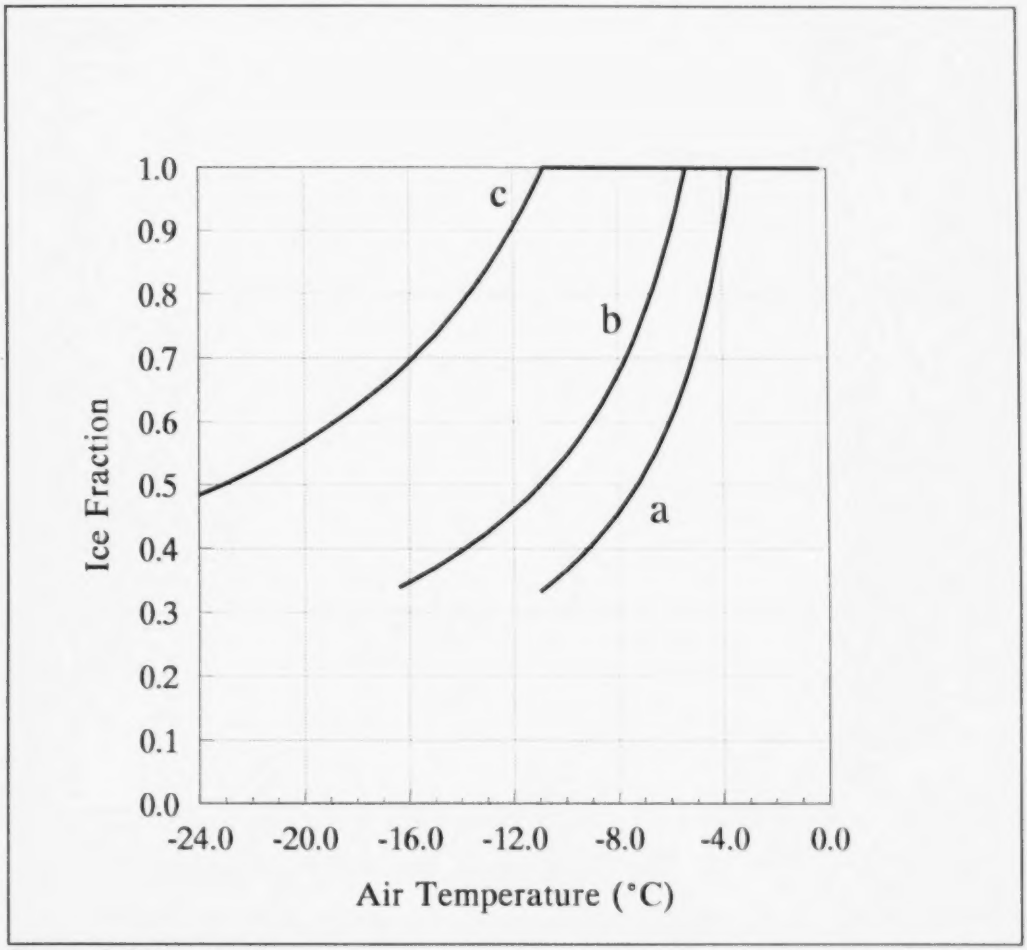

Figure 3.10 Ice fraction versus air temperature for three spray temperatures (a) $T_4=T_a$, (b) $T_4=T_a/2$, and (c) $T_4=0°C$. (conditions as given in Section 3.7.3)

In this case, the measured ice fraction was constant over the air temperature range at a value of 0.47 with the standard condition's liquid water content of 15 gm^{-3} (cf. Fig. 3.6). The explanation of this discrepancy between the substantial sensitivity of the model's prediction of ice fraction (i.e. 0.34 to 1.0) and the constancy of the measured ice fraction with air temperature, remains elusive.

As in Fig. 3.6, curves "a" and "b" in Fig. 3.10 are truncated due to a lack of numerical convergence in the model's computational algorithm at low air temperatures. Under these circumstances, the thin falling film is likely unstable due to rapid growth at

the icing interface. At present, the model is unable to resolve this transition from spongy ice growth to rime icing since rime was not considered in the model's development. The porous ice accretion regime described in Section 3.5.3 is not a very satisfactory model of rime icing. Although it occurs at low air and spray temperatures, it is unrealistic inasmuch as the liquid which is trapped within the porous accretion yields a low ice fraction for the accretion which is not characteristic of rime. Even though the accretion density in the porous ice regime resembles that of rime, the low ice fraction does not.

Fig. 3.11 shows the model-predicted ice fraction as a function of airspeed and relative humidity for the standard condition with T_4=-5°C. The ice fraction is not strongly

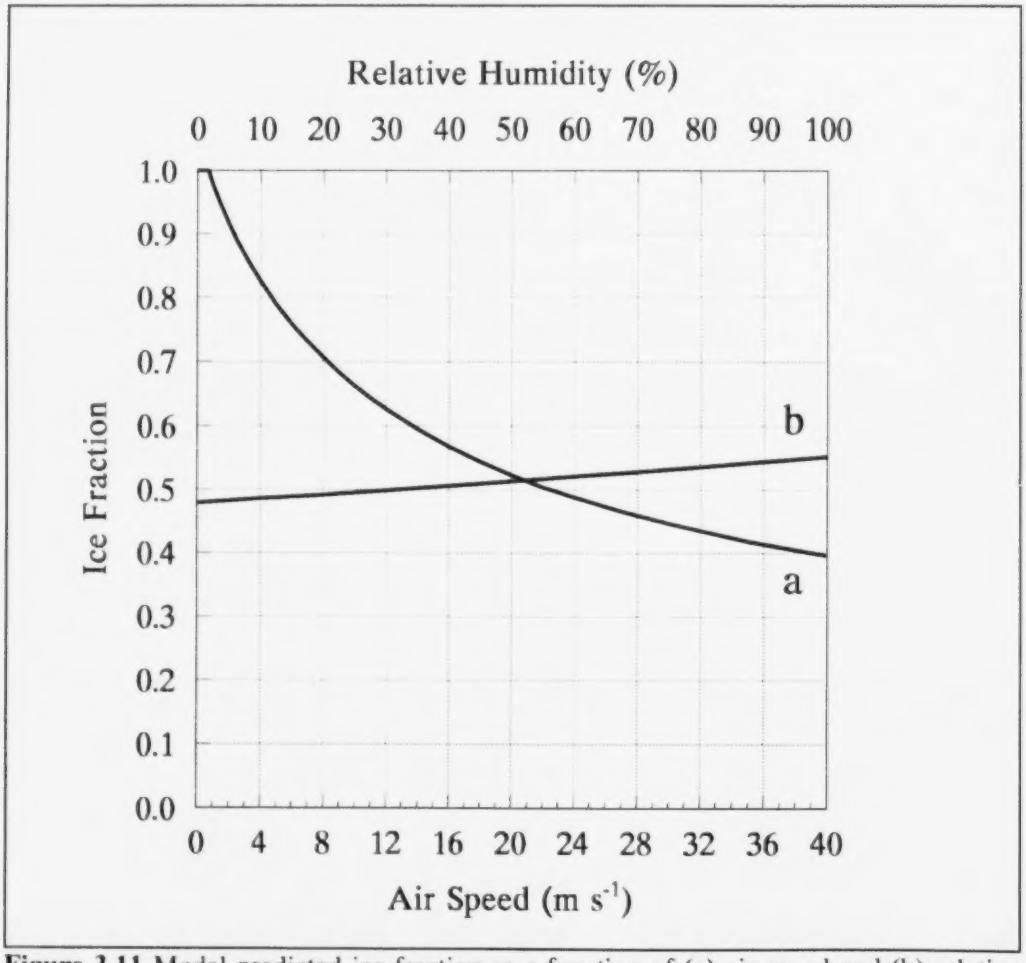

Figure 3.11 Model-predicted ice fraction as a function of (a) air speed and (b) relative humidity for the standard condition (as given in Section 3.7.3).

influenced by the relative humidity of the airstream but it does increase by about 15% as RH increases from 0% to 100%. The model is more sensitive to airspeed. The increase in the heat loss from the icing surface as the airspeed increases causes an increased evolution of latent heat in the freezing zone and a considerable increase in the icing interface supercooling. Because of this, the rate of advance of the icing interface increases, resulting in a considerable increase in both the sponginess (decrease in ice fraction) and the ice accretion flux as the airspeed rises. The effect of wind shear on the falling film is not included in the model, and this would likely have some influence on these results. However, understanding the effect of wind shear on the falling film and on the icing must remain an objective for future work.

3.8.4 Model evaluation with the icing data of Shi (pers. comm.)

A set of nine spray icing data measurements made on horizontal rotating cylinders of diameter 4 cm in the Marine Icing Wind Tunnel at the University of Alberta (Shi, pers. comm.) were compared with the predictions of the model. These cases of spongy spray icing data, and another group of nine icing cases that were used to calibrate the model, are documented in Appendix 9. The experiments are described more fully in Section 3.7.2. where the method used to calibrate the model is given.

The model predicted icing for seven of these cases, but it did not converge to a solution for the other two cases. Fig. 3.12 shows these seven cases as solid circles for which the model predicted three cases of spongy icing. These three cases are shown in Fig 3.12 as solid circles labelled with the model's predicted ice fraction while the other four glaze icing cases (at lower ice accretion fluxes) are given without ice fractions. The model predictions of accretion flux have a smaller relative error when the model predicts a spongy ice accretion. This is evident from the Willmott index of agreement, which for the glaze icing cases is 0.67 while for the spongy growth cases it is 0.9. Although the model underpredicts the measured ice accretion flux for both glaze and spongy cases, the correlation between the model and the experiments is good. This is evident from the coefficient of determination, which for all seven glaze and spongy cases is 0.96 and from

the Willmott index of agreement which is 0.94. Even though the model was developed to predict icing on a vertical cylinder, it has a comparable ability to predict accretion flux for horizontal cylinders. This is consistent with Stallabrass and Hearty (1967) who say that accretion rates for the vertical and horizontal orientations were indistinguishable under similar icing conditions.

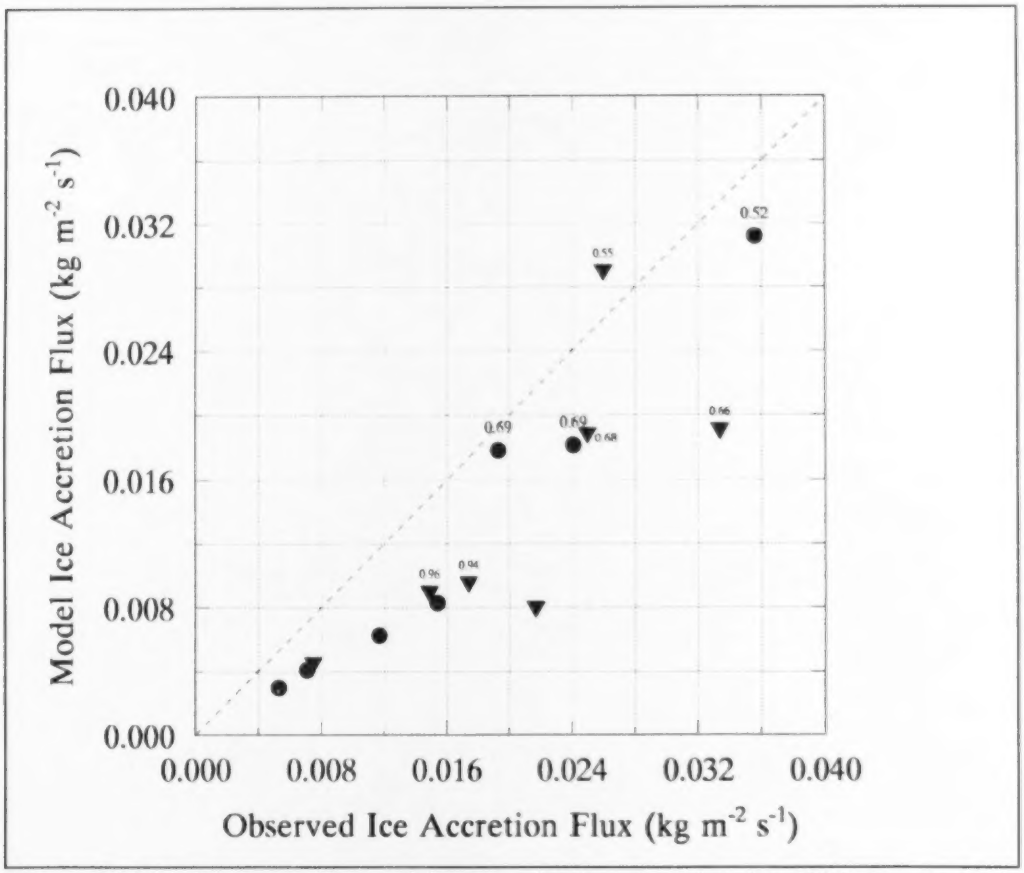

Figure 3.12 Model versus observed ice accretion flux for icing data (Shi, pers. comm.). Cases used to calibrate the model (triangles) and for performance evaluation (circles) are given. Spongy predictions are shown with ice fractions.

Fig. 3.12 also includes seven cases for which the model was used to predict icing based on the data set that was used in Section 3.7.2 to calibrate the model. These cases are shown as inverted solid triangles where the spongy cases are labelled with the model's predicted ice fraction. Although the model has empirical dependence on these experimental cases of icing, the model does not predict ice accretion flux as well as it

does for the independent cases discussed above. This is evident from the coefficient of determination, which for these cases is 0.56 and from the Willmott index of agreement which is 0.73. The reason for the model's reduced predictive capability with these cases remains unclear, although it may be partially due to the calibration method which depends only on a portion of the model's structure (i.e. the freezing zone and its thermodynamics).

The majority of the glaze ice predictions shown in Fig. 3.12 underpredict the observed ice accretion flux by factors in the range 2-3. This underprediction could be caused by model assumptions, such as a heat transfer coefficient that is too small due to unaccounted for roughness, or by assumptions concerning the input conditions, such as the assumed spray impingement temperature.

3.9 Summary Results Conclusions and Recommendations

A new, physically based, exploratory model of freshwater spongy spray icing on a vertically-oriented non-rotating cylinder has been developed. It includes many of the elements that are common to traditional spray icing models, but incorporates many new elements as well.

3.9.1 Summary

A surficial structure is postulated and heat and mass conservation are applied to yield predictions of both ice accretion flux and ice fraction. Predicting ice fraction is a unique feature of the present model which has not been accomplished before. A falling liquid film model has been adapted to describe the dynamics of the unfrozen surficial liquid film. A new model of the icing surface has been developed to describe the evolution of latent heat and its transfer within the freezing zone. The thickness of the freezing zone and the rate of advance of the icing interface are modelled using an analogy with freely-growing ice crystals. The growth rate of the ice accretion matrix is determined by both the solid ice flux and the flux of liquid water entrapped in the ice

matrix. What emerges from analysis of the performance of the model is a picture of spongy spray icing that portrays the complex interaction among the ice accretion matrix, the freezing zone, the falling surficial liquid, and the environmental conditions that drive the icing process.

The model was calibrated by determining the freezing zone parameter, C_r, from experimental measurements of ice accretion flux and ice fraction. A range of values $1.09 \leq C_r \leq 1.56$ was estimated and the average value of 1.33 was used in the model. Both ice fraction and ice accretion flux are strongly dependent on the value of the freezing zone parameter.

3.9.2 Results

A comparison of the model's performance with the empirical observations of Lesins et al. (1980) shows reasonable agreement for ice fraction as a function of liquid water content provided that the impinging spray temperature (unfortunately not measured) is taken to be in the range, $-5.0°C \geq T_4 \geq -10°C$. The model's prediction of ice accretion flux using a spray temperature of -5°C agrees closely with the results of Lesins et al. (1980). Unmeasured spray temperatures also led to difficulty when comparing the model-predicted ice accretion flux with the icing observations of Shi (pers. comm.). Even so, the model predictions of ice accretion flux compared reasonably well with the observations for horizontal cylinders, especially for those where spongy growth was predicted. The sensitivity analysis of Section 3.8 confirms the importance of spray temperature.

A sensitivity analysis of the model's prediction of ice fraction and ice accretion flux over the spray flux range, 0.1 $kgm^{-2}s^{-1}$ to 10.0 $kgm^{-2}s^{-1}$, showed that sponginess has an important influence on the ice accretion flux. This analysis also showed that the freezing zone and the falling film are thermodynamically coupled and that their interaction produces complex tendencies in ice fraction and ice accretion flux, with increasing spray flux. However, the assumptions concerning the surficial icing structure can affect model performance significantly. For example, the assumption of an isothermal

mixed layer is largely responsible for the predicted rapid change in ice fraction and ice accretion flux at the onset of mixed layer formation.

The model's prediction of ice fraction was found to be quite sensitive to air temperature. This finding is in contrast to observations of a relatively constant ice fraction with air temperature in the range, $-4°C \geq T_a \geq -16°C$ (Lesins et al., 1980). The explanation of this discrepancy between the model predictions and the observations of Lesins et al. (1980) remains elusive.

The model's prediction of ice fraction was shown to be insensitive to the relative humidity of the airstream. The airspeed however, does have a significant influence on model-predicted ice fraction. Shear stress due to the flow of air past the cylinder will decrease the thickness of the laminar and mixed layers and influence the transition to turbulence. This could enhance heat loss from the icing surface, decrease the icing interface temperature and increase the accretion flux and sponginess.

3.9.3 Conclusions

1. The present model is unable to describe the transition from spongy ice growth to rime icing, and the hypothesized porous ice accretion regime was of little help in gaining further insight concerning this transition. The glaze ice accretion regime occurred at the lower interfacial growth rates typical of smaller supercoolings. These smaller supercoolings at the icing interface are more likely at higher air temperatures, smaller impinging spray supercooling, and higher spray fluxes. The glaze ice accretion regime typically leads to the runoff of a substantial fraction of the model's impinging spray. The discovery that the crystal growth submodel predicts a rate of advance of the icing interface that is less than that of the thermodynamic submodel suggests that an amendment to the model is a worthwhile objective for future work.

2. The model's spongy ice accretion regime showed the greatest potential for spray ice accretion prediction, exhibiting favourable comparison with the observations of Lesins et al. (1980) and the spongy spray icing data of Shi (pers. comm.). Experience with the present model suggests that the emphasis of traditional icing models on the heat

balance at the icing surface is a proper one. The convective, evaporative, radiative and sensible heat fluxes together drive the ice accretion process. However, if these heat fluxes act on an icing surface which has a falling liquid film and freezing zone that are favourably organized to produce a spongy accretion, the mass accretion flux can become very much larger than the solid accretion typically predicted by traditional models.

3. Along with confirming the importance of the driving heat flux terms, the present work emphasizes the importance of the impinging spray temperature on the sensible heat transfer and thereby on the accretion sponginess. This conclusion implies that the heat transfer processes that govern the thermal evolution of in-cloud spray conditions are likely to have significant effects on accretion flux. For example, in vessel spray icing, droplet size, flux intensity, and flight distance will influence the droplet impingement temperature, and hence the sponginess of the ice deposit and ice accretion flux. For this reason, effective models of spray formation and thermal evolution may be required as a basis for effective modelling of spray ice accretion.

4. In addition, the sensitivity analysis of Fig. 3.9 suggests that water at the outer surface of the falling film may supercool several degrees. This result is in agreement with measurements of surficial water supercoolings of up to 7 °C on artificial hailstones (List, 1990), and the recent surficial liquid film modelling of Lozowski at al. (1995). In fact, the present model suggests that the film temperature may approach within a few degrees of the air temperature in cases where the spray has cooled to near the air temperature prior to collision with the icing surface.

3.9.4 Recommendations

1. Future modelling of the freezing zone should consider a better model or analogy for describing the rate of advance of the icing interface and the thickness of the freezing zone. A better analogy or model might be sought that would produce predictions of the rate of advance at the icing interface equal to that of the thermodynamic submodel for the glaze ice accretion regime. Improved modelling might also include an approach to the transition from spongy ice growth to rime icing. Although improvements in the

model's thermodynamics might be valuable, improvements in the modelling of the freezing zone is likely to be more fruitful. Perhaps a simplified theoretical model of the freezing zone based on crystal growth theory like the one proposed by Makkonen (1990) could be developed and adapted for use with the present modelling approach.

2. Future modelling of the surficial liquid film should consider: (i) the effect of impinging spray droplets on the structure of the falling film including splashing and the initiation of waves in the surficial liquid, (ii) the effect of the roughness of the icing interface on the dynamics of the surficial film, (iii) the effect of waves on the outer surface of the liquid film on the heat transfer to the airstream and the mass flux in the film, and (iv) the influence of wind shear on the thickness of the falling film as well as its direction of flow over the icing surface.

3. Future modelling work should consider the effects of the diffusion of impurities (e.g. salt) in the liquid film, as well as impurity entrapment in the freezing zone. In this way, the present model could be made more relevant to marine spray icing.

4. Data collected for verifying spongy growth model predictions should include not only ice fraction and ice accretion flux, but also impinging spray temperature. This is important in view of the sensitivity of the spongy growth process to spray temperature.

5. Thin section analysis may be of some help in the investigation of the relationship between ice crystal structure in the matrix and surficial growth conditions. The occurrence of the freezing zone and its nature might also be elucidated by crystallographic analysis. Körber and Schiewe (1983) have used microphotography to observe the dendritic growth of a freezing zone in aqueous salt solutions. Such a method could perhaps be adapted and used to examine the freezing zone in spongy spray icing.

List of References

Chalmers, B., 1964: *Principles of solidification.* John Wiley and Sons Inc., New York, 319 pp.

Dukler, A. E. and O. P. Bergelin, 1952: Characteristics of flow in falling liquid films. *Chem. Eng. Prog.*, **48(11),** 557-563.

Finstad, K., E. P. Lozowski and E. M. Gates, 1988: A Computational investigation of water droplet trajectories. *J. Atmos. Ocean. Tech.*, **5(1),** 160-170.

Foy, C. E., 1988: The design, instrumentation and performance of a refrigerated marine icing wind tunnel. M.Sc. thesis., University of Alberta, 117 pp.

Fraser, D., C.K. Rush and D. Baxter, 1952: Thermodynamic limitations of ice accretion instruments. NRC NAE Laboratory Report LR-32.

Fulford, G. D., 1964: The flow of liquids in thin films. *Advan. Chem. Eng.*, **5,** 151-236.

Hobbs, P. V., 1974: *Ice Physics.* Clarendon Press, Oxford, 837 pp.

Holman, J. P., 1990: *Heat transfer.* McGraw Hill, New York, 714 pp.

Incropera, F. P., and D. P. DeWitt, 1990: *Introduction to heat transfer.* John Wiley and Sons, New York, 824 pp.

Kachurin, L. G., L. I. Gashin and I. A. Smirnov, 1974: Icing rate of small displacement fishing boats under various hydrometeorological conditions. *Meteorologiya i Gidrologiya*, **3**, 50-60. [in Russian]

Kachurin, L.G. and V.G. Morachevskii, 1965: *Kinetics of phase transitions of water in the atmosphere*. Leningrad State University, Leningrad. (translated by Z. Lerman, Israel Program for Scientific Translations, Ltd., IPST Cat. No. 1807, 1966), 124 pp.

Knight, C. A., 1968: On the mechanism of spongy hailstone growth. *J. Atmos. Sci.*, **25,** 440-444.

Knight, C. A., and N. C. Knight, 1968: Spongy hailstone growth criteria I. Orientation fabrics. *J. Atmos. Sci.*, **25,** 445-452.

Körber, Ch., and M. W. Scheiwe, 1983: Observations on the non-planar freezing of aqueous salt solutions. *J. Cry. Grow.*, **61,** 307-316.

Kurz, W., and D. J. Fisher 1986: *Fundamentals of solidification.* Trans Tech Publications Ltd., Switzerland, 244 pp.

Lesins, G. B., R. List and P. I. Joe, 1980: Ice Accretions. Part I: Testing of new atmospheric icing concepts. *J. Rech. Atmos.*, **14(3-4):** 347-356.

List, R., 1959: The growth of ice-water composition in an experimental tunnel. *Helvetica Physica Acta,* **32,** 293-296.

List, R., 1963: General heat and mass exchange of spherical hailstones. *J. Atmos. Sci.*, **20,** 189-197.

List, R., 1990: Physics of supercooling of thin water skins covering gyrating hailstones. *J. Atmos. Sci.,* **47(15),** 1919-1925.

Lock, G. S. H., and I. B. Foster, 1990: Experiments on the growth of spongy ice near a stagnation point. *J. Glaciol.,* **36(123),** 143-150.

Lozowski E. P., A. M. Kobos, and L. G. Kachurin, 1995: Influence of the surface liquid film on cylinder icing under marine conditions. In: Proceedings of the 14th International Conference on Offshore Mechanics and Arctic Engineering (OMAE), Copenhagen, Vol. IV, Arctic/Polar Technology ASME 199, 115-122.

Macklin, W. C., 1977: The characteristics of natural hailstones and their interpretation. *Meteor. Monogr.*, **38**, 65-88.

Macklin, W. C., and B. F. Ryan, 1962: On the formation of spongy ice. *Q. J. R. Meteorol. Soc.*, **88,** 548-549.

Makkonen, L., 1984: Modelling of ice accretion on wires. *J. Climate Appl. Meteor.*, **23**, 929-939.

Makkonen, L., 1987: Salinity and growth rate of ice formed by sea spray. *Cold Reg. Sci. Tech.*, **14,** 163-171.

Makkonen, L., 1988: A model of icicle growth. *J. Glaciol.*, **34,** 64-70.

Makkonen, L., 1990: Origin of spongy ice. In: Proceedings of the 10th International Association for Hydraulic Research (IAHR) Ice Symposium, Espoo, Finland, 1022-1030.

Press, W. H., B. P. Flannery, S. A. Teukolsky and W. T. Vetterling, 1990: *Numerical recipes. The art of scientific computing (Fortran version).* Cambridge University Press, 702pp.

Roos, D. v. d. S., and H. -D. R. Pum, 1974: Sponginess in ice grown by accretion. *Q. J. R. Meteorol. Soc.*, **100,** 640-657.

Ryerson, C. C. and P. Longo, 1992: Ship superstructure icing: data collection and instrument performance on the USCGC MIDGETT Research Cruise. USA Cold Regions Research and Engineering Laboratory, CRREL Report 92-23, 56 pp.

Schlichting, H., 1979: *Boundary-layer theory.* McGraw Hill, New York, 817 pp.

Stallabrass, J. R., and P. F. Hearty, 1967: The icing of cylinders in conditions of simulated freezing sea spray. Mech. Eng. Rep. No. MD-50, NRC No. 9782, National Research Council of Canada, Ottawa, 10 pp.

Tirmizi, S. H., and W. N. Gill, 1987: Effect of natural convection on growth velocity and morphology of dendritic ice crystals. *J. Cry. Grow.*, *85*, 488-502.

Trela, M., 1988: Minimum wetting rate for a decelerating liquid film. *Int. J. Heat Fluid Flow,* **9(4),** 415-420.

von Kármán, T., 1939: The analogy between fluid friction and heat transfer. *Trans. Am. Soc. Mech. Engrs.*, **61,** 705.

Wasden, F., and A. E. Dukler, 1989: Insights into the hydrodynamics of free falling wavy films. *AIChE J.*, **35(2),** 187-195.

Zakrzewski, W. P., 1986: Icing of ships. Part I: Splashing a ship with spray. NOAA Tech. Memo., ERL PMEL-66, Pacific Marine Environmental Laboratory, Seattle, WA, 74 pp.

Zakrzewski, W. P., and E. P. Lozowski, 1991: Modelling and forecasting vessel icing. In: *Freezing and Melting Heat Transfer in Engineering,* K. C. Cheng and N. Seki, eds., Hemisphere Publishing Corp., 661-706.

4. CONCLUSIONS

The research described in the first three chapters is strongly interrelated. Since each chapter draws its own specific conclusions, this fourth chapter begins with an overview of the preceding chapters, and then presents overall conclusions and recommendations concerning vessel spray icing and spongy ice growth.

4.1 Overview

This dissertation began with a review of the physics of vessel spray icing to prepare for the novel research presented in Chapters 2 and 3. The review was structured so as to provide a context for the constituent physical processes and the conditions favourable to freezing spray. A similar framework was used in the development of the heuristic vessel icing model of Chapter 2. Also included was a detailed review of previous physical modelling of the distribution of spray ice accretion on vessels, as well as previous physical modelling of the particular problem of spongy ice growth. The second chapter presented a relatively simple physical model of overall spray ice accretion that can be applied to any vessel. The development of this vessel icing model included the assumption that the accretion is solid, in order to avoid the rather substantial difficulties of modelling the growth of spongy marine ice. To illustrate the challenges of this kind of modelling, the third chapter developed a model of spongy spray icing for a vertical cylinder (i.e. a typical vessel component). This model predicts both the ice accretion rate and the liquid fraction of the accretion.

4.2 Conclusions

1. The overall accretion of spray ice on a variety of vessels can be modelled in a relatively simple manner. The heuristic vessel spray icing model of Chapter 2 predicts the overall accretion rate based on reasonable assumptions, physical arguments, and an empirical description of bow spray generation. This model demonstrates that vessel spray

icing can be modelled without a substantial dependence on statistical methods or the considerable detail of three-dimensional modelling. This vessel icing model represents a rational compromise between the statistical-physical approach to freezing spray prediction and the vessel-specific approach. It is the only simple model that has the capability to make individual predictions for particular vessels. Since detailed vessel-specific models usually involve large, intricate codes, the heuristic spray icing model is much faster to run on a personal computer, requiring less than a second rather than several hours. This is especially helpful if many icing predictions are needed (e.g. for making maps of potential icing severity).

2. The aerodynamics and thermodynamics of the spray cloud are very important for the icing of vessels. The heuristic vessel icing model uses a spray/air heat balance to calculate the icing rate, unlike traditional models which consider heat transfer from the icing surfaces. Nevertheless, the model performed well against data and a version of the Kachurin et al. (1974) nomogram. We suggest that the heuristic model's successful performance implies that our emphasis on the spraying process was reasonable and valid, and that spraying processes are indeed very important in vessel icing.

3. A hypothetical icing mechanism, which we called nucleated spray icing, may be responsible for severe icing events. This mechanism, which depends on the presence of ice in the spray droplets, was described in Chapter 1, and modelled in Chapter 2. The substantial increase in vessel icing rate with nucleated spray icing suggests that this mechanism could explain severe icing incidents, and also, perhaps, a component of the heretofore unexplained noise in vessel icing data.

4. A theoretical sea-surface temperature limit to vessel spray icing is unlikely. A sensitivity analysis of the heuristic vessel icing model suggests that icing occurs over a wide range of sea-surface temperature, except extremely warm seas (i.e. T_{ss}>10°C).

5. The spongy ice accretion regime of the exploratory spray icing model would seem to have good potential for spray ice accretion prediction. The model's spongy growth regime compares favourably with data and shows that spongy spray ice accretion can be successfully modelled with a traditional heat balance at the icing surface, and a surficial structure that includes a freezing zone and surface liquid film. The model's

sensitivity to the value of the freezing zone parameter, suggests the importance of the freezing zone in spray icing as well as the importance of how the freezing zone is modelled. A sensitivity analysis demonstrates the importance of the liquid film in the spongy ice accretion regime. The ice accretion flux can become very much larger than that predicted by traditional models which ignore entrapped brine.

6. In the spongy regime, the impinging spray temperature has a considerable influence on the sensible heat flux at the icing surface, the icing interface temperature, the rate of advance of the icing interface, and the accretion's liquid fraction. Consequently, the thermal evolution of the spray in the airstream prior to impingement, is of critical significance, since it affects the sponginess and the rate of ice accretion.

7. The hypothesized porous ice accretion regime in the exploratory spray icing model of the third chapter was unsuccessful in describing the transition from spongy ice growth to rime ice growth. Even though the model's porous ice accretion has a low density due to the inclusion of air, like rime ice, it also has a low ice fraction, which is very unlike rime.

8. The glaze ice accretion regime of the exploratory spray icing model shows promise in predicting the accretion of solid ice. Even though the model's glaze icing regime was not tested against observations of glaze ice accretion, the model performs well (i.e. converges to a solution) near the transition between the spongy and glaze regimes. This regime is associated with high air temperature and impinging spray temperature, small icing interface supercooling, low growth rates, and high fluxes of liquid in the falling film.

9. In the exploratory spray icing model, the film surface may supercool up to 8°C with fluxes up to 10 $kgm^{-2}s^{-1}$ of strongly supercooled spray at a temperature of -10°C or less. This prediction is in general agreement with measurements of surficial water supercoolings up to 7°C on artificial hailstones (List, 1990), and the recent surficial liquid film modelling of Lozowski et al. (1995).

4.3 Recommendations

1. It would be timely and valuable to prepare a major review of vessel spray icing. The largely descriptive and qualitative review presented in the first chapter shows that there have been many developments in vessel spray icing research since the reviews of Zakrzewski and Lozowski (1991), Jessup (1985), Brown and Roebber (1985) and Shellard (1974). For example, a large vessel-specific model has been completed (Zakrzewski et al., 1993) which describes the accretion of ice over a vessel in a detailed manner. The influence of spray icing on the dynamics of a vessel has been studied by Chung et al. (1995), and modelling of spongy spray ice accretion has been given increasing attention (Makkonen, 1987). The hydrodynamics of excess liquid on the icing surface has been studied, along with its effect on the icing rate (Lozowski et al., 1995). These and other advances need to be assessed quantitatively and placed in context.

2. A comprehensive up-to-date bibliography on vessel spray icing and related research topics, available in hard copy and on disc, would be an invaluable resource to researchers investigating all aspects of vessel spraying and icing. Such a resource could be made available to the marine icing research community through the "Marine Icing Newsletter", or via the World Wide Web on the Marine Icing Home Page.

3. The heuristic vessel spray icing model of Chapter 2 could be used to research the relative importance of such vessel icing subprocesses as brine jet development, spray droplet formation, spray aerodynamics and thermodynamics, and surficial icing processes such as excess brine shedding and spongy growth. For example, the model could be modified to separate the modelling of icing on the vessel's topside from the modelling of spray aerodynamics and thermodynamics. Such a separation would lead to two submodels and allow for a performance comparison that could demonstrate the relative importance of these two processes.

4. With further development, the heuristic vessel spray icing model could be used as a vessel-specific operational forecast model of vessel icing. Other physical subprocesses to include in the model are: (i) brine jet hydrodynamics, (ii) spray droplet formation, and (iii) vessel dynamics. At present, a simple geometric approximation to the

a vessel's topside is included in the model. Perhaps a simple parallelepiped hull model would permit hydrodynamic predictions of brine jet formation as well as vessel motion, while remaining computationally simple.

5. In the exploratory spray icing model of Chapter 3, the rate of advance of the icing interface, and the thickness of the freezing zone should be described more realistically. In the glaze ice accretion regime, the freezing zone model should predict a rate of advance of the icing interface which is consistent with the thermodynamic submodel. Improved modelling of the freezing zone should also include an approach to the transition from spongy ice growth to rime icing. A theoretical model of the growth of an ensemble of ice crystals or a model based on an assumed ice crystal morphology, such as the one proposed by Makkonen (1990), could be developed and included.

6. The exploratory spray icing model could be further extended by incorporating the following liquid film phenomena: (i) the effect of impinging spray on the film (e.g. splashing and capillary wave initiation), (ii) the change in heat transfer to the airstream due to waves and splashing, (iii) the effect of the roughness of the ice surface on the dynamics of the surficial film, and (iv) the influence of wind shear on the film.

7. The surficial structure and modelling assumptions of the exploratory spray icing model could be introduced into icing models for other substrates, such as horizontal rotating and non-rotating cylinders, flat plates and spheres (hailstones). Such substrate configurations could also be used to test the surficial structure and modelling assumptions, through wind tunnel experiments.

8. Future modelling should consider the transport of salt in the brine film and in the freezing zone, and incorporate the other well-known salinity effects of marine spray icing (Makkonen, 1987). In this way, the freshwater spray icing model of Chapter 3 could be made more relevant to the spray icing of vessels. A performance comparison between the freshwater and saltwater spray icing models would yield further insight into the relative severity of the two kinds of spray icing.

9. The exploratory spray icing model needs to be tested further against experimental data taken in an icing wind tunnel. A non-rotating vertical cylinder could be mounted in a horizontal refrigerated wind tunnel with freezing spray. Measurements

should include ice fraction, ice accretion flux, and impinging spray temperature. If a means to measure the impinging spray temperature is not devised, then a model of the motion and cooling of an ensemble of droplets might be used to provide an estimate of the spray temperature.

10. Thin section analysis, often used in studying hailstones and other types of ice, may be of help in investigating the relationship between the ice crystal structure of the accreted ice matrix and the surficial growth conditions. The occurrence of the freezing zone and its morphology may also be elucidated by crystallographic analysis.

List of References

Brown, R. D., and P. Roebber, 1985: The scope of the ice accretion problem in Canadian waters related to offshore energy and transportation. Rep. 85-13, Canadian Climate Centre, Downsview, Ont., 295 pp. [unpublished manuscript]

Chung, K. K., Lozowski, E. P., J. S. Pawlowski and Q. Xu, 1995: Ship icing and stability. In: Proceedings of the 1st Asian Computational Fluid Dynamics Conference, Jan. 16-19, Hong Kong, Vol. 1, 275-280.

Jessup, R. G., 1985: Forecast techniques for ice accretion on different types of marine structures, including ships, platforms and coastal facilities. Marine Meteorology and Related Oceanographic Activities, Rep. 15, WMO, Canada, 90 pp.

Kachurin, L. G., L. I. Gashin and I. A. Smirnov, 1974: Icing rate of small displacement fishing boats under various hydrometeorological conditions. *Meteorologiya i Gidrologiya*, **3**, 50-60. [in Russian]

List, R., 1990: Physics of supercooling of thin water skins covering gyrating hailstones. *J. Atmos. Sci.*, **47(15)**, 1919-1925.

Lozowski E. P., A. M. Kobos, and L. G. Kachurin, 1995: Influence of the surface liquid film on cylinder icing under marine conditions. In: Proceedings of the 14th International Conference on Offshore Mechanics and Arctic Engineering (OMAE), Copenhagen, Vol. IV, Arctic/Polar Technolog ASME 199, 115-122.

Makkonen, L., 1987: Salinity and growth rate of ice formed by sea spray. *Cold Reg. Sci. Tech.*, **14**, 163-171.

Makkonen, L., 1990: Origin of spongy ice. In: Proceedings of the 10th International Association for Hydraulic Research (IAHR) Ice Symposium, Espoo, Finland, 1022-1030.

Shellard, H. C., 1974: The meteorological aspects of ice accretion of ships. Marine Science Affairs, Rep. No. 10, WMO-No. 397, World Meteorological Organization, Geneva, 34 pp.

Zakrzewski, W. P., and E. P. Lozowski, 1991: Modelling and forecasting vessel icing. In: *Freezing and Melting Heat Transfer in Engineering*, K. C. Cheng and N. Seki, eds., Hemisphere Publishing Corp., 661-706.

Zakrzewski, W. P., E. P. Lozowski, W. L. Thomas, M. Bourassa, R.Z. Blackmore, K. Szilder and A. Kobos, 1993: A three-dimensional time-dependent ship icing model. In: Proceedings of the 12th International Conference on Port and Ocean Engineering under Arctic Conditions (POAC), Vol. 2, Hamburg, 857-873.

APPENDIX 1: Spray Model Calibration in the Heuristic Vessel Icing Model

The following discussion sets out the rationale for the choices of k_z=0.085 s and k_r=0.15 s^{-1} in Section 2.4. First, we present an evaluation of k_z, the empirical coefficient (Eqn. 2.10b) which determines the time-averaged height of the spray window, Z. Once k_z has been determined, the empirical coefficient used to describe spray flux intensity, k_r, is evaluated.

The approach taken is to use physical reasoning, and spraying field data for the Soviet medium-sized fishing vessel (MFV) "Narva" (Zakrzewski, 1987), to arrive at the values of the empirical coefficients. The spraying data were taken while the vessel had an average speed of 2.83 ms^{-1}, with an average wind speed of 11 ms^{-1}, and an encountering angle of 100 degrees. Zakrzewski (1987) suggests a probable fetch of 200 nm, from which he deduces a significant wave height of 3.09 m, and a significant wave phase speed relative to the vessel of 11.01 ms^{-1}. Using Eqn. 25 from Zakrzewski (1987):

$$V_r = C_w - V_v \cos\alpha \qquad \textbf{(A1.1)}$$

where α is the encountering angle (180° for head seas; 90° for beam seas), V_v is the ship speed, and V_r is the wave phase speed relative to the vessel, the significant wave phase speed is calculated to be C_w=10.5 ms^{-1}. The Stokes' formula for deep-water waves is used to give a relationship between the phase speed and the period of wind waves (Khandekar, 1989):

$$C_w = 1.56P \qquad \textbf{(A1.2)}$$

where P is the period of the significant wave. Using Eqn. A1.2, the significant wave period is calculated to be P=6.75 s corresponding to a wave frequency, f=0.148 Hz.

A well-known equation for the radian frequency of encounter by a vessel, ω_e, is:

$$\omega_e = \omega\left(1 - \frac{\omega V_v}{g}\cos\alpha\right) \qquad \textbf{(A1.3)}$$

where ω is the radian frequency of the waves. Eqn. A1.3 can be transformed to:

$$f_e = f\left(1 - \frac{V_v}{C_w}\cos\alpha\right) \qquad \textbf{(A1.4)}$$

where f_e is the frequency (Hz) of encounter by the vessel, and f is the frequency (Hz) of the waves. Using Eqn. A1.4 with the required input parameter values from the "Narva" spraying data, results in a frequency of encounter, f_e=0.1551 Hz. Since Zakrzewski (1987) suggests that a good estimate for the frequency of spray generation is half the frequency of encounter, we assume that the spray frequency, f_{sp}=0.078 Hz.

In order to calculate estimates for the empirical parameters, k_z and k_r, assumptions concerning the nature of each spray event must be made along with the above calculated frequency of spraying, f_{sp}. We assume that gravitational acceleration essentially controls the rise and fall of the spray with droplet drag neglected. Under this assumption it can be shown that for a gravitational trajectory the time to rise and fall above the ship's bulwarks is:

$$\tau = 2\sqrt{\frac{2\Delta Z}{g}} \qquad \textbf{(A1.5)}$$

where ΔZ is the maximum height of the trajectory (in metres) above the ship's bulwarks. For a Soviet medium-sized fishing vessel like the "Narva", $\Delta Z=(Z_{max}-0.75)$, where 0.75 represents the height of the bulwarks (in metres), and where Z_{max} is the maximum height of the spray above the deck. For evaluating Z_{max}, Zakrzewski et al. (1988) suggest:

$$Z_{max} = 0.535\,V_r \qquad \textbf{(A1.6)}$$

From Eqn. A1.6, the maximum height for the "Narva" case can be calculated as Z_{max}=5.89 m, and therefore ΔZ=5.14 m. Once ΔZ is known, the flight time to complete the trajectory is calculated as τ=2.05 s from Eqn. A1.5.

We suggest here a simple understanding of spray generation based on the above trajectory calculation. The following assumptions are made to account for the temporal effects of the frequency of spraying and the time taken by the spray to rise and fall over the vessel on the time-averaged height of the spray window, Z. We assume that the initial

vertical spray jet speed is a maximum, and that subsequently the vertical spray jet speed decreases as the liquid approaches the top of the spray cloud envelope which forms over the vessel. Furthermore, it is assumed that the spray jet formation process, which results from the wave/hull interaction diminishes as the initial spray brine rises toward it's maximum height and stops at about the same time that the initial spray brine is back at the level of the top of the vessel's bulwarks. In other words, this understanding of the spraying event suggests that the trajectory of the initial spray brine defines the height, and is strongly related to the duration of the spray cloud over the vessel. This understanding is, at present, unsubstantiated, and is offered here as a working hypothesis. It is interesting to note however, that Zakrzewski and Lozowski (1991) recommend that a value for spray duration of 1 to 3 seconds be used for a Soviet medium-sized fishing vessel. The calculated value of τ=2.05 s, falls within this suggested range of spray duration.

The spray duration of 2.05 s, and the frequency of spraying, f_{sp}, as calculated above, are needed in order to adjust the trajectory height, ΔZ, in such a way as to take into account two important temporal effects. The first effect has to do with the influence of the spray generation frequency on the time-averaged height for the spray, Z, which is related to ΔZ by $Z=\tau f_{sp}\Delta Z$. The second effect on the time-averaged spray height has to do with the time it takes for spray to rise and fall during an individual spraying event. Since the time-averaged height of a gravitational trajectory is 2/3 of the maximum height of the trajectory, this factor must also be included in the calculation of the time-averaged spray height. Combining these two factors results in a spray access window height, $Z=2\tau f_{sp}\Delta Z/3$ (i.e. Z=0.5448 m). This value of the spray access window height along with a value for C_{gr}, can be used to calculate the empirical constant k_z from the equation:

$$Z = k_z C_{gr} \qquad \textbf{(A1.7)}$$

where the required value of C_{gr} can be obtained in turn from:

$$C_{gr}=\sqrt{V_v^2+C_g^2-2V_vC_g\cos\alpha} \qquad \textbf{(A1.8)}$$

and where the vessel speed, V_v, is known and the group velocity of the significant wave is, C_g=5.259 ms^{-1}, (i.e. $C_g=C_w/2$). Using Eqn. A1.7, the value of k_z is 0.085 s.

In order to begin the evaluation of the spray intensity coefficient, k_r, we use the fact that the flux of spray per unit width of wave exposure is:

$$F=U\int_{0.75}^{Z_{max}} w(z)dz \qquad \textbf{(A1.9)}$$

where U is the relative wind speed (assumed independent of height), and w(z) is the liquid water content as a function of height. According to Borisenkov et al. (1975), the liquid water content may be expressed as a function of height by:

$$w(z)=2.42\times10^{-2}\ \exp(-0.55z) \qquad \textbf{(A1.10)}$$

where z is the height above the deck of a Soviet medium-sized fishing vessel. Substituting Eqn. A1.10 into A1.9 and integrating yields a value of F for the "Narva" of 0.3014 $kgm^{-1}s^{-1}$. This value of F is used to determine the value of the empirical coefficient k_r. The empirical equation from Section 2.4 (Eqn. 2.9) which describes the rate of spray mass impingement on the vessel per unit width is:

$$F_{ws}=K\rho_a\frac{H_s^2}{F_B}C_{gr} \qquad \textbf{(A1.11)}$$

where the freeboard, F_B, is 3.5 m for an MFV, and where air density is 1.32 kgm^{-3} at an air temperature of -10°C, and a pressure of 10^5 Pa. From Eqns. A1.9 and A1.11, the value of the empirical coefficient K is calculated to be 0.0131 under the assumption that $F=F_{ws}$. Since we do not know exactly what portion of the generated spray is collected by the decks and superstructure of the "Narva", we make the assumption that all if it is collected. This assumption is inherent in the simple equation, $F=F_{ws}$. Since $K=k_rk_z$, the value of k_r can now be computed as k_r=0.1536 s^{-1}.

APPENDIX 2: Spray Collision Geometry in the Heuristic Vessel Icing Model

The equations and geometry that describe the motion of the air and wave energy relative to the model vessel of Chapter 2 are presented below. This will make it possible to understand the details of the model's algorithm for calculating the spray flux collected by the vessel. The basic vector equations are presented in Chapter 2, and Fig. 2.2 shows how the vectors add to give the group velocity and air velocity relative to the vessel.

The three input variables that influence spray generation are the encountering angle, α, the wind speed, V_w, and the vessel speed, V_v. As stated in Chapter 2, the encountering angle is 180° for head winds and seas (since the waves are wind waves moving in the same direction as the wind), 90° for beam winds and seas, and 0° for following winds and seas. A coordinate system is assigned to the vessel such that the y-axis is oriented parallel to the length of the vessel with the unit vector **j** directed forward over the bow and the unit vector **i** is directed toward starboard. Then the wind vector relative to the vessel is:

$$\mathbf{V}_{ar} = (V_w \sin\alpha)\mathbf{i} + (V_w \cos\alpha - V_v)\mathbf{j} \qquad \textbf{(A2.1)}$$

Eqn. A2.1 can be derived directly from Eqn. 2.11. The magnitude of the relative wind speed vector, $\mathbf{V}_{ar}$ is:

$$V_{ar} = (V_w^2 + V_v^2 - 2V_w V_v \cos\alpha)^{1/2} \qquad \textbf{(A2.2)}$$

Taking the dot product of the relative wind speed, $\mathbf{V}_{ar}$, and the unit vector, **j**, yields an expression for the apparent wind encountering angle (in the vessel's frame of reference):

$$\alpha_{ar} = \cos^{-1}\left(\frac{V_w \cos\alpha - V_v}{V_{ar}}\right) \qquad \textbf{(A2.3)}$$

In a way analogous to Eqn. A2.2, the relative group velocity may be written:

$$C_{gr} = (C_g^2 + V_v^2 - 2C_g V_v \cos\alpha)^{1/2} \qquad \textbf{(A2.4)}$$

and in a way analogous to Eqn. A2.3 the relative wave group encountering angle is:

$$\alpha_{gr} = \cos^{-1}\left(\frac{C_g \cos\alpha - V_v}{C_{gr}}\right) \qquad \textbf{(A2.5)}$$

where C_g is the group velocity. These vectors are shown in Fig. 2.2.

In order to determine V_a in Eqn. 2.1, the magnitude of the component of the relative wind vector, $\mathbf{V}_{ar}$, along the relative group velocity vector must be found. Fig. 2.3 shows vector $\mathbf{C}_{gr}$ perpendicular to the projected width, P, with the relative wind vector, $\mathbf{V}_{ar}$, at a small angle to $\mathbf{C}_{gr}$. The scalar component of the relative wind vector directed along the relative group velocity vector is:

$$V_a = \frac{\mathbf{V}_{wr} \cdot \mathbf{C}_{gr}}{C_{gr}} \qquad \textbf{(A2.6)}$$

Experience shows that this component of the wind usually has a positive value. A positive value of V_a implies positive air momentum for spray cloud development. If on the other hand, the value of V_a in Eqn. A2.6 is negative, there is no momentum for spray cloud development, and the algorithm for spray calculation in this case will produce a "no spray" condition. This condition may occur if the vessel proceeds in a following sea in which the group velocity is less than the vessel's velocity (i.e. the wave group does not overtake the vessel). However, the wind, which is generally faster then the wave group velocity, overtakes the vessel from behind. In this case a spray jet is hypothesized at the bow, while the relative wind approaches from the opposite direction blowing the spray away from the bow and the vessel. Eqn. A2.6 is very helpful in this way, as Eqns. A2.3 and A2.5 could not in themselves have been used to determine this "no spray" condition. If V_a is positive then the two vectors have the same general direction and imply that spray is rafted by the relative wind.

The component of wind speed relative to the vessel along the relative group velocity vector is perpendicular to the projected spray access window. As mentioned in Chapter 2 the width of the spray access window is necessary for calculating its area. This upwind projected width is:

$$P = \frac{L}{2}\sin\alpha_{gr} - B\cos\alpha_{gr} \quad \text{for: } 180 \geq \alpha_{gr} \geq 90$$
$$P = \frac{L}{2}\sin\alpha_{gr} + B\cos\alpha_{gr} \quad \text{for: } 90 > \alpha_{gr} \geq 0 \qquad \text{(A2.7)}$$

These equations take into account the geometry of the encountering angle of the group velocity with respect to the rectangular cross-section of the vessel in plan view (Fig. 2.3).

There is a small probability that the empirically assigned mass flux of brine, R_{ws} could be larger than the available flux of momentum, R_{ae}. These parameters appear in Eqn. 2.1, and imply a negative mass flux of entrained air, R_{as}. This clearly cannot be the case; therefore under these circumstances, the value of R_{as} is set to zero. Under this condition, the thermodynamics of the model dictate that there will be no icing if the sea-surface temperature is higher than the equilibrium freezing temperature. This is most likely, as the sea-surface temperature will usually be above the equilibrium freezing temperature. Supercooling of the sea-surface brine, if it occurs at all, is probably small and may be eliminated quickly by either turbulent mixing with deeper water or by the formation of frazil ice (Martin and Kauffman, 1981).

APPENDIX 3: Soviet Vessel Icing Data

The data presented in Table A3.1 are taken from Zakrzewski and Lozowski (1989), and have been modified where necessary for use in evaluating the BLS model described in Chapter 2 (Section 2.7). All cases assume a fetch of 200 nm and a sea-surface salinity of 32.5 ppt, except those cases in the data table with single starred cases numbers. Those cases with a single star have been assigned a fetch of 100 nm and a sea-surface salinity of 5 ppt, which are values likely to characterize icing events in the Baltic Sea. Those cases with a double star are events in which the observed icing rate, I, as given in Table A3.1, is a thickness growth rate in cm hr^{-1}. The icing rate, I, is otherwise a mass accumulation rate in tonnes hr^{-1}.

Table A3.1 The sixty icing events used to evaluate the performance of the BLS model in Chapter 2.

Case No.	V_v ms^{-1}	V_w ms^{-1}	α deg.	T_a °C	T_{ss} °C	L m	B m	F_B m	I thr^{-1}
2	3.1	16.0	155	-5.0	0.0	30.0	5.5	2.7	0.5
3	3.0	17.0	170	-9.2	0.3	54.0	9.3	4.7	5.5
7	2.6	14.0	50	-8.0	1.0	39.2	7.3	3.5	1.7
8	2.6	11.5	10	-10.0	1.2	39.2	7.3	3.5	1.7
9	2.6	11.6	120	-10.0	1.0	39.2	7.3	3.5	6.2
10	2.1	12.2	150	-11.2	1.6	39.2	7.3	3.5	2.1
11	2.1	17.5	150	-11.0	0.8	39.2	7.3	3.5	6.1
12	1.5	14.5	110	-9.0	2.4	39.2	7.3	3.5	4.5
13	2.1	6.0	120	-13.8	0.8	39.2	7.3	3.5	2.8
14**	2.5	14.0	180	-7.5	0.5	39.2	7.3	3.5	0.95
15**	2.5	8.0	180	-4.0	1.0	30.0	5.5	2.7	0.15
16**	1.75	14.0	180	-5.0	1.0	35.0	6.5	3.5	0.35
17**	2.0	14.0	180	-6.0	1.0	30.0	5.5	2.7	0.60
18**	2.0	14.0	180	-7.0	1.0	30.0	5.5	2.7	0.70

19**	2.0	14.0	180	-7.0	0.0	30.0	5.5	2.7	0.90
20**	2.0	14.0	180	-9.0	0.0	30.0	5.5	2.7	1.10
21	3.6	17.0	140	-4.2	-0.2	39.2	7.3	3.5	0.75
22	2.6	14.0	80	-10.0	1.8	38.5	7.2	3.5	0.40
23	2.1	14.5	150	-4.0	-1.0	38.5	7.2	3.5	0.30
24	2.1	11.0	150	-12.0	-1.8	38.5	7.2	3.5	2.80
25	4.6	17.4	130	-10.8	-1.6	54.2	9.3	4.7	7.3
26	4.6	13.2	130	-12.2	-1.6	54.2	9.3	4.7	5.0
33	4.8	20.0	125	-3.0	0.5	30.0	5.5	2.7	3.9
39*	2.6	13.0	175	-10.0	5.0	39.0	7.3	3.5	0.15
44*	4.6	12.0	53	-9.0	1.9	39.0	7.3	3.5	0.54
45*	3.3	5.0	73	-3.0	2.0	39.0	7.3	3.5	0.67
46*	4.1	25.0	82	-9.0	1.0	39.0	7.3	3.5	5.50
47*	4.1	11.0	135	-6.0	2.0	39.0	7.3	3.5	0.10
48*	4.4	14.0	97	-4.0	0.7	39.0	7.3	3.5	1.0
62	0.0	11.0	180	-14.5	0.0	34.2	6.3	3.0	1.55
65	0.75	16.0	147	-9.5	1.0	39.2	7.3	3.5	5.9
71	4.7	19.0	50	-10.0	-0.6	54.2	9.3	4.7	2.7
72	4.6	15.0	153	-13.8	-0.1	54.2	9.3	4.7	2.6
73	4.6	23.0	60	-14.1	0.7	54.2	9.3	4.7	8.6
80	3.8	9.5	85	-10.0	2.0	30.0	5.5	2.7	0.75
81	1.0	27.0	180	-3.0	1.0	39.2	7.3	3.5	0.9
87	4.6	12.5	140	-10.8	0.65	39.2	7.3	3.5	2.3
88	2.1	18.0	30	-5.4	2.5	54.0	9.3	4.7	1.7
89	1.6	18.0	165	-5.3	2.5	54.0	9.3	4.7	0.3
90	1.6	18.0	175	-5.6	2.4	54.0	9.3	4.7	0.5
91	1.6	18.0	175	-6.6	2.2	54.0	9.3	4.7	0.7
92	0.5	17.0	175	-8.6	1.4	54.0	9.3	4.7	0.8

93	0.5	14.0	165	-10.1	1.2	54.0	9.3	4.7	2.9
94	1.0	13.0	175	-11.1	1.1	54.0	9.3	4.7	1.6
95	2.1	13.0	175	-11.6	1.0	54.0	9.3	4.7	1.2
96	2.1	13.0	155	-11.7	0.6	54.0	9.3	4.7	1.2
97	3.1	13.0	150	-10.3	0.6	54.0	9.3	4.7	1.2
98	4.1	16.0	160	-15.0	-1.6	54.0	9.3	4.7	6.6
99	4.6	13.5	120	-5.4	0.6	39.5	7.3	3.5	1.0
100	4.6	14.5	115	-14.9	-1.1	39.5	7.3	3.5	2.7
101	4.6	6.5	15	-7.0	1.0	39.5	7.3	3.5	1.2
102	4.35	16.0	138	-11.8	0.3	39.5	7.3	3.5	3.0
103	4.6	14.0	170	-9.5	0.0	39.5	7.3	3.5	3.37
104	4.1	19.5	160	-13.2	0.9	39.5	7.3	3.5	2.1
105	4.1	17.0	170	-14.1	0.9	39.5	7.3	3.5	3.3
106	4.6	16.0	170	-10.2	0.5	39.5	7.3	3.5	1.6
112*	2.6	14.0	115	-5.0	-0.2	39.5	7.3	3.5	1.0
113*	2.3	14.0	135	-5.0	-0.1	39.5	7.3	3.5	2.0
114*	2.3	17.5	135	-5.0	-0.25	39.5	7.3	3.5	2.7
115*	4.6	17.5	140	-5.7	-0.4	39.5	7.3	3.5	4.7

Table A3.2 gives the twelve icing events used to evaluate the performance of the BLN heuristic model. All of the conventions specified for Table A3.1 apply to Table A3.2 as well.

Table A3.2 The twelve icing cases used to evaluate the performance of the BLN model.

Case No.	V_v ms^{-1}	V_w ms^{-1}	α deg.	T_a °C	T_{ss} °C	L m	B m	F_B m	I thr^{-1}
1	2.1	14.0	180	-17.0	1.0	30.0	5.5	2.7	7.0
36**	2.0	32.0	180	-8.0	1.0	110	20	9.7	4.5
41*	4.1	4.2	153	-10.0	0.0	39.0	7.3	3.5	0.37
42*	4.1	5.0	130	-10.0	-0.5	39.0	7.3	3.5	0.52
43*	4.6	7.0	102	-4.5	-1.5	39.0	7.3	3.5	1.0
55*	0.5	15.2	160	-4.2	-0.2	39.2	7.3	3.5	12.0
56*	2.6	14.8	140	-4.5	-0.3	39.2	7.3	3.5	6.0
57*	1.8	12.4	80	-5.6	0.5	39.2	7.3	3.5	6.0
58*	2.3	14.0	105	-4.6	-0.1	39.2	7.3	3.5	12.0
59*	2.6	13.8	115	-6.6	-0.4	39.2	7.3	3.5	44.0
60*	4.6	13.8	115	-5.7	-0.4	39.2	7.3	3.5	28.0
78	1.0	27.5	180	-12.0	-1.0	39.2	7.3	3.5	17.5

APPENDIX 4: The E-folding Time for Falling Film Development

We describe here a method for estimating the e-folding time for the hydrodynamic development of a steady laminar falling liquid film. We begin with an infinite vertical plate (i.e. at t=0) with a uniform motionless liquid film residing on it. This initial condition is chosen for the purpose of estimating how long a laminar falling layer will take to form. The kinetic energy of the spray is ignored in the present approach in order to make the following analysis possible. The resulting characteristic e-folding time for the establishment of a laminar layer will be compared to the characteristic period between spraying events as well as the characteristic period between droplet impacts. This comparison will give an appreciation for whether a steady laminar layer can re-establish itself between spraying events or between droplet impacts.

We also assume that the liquid velocity, u, varies linearly with distance, y, from the wall, and that the film is always laminar. We accept this kinematic assumption to achieve a first estimate of the time of film development, even though it is clear that the Navier-Stokes equations must be invoked for a fully rigorous approach. Therefore, assuming a no-slip boundary condition (i.e. u(0)=0), the velocity shear in the film is:

$$\frac{\partial u}{\partial y} = \frac{u_a}{(\frac{\delta}{2})} = \frac{2u_a}{\delta} \qquad \textbf{(A4.1)}$$

where u_a is the average film velocity, and δ is the liquid film thickness. At time t=0, the film velocity is zero. Therefore, initially the liquid film begins to accelerate at the rate g. As the liquid acquires motion relative to the wall, a shear stress is set up which decelerates the film. The wall shear stress is:

$$\tau = \mu \frac{\partial u}{\partial y} \qquad \textbf{(A4.2)}$$

where μ is the dynamic viscosity of the liquid. We assume that there is no stress exerted on the outer surface of the film. The acceleration produced by this upward directed shear stress on the laminar film is opposite in direction to g the gravitational acceleration. The

acceleration given to the liquid layer by the shear stress is:

$$a = \frac{\mu \frac{\partial u}{\partial y}}{\rho \delta} \qquad \textbf{(A4.3)}$$

where the numerator is the shearing force per unit area, and the denominator is the liquid mass per unit area. Substitution of Eqn. A4.1 into A4.3 results in:

$$a = \frac{2\mu u_a}{\rho \delta^2} \qquad \textbf{(A4.4)}$$

The rate of change of the mean velocity in the film with time is:

$$\frac{du_a}{dt} = g - \frac{2\mu u_a}{\rho \delta^2} \qquad \textbf{(A4.5)}$$

where acceleration down the vertical surface is taken as positive. Eqn. A4.5 is a linear first order differential equation with the general solution:

$$u_a = \frac{g}{k}(1 - e^{-kt}) \qquad \textbf{(A4.6)}$$

where k is:

$$k = \frac{2\mu}{\rho \delta^2} \qquad \textbf{(A4.7)}$$

The e-folding time from Eqn. A4.6 is:

$$t_e = \frac{1}{k} = \frac{\rho \delta^2}{2\mu} \qquad \textbf{(A4.8)}$$

In order to calculate the e-folding time we use for water, ρ=1000 kgm^{-3} and μ=1.75X10^{-3} Nsm^{-2}. The choice of thickness for the laminar layer, δ, is not readily apparent. However, the Dukler and Bergelin (1952) model for a falling film gives a maximum laminar layer thickness of approximately 200 μm.

Eqn. A4.8 produces e-folding times of 0.0029s, 0.0114s and 0.29s for 100 μm, 200 μm and 1 mm thick laminar layers, respectively. A falling film of 1 mm thickness is however likely to become turbulent according to the Dukler and Bergelin (1952) model.

APPENDIX 5: The Mean Period between Droplet Collisions

In order to estimate the mean period between spray droplet impacts on a surface, a spray collision efficiency of unity is assumed for the wetted surface. For a monodisperse spray the number of droplets per second passing through one square metre normal to the spray's velocity is:

$$N_R = \frac{R}{m_d} \qquad \textbf{(A5.1)}$$

where R is the impinging flux (units of $kgm^{-2}s^{-1}$) and m_d is the mass of the droplets. The mass of a spray droplet is:

$$m_d = \frac{\pi}{6}\rho_w d^3 \qquad \textbf{(A5.2)}$$

where ρ_w is the density of brine and d is the spray droplet diameter. Since the impact of a droplet with a surface that is covered by a falling film is probably a complex process, it is necessary to make a simplifying assumption in order to estimate the mean period between droplet collisions. We assume that the effective diameter of impact influence of an impinging droplet is twice the diameter of the droplet. It is likely that the area of impact influence is a function of droplet velocity and liquid film thickness among other factors, but for the moment, D=2d where D is the diameter of the effective area of impact, A.

Next, the rate at which droplets will disturb the liquid film at a specific point by impinging on the surface is:

$$N = N_R A \qquad \textbf{(A5.3)}$$

where A is the area of impact influence ($A=\pi D^2/4=\pi d^2$) around the specified surficial point. Combining Eqns. A5.1, A5.2 and A5.3 we obtain:

$$N = \frac{6R}{d\rho_w} \qquad \textbf{(A5.4)}$$

The inverse of N is the mean period between droplet impacts at a point. Hence the mean period between impacts on a point is:

$$\tau_d = \frac{d\rho_w}{6R} \qquad \text{(A5.5)}$$

For brine of density, ρ_w=1000 kgm^{-3}, a droplet diameter of d=1 mm, and an impinging spray flux, R=10 kgm^{-2}s^{-1}, the mean period is τ_d=0.0166 s. This value of τ_d is likely a low estimate because R=10 kgm^{-2}s^{-1} is a large value of spray flux on a Soviet medium-sized fishing trawler (Zakrzewski, 1986).

APPENDIX 6: The Reynolds and Rayleigh Numbers for a Falling Film

Both the Reynolds number and the Rayleigh number increase with increased characteristic length. In the case of a falling film, the characteristic length is the film's thickness, δ. Using the Dukler and Bergelin (1952) model (Eqns. 3.1, 3.2, 3.3 and 3.14) the maximum laminar layer thickness is given by:

$$\delta_{max}=\left(\frac{5\mu}{g^{1/2}\rho}\right)^{2/3} \qquad \textbf{(A6.1)}$$

where μ is the dynamic viscosity of water, g is the gravitational acceleration, and ρ is the density of water. This maximum value of the laminar layer thickness is estimated to be δ_{max}=198 μm. At greater film thicknesses and liquid flow rates, the laminar sublayer of the Dukler and Bergelin (1952) model is subjected to increased shear by the buffer layer and the turbulent layer. This increased shear causes the model's laminar sublayer to decrease in thickness even though the sublayer flow itself is conserved. As the film thickness and the liquid flow rates of the film decrease the laminar layer becomes increasingly stable.

The Reynolds number for a falling film is given by:

$$\mathbf{Re}=\frac{4\Gamma}{\mu} \qquad \textbf{(A6.2)}$$

where Γ is the mass flow rate per unit breath of the falling film (defined in Eqn. 3.7). If the film is laminar, the Reynolds number may be represented as (Incropera and DeWitt, 1990):

$$\mathbf{Re}=\frac{4g\rho^2\delta^3}{3\mu^2} \qquad \textbf{(A6.3)}$$

Using δ=198 μm, the film Reynolds number is Re=33. Incropera and DeWitt (1990) give a Reynolds number based on thickness of Re≈30 as the criterion for the onset of wavy laminar flow. Therefore, the development of the buffer layer in the Dukler and Bergelin

(1952) model is approximately coincident with the development of waves on the outer surface of the falling film. Dukler and Bergelin (1952) also give a Reynolds number based on film thickness of Re≈1100 as the criterion for the development of turbulence in the falling film which agreed well with their data. It is clear that if droplet bombardment, wind shear and icing interface roughness are neglected, that the laminar layer of the Dukler and Bergelin (1952) model is likely to be a robust hydrodynamic structure as far as mechanically induced turbulence is concerned.

Convective instability cannot develop for the laminar layer of a falling film on a vertical surface. It requires that the gravitational body force be aligned with the density gradient, and in this case the density gradient of the laminar layer is normal to the gravitational body force. However, even though the convective stability is not strictly applicable to the present modelling, it is included for its potential relevance to horizontal films. Therefore, the convective stability of the same laminar layer as above is considered using the Rayleigh number. The Rayleigh number is defined as:

$$Ra = \frac{g\beta \Delta T \delta^3}{\nu \alpha} \qquad \textbf{(A6.4)}$$

where β is the thermal expansion coefficient (i.e. β=-68.05X10^{-6}°C^{-1} for water at 0°C), ν is the kinematic viscosity of water (i.e. ν=1.75X10^{-6}m^{2}s^{-1}), and α is the thermal diffusivity of water (i.e. α=1.3X10^{-7}m^{2}s^{-1}). Using a value for the temperature difference across the laminar layer of ΔT=-15°C (a large temperature difference), a conservative estimate of the Rayleigh number is produced. In the present case, the laminar layer must be considered as convectively stable with a Rayleigh number estimate of Ra=0.34. List (1990) used ΔT=-3°C as a temperature difference across a liquid layer on a hailstone to estimate Ra=0.93. These estimates are much smaller than the critical Rayleigh number of 1240 for a fluid between flat plats. Therefore, the integrity of the laminar layer as given by the Dukler and Bergelin (1952) model is very likely maintained for both the mechanical and convective mechanisms of turbulence induction.

APPENDIX 7: The Algorithm for the Spray Icing Model

This appendix documents the way in which the model's equations (cf. Section 3.6) are used to solve for the ice accretion flux and the ice fraction. A flow chart which illustrates the structure of the algorithm, the structure of the computer code, and the sequence of subroutines is shown in Fig. A7.1. Each of the steps in the algorithm is described and explained below.

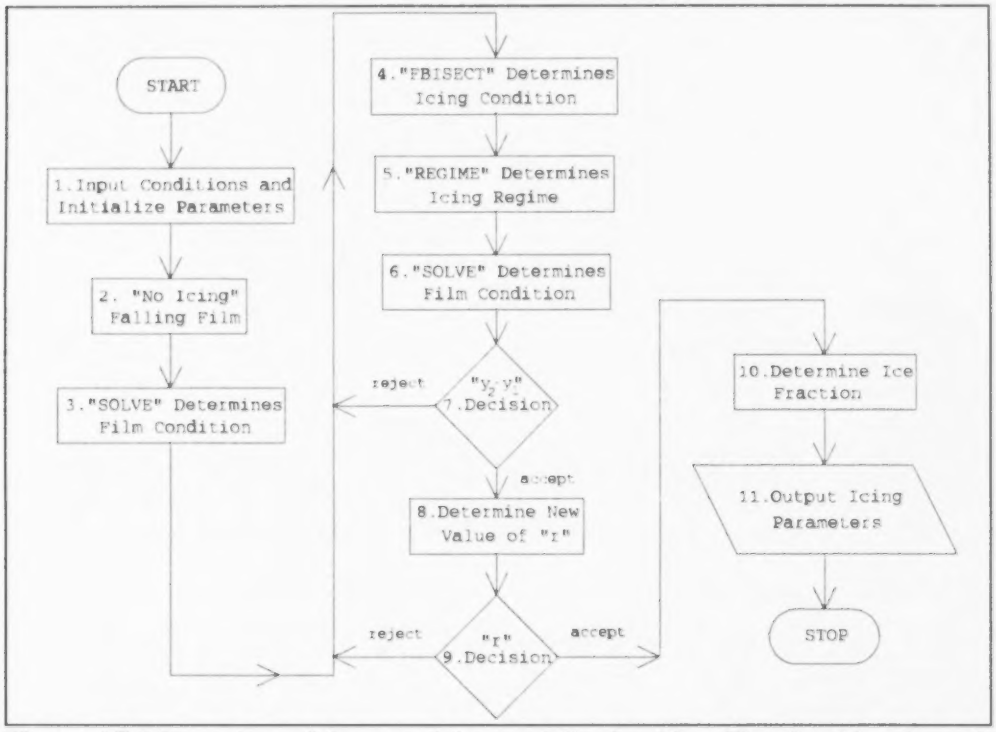

Figure A7.1 Flow chart of the spray icing model's algorithm. The algorithm depends on convergence for successive calculations of the laminar layer thickness, (y_2-y_1), and the temperature ratio, r.

1. Input conditions and initialize parameters. The environmental conditions are input (e.g. T_a, RH, V_a, T_4, R_4) and model parameters such as the heat transfer coefficient and the saturation vapour pressure of the air are computed. The freezing zone/laminar layer temperature ratio, r, (defined in Eqns. 3.26 and 3.64) is initialized to a value of 0.1 in preparation for its comparison with the first calculated value of r at Step 9.

2. No icing. Falling film. This step assumes that no ice accretion is occurring and that all of the water entering or impinging on the segment is shed. Eqns. 3.59 and 3.63 are used to calculate the total flux of the falling film under the tentative assumption that no ice is accreted (i.e. $I_0=R_0=0$).

3. "SOLVE". This subroutine determines the condition of the falling film and requires the segment's total flux of shed water as an input. "SOLVE" depends on Eqns. 3.58 to 3.63 to determine the thickness of the falling film, the thickness of the laminar layer, the flux of the laminar layer, and the flux of the mixed layer, if one is present. Since the total film flux is calculated in Step 2 under the "no icing" assumption, a first estimate of the laminar layer thickness is calculated in preparation for its first error comparison with a newly calculated value at Step 7. Steps 4, 5 and 6 produce the new estimate for the laminar layer thickness with ice growth taken into account, and along with Step 7, forms a computation loop. This computational loop (Steps 4-7) is inside another computation loop that searches until a sufficiently small error in the freezing zone/laminar layer temperature ratio, r, occurs (Steps 4-9).

4. "FBISECT". This subroutine determines the temperature at the surface of the falling film, T_3, the temperature at the icing interface, T_1, and the pure ice flux, I_0. "FBISECT" solves Eqns. 3.68 and 3.69 for T_2 (i.e. $T_2=T_3$) and T_1 using the freezing zone/laminar layer temperature ratio ($r=(T_0-T_1)/(T_1-T_2)$). From the definition of this temperature ratio, the temperature difference across the laminar layer is:

$$(T_2-T_1)=\frac{1}{1+r}(T_2-T_0) \tag{A7.1}$$

Substitution of Eqn. A7.1 into the first term of Eqn. 3.68 results in:

$$-\frac{k_w}{(1+r)}\frac{(T_2-T_0)}{(y_2-y_1)}-h(T_2-T_a)-\frac{\varepsilon h L_v}{c_p P_a}\left(\frac{P_r}{S_c}\right)^{0.63}(e_2-RHe_a) \tag{A7.2}$$

$$-\sigma a(T_2-T_a)+c_w R_{i3}(T_{i3}-T_2)-c_w R_4(T_2-T_4)=0$$

Since all of the parameters of Eqn. A7.2, except T_2, are known when subroutine

"FBISECT" is called, the temperature at the interface of the laminar and mixed layer, T_2, can be calculated. This is accomplished with a bisection search for T_2 over the range $0°C \le T_2 \le T_a$. The bisection search method is documented in Press et al. (1990) and serves as a reliable and robust method for calculating numerical solutions to equations such as Eqn. A7.2. Once T_2 is known, the icing interface temperature is calculated with:

$$T_1 = \frac{1}{1+r} T_0 + \frac{r}{1+r} T_2 \qquad \textbf{(A7.3)}$$

which is derived from Eqn. A7.1. Once T_2 and T_1 are known, Eqn. 3.69 is used in "FBISECT" to solve for the pure ice flux, I_0.

5. "REGIME". This subroutine begins by calculating the rate of advance of the icing interface according to Eqn. 3.71 based on the icing interface temperature, T_1, calculated in subroutine "FBISECT" in Step 4. Once the rate of advance of the icing interface is known, estimates for the flux of entrapped water, R_0, and the flux of entrapped air, R_a, are calculated according to Eqns. 3.72 and 3.73, respectively. These fluxes serve to identify the model's icing regime according to the criteria given in Section 3.6., namely, that: (1) if $R_0 \le 0$, the glaze ice accretion regime occurs with $R_0=0$ and $R_a=0$; (2) is $R_0>0$ and $R_a \le 0$, the spongy ice accretion regime occurs with a mass flux of entrapped water, R_0, and a mass flux of entrapped air, $R_a=0$, and (3) if $R_0>0$ and $R_a>0$, the porous ice accretion regime occurs with a mass flux of entrapped water, R_0, and a mass flux of entrapped air, R_a. Once R_0 and R_a are known, along with the pure ice flux, I_0, the ice fraction, I, and the density of the accretion, ρ_{ac}, are calculated according to Eqns. 3.67 and 3.57, respectively. Subroutine "REGIME" also determines the total flux for the film in preparation for subroutine "SOLVE" which will calculate the new condition of the falling film. The equation used to calculate the total film flux is produced by substituting Eqn. 3.59 into Eqn. 3.16:

$$R_T = R_{i2} + R_{i3} + R_4 - I_0 - R_0 \qquad \textbf{(A7.4)}$$

Subroutine "REGIME" determines the prevailing icing regime and the flux of entrapped air and water as well as the accretion density and ice fraction.

6. "SOLVE". Subroutine "SOLVE" is called at Step 6 in order to determine the conditions of the falling film as for Step 3. "SOLVE" determines the thickness of the falling film, the thickness of the laminar layer, the flux of the laminar layer, and the flux of the mixed layer if a mixed layer is present. The thickness of the laminar layer, (y_2-y_1), is calculated in preparation for its comparison to the previous estimate of laminar layer thickness calculated at Step 3 on the first iteration, and at Step 6 of a previous iteration.

7. Decision. The new value of laminar layer thickness, (y_2-y_1) is compared to the previous value of laminar layer thickness. If the new value of laminar layer thickness calculated at Step 6 is different from its value on the previous iteration by more than 0.001%, the previous value of the laminar layer thickness is rejected and new icing conditions will be calculated with a return to subroutine "FBISECT" at Step 4. If the new value of laminar layer thickness calculated at Step 6 is different from its value on the previous iteration by less than 0.001%, the new value of laminar layer thickness is accepted and icing conditions are solved for the current value of the temperature ratio, r, in preparation for Step 8.

8. Determine new temperature ratio. Once a new value for the laminar layer thickness is made available by the first calculation loop (Steps 4-7), a new value for the temperature ratio is calculated according to Eqn. 3.33.

9. Decision. The new value of the temperature ratio, r, calculated in Step 8 is compared to its previous value of 0.1 for the first pass through the calculation loop (Steps 4-9) or to its value on the previous pass through the calculation loop. If the new value of the temperature ratio is different from its value on the previous iteration by more than 0.001%, the previous value of the temperature ratio is rejected and new icing conditions will be calculated with a return to subroutine "FBISECT" at Step 4. If the new value of the temperature ratio calculated at Step 8 is different from its value on the previous iteration by less than 0.001%, the new value is accepted and the model's equations have been solved numerically.

10. Determine ice fraction. The equations of Section 3.5.5 are used to determine the ice fraction and density of the model ice accretion once I_0, R_0, and R_a are known from steps 1-9.

11. Output icing parameters. The icing parameters that describe the model's accretion (I_0, R_0, R_a, I and ρ_{ac}) are made available following their calculation in steps 1-10.

APPENDIX 8: The Icing Data used to Calibrate the Spray Icing Model

This appendix documents the spray icing data of Shi (pers. comm.) that was used to determine the value of the freezing zone parameter, C_r (Eqn. 3.29) for use in the spray icing model described in Chapter 3. The experiments and the method used by Shi (pers. comm.) are described in Section 3.7.2. Table A8.1 gives the case number for each of the spray icing measurements that were used to calibrate the model. For each case, the air temperature,T_a, air velocity, V_a, spray flux, R_s, ice accretion flux, (I_0+R_0), and sponginess, λ, were measured. The ice fraction, I, and the ice accretion flux, (I_0+R_0), for each icing case, were used to calculate a value for the freezing zone parameter, C_r (see Table A8.1). The method and equations used for these calculations of C_r are given in Section 3.7.1 and 3.7.2.

Case 1 could not be included in the evaluation of the freezing zone parameter because the sponginess, λ, (or ice fraction, I) was not measured, and it must be known to evaluate C_r. However, case 9 was included even though the ice accretion flux, (I_0+R_0), was not measured. Case 9 was included on the assumption that the ice accretion flux for case 10 would be little different from that of case 9, and therefore the ice accretion flux of case 10 was used for case 9. This is justified here because the air temperatures, air velocities, spray fluxes, and measured ice fractions for the two cases are negligibly different. For example, the measured ice fraction for case 9 is within 3.6% of that of case 10. Excluding case 1, and including case 9 produced the list of freezing zone parameters given in Table A8.1. The mean value of these freezing zone parameters is 1.33, and the standard deviation is 0.16. This value of C_r=1.33 is used in the model throughout Section 3.8 to evaluate the model's performance and sensitivity.

Table A8.1 The Shi (pers. comm.) spray icing data used to evaluate the performance of the spray icing model's freezing zone parameter, C_r.

Case No.	T_a °C	V_a ms^{-1}	R_s $kgm^{-2}s^{-1}$	(I_0+R_0) $kgm^{-2}s^{-1}$	λ	I	C_r
2	-6.2	20.0	0.102	0.0217	0.371	0.629	1.31
3	-5.5	30.0	0.100	0.0174	0.415	0.585	1.45
4	-10.0	30.0	0.105	0.0260	0.362	0.638	1.23
5	-15.4	10.0	0.088	0.0334	0.460	0.540	1.26
6	-15.8	20.0	0.108	0.0392	0.471	0.583	1.15
7	-15.0	30.0	0.105	0.0478	0.429	0.571	1.09
8	-10.0	20.0	0.105	0.0250	0.455	0.545	1.37
9	-10.4	10.0	0.092	0.0149[1]	0.442	0.558	1.56
10	-10.0	10.0	0.091	0.0149	0.421	0.579	1.53

[1] The ice accretion flux for case 9 was not measured. Therefore, the value for case 10 was assumed because of the similarity of the two cases.

APPENDIX 9: The Icing Data used to Evaluate the Spray Icing Model

This appendix documents the spray icing data of Shi (pers. comm.) that was used to evaluate the performance of the spray icing model. The results are shown in Fig. 3.12 and the experiments along with the method used by Shi (pers. comm.) are described in Section 3.7.2. Table A9.1 gives the case number for each of the spray icing measurements that are used to evaluate the model's performance in Section 3.8.4. The model does not provide an icing prediction for cases 14 or 19, and therefore, does not provide a performance comparison in these two cases. For this reason, 7 of the 9 cases are shown in Fig. 3.12 of Section 3.84. These 7 cases have a coefficient of determination of 0.96 while the Willmott index of agreement is 0.94.

Table A9.1 The spray icing data (Shi, pers. comm.) used to evaluate the performance of the spray icing model.

Case No.	T_a °C	V_a ms^{-1}	R_s $kgm^{-2}s^{-1}$	(I_0+R_0) $kgm^{-2}s^{-1}$	$(I_0+R_0)^2$ $kgm^{-2}s^{-1}$	I	I[3]
11	-9.7	10.0	0.0846	0.0154	0.0083	0.57	1.0
12	-9.8	20.0	0.1040	0.0241	0.0181	0.58	0.69
13	-19.8	10.0	0.0897	0.0356	0.0312	0.54	0.52
14[4]	-19.0	20.0	0.0972	0.0493	NA	0.56	NA
15	-4.6	10.0	0.0831	0.0071	0.0041	0.59	1.0
16	-4.7	20.0	0.1020	0.0117	0.0063	0.55	1.0
17	-7.7	30.0	0.0960	0.0193	0.0178	0.60	0.69
18	-2.1	20.0	0.0990	0.0053	0.0030	0.68	1.0
19[5]	-25.4	20.0	0.0850	0.0550	NA	0.63	NA

[2] The model's prediction of ice accretion flux.

[3] The model's prediction of ice fraction.

[4] Icing case 14 for which the model did not converge, and for this reason, did not provide a prediction.

[5] Icing case 19 for which the model did not converge, and for this reason, did not provide a prediction.

Table A9.2 gives the spray icing data that was used to calibrate the spray icing model and the spray icing model's predictions for these cases. Therefore, Table A9.2 presents a comparison of data with a model that partially depends on the data. Case 1 which was not used to calibrate the model (see Appendix 8) is included in Table A9.2 and Fig. 3.12. Since the model did not provide predictions for cases 6 and 7, and since the ice accretion flux for case 9 is not available, seven cases are available for a comparison in which the model is partially dependent on the data. These seven cases have a coefficient of determination of 0.56 and a Willmott index of agreement of 0.73.

Table A9.2 The spray icing data (Shi, pers. comm.) that was used to estimate the freezing zone parameter in Section 3.7.2 are presented and compared to the predictions of the spray icing model. Case 1, although not used in the model's calibration, is included even though the ice fraction is not available.

Case No.	T_a °C	V_a ms^{-1}	R_s $kgm^{-2}s^{-1}$	(I_0+R_0) $kgm^{-2}s^{-1}$	$(I_0+R_0)^6$ $kgm^{-2}s^{-1}$	I	I[7]
2	-6.2	20.0	0.102	0.0217	0.0080	0.63	1.0
3	-5.5	30.0	0.100	0.0174	0.0096	0.58	0.94
4	-10.0	30.0	0.105	0.0260	0.0290	0.64	0.55
5	-15.4	10.0	0.088	0.0334	0.0191	0.54	0.66
6[8]	-15.8	20.0	0.108	0.0392	NA	0.53	NA
7[9]	-15.0	30.0	0.105	0.0478	NA	0.57	NA
8	-10.0	20.0	0.105	0.0250	0.01885	0.54	0.68
9[10]	-10.4	10.0	0.092	NA	0.0094	0.56	0.96
10	-10.0	10.0	0.091	0.0149	0.0090	0.58	0.96
1	-5.2	10.0	0.079	0.0075	0.0046	NA	1.0

[6] The model's prediction of ice accretion flux.

[7] The model's prediction of ice fraction.

[8] Icing case 6 for which the model did not converge and for this reason did not provide a prediction.

[9] Icing case 7 for which the model did not converge and for this reason did not provide a prediction.

[10] The ice accretion flux for case 9 is not available.

VITAE

Ryan Z. Blackmore

11391-22 Ave
Edmonton, Alberta
T6J 4V8
Phone: (403) 434-4391

Department of Earth
and Atmospheric Sciences
University of Alberta
Edmonton, Alberta T6G 2E3
Phone: (403) 492-5405

EDUCATION

1988 M.Sc. Meteorology, University of Alberta
1985 B.Sc. Meteorology (Specialization), University of Alberta
1976 B.Sc. Mechanical Engineering, University of Alberta

SCHOLARSHIPS, AWARDS AND RESEARCH WORK

1996-1995	Research Assistantship, Department of Earth and Atmospheric Sciences, University of Alberta
1995-1993	Research Assistantship, Department of Geography (Meteorology), University of Alberta
1992	Province of Alberta Graduate Fellowship
1991	AES Scholarship for Graduate Studies in Meteorology and Atmospheric Science
1990	Andrew Stewart Graduate Prize, University of Alberta
1989,1988	NSERC Postgraduate Doctoral Scholarship, University of Alberta
1989,1988	Graduate Faculty Fellowship, University of Alberta
1988	Graduate Research Travel Award, Faculty of Graduate Studies and Research, University of Alberta, to attend the 10th Port and Ocean Engineering under Arctic Conditions Conference in Luleä, Sweden
1987	Intersession Bursary, Department of Geography, University of Alberta
1987	Graduate Research Travel Award, Faculty of Graduate Studies and Research, University of Alberta, to attend the 2nd Workshop on Operational Meteorology in Halifax, Canada
1986	Research Assistantship, Department of Geography (Meteorology), University of Alberta
1985	Dean's Honor Roll, Faculty of Science, University of Alberta
1985	NSERC Undergraduate Summer Research Award, University of Alberta
1984	AES/NSERC Studentship, University of Alberta

PUBLICATIONS AND WORK IN PROGRESS

Blackmore, R. Z., 1988: Spongy ice formation. M.Sc. thesis. University of Alberta, 140 pp (unpublished).

Blackmore, R. Z., 1986: Innovations to the Lozowski/Stallabrass/ Hearty icing model. In: Lozowski, E. P., and E. M. Gates, 1986: Applied research in atmospheric Icing: final report to the Department of National Defense. University of Alberta, Edmonton, Alberta, 96-103.

Blackmore, R. Z., W. P. Zakrzewski, and E. P. Lozowski, 1989: Ice growth on a ship's mast. In: Proceedings of the 10th International Conference on Port and Ocean Engineering under Arctic Conditions, (POAC), Lulëa, Sweden, Vol. 3, 1440-1453.

Blackmore, R. Z., and E. P. Lozowski, 1992: An uncomplicated model of ship icing. In: Proceedings of the 11th International Association for Hydraulic Research Symposium on Ice (IAHR), Banff, Canada, Vol. 2, 607-621.

Blackmore, R. Z., and E. P. Lozowski, 1993: An heuristic freezing spray model of vessel icing. In: Proceedings of the 3rd International Society of Offshore and Polar Engineering Conference (ISOPE), Singapore, Vol. 2, 648-654.

Blackmore, R. Z., and E. P. Lozowski, 1994: An heuristic freezing spray model of vessel icing. *Int. J. Offshore Polar Eng.*, **4(2)**, 119-126.

Blackmore, R. Z., and E. P. Lozowski, 1996: A freshwater spongy spray icing model with surficial structure. In: Proceedings of the 7th International Workshop on Atmospheric Icing of Structures (IWAIS), Chicoutimi, Quebec, June 3-6, 33-38.

Lozowski, E., R. Blackmore, T. Forest, and J. Shi 1996: Spongy icing in the marine environment. In: Proceedings of the 15th International Conference on Offshore Mechanics and Arctic Engineering (OMAE), Florence, Vol. IV, Arctic/Polar Technology ASME, 55-61.

Zakrzewski, W. P., E. P. Lozowski, and R. Z. Blackmore, 1988: Atmospheric icing of ships and an overview of the research on atmospheric icing modelling applicable to ship icing. In: Proceedings of the 4th International Symposium on Atmospheric Icing on Structures (IWAIS), Paris, 202-207.

Zakrzewski, W. P., E .P. Lozowski, and R. Z. Blackmore, 1988: Computer modelling of ship icing. In: Proceedings of the 9th International Association for Hydraulic Research (IAHR), Symposium on Ice, Sapporo, Vol. 2, 446-457.

Zakrzewski, W. P., R. Z. Blackmore, and E. P. Lozowski, 1987: Mapping the ice growth rates on sea-going ships in water east of Canada. In: Proceedings of 2nd Canadian Workshop on Operational Meteorology, Halifax, NS, 77-99.

Zakrzewski, W. P., R. Z. Blackmore, and E. P. Lozowski, 1988: Mapping icing rates on sea-going ships. *J. Meteor. Soc. Jpn*, **66,** 661-675.

Zakrzewski, W. P., E. P. Lozowski, and R. Z. Blackmore, 1988: The use of a ship icing model to estimate the direct spray fluxes. In: Proceedings of the 4th International Symposium on Atmospheric Icing of Structures (IWAIS), Paris, 399-404.

Zakrzewski, W. P., E. P. Lozowski, R. Z. Blackmore, and R. Gagnon, 1988: Recent approaches in the modelling of ship icing. In: Proceedings of the 9th International Association for Hydraulic Research (IAHR) Symposium on Ice, Vol. 2, Sapporo, 458-476.

Zakrzewski, W. P., E. P. Lozowski, W. L. Thomas, M. Bourassa, R.Z. Blackmore, K. Szilder, and A. Kobos, 1993: A three-dimensional time-dependent ship icing model. In: Proceedings of the 12th International Conference on Port and Ocean Engineering under Arctic Conditions (POAC), Vol. 2, Hamburg, 857-873.

PRESENTATIONS

1996 Presented the paper "A Freshwater Spongy Spray Icing Model with Surficial Structure" (R.Z. Blackmore and E.P. Lozowski) at the 7th International Workshop on Atmospheric Icing of Structures, Chicoutimi, Quebec, Canada.

1993 Presented the paper "An Heuristic Freezing Spray Model of Vessel Icing" (R.Z. Blackmore and E.P. Lozowski) at the 3rd International Society of Offshore and Polar Engineering Conference, Singapore.

1992 Presented the paper "An Uncomplicated Model of Ship Icing" (R.Z. Blackmore and E.P. Lozowski) at the 11th International Symposium on Ice, International Association for Hydraulic Research, Banff, Canada.

1989 Presented the paper "Ice Growth on a Ship's Mast" (R.Z. Blackmore, W.P. Zakrzewski and E.P. Lozowski) at the 10th International Conference on Port and Ocean Engineering under Arctic Conditions, Lulëa, Sweden.

1987 Presented the paper "Mapping the Ice Growth Rates on Sea-going Ships in Waters East of Canada" (W.P. Zakrzewski, R.Z. Blackmore, and E.P. Lozowski) at the 2nd Workshop on Operational Meteorology, Halifax, Canada.

PROFESSIONAL ASSOCIATIONS

American Meteorological Society
Canadian Meteorological and Oceanographic Society
American Geophysical Union
The International Society of Offshore and Polar Engineers
The International Society for the Prevention and Mitigation of Natural Hazards